POSITRON EMISSION TOMOGRAPHY IN ATHEROSCLEROSIS

POSITRON EMISSION TOMOGRAPHY IN ATHEROSCLEROSIS

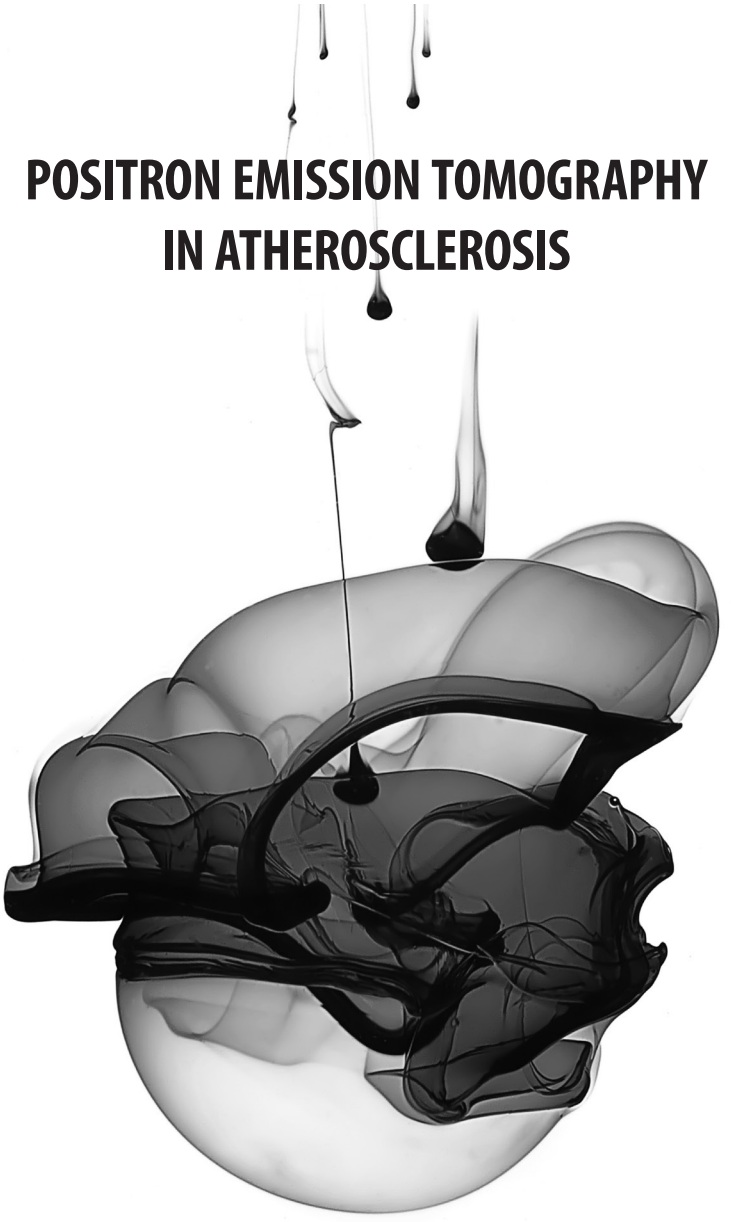

Björn Alexander Blomberg

Positron Emission Tomography in Atherosclerosis
Thesis, Utrecht University, the Netherlands

ISBN/EAN: 978-90-393-6443-7
Cover art: Studio 37
Printed by: Ridderprint B.V., Ridderkerk

POSITRON EMISSION TOMOGRAPHY IN ATHEROSCLEROSIS

Functionele beeldvorming van slagaderverkalking
(met een samenvatting in het Nederlands)

Proefschrift

ter verkrijging van de graad van doctor aan de Universiteit Utrecht
op gezag van de rector magnificus, prof. dr. G.J. van der Zwaan,
ingevolge het besluit van het college van promoties
in het openbaar te verdedigen op
donderdag 10 december 2015 des middags te 12.45 uur

door

Björn Alexander Blomberg

geboren op 4 december 1987 te Rockanje

Promotoren: Prof. dr. W.P.T.M. Mali
Prof. dr. P.F. Høilund-Carlsen

Copromotoren: Dr. P.A. de Jong
Dr. M.G.E.H. Lam

The research presented in this thesis was financially supported by the 'Alexandre Suerman' MD/PhD program of the University Medical Center Utrecht, Utrecht, the Netherlands, the Anne Marie and Christian Rasmussen's Memorial Foundation of the University of Southern Denmark, Odense, Denmark, the Jørgen and Gisela Thrane's Philantrophic Research Foundation, Broager, Denmark, and the United States Department of Veterans Affairs, United States of America.

Financial support by the Dutch Heart Foundation for the publication of this thesis is gratefully acknowledged.

Additional financial support for publication of this thesis was kindly provided by the Department of Nuclear Medicine at Odense University Hospital, ChipSoft B.V., Sectra BeNeLux, and ABN AMRO Bank N.V.

Aan mijn ouders

"It ain't what you don't know that gets you into trouble.
It's what you know for sure that just ain't so."

Mark Twain

TABLE OF CONTENTS

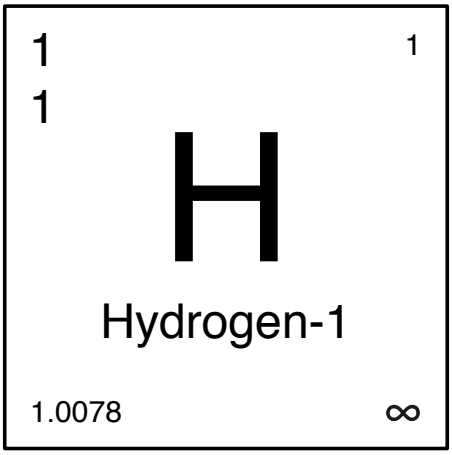
1
1
1
H
Hydrogen-1
1.0078
∞

Chapter 1

General Introduction

Atherosclerosis is a cardiovascular disease characterized by deposition of plaques within arterial walls **(1)**. These plaques contain lipids, calcium, and various types of inflammatory cells **(2)**. Although plaques develop slowly and generally remain asymptomatic for decades, the clinical manifestation of atherosclerosis is often abrupt and without warning. Typically, atherosclerosis becomes clinically manifest in the form of an adverse cardiovascular event, such as acute myocardial infarction **(3)** or stroke **(4)**.

Adverse cardiovascular events and their sequelae are a major health hazard in Western societies **(5)**. Hence, strategies to prevent adverse cardiovascular events are among our most important public health priorities **(6, 7)**. Preventive strategies have focused primarily on identifying asymptomatic individuals at high cardiovascular disease risk, the so-called "vulnerable" patient **(7)**. In theory, vulnerable patients benefit most from intensive evidence-based medical interventions. However, early identification of vulnerable patients remains a major ongoing challenge **(6)**. Numerous factors, such as smoking, obesity, dyslipidemia, hypertension, and diabetes mellitus, are associated with increased rates of adverse cardiovascular events; nonetheless, their hazard rates are too small for accurate individual risk assessment **(8)**. Even comprehensive risk scores, such as the Framingham Risk Score **(9)** or HeartSCORE **(10)**, provide insufficient predictive accuracy for adequate individual risk assessment, leading to substantial over-treatment and under-treatment with associated morbidity and societal costs **(11)**.

Recent developments in cardiovascular imaging offer new opportunities for early and individual cardiovascular disease risk assessment. Next to computed tomography (CT) imaging of vascular calcifications **(12)**, functional imaging techniques, aimed at visualizing and quantifying key pathophysiological mechanisms of atherosclerotic cardiovascular disease, have gained interest as potent markers of risk for adverse cardiovascular events. The key pathophysiological mechanisms of atherosclerosis include arterial inflammation **(13)** and vascular calcification **(14)**, which can be evaluated by [^{18}F]-fluorodeoxyglucose positron emission tomography/computed tomography (^{18}FDG PET/CT) **(15, 16)** and sodium [^{18}F]-fluoride positron emission tomography/computed tomography (Na^{18}F PET/CT) imaging **(17)**, respectively (**FIGURE 1**). Although these imaging techniques appear promising for the purpose of cardiovascular disease risk assessment, rigorous technical and clinical validation are required before these imaging modalities can be reliably implemented into daily clinical practice. Consequently, the aim of this thesis was to evaluate the technical and clinical validity of ^{18}FDG PET/CT and Na^{18}F PET/CT for the purpose of cardiovascular risk assessment.

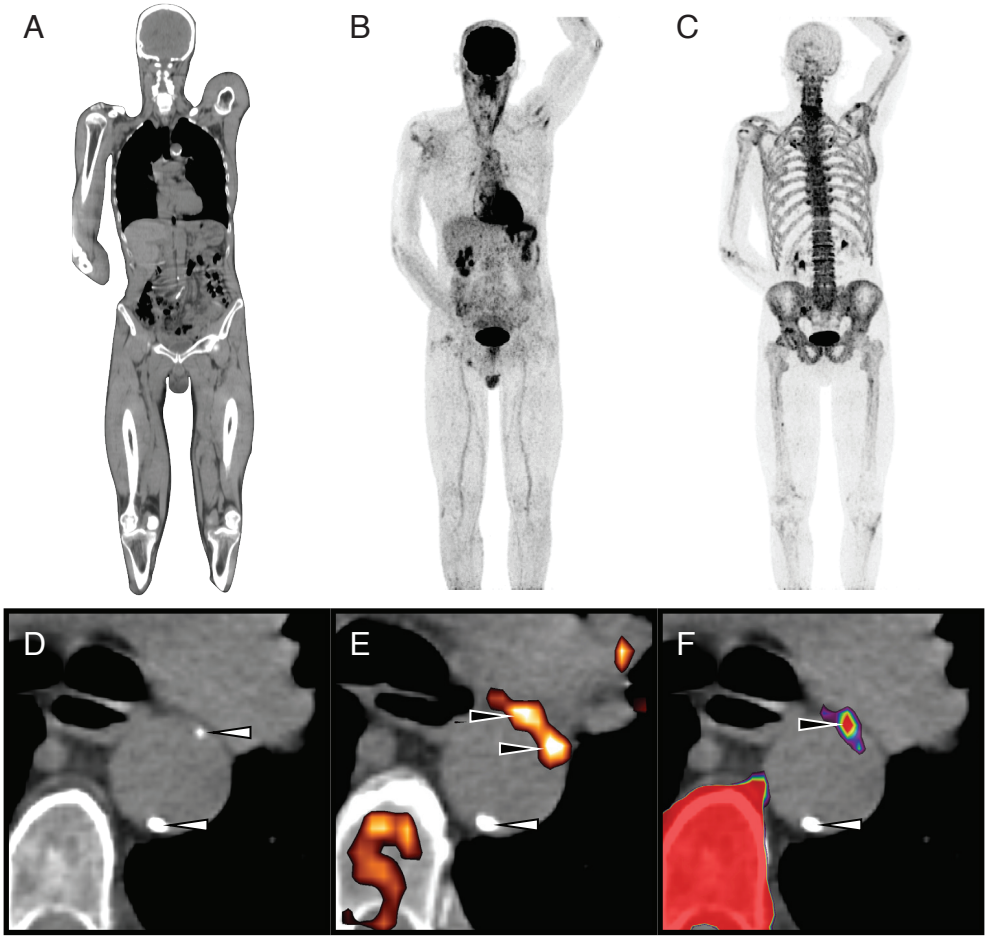

FIGURE 1 – Atherosclerosis assessment with computed tomography (CT) (**A**, **D**), [^{18}F]-fluorodeoxyglucose positron emission tomography/computed tomography (^{18}FDG PET/CT) (**B**, **E**), and sodium [^{18}F]-fluoride positron emission tomography/computed tomography (Na^{18}F PET/CT) (**C**, **F**). All images were obtained in a 65-year old male volunteer. Axial CT images reveal the presence of vascular calcifications in the aorta (*white arrowheads* in **D**). Superimposed ^{18}FDG PET images demonstrate that the posterior calcified lesion is associated with arterial inflammation (*black arrowheads* in **E**), whereas the anterior lesion (*white arrowhead* in **E**) is not. Superimposed Na^{18}F PET images demonstrate that the posterior calcified lesion is associated with active calcification (*black arrowhead* in **F**), whereas the anterior lesion (*white arrowhead* in **F**) is not. The imaging characteristics presented in **D**, **E**, and **F** are all associated with an increased risk for adverse cardiovascular events.

CAMONA STUDY

The technical and clinical validity of ^{18}FDG PET/CT and Na^{18}F PET/CT for the purpose of cardiovascular risk assessment was studied in context of the "Cardiovascular Molecular Calcification Assessed by ^{18}F-NaF PET/CT" (CAMONA) study. CAMONA is a single center prospective observational study that recruited healthy volunteers as well as patients with chest pain syndromes. Recruited subjects were evaluated by ^{18}FDG PET/CT, Na^{18}F PET/CT, and various other cardiovascular disease risk evaluation tools, including cardiac CT imaging, the Framingham Risk Score **(9)**, and HeartSCORE **(10)**. The primary aim of CAMONA was to relate the prevalence and degree of arterial ^{18}FDG and Na^{18}F uptake to the cardiovascular risk profile of the study subject. This aim was based on the hypothesis that the degree of arterial ^{18}FDG and Na^{18}F uptake reflects atherosclerosis severity and hence is a function of hazard suffered from a life-long exposure to both known and unknown cardiovascular risk factors. This hypothesis suggests that subjects with increased tracer uptake in their arteries are at increased risk for adverse cardiovascular events. Secondary aims of the CAMONA study included validation, and where possible, improvement of currently applied ^{18}FDG PET/CT and Na^{18}F PET/CT imaging and quantification protocols.

Two-years after the baseline examinations, all CAMONA participants will be evaluated again by ^{18}FDG PET/CT, Na^{18}F PET/CT, and cardiac CT imaging. The follow-up data, however, are not yet available. Therefore, this thesis focused solely on results obtained as part of the baseline CAMONA examinations. In the near future, the follow-up data will become available. The follow-up data will be used to investigate the relationship between risk for adverse cardiovascular events and temporal changes in arterial inflammation and vascular calcification. These relations might give insight into the mechanisms responsible for atherosclerotic cardiovascular disease progression and potentially patient vulnerability for adverse cardiovascular events.

THESIS OUTLINE

This thesis consists of two parts. **Part I**, comprising 5 chapters, focuses on the technical validity of ^{18}FDG PET/CT and Na^{18}F PET/CT imaging for the purpose of cardiovascular risk assessment. **Chapters 2** and **3** describe the results of a prospective study that investigated whether delayed PET/CT imaging improves assessment of arterial inflammation and vascular calcification by ^{18}FDG PET/CT and Na^{18}F PET/CT imaging, respectively. **Chapter 4** discusses the results of a retrospective study that investigated whether partial volume effects influence

quantification of arterial inflammation as assessed by delayed ^{18}FDG PET/CT imaging. **Chapters 5** and **6** report the results of a prospective study that investigated the impact of personal characteristics and technical factors on quantification of ^{18}FDG and Na^{18}F uptake in human arteries, respectively. In addition, **chapters 5** and **6** aimed to optimize methodologies to quantify the degree of ^{18}FDG and Na^{18}F uptake in the arterial system, respectively.

Part II, comprising 3 chapters, focuses on the clinical validity of ^{18}FDG PET/CT and Na^{18}F PET/CT imaging for the purpose of cardiovascular risk assessment. **Chapter 7** describes the results of a prospective study that aimed to establish reference values for ^{18}FDG and Na^{18}F uptake in human arteries. **Chapter 8** presents the results from a prospective study that investigated whether coronary artery Na^{18}F uptake is related to the cardiovascular risk profile of healthy adults. **Chapter 9** discusses the results from a prospective study that investigated the relationship between cardiovascular disease risk and arterial inflammation and vascular calcification of the thoracic aorta.

General discussion of study findings, future perspectives, and closing remarks are stated in **chapter 10**.

REFERENCES

1. Weber C, Noels H. Atherosclerosis: Current Pathogenesis and Therapeutic Options. *Nat Med.* 2011; **17**: 1410-1422.
2. Moore KJ, Tabas I. Macrophages in the Pathogenesis of Atherosclerosis. *Cell.* 2011; **145**: 341-355.
3. Libby P. Mechanisms of Acute Coronary Syndromes and Their Implications for Therapy. *N Engl J Med.* 2013; **368**: 2004-2013.
4. Donnan GA, Fisher M, Macleod M, et al. Stroke. *Lancet.* 2008; **371**: 1612-1623.
5. Mozaffarian D, Benjamin EJ, Go AS, et al. Heart Disease and Stroke Statistics – 2015 Update: A Report from the American Heart Association. *Circulation*. 2015; **131**: e29-322.
6. Franco M, Cooper RS, Bilal U, et al. Challenges and Opportunities for Cardiovascular Disease Prevention. *Am J Med.* 2011; **124**: 95-102.
7. Arbab-Zadeh A, Fuster V. The Myth of the "Vulnerable Plaque": Transitioning from a Focus on Individual Lesions to Atherosclerotic Disease Burden for Coronary Artery Disease Risk Assessment. *J Am Coll Cardiol.* 2015; **65**: 846-855.
8. Greenland P, Knoll MD, Stamler J, et al. Major Risk Factors as Antecedents of Fatal and Nonfatal Coronary Heart Disease Events. *JAMA.* 2003; **290**: 891-897.
9. D'Agostino RB, Vasan RS, Pencina MJ, et al. General Cardiovascular Risk Profile for Use in Primary Care: The Framingham Heart Study. *Circulation.* 2008; **117**: 743-753.
10. Conroy RM, Pyorala K, Fitzgerald AP, et al. Estimation of Ten-Year Risk of Fatal Cardiovascular Disease in Europe: The SCORE Project. *Eur Heart J.* 2003; **24**: 987-1003.
11. Detrano R, Guerci AD, Carr JJ, et al. Coronary Calcium as a Predictor of Coronary Events in Four Racial or Ethnic Groups. *N Engl J Med.* 2008; **358**: 1336-1345.
12. Budoff MJ, Shaw LJ, Liu ST et al. Long-term prognosis associated with coronary calcification: observations from a registry of 25,253 patients. J Am Coll Cardiol 2007;49:1860-70.
13. Hansson GK. Inflammation, Atherosclerosis, and Coronary Artery Disease. *N Engl J Med.* 2005; **352**: 1685-1695.
14. Demer LL, Tintut Y. Vascular Calcification: Pathobiology of a Multifaceted Disease. *Circulation.* 2008; **117**: 2938-2948.
15. Figueroa AL, Abdelbaky A, Truong QA, et al. Measurement of Arterial Activity on Routine FDG PET/CT Images Improves Prediction of Risk of Future CV Events. *J Am Coll Cardiol Img.* 2013; **6**: 1250-1259.
16. Tarkin JM, Joshi FR, Rudd JH. PET Imaging of Inflammation in Atherosclerosis. *Nat Rev Cardiol.* 2014; **11**: 443-457.

17. Joshi NV, Vesey A, Newby DE, et al. Will ^{18}F-Sodium Fluoride PET-CT Imaging be the Magic Bullet for Identifying Vulnerable Coronary Atherosclerotic Plaques? *Curr Cardiol Rep.* 2014; **16**: 521-528.

PART I

Technical Developments

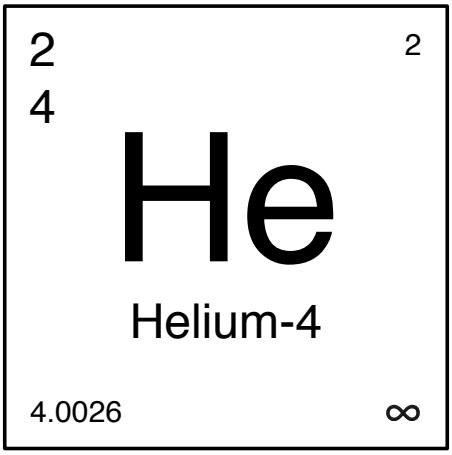
2
4
2
He
Helium-4
4.0026
∞

Chapter 2

Delayed [^{18}F]-Fluorodeoxyglucose PET/CT Imaging Improves Quantitation of Atherosclerotic Plaque Inflammation: Results from the CAMONA Study

Björn A. Blomberg
Anders Thomassen
Richard A.P. Takx
Malene G. Hildebrandt
Jane A. Simonsen
Karen M. Buch-Olsen
Axel C.P. Diederichsen
Hans Mickley
Abass Alavi
Poul F. Høilund-Carlsen

Published in the *Journal of Nuclear Cardiology*, 2014

ABSTRACT

Background: This study aimed to determine if delayed [^{18}F]-fluorodeoxyglucose (^{18}FDG) PET/CT imaging improves quantitation of atherosclerotic plaque inflammation. Blood-pool activity can disturb the arterial ^{18}FDG signal. With time, blood-pool activity declines. Therefore, delayed imaging can potentially improve quantitation of atherosclerotic plaque inflammation.

Methods: 40 subjects were prospectively assessed by dual time-point PET/CT imaging at approximately 90 and 180 minutes after ^{18}FDG administration. For both time-points, global uptake of ^{18}FDG was determined in the carotid arteries and thoracic aorta by calculating the blood-pool corrected maximum standardized uptake value ($cSUV_{MAX}$). A target-to-background ratio (TBR) was calculated to determine the contrast resolution at 90 and 180 minutes. Furthermore, we assessed whether the acquisition time-point affected the relation between $cSUV_{MAX}$ and the estimated 10-year risk for fatal cardiovascular disease (SCORE %).

Results: A significant increase in carotid $cSUV_{MAX}$ (23 %; $P < .001$), carotid TBR (20 %; $P < .001$), aortic $cSUV_{MAX}$ (14 %; $P < .001$), and aortic TBR (20 %; $P < .001$) was observed with time. At 90 minutes, $cSUV_{MAX}$ did not relate to SCORE %, whereas at 180 minutes significant positive relations were observed between SCORE % and carotid ($\tau = 0.25$; $P = .045$) and aortic ($\tau = 0.33$; $P = .008$) $cSUV_{MAX}$.

Conclusions: Delayed ^{18}FDG PET/CT imaging at 180 minutes improves quantitation of atherosclerotic plaque inflammation over imaging at 90 minutes. Therefore, the optimal acquisition time-point to assess atherosclerotic plaque inflammation lies beyond the advocated time-point of 90 minutes after ^{18}FDG administration.

INTRODUCTION

[^{18}F]-fluorodeoxyglucose positron emission tomography/computed tomography (^{18}FDG PET/CT) is a promising non-invasive imaging technique for assessment of atherosclerosis. By targeting atherosclerotic plaque glycolysis, a surrogate marker of plaque inflammation and hypoxia **(1, 2)**, ^{18}FDG PET/CT imaging can potentially detect active atherosclerosis **(2)**, quantitate its degree, evaluate response to treatment **(3, 4)**, and prognosticate risk for atherosclerosis related disease **(5)**.

Although several prospective studies reported promising results **(6-9)**, ^{18}FDG PET/CT imaging of atherosclerosis has limitations. An important limitation is poor contrast resolution **(10)**. As ^{18}FDG is injected intravenously, persistent blood activity can disturb the arterial wall signal, which can compromise quantitation of atherosclerotic plaque ^{18}FDG avidity. With time, blood activity declines (**FIGURE 1**). Therefore, delayed ^{18}FDG PET/CT imaging beyond the advocated 90 minute time-point **(7)** can potentially improve quantitation of atherosclerotic plaque inflammation **(11)**.

To test the hypothesis that delayed ^{18}FDG PET/CT imaging improves quantitation of atherosclerotic plaque inflammation, we prospectively performed dual time-point ^{18}FDG PET/CT imaging at approximately 90 and 180 minutes after ^{18}FDG administration in healthy controls as well as patients with chest pain referred for a coronary CT-angiography.

METHODS

This study is part of the "Cardiovascular Molecular Calcification Assessed by ^{18}F-NaF PET/CT" (CAMONA) protocol. CAMONA was approved by the Danish National Committee on Biomedical Research Ethics, registered at ClinicalTrials.gov (NCT01724749), and conducted in accordance with the Declaration of Helsinki. Written informed consent was obtained from all study subjects.

Subject Selection

We recruited a heterogeneous population of subjects, including healthy controls and patients with chest pain. This allowed us to assess the effect of delayed ^{18}FDG PET/CT imaging on a wide range of subjects with varying degrees of cardiovascular risk to ensure the translation of our findings to various settings. Healthy controls were recruited from the general population by local advertisement and from the local

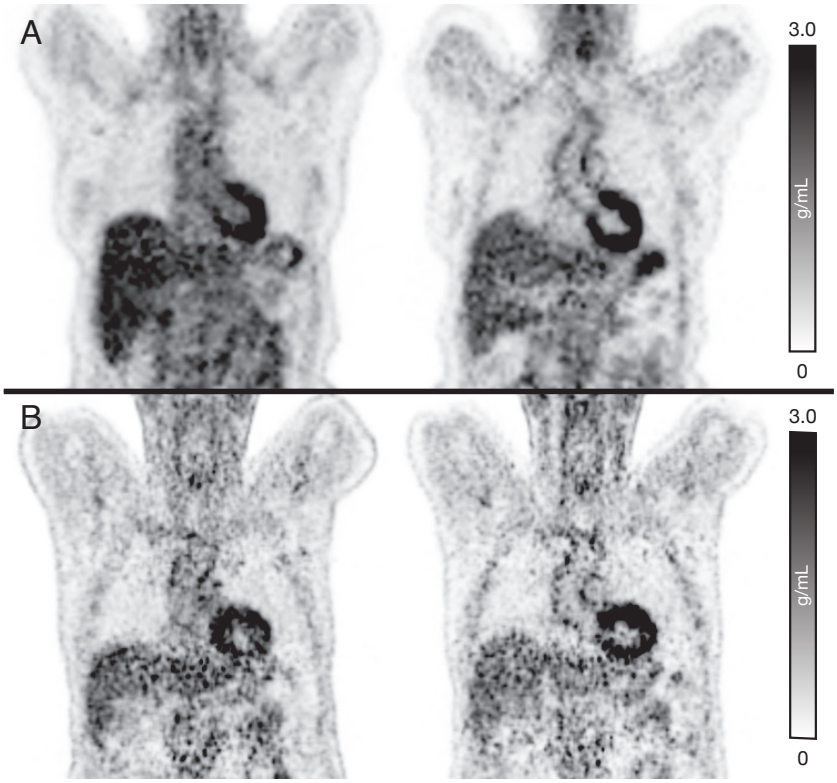

FIGURE 1 – Coronal PET images show ^{18}FDG activity concentrations in the ascending aorta and luminal blood. (**A**) PET images acquired for a different purpose at 60 (*left*) and 187 minutes (*right*) after ^{18}FDG administration in a 62-year-old female. The aortic wall-to-blood contrast (i.e. target-to-background ratio; TBR) improves with time. (**B**) PET images acquired at 94 (*left*) and 179 minutes (*right*) after ^{18}FDG administration in a 69-year-old male with increased cardiovascular risk (calcium score > 1000 Agatston units and SCORE of 3 %). With time, luminal blood activity decreases whereas the aortic wall activity increases, resulting in a superior TBR with time (2.4 *versus* 3.2; 33 % increase).

blood bank. Non-smokers with a negative history of cardiovascular disease, a systolic blood pressure below 160 mmHg, a diastolic blood pressure below 100 mmHg, total serum cholesterol below 6.2 mmol/L, and glycated hemoglobin (HbA1c) below 48 mmol/mol were eligible for inclusion. Patients with chest pain were recruited from those referred for a coronary CT-angiography. Only patients with a 10-year risk for fatal cardiovascular disease equal to or above 1 %, as calculated by the body mass index (kg/m^2) based Systematic COronary Risk Evaluation (SCORE) tool, were eligible for inclusion. We excluded subjects with cancer or a chronic inflammatory disease because these diseases may influence arterial ^{18}FDG avidity. Also, subjects with a history of major cardiovascular events (i.e. acute myocardial

infarction, transient ischemic attack, and ischemic stroke) were excluded. These patients are already at high cardiovascular risk and are less likely to benefit from atherosclerosis imaging with PET. Between November 2012 and March 2013, we enrolled 21 controls and 20 patients. One patient was excluded from the analysis because a cancer was diagnosed with PET. Apart from age, prescribed medication, and SCORE %, subject demographics were not statistically different between patients and controls (**TABLE 1**).

Study Design

Subjects were evaluated by questionnaires, blood pressure measurements, blood analyses, dual time-point ^{18}FDG PET/CT imaging, and non-contrast enhanced cardiac CT imaging. Questionnaires yielded information about prescribed medication, history of cardiovascular disease, and cardiovascular risk factors. Blood pressure measurements were performed thrice after a supine rest of at least 30 minutes. The average of the last two measurements determined the systolic and diastolic blood pressure. Blood analyses determined fasting serum total cholesterol, serum LDL cholesterol, serum HDL cholesterol, fasting plasma glucose, HbA1c, serum creatinine, and the Modification of Diet and Renal Disease (MDRD) estimated glomerular filtration rate (eGFR). For each subject, the SCORE % was recalculated based on age, gender, systolic blood pressure, total serum cholesterol, serum HDL cholesterol, and smoking status **(12)**. ^{18}FDG PET/CT imaging was performed on integrated PET/CT scanners (GE Discovery 690, VCT, RX, and STE) with comparable spatial resolution. Each subject underwent dual time-point PET/CT imaging at 90 and 180 minutes after intravenous injection of approximately 4.0 MBq of ^{18}FDG per kilogram of body weight. The ^{18}FDG was administered after an overnight fast of at least 8 hours. Prior to ^{18}FDG injection, the blood glucose concentration was determined to secure a value below 8 mmol/L. After injection and in between scans, patients rested in a quiet and warm room. The acquisition time per bed position was 2.5 minutes at 90 minutes and 3.5 minutes at 180 minutes. Total body PET images were acquired in 3D-mode and reconstructed into coronal, transverse, and sagittal planes by an iterative reconstruction algorithm (GE VUE Point). Corrections were applied for attenuation, scatter, random coincidences, and scanner dead time. Low-dose CT imaging (140 kV, 30-110 mA, noise index 25, 0.8 seconds per rotation, slice thickness 3.75 mm) was performed for attenuation correction and anatomic orientation. To determine the coronary calcium score, non-contrast enhanced, breath-hold, cardiac CT imaging (120 kV, 100 mA, 0.4 seconds per rotation, slice thickness 2.5 mm) was performed with electrocardiogram gating at 50 % of the R-R interval. The effective radiation dosage received for the entire imaging protocol was approximately 10 mSv.

Quantitative Image Analyses

All images were analyzed by version 4.0 of the Philips IntelliSpace Portal client. The image analyst was blinded to subject demographics and ^{18}FDG circulating time. For each subject, for

TABLE 1 - Subject demographics

	Controls (*n* = 21)	**Patients** (*n* = 19)	***P* value**	**Total** (*N* = 40)
Age, years	42.6 ± 14.7	54.0 ± 13.0	**.019**	48.0 ± 14.9
Male, %	48	47	.999	47
Active smoking, %	0	16	.098	8
Blood pressure, mmHg				
- Systolic	130.3 ± 15.5	133.3 ± 19.4	.592	131.8 ± 17.3
- Diastolic	79.7 ± 8.6	80.3 ± 8.3	.839	80.0 ± 5.2
Heart rate, beats/minute	63.9 ± 14.0	65.2 ± 10.7	.736	64.5 ± 12.4
Body mass index, kg/m^2	26.8 ± 5.0	27.4 ± 4.2	.664	27.1 ± 4.6
Diabetes mellitus, %	0	0	.999	0
Cholesterol, mmol/L				
- Total	5.0 ± 0.8	5.3 ± 1.0	.428	5.2 ± 0.9
- LDL	3.2 ± 0.9	3.4 ± 1.0	.512	3.3 ± 0.9
- HDL	1.4 ± 0.5	1.4 ± 0.4	.646	1.4 ± 0.5
Plasma glucose, mmol/L	5.4 ± 0.4	5.7 ± 0.6	.051	5.5 ± 0.5
HbA1c, mmol/mol	34.6 ± 5.0	36.8 ± 3.0	.100	35.7 ± 4.3
Creatinine, µmol/L	78.0 ± 13.1	78.0 ± 15.6	.999	78.0 ± 14.1
MDRD-eGFR, mL/min/1.73 m^2	89.9 ± 17.2	85.9 ± 17.2	.458	88.0 ± 17.1
Medication, %				
- Lipid lowering drugs	0	21	**.042**	10
- Antihypertensive drugs	0	42	**.001**	20
Coronary calcium score				
- Agatston, arbitrary units	0 [0 – 4]	0 [0 – 114]	.469	0 [0 – 15]
- volume, mm^3	0 [0 – 8]	0 [0 – 55]	.537	0 [0 – 14]
SCORE, %	0 [0 – 1]	1 [0 – 3]	**.029**	1 [0 – 1]

Values are mean ± the standard deviation, %, or median [25 – 75 percentiles]. HbA1c, MDRD-eGFR, and SCORE indicate glycated hemoglobin, glomerular filtration rate estimated by the Modification of Diet and Renal Disease formula, and 10-year risk for fatal cardiovascular disease according to the Systematic COronary Risk Evaluation tool based on age, gender, systolic blood pressure, total serum cholesterol, serum HDL cholesterol, and smoking status, respectively.

each time point, global uptake of ^{18}FDG was determined in the carotid arteries and the thoracic aorta according to previously published methods **(7)**. In summary, an oval region of interest (ROI) was manually placed around the outer perimeter of the right and left common carotid artery and thoracic aorta on every slice of the attenuation corrected transverse PET/CT images. We carefully excluded cardiac and bone marrow derived ^{18}FDG activity by eliminating these areas from the ROI. Per ROI, the maximum ^{18}FDG activity concentration (Bq/mL) was determined and transformed into the radiotracer-decay and body weight (kg) corrected maximum standardized uptake value (SUV_{MAX}). Per arterial bed, SUV_{MAX} values were summed and divided by the number of ROIs resulting in a single averaged SUV_{MAX} value for the carotid arteries and for the thoracic aorta. Subsequently, the averaged SUV_{MAX} value was corrected for blood-pool ^{18}FDG activity by subtraction of the blood activity, resulting in the blood-pool corrected SUV_{MAX} ($cSUV_{MAX}$) (**FIGURE 2**). The blood-pool ^{18}FDG activity was determined by drawing a single spherical volume of interest (approximately 400 mm^3) in the center of the right atrium and was quantified as the radiotracer-decay and body weight (kg) corrected mean SUV (SUV_{MEAN}). The blood-pool SUV_{MAX} was determined to demonstrate that $cSUV_{MAX}$ does not simply quantifies blood-pool noise. To quantitate the contrast resolution, target-to-background ratios (TBR) were calculated by dividing the averaged arterial SUV_{MAX} with the blood-pool SUV_{MEAN}. The coronary calcium score, obtained from the cardiac CT images, was quantified in arbitrary units according to Agatston and as a volumetric score (mm^3) **(13)**. The arbitrary units were multiplied by a cofactor of 2.5/3.0 to correct for the tomographic slice thickness of 2.5 mm. The detection threshold for coronary calcium was set at 130 Hounsfield units.

Rater Agreement

Inter- and intra-rater agreement of $cSUV_{MAX}$ and the TBR was assessed two months after the initial analysis in a randomly selected sample of 10 subjects. Raters were blinded for subject demographics, ^{18}FDG circulating time, and results from the initial analysis.

Statistical Analysis

Demographics, arterial SUV_{MAX}, blood-pool SUV_{MEAN}/SUV_{MAX}, arterial $cSUV_{MAX}$, and the TBR were summarized and compared between patients and controls. Continuous variables were summarized as means ± the standard deviation and compared with the unpaired Student's *t* test. Non-parametric continuous variables were summarized as medians with 25 – 75 percentiles and compared with the Mann-Whitney *U* test. Categorical variables were summarized as percentages and compared with Fisher's exact test. Subsequent analyses were

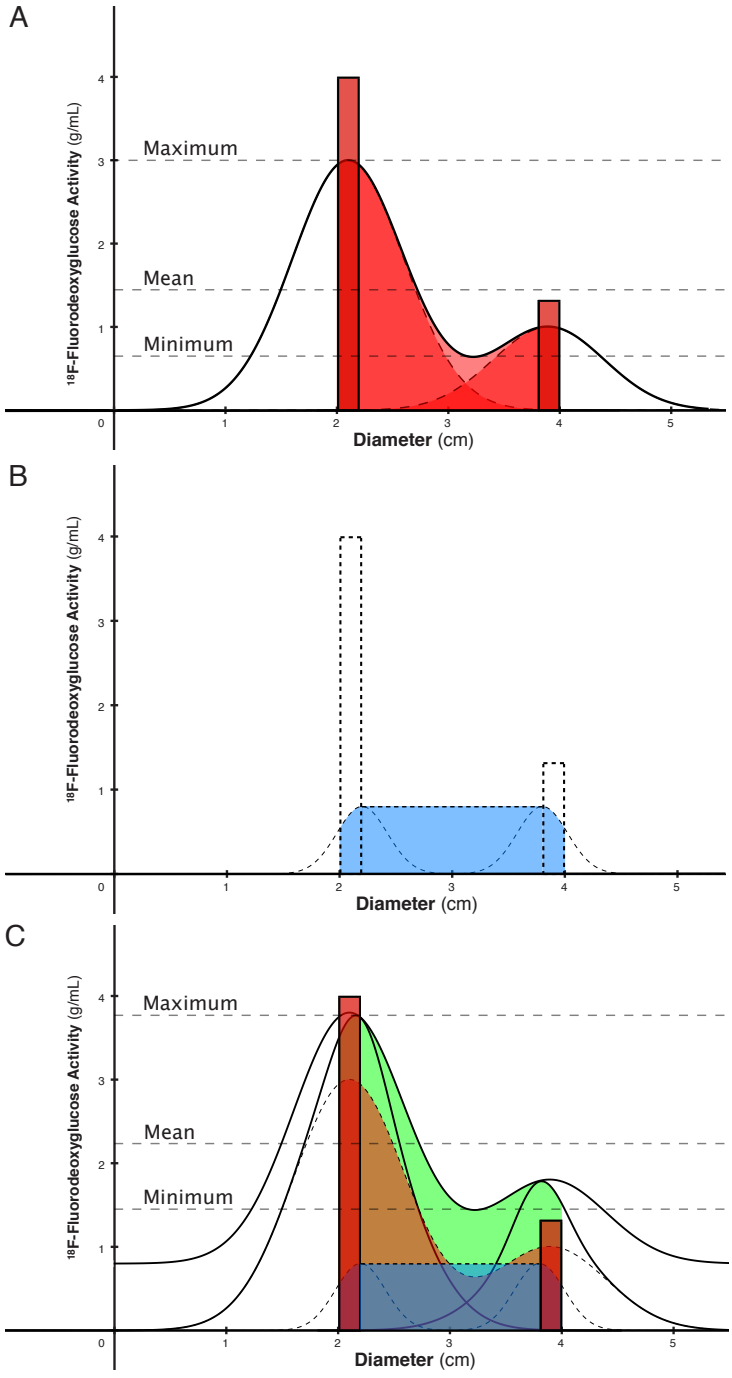
A
Maximum
Mean
Minimum
^{18}F-Fluorodeoxyglucose Activity (g/mL)
Diameter (cm)
B
^{18}F-Fluorodeoxyglucose Activity (g/mL)
Diameter (cm)
C
Maximum
Mean
Minimum
^{18}F-Fluorodeoxyglucose Activity (g/mL)
Diameter (cm)

FIGURE 2 – (**A**) Aortic wall ^{18}FDG activity concentration (standardized uptake value; SUV) modeled assuming no background and no luminal blood activity. To appreciate the focal nature of aortic ^{18}FDG accumulation, activity concentrations were modeled more intense in the left compared to the right aortic wall. Note that the retrieved maximum and mean SUV is lower than the true aortic activity concentration (*red bars*) because of partial volume errors (PVEs). Conversely, PVEs result in overestimated values of the minimum activity. (**B**) Luminal blood activity modeled assuming no background and no aortic wall activity. Note that luminal blood activity spills-out onto the aortic wall because of PVEs. (**C**) Combined aortic wall and luminal blood activity modeled assuming no background activity. The color pallet (*red* = aortic wall activity, *blue* = luminal blood activity, and *green* = combined aortic and luminal blood activity) represents the activity concentration as retrieved by PET/CT in a region of interest encompassing the outer aortic wall. Note that the PET/CT recovered SUV_{MAX} (i.e. SUV_{MAX} in **C**) is the sum of aortic wall SUV_{MAX} (i.e. SUV_{MAX} as in **A**) and luminal blood activity. Therefore, the aortic wall SUV_{MAX} (as in **A**) can be estimated by subtracting luminal blood SUV_{MEAN} from the recovered SUV_{MAX} (as in **C**) resulting in the blood-pool corrected SUV_{MAX} ($cSUV_{MAX}$). Note that $cSUV_{MAX}$ has no dependence on luminal blood SUV_{MEAN}, whereas the ratio between SUV_{MAX} and blood-pool SUV_{MEAN} (i.e. target-to-background ratio; TBR) has. To illustrate, if SUV_{MAX} is 3.8 (derived from **C**) and luminal blood SUV_{MEAN} is 0.8 (derived from **B**), the $cSUV_{MAX}$ is 3.0 (result as in **A**). These values make a TBR of 4.75. If the true aortic wall activity remains unchanged (result as in **A**), but luminal blood SUV_{MEAN} decreases to 0.6, the $cSUV_{MAX}$ remains 3 (3.6 – 0.6). However, the TBR increases by 26 % to 6 (3.6 / 0.6). To calculate the true aortic activity concentration (*red bars*), corrections for both luminal blood SUV_{MEAN} and PVE need to be applied.

performed on the pooled data of patients and controls. The variation in SUV_{MAX}, blood-pool SUV_{MEAN}, $cSUV_{MAX}$, and the TBR as a function of time was evaluated by the paired Student's *t* test. Subsequently, a mixed-design analysis of variance evaluated whether $cSUV_{MAX}$ as a function of time was interacted by the difference in subject recruitment (i.e. patients *versus* controls). To assess the impact of ^{18}FDG circulating time on atherosclerosis quantitation, we first evaluated the strength of the relationship between SCORE % and $cSUV_{MAX}$ and SCORE % and the TBR at both 90 and 180 minutes by the Kendall rank correlation coefficient (τ). Second, we evaluated the linear relationship between carotid and aortic $cSUV_{MAX}$ by the Pearson correlation coefficient (*r*). Finally, multivariate linear regression analysis was performed by backwards elimination of variables. The variables included were those of SCORE %. To correct for the effect of medication, we added lipid lowering and antihypertensive drugs as additional variables. Variables with a *P* value less than .10 were retained in the model. Rater agreement of $cSUV_{MAX}$ and the TBR was assessed by intraclass correlation coefficients (ICC) (two-way random effects model assessing absolute agreement of single measures) **(14)** as well as the 95 % limits of agreement according to Bland and Altman **(15)**. A two-tailed *P* value below .05 was regarded statistically significant. Except for the multivariate linear regression analysis, presented *P* values and 95 % confidence intervals were determined by a bootstrap of 2,000 samples. Statistical analyses were performed by IBM SPSS Statistics version 21.

RESULTS

PET/CT imaging commenced at 90 ± 8 and 181 ± 3 minutes after ^{18}FDG administration. The blood-pool SUV_{MEAN} (P < .001) significantly declined with time, whereas carotid $cSUV_{MAX}$ (P < .001), carotid TBR (P < .001), aortic $cSUV_{MAX}$ (P < .001), and aortic TBR (P < .001) significantly increased with time (**FIGURE 3**). Carotid SUV_{MAX} (P = .486) and aortic SUV_{MAX} (P = .565) were invariant to the ^{18}FDG circulating time. The increase in carotid and aortic $cSUV_{MAX}$ with time was not interacted by the difference in subject recruitment (P > .209). No significant difference in mean carotid and aortic $cSUV_{MAX}$ was observed between patients and controls (**TABLE 2**).

At 180 minutes, a significant positive relationship was observed between SCORE % and carotid and aortic $cSUV_{MAX}$ (**TABLE 3**). This finding was not observed at 90 minutes. No relation was observed between SCORE % and the carotid or aortic TBR, neither at 90 minutes nor at 180 minutes. At 90 and 180 minutes, carotid and aortic $cSUV_{MAX}$ were significantly related to each other (**TABLE 4**).

At 90 minutes, multivariable linear regression analysis with backwards elimination established a significant relationship between carotid $cSUV_{MAX}$ and age

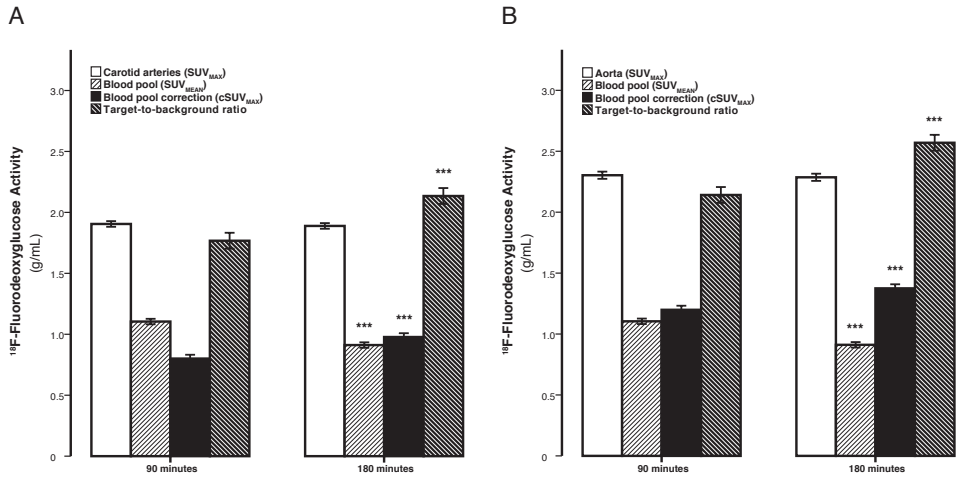

Figure 3 – The average maximum carotid (**A**) and aortic (**B**) ^{18}FDG activity was invariant to time, whereas blood-pool activity significantly decreased and blood-pool corrected values and the target-to-background ratio significantly increased with time. *Error bars* represent the 95 % confidence interval of the mean. *** P < .001 decline or increase compared to previous time point established by the paired Student's t test.

TABLE 2 – ^{18}F-fluorodeoxyglucose activity in the aorta, carotid arteries, and blood-pool

	Controls	Patients	*P* value	Total
Carotid SUV_{MAX}				
- 90 minutes	1.90 ± 0.71	1.91 ± 0.54	.976	1.91 ± 0.62
- 180 minutes	1.84 ± 0.60	1.94 ± 0.55	.595	1.89 ± 0.57
Aortic SUV_{MAX}				
- 90 minutes	2.24 ± 0.39	2.37 ± 0.64	.431	2.30 ± 0.52
- 180 minutes	2.18 ± 0.47	2.40 ± 0.79	.303	2.28 ± 0.64
Blood-pool SUV_{MEAN}				
- 90 minutes	1.09 ± 0.28	1.12 ± 0.31	.686	1.10 ± 0.29
- 180 minutes	0.88 ± 0.20	0.94 ± 0.27	.455	0.91 ± 0.24
Blood-pool SUV_{MAX}				
- 90 minutes	1.47 ± 0.43	1.52 ± 0.56	.731	1.49 ± 0.49
- 180 minutes	1.10 ± 0.37	1.18 ± 0.46	.571	1.14 ± 0.41
Carotid $cSUV_{MAX}$				
- 90 minutes	0.82 ± 0.62	0.78 ± 0.35	.863	0.80 ± 0.50
- 180 minutes	0.95 ± 0.54	1.00 ± 0.39	.763	0.98 ± 0.47
Aortic $cSUV_{MAX}$				
- 90 minutes	1.15 ± 0.33	1.25 ± 0.41	.398	1.20 ± 0.35
- 180 minutes	1.30 ± 0.38	1.46 ± 0.59	.329	1.37 ± 0.49
Carotid TBR				
- 90 minutes	1.80 ± 0.61	1.73 ± 0.33	.674	1.77 ± 0.49
- 180 minutes	2.12 ± 0.62	2.15 ± 0.58	.901	2.13 ± 0.59
Aortic TBR				
- 90 minutes	2.13 ± 0.42	2.15 ± 0.36	.879	2.14 ± 0.39
- 180 minutes	2.52 ± 0.50	2.62 ± 0.62	.573	2.57 ± 0.55

Values are mean ± the standard deviation for 21 controls and 19 patients. SUV_{MAX}, SUV_{MEAN}, $cSUV_{MAX}$, and TBR indicate radiotracer-decay and body weight corrected maximum standardized uptake value, radiotracer-decay and body weight corrected mean standardized uptake value, blood-pool corrected SUV_{MAX}, and target-to-background ratio, respectively.

(β = 0.32)(adjusted R^2 = 0.08; P = .044). At 180 minutes, age (β = 0.57), total cholesterol (β = -0.31), and lipid lowering medication (β = -0.42) were independently related to carotid $cSUV_{MAX}$ (adjusted R^2 = 0.26; P = .003). Similar relations were observed with carotid TBR as the dependent variable, although the model as well as the relations with cardiovascular risk factors was less strong (**TABLE 5**).

TABLE 3 - Relationship between arterial ^{18}F-fluorodeoxyglucose activity and SCORE %

	Kendall's τ	95 % confidence interval	*P* value
Carotid $cSUV_{MAX}$			
- 90 minutes	0.23	-0.03 to 0.45	.068
- 180 minutes	0.25	0.01 to 0.47	**.045**
Aortic $cSUV_{MAX}$			
- 90 minutes	0.24	-0.01 to 0.46	.051
- 180 minutes	0.33	0.12 to 0.51	**.008**
Carotid TBR			
- 90 minutes	0.13	-0.11 to 0.39	.287
- 180 minutes	0.11	-0.12 to 0.34	.388
Aortic TBR			
- 90 minutes	0.11	-0.14 to 0.38	.361
- 180 minutes	0.17	-0.07 to 0.40	.174

Abbreviations as in **TABLE 2.**

At 90 minutes, multivariable linear regression analysis with backwards elimination established a significant relationship between aortic $cSUV_{MAX}$ and antihypertensive drugs (β = 0.47)(adjusted R^2 = 0.20; P = .002). At 180 minutes, age (β = 0.33), antihypertensive drugs (β = 0.48), and lipid lowering medication (β = -0.32) were independently related to aortic $cSUV_{MAX}$ (adjusted R^2 = 0.31; P = .001). Similar relations were observed with aortic TBR as the dependent variable, although the model as well as the relations with cardiovascular risk factors was less strong (**TABLE 6**).

Strong inter- and intra-rater agreement was observed for both $cSUV_{MAX}$ and the TBR as indicated by ICCs in the range of 0.98 and 1.00 (**SUPPLEMENTARY TABLES 1**, **2**). Furthermore, the 95 % limits of agreement were considered small (**SUPPLEMENTARY FIGURES 1**, **2**). This finding was observed at both 90 and 180 minutes.

TABLE 4 - Relationship between carotid and aortic $cSUV_{MAX}$

Time-point	Pearson's *r*	95 % confidence interval	*P* value
90 minutes	0.48	0.20 to 0.86	**.002**
180 minutes	0.60	0.37 to 0.82	**< .001**

Abbreviations as in **TABLE 2**.

DISCUSSION

Our study demonstrates that quantitation of atherosclerotic plaque inflammation improves by delayed time-point ^{18}FDG PET/CT imaging. Therefore, the optimal acquisition time-point to assess atherosclerotic plaque inflammation lies beyond the advocated time-point of 90 minutes after ^{18}FDG administration. Delayed imaging at 180 minutes results in superior contrast between blood-pool and arterial ^{18}FDG activity compared to imaging at earlier time points. Declining blood-pool ^{18}FDG activity and prolonged accumulation of ^{18}FDG in atherosclerotic plaque with time likely account for the superior contrast observed at 180 minutes over imaging at 90 minutes. The favorable ^{18}FDG kinetics at 180 minutes improves the relationship between arterial ^{18}FDG avidity ($cSUV_{MAX}$) and cardiovascular risk (SCORE %). Furthermore, improved relations were observed between carotid $cSUV_{MAX}$ and aortic $cSUV_{MAX}$ and $cSUV_{MAX}$ and cardiovascular risk factors at 180 minutes over imaging at 90 minutes.

TABLE 5 – Dependence of carotid ^{18}F-fluorodeoxyglucose activity on cardiovascular risk factors

	B	SE of *B*	β	Adjusted R^2	*P* value
Carotid $cSUV_{MAX}$ – 90 minutes				0.08	**.044**
- Constant	0.29	0.26			.279
- Age	0.01	0.01	0.32		**.044**
Carotid $cSUV_{MAX}$ – 180 minutes				0.26	**.003**
- Constant	1.00	0.42			**.022**
- Age	0.02	0.01	0.57		**.001**
- Cholesterol, Total	-0.16	0.07	-0.31		**.037**
- Lipid lowering drugs	-0.62	0.24	-0.40		**.015**
Carotid TBR – 90 minutes				0.09	**.036**
- Constant	2.26	0.24			**< .001**
- Cholesterol, HDL	-0.35	0.16	-0.33		**.036**
Carotid TBR – 180 minutes				0.18	**.019**
- Constant	2.12	0.40			**< .001**
- Age	0.01	0.01	0.34		**.037**
- Cholesterol, HDL	-0.41	0.19	-0.32		**.032**
- Lipid lowering drugs	-0.66	0.31	-0.34		**.040**

Abbreviations as in **TABLE 2**. *B*, SE, and β indicate regression coefficient, standard error, and the standardized regression coefficient, respectively.

Previous reports contradicted in recommending delayed ^{18}FDG PET/CT imaging for assessment of atherosclerotic plaque inflammation. A prospective study in patients with carotid atherosclerosis demonstrated that the optimal interval between ^{18}FDG administration and PET/CT acquisition is approximately 180 minutes **(2)**. More recent work by the same investigators advocated an interval of at least 90 minutes between ^{18}FDG administration and PET/CT acquisition **(7)**. In another study, ^{18}FDG circulating-time neither correlated to the carotid TBR (r = 0.20; P = .08) nor to the carotid ^{18}FDG activity concentration (kBq/mL) (r = -0.07; P = .57) **(9)**. A subsequently published prospective multiple time-point ^{18}FDG PET/CT imaging study could not demonstrate a significant advantage of imaging aortic abdominal aneurysms at 180 minutes over imaging at 60 minutes **(10)**. The methodology of the latter study, however, raised concerns. The main concerns related to the quantitative imaging analysis (e.g. deriving background activity from the aortic lumen instead of a venous structure and utilizing the most intense voxel instead of global quantification as an outcome variable) and whether patients with abdominal aortic aneurysms form a representative domain to

TABLE 6 – Dependence of aortic ^{18}F-fluorodeoxyglucose activity on cardiovascular risk factors

	B	SE of *B*	β	Adjusted R^2	*P* value
Aortic $cSUV_{MAX}$ – 90 minutes				0.20	**.002**
- Constant	1.20	0.06			**< .001**
- Antihypertensive drugs	0.40	0.12	0.47		**.002**
Aortic $cSUV_{MAX}$ – 180 minutes				0.31	**.001**
- Constant	0.79	0.24			**.001**
- Age	0.01	0.01	0.33		**.043**
- Antihypertensive drugs	0.58	0.19	0.48		**.005**
- Lipid lowering drugs	-0.51	0.25	-0.32		**.046**
Aortic TBR – 90 minutes				0.12	**.016**
- Constant	2.00	0.08			**< .001**
- Male	0.29	0.12	0.38		**.016**
Aortic TBR – 180 minutes				0.16	**.028**
- Constant	2.37	0.12			**< .001**
- Male	0.32	0.16	0.29		.055
- Antihypertensive drugs	0.52	0.23	0.38		**.029**
- Lipid lowering drugs	-0.58	0.30	-0.32		.065

Abbreviations as in **TABLE 2**. *B*, SE, and β indicate regression coefficient, standard error, and the standardized regression coefficient, respectively.

investigate the optimal acquisition time-point for atherosclerosis imaging with ^{18}FDG PET/CT **(16)**. To overcome these limitations, a triple time-point ^{18}FDG PET/CT imaging study in patients with lung cancer was conducted and could demonstrate significantly higher carotid and aortic TBRs at 180 minutes over imaging at 60 and 120 minutes **(11)**. Although this study demonstrated significantly better contrast resolution between the arterial wall and blood-pool activity at 180 minutes, the study was insufficiently powered to determine whether delayed imaging improves correlations with cardiovascular risk or cardiovascular risk factors. Our study was specifically designed to overcome this particular limitation and could demonstrate that quantitation of atherosclerotic plaque inflammation improves by delayed imaging at 180 minutes over imaging at 90 minutes. Another important advantage of our study is the within-person comparison. Each subject was imaged at both 90 and 180 minutes after injection of ^{18}FDG. This paired study design eliminated potential confounding effects due to uncontrollable variation in subject demographics, imaging parameters, and subject preparation.

Besides the finding that delayed imaging improves quantitation of atherosclerotic plaque inflammation, our study demonstrated a significant relationship between the degree of carotid and aortic ^{18}FDG avidity and cardiovascular risk (SCORE %). This observation suggests that ^{18}FDG PET/CT imaging of atherosclerosis may be utilized to prognosticate cardiovascular risk. Furthermore, our results support the notion that statins attenuate both carotid and aortic ^{18}FDG activity **(3, 4)**. Contrary to statins, patients taking antihypertensive drugs appear to have increased levels of aortic atherosclerotic plaque inflammation. Whether this relates to an echo effect of hypertension or is genuinely related to antihypertensive drugs remains to be elucidated. Also, our study demonstrated that quantitation of arterial ^{18}FDG activity could be achieved with very high inter- and intra-rater agreement. This finding is consistent with previously published agreement studies **(7, 17)**. Remarkably, our study could not demonstrate a significant difference in carotid and aortic ^{18}FDG avidity between patients and controls. A limited sample size, large inter-subject variation in carotid and aortic ^{18}FDG avidity, and small differences in patient and control demographics may account for this observation.

Our study further suggests that quantitation of atherosclerotic plaque inflammation by the TBR is suboptimal compared to $cSUV_{MAX}$. Notably, we showed that carotid and aortic $cSUV_{MAX}$ at 180 minutes were positively related to SCORE %, whereas the TBR was not. Also, relations between arterial ^{18}FDG avidity and cardiovascular risk factors were stronger when arterial ^{18}FDG avidity was quantified as $cSUV_{MAX}$. Although it is very common to quantitate arterial ^{18}FDG activity as a TBR **(3-10)**, the TBR method is associated with limitations. Most

importantly, the TBR is dependent on blood-pool ^{18}FDG activity (**FIGURE 2**). We demonstrated that blood-pool ^{18}FDG activity is dependent on the circulating time of ^{18}FDG. Independent of $cSUV_{MAX}$, blood-pool SUV_{MEAN} decreases with time and, as a result, the TBR increases with time. This makes the circulation time of the radiopharmaceutical a major determinant of the TBR, a circumstance that may explain why the TBR was not related to cardiovascular risk and less strongly related to cardiovascular risk factors as compared to quantitation of vascular ^{18}FDG avidity by $cSUV_{MAX}$.

Limitations

First, our study did not assess atherosclerotic plaque inflammation via histopathology. Therefore, correlations between arterial ^{18}FDG avidity, the acquisition time-point, and histological confirmation of plaque inflammation cannot be substantiated by our data. Nonetheless, our study could demonstrate an increase in image contrast resolution with time, an increase in aortic and carotid ^{18}FDG avidity with time, and improved correlations between arterial ^{18}FDG avidity and cardiovascular risk and cardiovascular risk factors with time. Although direct comparison with histological correlates of plaque inflammation lacks, our findings support the statement that delayed ^{18}FDG PET/CT imaging at 180 minutes improves the quantitation of atherosclerotic plaque inflammation over imaging at 90 minutes.

Second, our semi-quantitative image analysis did not correct for partial volume errors (PVEs), which could have significantly influenced study results **(18)**. As the size of the average non-calcified atherosclerotic plaque is far smaller than the spatial resolution of PET (9 mm^3 *versus* 125 mm^3 **(19, 20)**), PVEs should be considered in atherosclerosis imaging with PET **(21)**. Moreover, patient movement and pulsatile blood flow further degrades spatial resolution, thereby intensifying PVEs **(22)**. The consequence of PVEs in atherosclerosis imaging is a signal spill-out from the atherosclerotic plaque and a signal spill-in from the blood-pool (**FIGURE 2**). PVEs necessitate correction for blood-pool activity in order to obtain reliable atherosclerotic plaque ^{18}FDG activity concentrations. Furthermore, as non-partial volume corrected data underestimates the true atherosclerotic plaque signal, partial volume correction may be able to generate higher and more reliable values. Thus, partial-volume correction may further improve quantitation of atherosclerotic plaque inflammation with ^{18}FDG PET/CT imaging. This task was not attempted in our study.

Third, the imaging time-points of 90 and 180 minutes were chosen based on expert opinion and recommendations by previous publications. Theoretically, the optimal ^{18}FDG

PET/CT acquisition time-point could have occurred between 90 and 180 minutes, or after 180 minutes. Still, our study had one important finding: delayed imaging beyond 90 minutes improves quantitation of atherosclerotic plaque inflammation demonstrating that ^{18}FDG PET/CT of atherosclerosis at 90 minutes is suboptimal compared to imaging at 180 minutes.

Conclusions

In conclusion, we have shown that delayed ^{18}FDG PET/CT imaging at 180 minutes improves quantitation of atherosclerotic plaque inflammation over imaging at 90 minutes. Therefore, the optimal acquisition time-point to assess atherosclerotic plaque inflammation lies beyond the advocated time-point of 90 minutes after ^{18}FDG administration.

REFERENCES

1. Folco EJ, Sheikine Y, Rocha VZ, et al. Hypoxia but not Inflammation Augments Glucose Uptake in Human Macrophages: Implications for Imaging Atherosclerosis with [^{18}F]-Fluorine-Labeled 2-Deoxy-D-Glucose Positron Emission Tomography. *J Am Coll Cardiol.* 2011; **58**: 603-14.

2. Rudd JH, Warburton EA, Fryer TD, et al. Imaging Atherosclerotic Plaque Inflammation with [^{18}F]-Fluorodeoxyglucose Positron Emission Tomography. *Circulation.* 2002; **105**: 2708-11.

3. Tawakol A, Fayad ZA, Mogg R, et al. Intensification of Statin Therapy Results in a Rapid Reduction in Atherosclerotic Inflammation: Results of a Multi-Center FDG-PET/CT Feasibility Study. *J Am Coll Cardiol*. 2013; **62**: 909-17.

4. Tahara N, Kai H, Ishibashi M, et al. Simvastatin Attenuates Plaque Inflammation: Evaluation by Fluorodeoxyglucose Positron Emission Tomography. *J Am Coll Cardiol.* 2006; **48**: 1825-31.

5. Rominger A, Saam T, Wolpers S, et al. ^{18}F-FDG PET/CT Identifies Patients at Risk for Future Vascular Events in an Otherwise Asymptomatic Cohort with Neoplastic Disease. *J Nucl Med.* 2009; **50**: 1611-20.

6. Bucerius J, Mani V, Moncrieff C, et al. Impact of Noninsulin-Dependent Type 2 Diabetes on Carotid Wall ^{18}F-Fluorodeoxyglucose Positron Emission Tomography Uptake. *J Am Coll Cardiol.* 2012; **59**: 2080-8.

7. Rudd JH, Myers KS, Bansilal S, et al. Atherosclerosis Inflammation Imaging with ^{18}F-FDG PET: Carotid, Iliac, and Femoral Uptake Reproducibility, Quantification Methods, and Recommendations. *J Nucl Med.* 2008; **49**: 871-8.

8. Kim TN, Kim S, Yang SJ, et al. Vascular Inflammation in Patients with Impaired Glucose Tolerance and Type 2 Diabetes: Analysis with ^{18}F-Fluorodeoxyglucose Positron Emission Tomography. *Circ Cardiovasc Imaging.* 2010; **3**: 142-8.

9. Bucerius J, Duivenvoorden R, Mani V, et al. Prevalence and Risk Factors of Carotid Vessel Wall Inflammation in Coronay Artery Disease Patients: FDG-PET and CT Imaging Study. *J Am Coll Cardiol Img.* 2011; **4**: 1195-205.

10. Menezes LJ, Kotze CW, Hutton BF, et al. Vascular Inflammation Imaging with ^{18}F-FDG PET/CT: When to Image? *J Nucl Med.* 2009; **50**: 854-7.

11. Blomberg BA, Akers SR, Saboury B, et al. Delayed Time-Point ^{18}F-FDG PET/CT Imaging Enhances Assessment of Atherosclerotic Plaque Inflammation. *Nucl Med Commun.* 2013; **34**: 860-7.

12. Conroy RM, Pyorala K, Fitzgerald AP, et al. Estimation of Ten-Year Risk of Fatal

Cardiovascular Disease in Europe: The SCORE Project. *Eur Heart J.* 2003; **24**: 987-1003.

13. Becker CR, Knez A, Ohnesorge B, et al. Visualization and Quantification of Coronary Calcifications with Electron Beam and Spiral Computed Tomography. *Eur Radiol.* 2000; **10**: 629-35.

14. Kottner J, Audige L, Brorson S, et al. Guidelines for Reporting Reliability and Agreement Studies (GRRAS) Were Proposed. *J Clin Epidemiol.* 2011; **64**: 96-106.

15. Bland JM, Altman DG. Statistical Methods for Assessing Agreement Between Two Methods of Clinical Measurement. *Lancet.* 1986; **1**: 307-10.

16. Rudd JH, Elkhawad M, Fayad ZA. Vascular Imaging with ^{18}F-FDG PET/CT: Optimal ^{18}F-FDG Circulation Time? *J Nucl Med.* 2009; **50**: 1560.

17. Rudd JH, Myers KS, Bansilal S, et al. ^{18}Fluorodeoxyglucose Positron Emission Tomography Imaging of Atherosclerotic Plaque Inflammation is Highly Reproducible: Implications for Atherosclerosis Therapy Trials. *J Am Coll Cardiol.* 2007; **50**: 892-6.

18. Hickeson M, Yun M, Matthies A, et al. Use of a Corrected Standardized Uptake Value Based on the Lesion Size on CT Permits Accurate Characterization of Lung Nodules on FDG-PET. *Eur J Nucl Med Mol Imaging.* 2002; **29**: 1639-47.

19. Fox JJ, Strauss HW. One Step Closer to Imaging Vulnerable Plaque in the Coronary Arteries. *J Nucl Med.* 2009; **50**: 497-500.

20. Otsuka M, Bruining N, Van Pelt NC, et al. Quantification of Coronary Plaque by 64-Slice Computed Tomography: A Comparison With Quantitative Intracoronary Ultrasound. *Invest Radiol.* 2008; **43**: 314-21.

21. Sanchez-Crespo A, Andreo P, Larsson SA. Positron Flight in Human Tissues and Its Influence on PET Image Spatial Resolution. *Eur J Nucl Med Mol Imaging.* 2004; **31**: 44-51.

22. Basu S, Zaidi H, Houseni M, et al. Novel Quantitative Techniques for Assessing Regional and Global Function and Structure Based on Modern Imaging Modalities: Implications for Normal Variation, Aging and Diseased States. *Semin Nucl Med*. 2007; **37**: 223-39.

SUPPLEMENTARY FIGURES

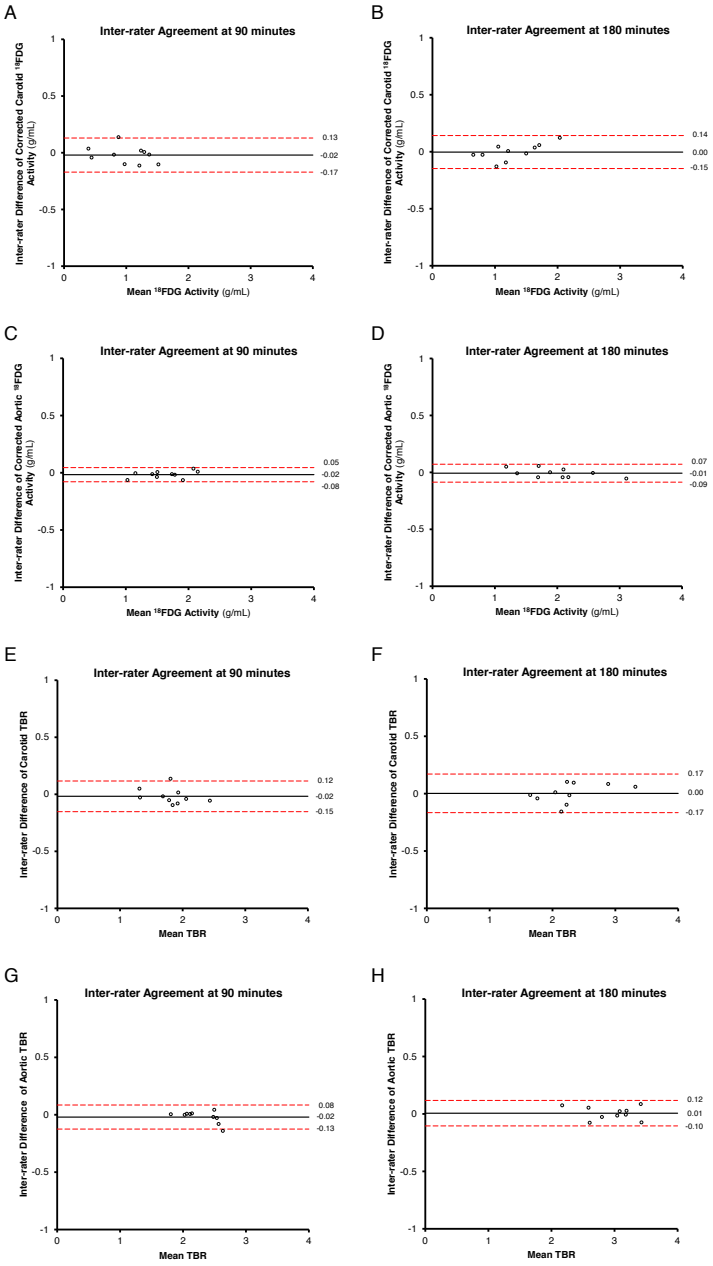

SUPPLEMENTARY FIGURE 1 – Inter-rater agreement of carotid $cSUV_{MAX}$ (**A**, **B**), aortic $cSUV_{MAX}$ (**C**, **D**), carotid TBR (**E**, **F**), and aortic TBR (**G**, **H**) at 90 (**A**, **C**, **E**, **G**) and 180 minutes (**B**, **D**, **F**, **H**).

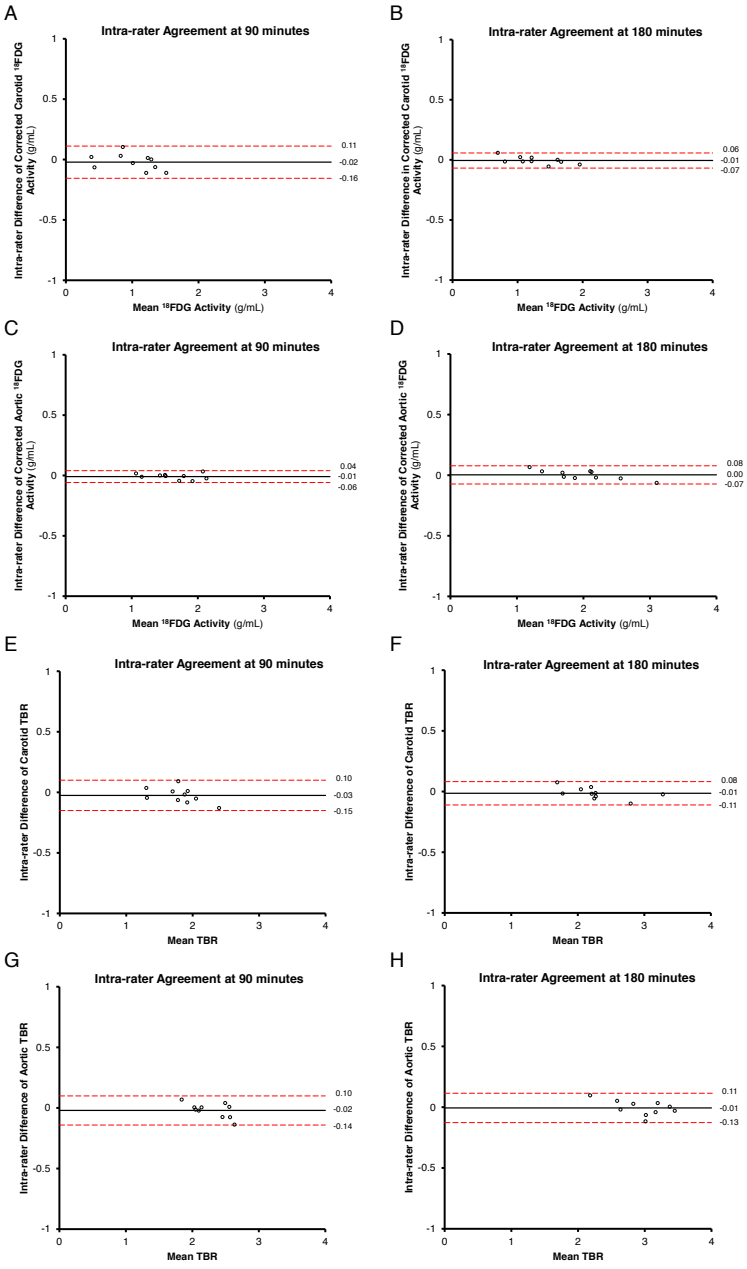

SUPPLEMENTARY FIGURE 2 – Intra-rater agreement of carotid $cSUV_{MAX}$ (**A**, **B**), aortic $cSUV_{MAX}$ (**C**, **D**), carotid TBR (**E**, **F**), and aortic TBR (**G**, **H**) at 90 (**A**, **C**, **E**, **G**) and 180 minutes (**B**, **D**, **F**, **H**).

SUPPLEMENTARY TABLES

SUPPLEMENTARY TABLE 1 – Inter-rater agreement

	ICC	95 % CI	Mean difference (g/mL)	95 % Limits of agreement
Carotid $cSUV_{MAX}$				
- 90 minutes	0.98 ***	0.93 to 1.00	-0.02	-0.17 to 0.13
- 180 minutes	0.99 ***	0.95 to 1.00	0.00	-0.15 to 0.14
Aortic $cSUV_{MAX}$				
- 90 minutes	1.00 ***	0.98 to 1.00	-0.02	-0.08 to 0.05
- 180 minutes	1.00 ***	0.99 to 1.00	-0.01	-0.09 to 0.07
Carotid TBR				
- 90 minutes	0.98 ***	0.92 to 1.00	-0.02	-0.15 to 0.12
- 180 minutes	0.99 ***	0.95 to 1.00	0.00	-0.17 to 0.17
Aortic TBR				
- 90 minutes	0.98 ***	0.93 to 1.00	-0.02	-0.13 to 0.08
- 180 minutes	0.99 ***	0.97 to 1.00	0.01	-0.10 to 0.12

ICC, CI, SUV_{MAX}, $cSUV_{MAX}$, and TBR indicate intraclass correlation coefficient (two-way random effects model assessing absolute agreement of single measures), confidence interval, radiotracer-decay and body weight corrected maximum standardized uptake value, blood-pool corrected SUV_{MAX}, and target-to-background ratio, respectively. *** $P < .001$.

SUPPLEMENTARY TABLE 2 – Intra-rater agreement

	ICC	95 % CI	Mean difference (g/mL)	95 % Limits of agreement
Carotid $cSUV_{MAX}$				
- 90 minutes	0.98 ***	0.94 to 1.00	-0.02	-0.16 to 0.11
- 180 minutes	1.00 ***	0.99 to 1.00	-0.01	-0.07 to 0.06
Aortic $cSUV_{MAX}$				
- 90 minutes	1.00 ***	0.99 to 1.00	-0.01	-0.06 to 0.04
- 180 minutes	1.00 ***	0.99 to 1.00	0.00	-0.07 to 0.08
Carotid TBR				
- 90 minutes	0.98 ***	0.92 to 0.99	-0.03	-0.15 to 0.10
- 180 minutes	0.99 ***	0.98 to 1.00	-0.01	-0.11 to 0.08
Aortic TBR				
- 90 minutes	0.98 ***	0.92 to 0.99	-0.02	-0.14 to 0.10
- 180 minutes	0.99 ***	0.96 to 1.00	-0.01	-0.13 to 0.11

Abbreviations as in **SUPPLEMENTARY TABLE 1**. *** $P < .001$.

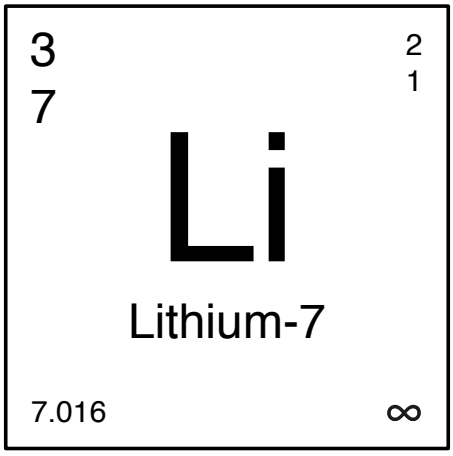
3
7
2
1
Li
Lithium-7
7.016
∞

Chapter 3

Delayed Sodium [^{18}F]-Fluoride PET/CT Imaging Does Not Improve Quantification of Vascular Calcification Metabolism: Results from the CAMONA Study

Björn A. Blomberg
Anders Thomassen
Richard A.P. Takx
Mie H. Vilstrup
Søren Hess
Anne L. Nielsen
Axel C.P. Diederichsen
Hans Mickley
Abass Alavi
Poul F. Høilund-Carlsen

Published in the *Journal of Nuclear Cardiology*, 2014

ABSTRACT

Background: This study aimed to determine if delayed sodium ^{18}F-fluoride ($Na^{18}F$) PET/CT imaging improves quantification of vascular calcification metabolism. Blood-pool activity can disturb the arterial $Na^{18}F$ signal. With time, blood-pool activity declines. Therefore, delayed imaging can potentially improve quantification of vascular calcification metabolism.

Methods: Twenty healthy volunteers and 18 patients with chest pain were prospectively assessed by triple time-point PET/CT imaging at approximately 45, 90, and 180 minutes after $Na^{18}F$ administration. For each time point, global uptake of $Na^{18}F$ was determined in the coronary arteries and thoracic aorta by calculating the blood-pool corrected maximum standardized uptake value ($cSUV_{MAX}$). A target-to-background ratio (TBR) was calculated to determine the contrast resolution at 45, 90, and 180 minutes. Lastly, we assessed whether the acquisition time-point affected the relation between $cSUV_{MAX}$ and the estimated 10-year risk for fatal cardiovascular disease (SCORE %).

Results: Coronary $cSUV_{MAX}$ (P = .533) and aortic $cSUV_{MAX}$ (P = .654) remained similar with time, whereas the coronary TBR (P < .001) and aortic TBR (P < .001) significantly increased with time. Although the contrast resolution improved with time, positive correlations between SCORE % and coronary $cSUV_{MAX}$ (P < .020) and aortic $cSUV_{MAX}$ (P < .005) were observed at all investigated time points.

Conclusions: Delayed $Na^{18}F$ PET/CT imaging does not improve quantification of vascular calcification metabolism. Although contrast resolution improves with time, arterial $Na^{18}F$ avidity is invariant to the time between $Na^{18}F$ administration and PET/CT acquisition. Therefore, the optimal PET/CT acquisition time-point to quantify vascular calcification metabolism is achieved as early as 45 minutes after $Na^{18}F$ administration.

INTRODUCTION

Vascular calcification is an important independent predictor of cardiovascular morbidity, cardiovascular mortality, and all-cause mortality **(1-3)**. Traditionally, vascular calcification is detected and quantified by electron beam or spiral computerized tomography (CT) imaging **(4)**. Nonetheless, CT imaging of vascular calcification is associated with two inherent limitations. First, the nature of CT prevents accurate detection of vascular calcification at the molecular level **(5)**. Second, CT cannot discriminate active from indolent vascular calcification, a possible biomarker for vulnerable and stabilized atherosclerotic plaque, respectively **(6-8)**. These limitations impede stratification of patients into well-defined cardiovascular risk groups by CT imaging of vascular calcification alone, as demonstrated in a cohort of smokers and non-smokers **(9)**.

Imaging vascular calcification by sodium ^{18}F-fluoride positron emission tomography/CT (Na^{18}F PET/CT) can possibly improve cardiovascular risk stratification. Na^{18}F PET/CT targets the active exchange of fluoride with the hydroxyl ions of hydroxylapatite crystals producing fluorapatite **(10)**. This process is believed to represent calcification metabolism of osseous tissue, including vascular calcification. Thereby, Na^{18}F PET/CT can detect vascular calcification at the molecular level as well as discriminate active from indolent vascular calcification **(11, 12)** (**FIGURE 1**). In support of the hypothesis that Na^{18}F PET/CT imaging can improve cardiovascular risk stratification are several retrospective studies that demonstrated positive correlations between arterial Na^{18}F accumulation and various cardiovascular risk factors, including age, gender, hypertension, hypercholesterolemia, and diabetes mellitus **(12-15)**. In addition, a prospective study demonstrated a significant positive relationship between the degree of coronary and aortic Na^{18}F accumulation and cardiovascular risk, as quantified by the coronary calcium score and Framingham Risk Score **(8)**.

Despite these promising results, current Na^{18}F PET/CT imaging protocols, primarily optimized for bone imaging, may limit quantification of vascular calcification metabolism. For example, the Society of Nuclear Medicine (SNM) Practice Guideline states that PET/CT imaging can commence as early as 30 – 45 minutes after administration of Na^{18}F **(16)**. At these time points, the remaining blood Na^{18}F activity might negatively affect quantification of Na^{18}F uptake in the arterial wall. Maximizing contrast between arterial wall and blood-pool Na^{18}F activity, achieved by increasing the Na^{18}F circulating time, has been proposed to improve assessment of vascular calcification metabolism **(13, 17)**. To test this hypothesis, we prospectively performed triple time-point Na^{18}F PET/CT imaging at approximately 45, 90, and

180 minutes after $Na^{18}F$ administration in both healthy controls and patients with chest pain referred for a coronary CT-angiography.

METHODS

This study is part of the CAMONA (Cardiovascular Molecular Calcification Assessed by ^{18}F-NaF PET/CT) protocol. CAMONA was approved by the Danish National Committee on Biomedical Research Ethics and registered at ClinicalTrials.gov (NCT01724749). The study was conducted in accordance with the Declaration of Helsinki and all study subjects provided written informed consent.

Subject Selection

Healthy controls were recruited from the general population by local advertisement and from the local blood bank. Controls with a negative history of cardiovascular disease and modifiable cardiovascular risk factors below upper limits of recommended levels (i.e. blood pressure below 160 mmHg systolic and 100 mmHg diastolic, total serum cholesterol below 6.2 mmol/L, glycated hemoglobin (HbA1c) below 48 mmol/mol, and a non-smoking status) were eligible for inclusion. Patients with chest pain were recruited from those referred for a coronary CT-angiography. Only patients with a 10-year risk for fatal cardiovascular disease equal to or above 1 %, as estimated by the body mass index (kg/m^2) based Systematic COronary Risk Evaluation (SCORE) tool, were eligible for inclusion. We excluded subjects with a history of major cardiovascular events (i.e. acute myocardial infarction, transient ischemic attack, ischemic stroke), cancer, chronic inflammatory disease, or kidney failure. These patients are already at increased cardiovascular risk and are less likely to benefit from vascular calcification imaging with PET. Study subjects were enrolled between November 2012 and March 2013. In total, 20 controls and 20 patients were recruited. One patient was excluded because of technical failure of the PET/CT scanner, and another patient was excluded because a malignant neoplasm was diagnosed on PET. Apart from age, plasma glucose, prescribed medication, and SCORE %, no significant differences in subject demographics were observed between patients and controls (**TABLE 1**).

Study Design

Each subject was evaluated by questionnaires, blood pressure measurements, blood analyses, triple time-point $Na^{18}F$ PET/CT imaging, and non-contrast enhanced cardiac CT imaging. Questionnaires collected information about cardiovascular risk factors, prescribed medication,

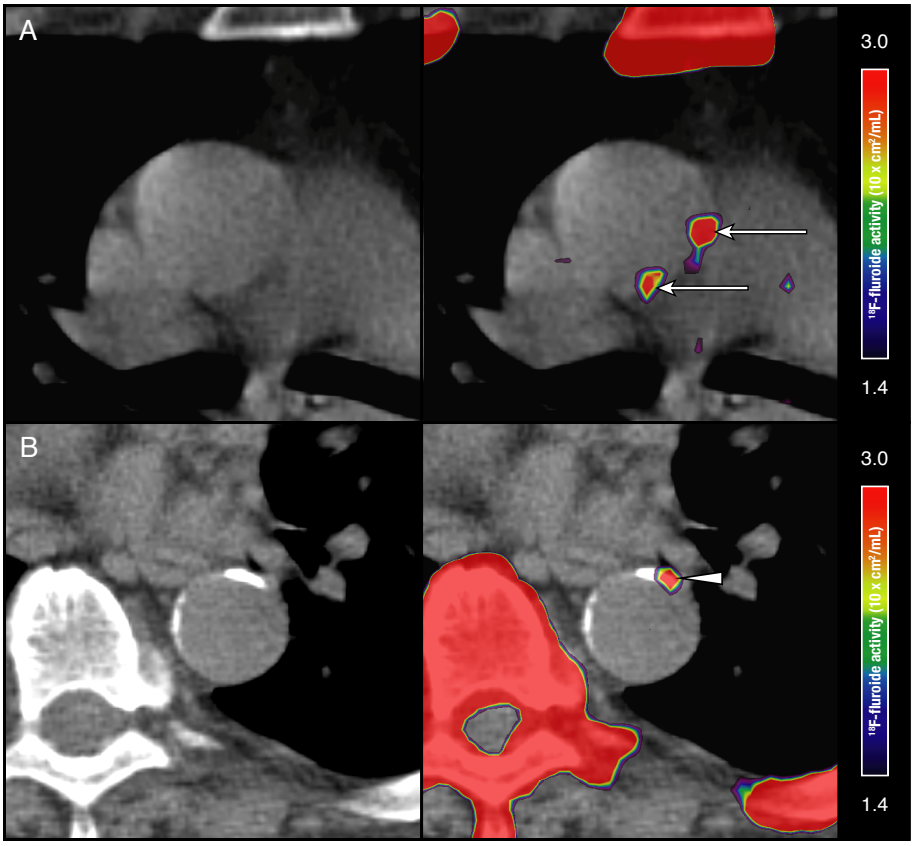

FIGURE 1 – (**A**) Patient without structural vascular calcification. A positive Na[18]F PET signal, representing molecular vascular calcification, was observed in the ascending aorta (*arrows*). (**B**) Patient with active (*arrowhead*) and indolent vascular calcification in the descending aorta. Further note the intense uptake of Na[18]F in the sternum, vertebra, and ribs.

and history of cardiovascular disease. Blood pressure measurements were performed thrice after a supine rest of at least 30 minutes. The systolic and diastolic blood pressure was derived from the average of the last two measurements. Blood analyses determined fasting serum total cholesterol, serum LDL cholesterol, serum HDL cholesterol, fasting plasma glucose, HbA1c, serum creatinine, and the MDRD (Modification of Diet and Renal Disease) estimated glomerular filtration rate (eGFR). For each subject, the SCORE % was recalculated based on age, gender, systolic blood pressure, total serum cholesterol, serum HDL cholesterol, and smoking status **(18)**. Na[18]F PET/CT imaging was performed on integrated PET/CT scanners (GE Discovery 690,

TABLE 1 - Subject demographics

	Controls (*n* = 20)	**Patients** (*n* = 18)	***P* value**	**Total** (*N* = 38)
Age, years	41.8 ± 14.5	54.7 ± 13.0	**.007**	47.9 ± 15.1
Male, %	50	50	.999	50
Active smoking, %	0	17	.097	8
Blood pressure, mmHg				
- Systolic	131.5 ± 15.0	133.8 ± 19.8	.677	132.6 ± 17.3
- Diastolic	80.2 ± 8.6	80.2 ± 8.6	.994	80.2 ± 8.5
Heart rate, beats/minute	63.6 ± 14.3	64.1 ± 9.9	.890	63.8 ± 12.3
Body mass index, kg/m^2	26.6 ± 5.0	27.5 ± 4.3	.523	27.0 ± 4.7
Diabetes mellitus, %	0	0	.999	0
Cholesterol, mmol/L				
- Total	5.1 ± 0.8	5.2 ± 1.0	.744	5.2 ± 0.9
- LDL	3.3 ± 0.9	3.3 ± 1.0	.821	3.3 ± 0.9
- HDL	1.5 ± 0.6	1.4 ± 0.4	.549	1.41 ± 0.5
Plasma glucose, mmol/L	5.4 ± 0.4	5.8 ± 0.6	**.027**	5.5 ± 0.5
HbA1c, mmol/mol	34.5 ± 5.1	36.8 ± 3.1	.099	35.6 ± 4.4
Creatinine, µmol/L	77.4 ± 13.1	79.1 ± 15.3	.712	78.2 ± 14.0
MDRD-eGFR, mL/min/1.73 m^2	91.4 ± 16.1	84.8 ± 17.0	.224	88.3 ± 16.6
Medication, %				
- Lipid lowering drugs	0	22	**.041**	11
- Antihypertensive drugs	0	44	**.001**	21
Coronary calcium score				
- Agatston, arbitrary units	0 [0 – 4]	0 [0 – 123]	.426	0 [0 – 16]
- volume, mm^3	0 [0 – 8]	0 [0 – 55]	.496	0 [0 – 18]
SCORE, %	0 [0 – 1]	1 [0 – 1]	**.013**	1 [0 – 1]

Values are mean ± the standard deviation, %, or median [25 – 75 percentiles]. HbA1c, MDRD-eGFR, and SCORE indicate glycated hemoglobin, glomerular filtration rate estimated by the Modification of Diet and Renal Disease formula, and 10-year risk for fatal cardiovascular disease according to the Systematic COronary Risk Evaluation tool based on age, gender, systolic blood pressure, total serum cholesterol, serum HDL cholesterol, and smoking status, respectively.

VCT, RX, and STE) with comparable spatial resolutions. Each subject underwent triple time-point PET/CT imaging at 45, 90, and 180 minutes after intravenous injection of approximately 2.2 MBq of $Na^{18}F$ per kilogram of body weight. The acquisition time per bed position was 2.5

minutes at 45 and 90 minutes. To compensate for radioactive decay of $Na^{18}F$, the acquisition time per bed position was extended to 3.5 minutes at 180 minutes. Total body PET images were acquired in 3D-mode and reconstructed into coronal, transverse, and sagittal slices by an iterative reconstruction algorithm (GE VUE Point). Corrections were applied for attenuation, scatter, random coincidences, and scanner dead time. Low-dose CT imaging (140 kV, 30-110 mA, noise index 25, 0.8 seconds per rotation, slice thickness 3.75 mm) was performed for attenuation correction and anatomic orientation. To determine the coronary calcium score, non-contrast enhanced, breath-hold, cardiac CT imaging (120 kV, 100 mA, 0.4 seconds per rotation, slice thickness 2.5 mm) was performed with electrocardiogram gating at 50 % of the R-R interval. On average, cardiac CT images were obtained within two weeks of the $Na^{18}F$ PET/CT images. The effective radiation dosage received for the entire imaging protocol was approximately 11 mSv.

Quantitative Image Analyses

All images were analyzed by version 4.0 of the Philips IntelliSpace Portal client. The image analyst was blinded to subject demographics and $Na^{18}F$ circulating time. For each subject, for each time point, global uptake of $Na^{18}F$ was determined in the coronary arteries **(14, 19)** and the thoracic aorta **(20)** as per published methods. In summary, for the coronary arteries, we manually drew a free-hand region of interest (ROI) around the cardiac silhouette on every slice of the attenuation corrected transverse PET/CT images. We carefully excluded $Na^{18}F$ activity originating from bone tissue, the aortic wall, and cardiac valves by eliminating these areas from the ROI. For the thoracic aorta, we manually drew a free-hand ROI around the outer perimeter of the arterial wall on every slice of the attenuation corrected transverse PET/CT images. We carefully excluded bone-derived $Na^{18}F$ activity by eliminating these areas from the ROI. Per ROI, the maximum $Na^{18}F$ activity concentration (Bq/mL) was determined and transformed into radiotracer-decay and body surface area corrected maximum standardized uptake value (SUV_{MAX}). Body surface area was calculated by the Du Bois formula in cm^2. Per arterial bed, SUV_{MAX} values were summed and divided by the number of ROIs to produce a single averaged value of SUV_{MAX} for the coronary arteries and for the thoracic aorta. Subsequently, the averaged SUV_{MAX} was corrected for blood-pool $Na^{18}F$ activity by subtraction of the blood-pool activity producing the blood-pool corrected SUV_{MAX} ($cSUV_{MAX}$) (**FIGURE 2**). The blood-pool $Na^{18}F$ activity was determined by drawing a single spherical volume of interest (400 mm^3) in the center of the right atrium and was quantified as the radiotracer-decay and body surface area corrected mean SUV (SUV_{MEAN}). To demonstrate that $cSUV_{MAX}$ does not simply quantifies blood-pool noise, blood-pool SUV_{MAX} was also determined. To quantify the contrast resolution,

FIGURE 2 – (**A**) Aortic wall sodium ^{18}F-fluoride ($Na^{18}F$) activity concentration (standardized uptake value; SUV) modeled assuming no background and no luminal blood activity. To appreciate the focal nature of aortic $Na^{18}F$ accumulation, activity concentrations were modeled more intense in the right compared to the left aortic wall. Note that the retrieved maximum and mean SUV is lower than the true aortic activity concentration (*red bars*) because of partial volume effects (PVEs). Conversely, PVEs result in overestimated values of the minimum activity. (**B**) Luminal blood activity modeled assuming no background and no aortic wall activity. Note that luminal blood activity bleeds-out onto the aortic wall because of PVEs. (**C**) Combined aortic wall and luminal blood activity modeled assuming no background activity. The color pallet (*red* = aortic wall activity, *blue* = luminal blood activity, *green* = combined aortic and luminal blood activity) represents the activity concentration as retrieved by PET/CT in a region of interest encompassing the outer aortic wall. Note that the PET/CT recovered SUV_{MAX} (i.e. SUV_{MAX} in **C**) is the sum of aortic wall SUV_{MAX} (i.e. SUV_{MAX} as in **A**) and luminal blood activity. Therefore, the aortic wall SUV_{MAX} (as in **A**) can be estimated by subtracting luminal blood SUV_{MEAN} from the recovered SUV_{MAX} (as in **C**) resulting in the blood-pool corrected SUV_{MAX} ($cSUV_{MAX}$). Note that $cSUV_{MAX}$ has no dependence on luminal blood SUV_{MEAN}, whereas the ratio between SUV_{MAX} and blood-pool SUV_{MEAN} (i.e. target-to-background ratio; TBR) has. To illustrate, if SUV_{MAX} is 4.0 (derived from **C**) and luminal blood SUV_{MEAN} is 1.5 (derived from **B**), the $cSUV_{MAX}$ is 2.5 (result as in **A**). These values make a TBR of 2.7. If the true aortic wall activity remains unchanged (result as in **A**), but luminal blood SUV_{MEAN} decreases to 0.8, the $cSUV_{MAX}$ remains 2.5 (3.3 – 0.8). However, the TBR (3.3 / 0.8) increases by 52 % to 4.1. To calculate the true aortic activity concentration (*red bars*), corrections for both luminal blood SUV_{MEAN} and PVEs need to be applied.

target-to-background ratios (TBR) were calculated by dividing the averaged arterial SUV_{MAX} with blood-pool SUV_{MEAN}. The coronary calcium score, obtained from the cardiac CT images, was quantified in arbitrary units according to Agatston and as a volumetric score (mm^3) **(4)**. To correct for the slice thickness of 2.5 mm, arbitrary units were multiplied by a cofactor of 2.5/3.0. The detection threshold for coronary calcium was set at 130 Hounsfield units.

Rater Agreement

Inter- and intra-rater agreement of $cSUV_{MAX}$ and the TBR was assessed one month after the initial analysis in a randomly selected sample of 10 subjects. Raters were blinded for subject demographics, $Na^{18}F$ circulating time, and results from the initial analysis.

Statistical Analysis

Demographics, arterial SUV_{MAX}, blood-pool SUV_{MEAN}/SUV_{MAX}, arterial $cSUV_{MAX}$, and the TBR were summarized and compared between controls and patients. Continuous variables were summarized as means ± the standard deviation and compared with the unpaired Student's *t* test. Non-parametric continues variables were summarized as medians with 25 – 75 percentiles and compared with the Mann-Whitney *U* test. Categorical variables were summarized as percentages and compared with the Fisher's exact test. Subsequent analyses

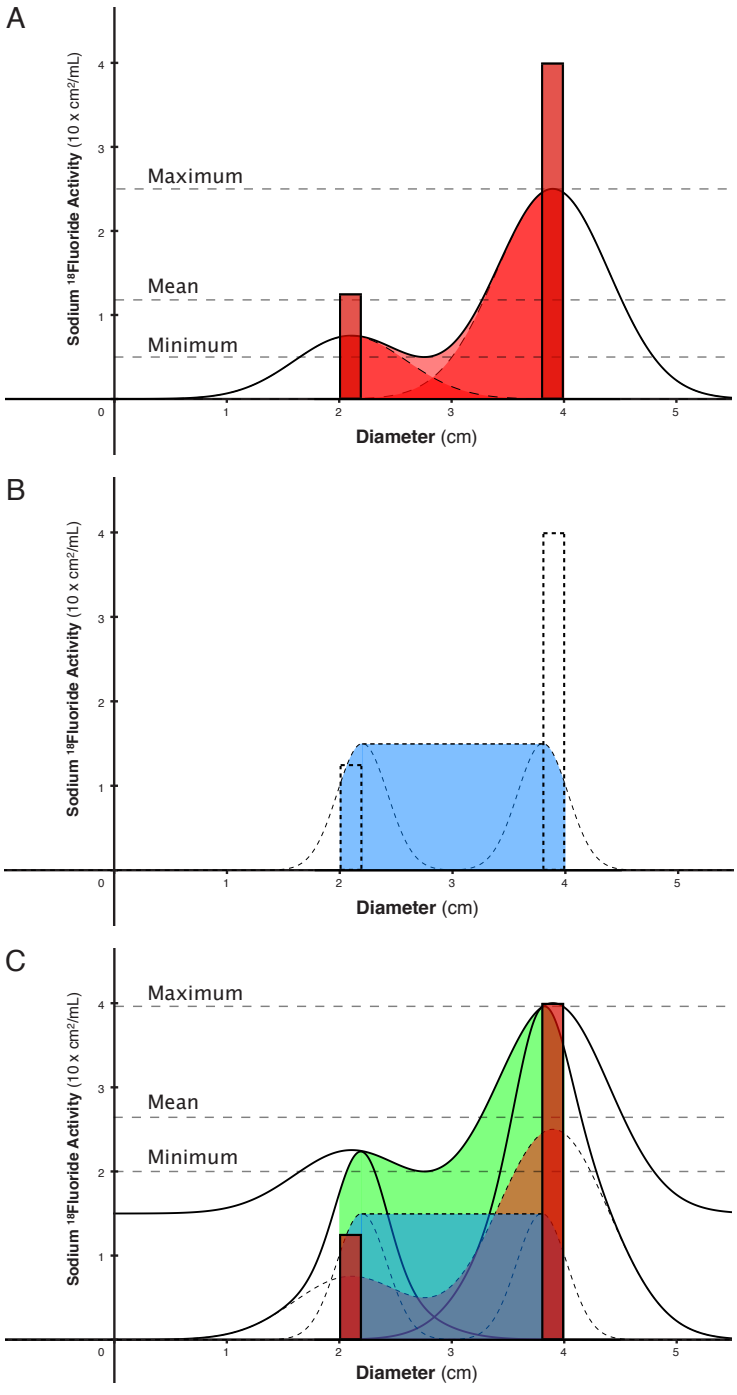
A
Sodium ^{18}Fluoride Activity (10 x cm^2/mL)
Maximum
Mean
Minimum
Diameter (cm)
B
Sodium ^{18}Fluoride Activity (10 x cm^2/mL)
Diameter (cm)
C
Sodium ^{18}Fluoride Activity (10 x cm^2/mL)
Maximum
Mean
Minimum
Diameter (cm)

were performed on the pooled data set of patients and controls. The variation in SUV_{MAX}, blood-pool SUV_{MEAN}, $cSUV_{MAX}$, and the TBR as a function of time was evaluated by the one-way analysis of variance (ANOVA) for matched pairs. If the assumption of sphericity was violated, as assessed by Mauchly's test, Greenhouse-Geisser corrected degrees of freedom and probability (*P*) values were reported. Post hoc analysis by pairwise comparison of means was conducted using the Student's *t* test for matched pairs with a Bonferroni correction. To determine the impact of $Na^{18}F$ circulating time on vascular calcification metabolism quantification, we first evaluated the strength of the relationship between SCORE % and $cSUV_{MAX}$ and SCORE % and the TBR by the Kendall rank correlation coefficient (τ). Second, we evaluated the linear relationship between coronary and aortic $cSUV_{MAX}$ by the Pearson correlation coefficient (*r*). Rater agreement was evaluated by intraclass correlation coefficients (ICC) (two-way random effects model assessing absolute agreement of single measures) as well as the 95 % limits of agreement according to Bland and Altman **(21)**. A two-tailed *P* value below .05 was regarded statistically significant. Presented *P* values and 95 % confidence intervals were calculated by a bootstrap of 2,000 samples. Statistical analyses were performed by IBM SPSS Statistics version 21.

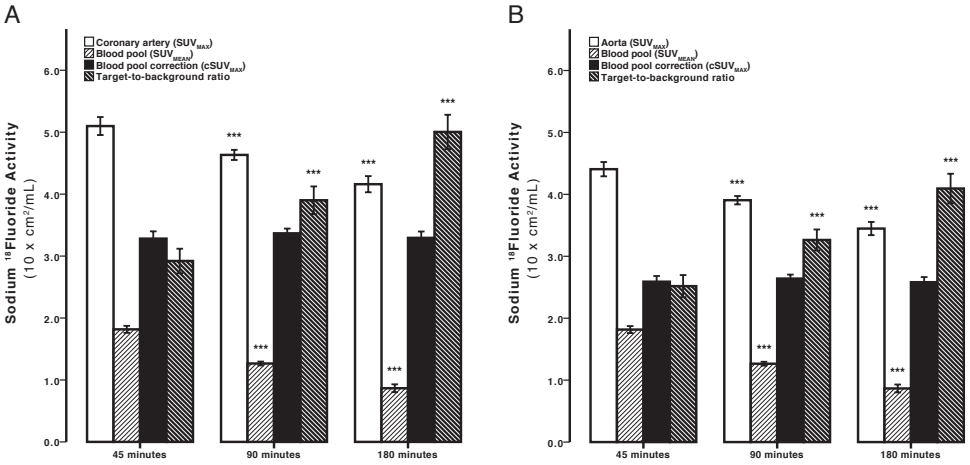

FIGURE 3 – Coronary SUV_{MAX} (**A**), aortic SUV_{MAX} (**B**), and blood-pool SUV_{MEAN} decreased with time, whereas the TBR significantly increased with time. Coronary and aortic $cSUV_{MAX}$ remained similar with time. *Error bars* represent 95 % confidence intervals of the mean. *** $P < .001$ decline or increase compared to previous time point established by the one-way ANOVA for matched pairs with a Bonferroni correction.

RESULTS

PET/CT imaging commenced at 47 ± 3, 90 ± 3, and 179 ± 3 minutes after $Na^{18}F$ administration. Coronary SUV_{MAX} (P < .001), aortic SUV_{MAX} (P < .001), and blood-pool SUV_{MEAN} (P < .001) significantly declined with time, whereas the coronary TBR (P < .001) and aortic TBR (P < .001) significantly increased with time (**FIGURE 3**). Coronary $cSUV_{MAX}$ (P = .533) and aortic $cSUV_{MAX}$ (P = .654) were invariant to $Na^{18}F$ circulating time (**SUPPLEMENTARY FIGURE 1**).

On average, coronary $cSUV_{MAX}$ was significantly higher in patients than in controls (**TABLE 2**) (**FIGURE 4**). The coronary TBR remained similar between patients and controls. These findings were consistent among the three investigated time points. At 45 minutes, aortic $cSUV_{MAX}$ was, on average, higher in patients than in controls. This finding could not be reproduced at 90 and 180 minutes. The aortic TBR remained similar between patients and controls.

A significant positive relationship was observed between SCORE % and coronary and aortic $cSUV_{MAX}$ (**TABLE 3**). This finding was consistent among time points. Similar relationships were observed between SCORE % and the coronary and aortic TBR, with exception of the coronary TBR at 45 minutes. At all investigated time points, coronary $cSUV_{MAX}$ significantly related to aortic $cSUV_{MAX}$ (**TABLE 4**).

Very strong inter- and intra-rater agreement was observed for coronary and aortic $cSUV_{MAX}$ as indicated by ICCs in the range of 0.98 and 1.00 (**SUPPLEMENTARY TABLES 1**, **2**). Furthermore, the observed 95 % limits of agreement were considered small (**SUPPLEMENTARY FIGURES 2**, **3**). These observations were consistent among the three investigated time points. Compared to $cSUV_{MAX}$, the inter- and intra-rater agreement of the coronary and aortic TBR was poorer as indicated by the larger 95 % limits of agreement.

DISCUSSION

Our study demonstrates that quantification of vascular calcification metabolism is invariant to the time between $Na^{18}F$ injection and PET/CT acquisition. Therefore, the optimal PET/CT acquisition time-point to quantify vascular calcification metabolism is achieved as early as 45 minutes after $Na^{18}F$ administration. Although delayed imaging at 90 and 180 minutes significantly improved contrast resolution over imaging at 45 minutes, the blood-pool corrected maximum standardized uptake value ($cSUV_{MAX}$) was unaffected by the $Na^{18}F$ circulating time.

TABLE 2 - Sodium ^{18}F-fluoride activity in the coronary arteries, aorta, and blood-pool

	Controls	Patients	*P* value	Total
Coronary SUV_{MAX}				
- 45 minutes	4.54 ± 1.00	5.72 ± 1.28	**.005**	5.10 ± 1.27
- 90 minutes	4.21 ± 0.96	5.10 ± 1.39	**.033**	4.63 ± 1.25
- 180 minutes	3.62 ± 1.01	4.77 ± 1.66	**.017**	4.16 ± 1.46
Aortic SUV_{MAX}				
- 45 minutes	4.06 ± 1.00	4.80 ± 1.09	**.031**	4.41 ± 1.09
- 90 minutes	3.57 ± 1.00	4.35 ± 1.24	.072	3.94 ± 1.12
- 180 minutes	3.05 ± 0.98	3.94 ± 1.48	.060	3.47 ± 1.30
Blood-pool SUV_{MEAN}				
- 45 minutes	1.76 ± 0.49	1.89 ± 0.49	.422	1.82 ± 0.49
- 90 minutes	1.21 ± 0.36	1.33 ± 0.39	.328	1.27 ± 0.38
- 180 minutes	0.81 ± 0.20	0.93 ± 0.28	.156	0.87 ± 0.24
Blood-pool SUV_{MAX}				
- 45 minutes	3.01 ± 0.86	3.46 ± 1.04	.158	3.22 ± 0.96
- 90 minutes	2.26 ± 0.79	2.60 ± 0.82	.217	2.42 ± 0.82
- 180 minutes	1.75 ± 0.61	2.01 ± 0.84	.278	1.87 ± 0.73
Coronary $cSUV_{MAX}$				
- 45 minutes	2.79 ± 0.66	3.83 ± 1.19	**.003**	3.28 ± 1.08
- 90 minutes	3.00 ± 0.78	3.77 ± 1.33	**.044**	3.37 ± 1.13
- 180 minutes	2.80 ± 0.92	3.84 ± 1.66	**.030**	3.29 ± 1.40
Aortic $cSUV_{MAX}$				
- 45 minutes	2.30 ± 0.71	2.91 ± 0.96	**.035**	2.59 ± 0.88
- 90 minutes	2.36 ± 0.81	2.95 ± 1.26	.099	2.64 ± 1.07
- 180 minutes	2.24 ± 0.86	2.30 ± 1.51	.095	2.58 ± 1.25
Coronary TBR				
- 45 minutes	2.70 ± 0.57	3.17 ± 0.92	.071	2.92 ± 0.78
- 90 minutes	3.77 ± 1.65	4.05 ± 1.41	.599	3.90 ± 1.53
- 180 minutes	4.58 ± 1.15	5.48 ± 2.44	.182	5.00 ± 1.90
Aortic TBR				
- 45 minutes	2.40 ± 0.55	2.64 ± 0.73	.277	2.52 ± 0.64
- 90 minutes	3.16 ± 1.30	3.38 ± 1.28	.604	3.26 ± 1.28
- 180 minutes	3.80 ± 0.87	4.42 ± 2.14	.279	4.09 ± 1.61

Values are mean ± the standard deviation for 20 controls and 18 patients. SUV_{MAX}, SUV_{MEAN}, $cSUV_{MAX}$, and TBR indicate radiotracer-decay and body surface area corrected maximum standardized uptake value, radiotracer-decay and body surface area corrected mean standardized uptake value, blood-pool corrected SUV_{MAX}, and target-to-background ratio, respectively.

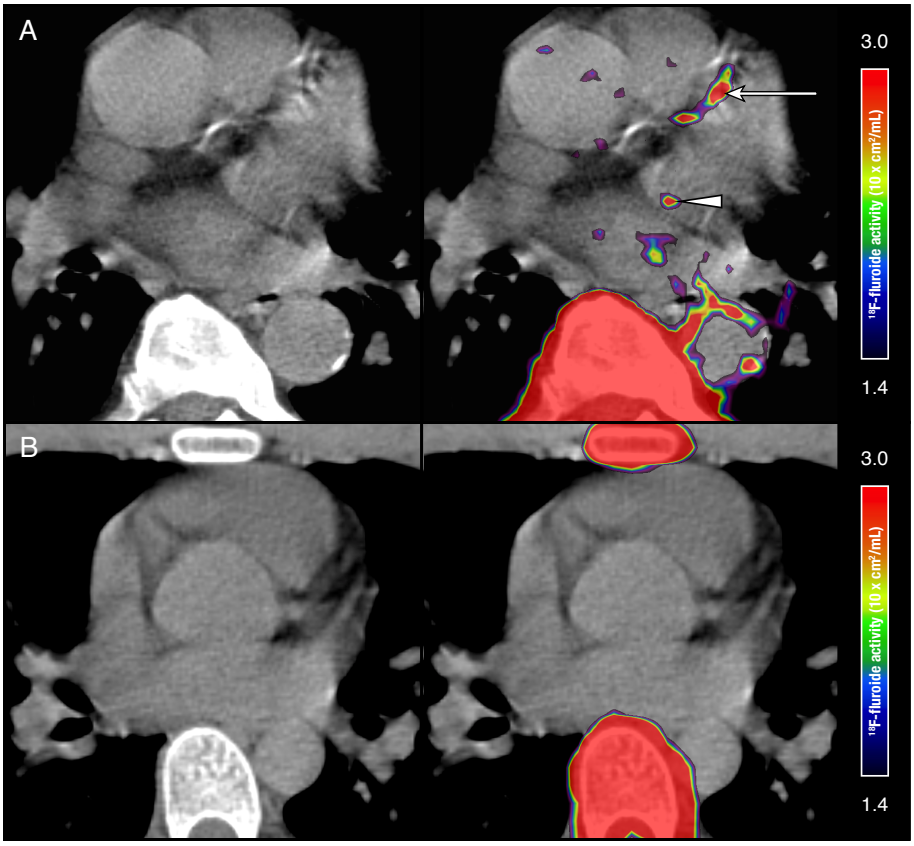

FIGURE 4 – **(A)** Patient with a SCORE of 3 %, a coronary calcium score of > 1,000 Agatston units, and intense focal Na^{18}F accumulation in the territory of the left anterior descending (*arrow*) and left circumflex (*arrowhead*) coronary artery. Furthermore, intense Na^{18}F accumulation was observed in the descending aorta, predominantly in areas without structural vascular calcification. **(B)** Healthy control with a SCORE of 0 %, no vascular calcifications, and no vascular Na^{18}F accumulation.

Furthermore, coronary cSUV$_{MAX}$ could discriminate patients from controls at all investigated time points. Also, significant positive relationships between cardiovascular risk (SCORE %) and coronary and aortic cSUV$_{MAX}$ were observed at all investigated time points. Finally, we observed high inter- and intra-rater agreement for coronary and aortic cSUV$_{MAX}$ at 45, 90, and 180 minutes. With cSUV$_{MAX}$ as the preferred quantifier of arterial Na^{18}F activity, the findings of our study support the statement that the optimal acquisition time-point to quantify vascular calcification metabolism with PET/CT imaging is achieved as early as 45 minutes after Na^{18}F administration.

Our findings challenge the notion that maximizing contrast between arterial wall and blood-pool $Na^{18}F$ activity improves quantification of vascular calcification metabolism. We speculate that the near instantaneous incorporation of $Na^{18}F$ in osseous tissue and the rapid decline of $Na^{18}F$ from the blood-pool are responsible for the satisfactory contrast resolution achieved at 45 minutes **(10, 22)**. Increasing contrast resolution, beyond what is achieved at 45 minutes, does not seem to add sensitivity to quantification of vascular calcification metabolism. We further speculate that $Na^{18}F$ accumulation in vascular calcifications saturate as early as 45 minutes after $Na^{18}F$ administration. This may explain the observation that $cSUV_{MAX}$ is invariant to time. Autoradiographic analyses of $Na^{18}F$ incorporation in vascular calcification combined with histopathology might be able to confirm these speculations.

Besides the finding that $cSUV_{MAX}$ is time invariant, our study demonstrated significantly higher values of $cSUV_{MAX}$ in patients compared to controls. This finding can be attributed to both age and the fact that patients had a significantly higher median SCORE % than controls. Furthermore, our results confirm the observation that coronary and aortic $Na^{18}F$ activity significantly relate to cardiovascular risk **(8)** even though arterial $Na^{18}F$ activity

TABLE 3 - Correlation between arterial sodium ^{18}F-fluoride activity and SCORE %

	Kendall's τ	95 % confidence interval	*P* value
Coronary $cSUV_{MAX}$			
- 45 minutes	0.40	0.17 to 0.61	**.002**
- 90 minutes	0.30	0.04 to 0.53	**.019**
- 180 minutes	0.32	0.06 to 0.54	**.013**
Coronary TBR			
- 45 minutes	0.17	-0.11 to 0.42	.172
- 90 minutes	0.57	0.42 to 0.71	**< .001**
- 180 minutes	0.68	0.57 to 0.79	**< .001**
Aortic $cSUV_{MAX}$			
- 45 minutes	0.37	0.13 to 0.56	**.003**
- 90 minutes	0.77	0.65 to 0.87	**< .001**
- 180 minutes	0.85	0.76 to 0.92	**< .001**
Aortic TBR			
- 45 minutes	0.26	0.02 to 0.47	**.040**
- 90 minutes	0.61	0.48 to 0.72	**< .001**
- 180 minutes	0.66	0.50 to 0.79	**< .001**

Abbreviations as in **TABLE 2**.

TABLE 4 - Relationship between coronary and aortic $cSUV_{MAX}$

Time-point	Pearson's *r*	95 % confidence interval	*P* value
45 minutes	0.82	0.70 to 0.91	**< .001**
90 minutes	0.77	0.64 to 0.87	**< .001**
180 minutes	0.80	0.67 to 0.90	**< .001**

Abbreviations as in **TABLE 2**.

($cSUV_{MAX}$ *versus* TBR) as well as cardiovascular risk (SCORE % *versus* Framingham Risk Score) were quantified differently in our study. We could also demonstrate a highly significant correlation between coronary and aortic $Na^{18}F$ activity, supporting the notion that vascular calcification is a systemic disorder. Finally, our study could demonstrate that the maximum $Na^{18}F$ activity concentration in the blood-pool remained substantially lower than the coronary and aortic SUV_{MAX}. This finding indicates that global assessment of arterial $Na^{18}F$ activity does not quantify blood-pool noise.

The results of our study suggest that quantification of vascular calcification metabolism by the TBR is suboptimal compared to $cSUV_{MAX}$. Notably, our study showed that coronary $cSUV_{MAX}$ could discriminate patients from controls, whereas the TBR could not. Although it is prevalent to quantify arterial $Na^{18}F$ avidity as a TBR **(13, 15, 17, 23)**, the TBR method is associated with limitations. First, the TBR is dependent on blood-pool $Na^{18}F$ activity (**FIGURE 2**). We demonstrated that blood-pool $Na^{18}F$ activity is highly dependent on the circulating time of $Na^{18}F$. Independent of vascular $Na^{18}F$ accumulation, the blood-pool activity decreases with time and, as a result, the TBR increases with time. This makes the circulating time of the radiopharmaceutical a major determinant of the TBR, especially for radiopharmaceuticals with rapid blood clearance, like $Na^{18}F$ **(22)**. Second, inter-subject variation in blood-pool $Na^{18}F$ clearance might bias quantification of vascular calcification metabolism. For example, the blood-pool clearance seems to depend on the eGFR **(10)**. It is well known that the GFR progressively decreases with age **(24)**. Although our study could not demonstrate a significant difference in eGFR or blood-pool $Na^{18}F$ activity between patients and controls, our significantly older patient cohort showed a trend towards lower eGFR and higher blood-pool $Na^{18}F$ activity over controls. This might result in underestimated values of true arterial $Na^{18}F$ uptake in older subjects compared to younger subjects. Third, the TBR is subject to larger inter- and intra-rater variation compared to the $cSUV_{MAX}$. Bias introduced by TBR quantification of vascular calcification metabolism might explain why coronary TBR could not discriminate patients from controls, whereas coronary $cSUV_{MAX}$ could.

Limitations

First, our semi-quantitative image analysis did not correct for partial volume effects (PVEs), which could have influenced study results **(25)**. As the average size of vascular calcifications approach the spatial resolution of PET (both approximately 125 mm^3) **(26, 27)**, PVEs should be considered in the quantification of vascular calcification metabolism. Moreover, PVEs are amplified by pulsatile blood flow, patient movement, and the cardiac and respiratory cycle **(28)**. This is particularly pertinent in the coronary arteries, because of their anatomic location **(29)**. The consequence of PVEs is a signal bleed-out from the arterial wall and signal bleed-in from the blood-pool. This blurring effect necessitates blood-pool corrections to obtain reliable vascular $Na^{18}F$ activity concentrations. To further improve quantification of vascular $Na^{18}F$ avidity, partial volume corrections need to be applied. This was not performed in our study and likely resulted in underestimated values of arterial $Na^{18}F$ activity concentrations.

Second, the time points of 45, 90, and 180 minutes were chosen based on empirical evidence provided by the SNM Practice Guideline for Sodium ^{18}F-Fluoride PET/CT Bone Scans **(16)**. Theoretically, the optimal $Na^{18}F$ PET/CT acquisition time-point could have occurred before 45 minutes or after 180 minutes. Nevertheless, the observation that a satisfactory contrast resolution can be achieved as early as 45 minutes after $Na^{18}F$ administration allows consideration of other factors, such as department logistics and patient comfort, determine the imaging time-point. For example, our department has adopted an imaging time-point of 90 minutes after $Na^{18}F$ injection for PET/CT quantification of vascular calcification metabolism.

Third, coronary uptake of $Na^{18}F$ was determined by global assessment. Global assessment of coronary $Na^{18}F$ accumulation is potentially limited by bleed-out activity from non-coronary derived $Na^{18}F$ activity **(29)**. Nevertheless, our study demonstrated that excluding non-coronary $Na^{18}F$ activity from the ROI could be achieved with high inter- and intra-rater agreement. In addition, global assessment of coronary $Na^{18}F$ avidity has advantages over focal quantification of coronary $Na^{18}F$ uptake. First, global assessment is not limited by difficulties localizing the coronary arteries on non-ECG-gated CT images acquired during PET/CT imaging. Localizing the coronary tree in subjects without coronary calcification is particularly difficult, as was the case in the majority of subjects included in our study. Second, global assessment evaluates the entire vasculature of the heart and is not limited to focal segments of the coronary tree. Despite these advantages, we encourage comparison of both techniques in a large sample of subjects to determine the technique of preference.

Conclusions

In conclusion, we have shown that delayed $Na^{18}F$ PET/CT imaging does not improve quantification of vascular calcification metabolism. Although contrast resolution improves with time, arterial $Na^{18}F$ avidity is invariant to the time between $Na^{18}F$ administration and PET/CT acquisition. Therefore, the optimal PET/CT acquisition time-point to quantify vascular calcification metabolism is achieved as early as 45 minutes after $Na^{18}F$ administration.

REFERENCES

1. Budoff MJ, Shaw LJ, Liu ST, et al. Long-Term Prognosis Associated with Coronary Calcification: Observations from a Registry of 25,253 Patients. *J Am Coll Cardiol.* 2007; **49**: 1860-70.

2. Hou ZH, Lu B, Gao Y, et al. Prognostic Value of Coronary CT Angiography and Calcium Score for Major Adverse Cardiac Events in Outpatients. *J Am Coll Cardiol Img.* 2012; **5**: 990-9.

3. Allison MA, Hsi S, Wassel CL, et al. Calcified Atherosclerosis in Different Vascular Beds and the Risk of Mortality. *Arterioscler Thromb Vasc Biol.* 2012; **32**: 140-6.

4. Becker CR, Knez A, Ohnesorge B, et al. Visualization and Quantification of Coronary Calcifications with Electron Beam and Spiral Computed Tomography. *Eur Radiol.* 2000; **10**: 629-35.

5. Ehara S, Kobayashi Y, Yoshiyama M, et al. Spotty Calcification Typifies the Culprit Plaque in Patients with Acute Myocardial Infarction: An Intravascular Ultrasound Study. *Circulation.* 2004; **110**: 3424-9.

6. Demer LL, Tintut Y. Vascular Calcification: Pathobiology of a Multifaceted Disease. *Circulation.* 2008; **117**: 2938-48.

7. Virmani R, Burke AP, Farb A, et al. Pathology of the Vulnerable Plaque. *J Am Coll Cardiol.* 2006; **47**: C13-8.

8. Dweck MR, Chow MW, Joshi NV, et al. Coronary Arterial ^{18}F-Sodium Fluoride Uptake: A Novel Marker of Plaque Biology. *J Am Coll Cardiol.* 2012; **59**: 1539-48.

9. McEvoy JW, Blaha MJ, Rivera JJ, et al. Mortality Rates in Smokers and Nonsmokers in the Presence or Absence of Coronary Artery Calcification. *J Am Coll Cardiol Img.* 2012; **5**: 1037-45.

10. Czernin J, Satyamurthy N, Schiepers C. Molecular Mechanisms of Bone ^{18}F-NaF Deposition. *J Nucl Med.* 2010; **51**: 1826-9.

11. Derlin T, Richter U, Bannas P, et al. Feasibility of ^{18}F-Sodium Fluoride PET/CT for Imaging of Atherosclerotic Plaque. *J Nucl Med.* 2010; **51**: 862-5.

12. Derlin T, Wisotzki C, Richter U, et al. In Vivo Imaging of Mineral Deposition in Carotid Plaque Using ^{18}F-Sodium Fluoride PET/CT: Correlation with Atherogenic Risk Factors. *J Nucl Med.* 2011; 52: 362-8.

13. Janssen T, Bannas P, Herrmann J, et al. Association of Linear ^{18}F-Sodium Fluoride Accumulation in Femoral Arteries as a Measure of Diffuse Calcification with Cardiovascular Risk Factors: A PET/CT Study. *J Nucl Cardiol.* 2013; **20**: 569-77.

14. Beheshti M, Saboury B, Mehta NN, et al. Detection and Global Quantification of

Cardiovascular Molecular Calcification by ^{18}F-Fluoride Positron Emission Tomography/Computed Tomography - A Novel Concept. *Hell J Nucl Med.* 2011; **14**: 114-20.

15. Li Y, Berenji GR, Shaba WF, et al. Association of Vascular Fluoride Uptake with Vascular Calcification and Coronary Artery Disease. *Nucl Med Commun.* 2012; **33**: 14-20.

16. Segall G, Delbeke D, Stabin MG, et al. SNM Practice Guideline for Sodium ^{18}F-Fluoride PET/CT Bone Scans 1.0. *J Nucl Med.* 2010; **51**: 1813-20.

17. Dweck MR, Joshi FR, Newby DE, et al. Noninvasive Imaging in Cardiovascular Therapy: The Promise of Coronary Arterial ^{18}F-Sodium Fluoride Uptake as a Marker of Plaque Biology. *Expert Rev Cardiovasc Ther.* 2012; **10**: 1075-7.

18. Conroy RM, Pyorala K, Fitzgerald AP, et al. Estimation of Ten-Year Risk of Fatal Cardiovascular Disease in Europe: The SCORE Project. *Eur Heart J.* 2003; **24**: 987-1003.

19. Basu S, Høilund-Carlsen PF, Alavi A. Assessing Global Cardiovascular Molecular Calcification with ^{18}F-Fluoride PET/CT: Will this Become a Clinical Reality and a Challenge to CT Calcification Scoring? *Eur J Nucl Med Mol Imaging.* 2012; **39**: 660-4.

20. Derlin T, Toth Z, Papp L, et al. Correlation of Inflammation Assessed by ^{18}F-FDG PET, Active Mineral Deposition Assessed by ^{18}F-Fluoride PET, and Vascular Calcification in Atherosclerotic Plaque: A Dual-Tracer PET/CT Study. *J Nucl Med.* 2011; **52**: 1020-7.

21. Bland JM, Altman DG. Statistical Methods for Assessing Agreement Between Two Methods of Clinical Measurement. *Lancet.* 1986; **1**: 307-10.

22. Kurdziel KA, Shih JH, Apolo AB, et al. The Kinetics and Reproducibility of ^{18}F-Sodium Fluoride for Oncology Using Current PET Camera Technology. *J Nucl Med.* 2012; **53**: 1175-84.

23. Dweck MR, Khaw HJ, Sng GK, et al. Aortic Stenosis, Atherosclerosis, and Skeletal Bone: Is there a Common Link with Calcification and Inflammation? *Eur Heart J.* 2013; **34**: 1567-74.

24. Levey AS, Bosch JP, Lewis JB, et al. A More Accurate Method to Estimate Glomerular Filtration Rate From Serum Creatinine: A New Prediction Equation. *Ann Intern Med.* 1999; **130**: 461-70.

25. Hickeson M, Yun M, Matthies A, et al. Use of a Corrected Standardized Uptake Value Based on the Lesion Size on CT Permits Accurate Characterization of Lung Nodules on FDG-PET. *Eur J Nucl Med Mol Imaging.* 2002; **29**: 1639-47.

26. Sanchez-Crespo A, Andreo P, Larsson SA. Positron Flight in Human Tissues and Its Influence on PET Image Spatial Resolution. *Eur J Nucl Med Mol Imaging.* 2004; **31**: 44-51.

27. Mets OM, Vliegenthart R, Gondrie MJ, et al. Lung Cancer Screening CT-Based Prediction of Cardiovascular Events. *J Am Coll Cardiol Img.* 2013; **6**: 899-907.

28. Basu S, Zaidi H, Houseni M, et al. Novel Quantitative Techniques for Assessing Regional and Global Function and Structure Based on Modern Imaging Modalities: Implications for Normal Variation, Aging, and Diseased States. *Semin Nucl Med.* 2007; **37**: 223-39.

29. Mohler ER, Alavi A, Wilensky RL. ^{18}F-Fluoride Imaging for Atherosclerosis. *J Am Coll Cardiol.* 2012; **60**: 1711-2.

SUPPLEMENTARY FIGURES

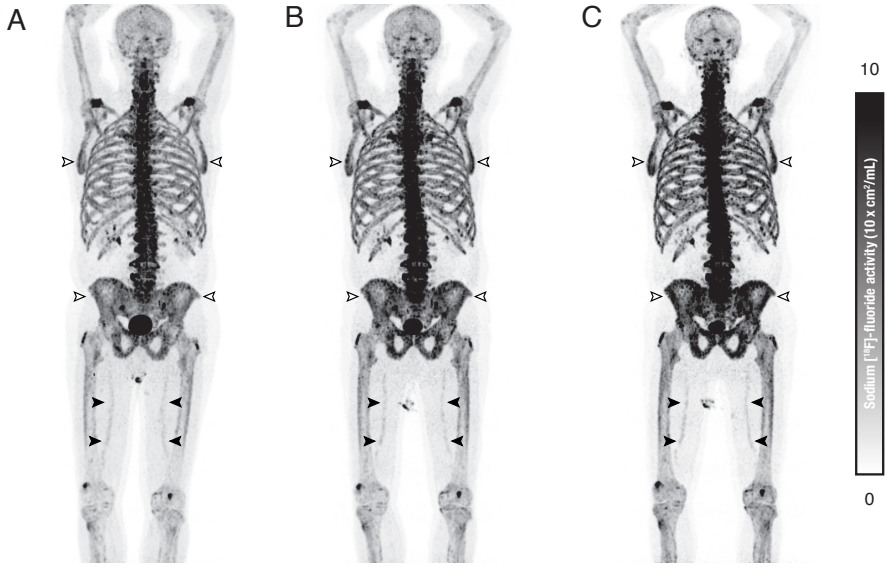

SUPPLEMENTARY FIGURE 1 – Maximum intensity projection PET/CT images acquired in a 50-year old male with hypertension at 45 (**A**), 90 (**B**), and 180 minutes (**C**) after administration of 150 MBq of $Na^{18}F$. Bone $Na^{18}F$ avidity increased with time (*white arrowheads in* **A**, **B**, and **C**), whereas femoral artery $Na^{18}F$ avidity appears to be indifferent to the effect of time (*black arrowheads* in **A**, **B**, and **C**).

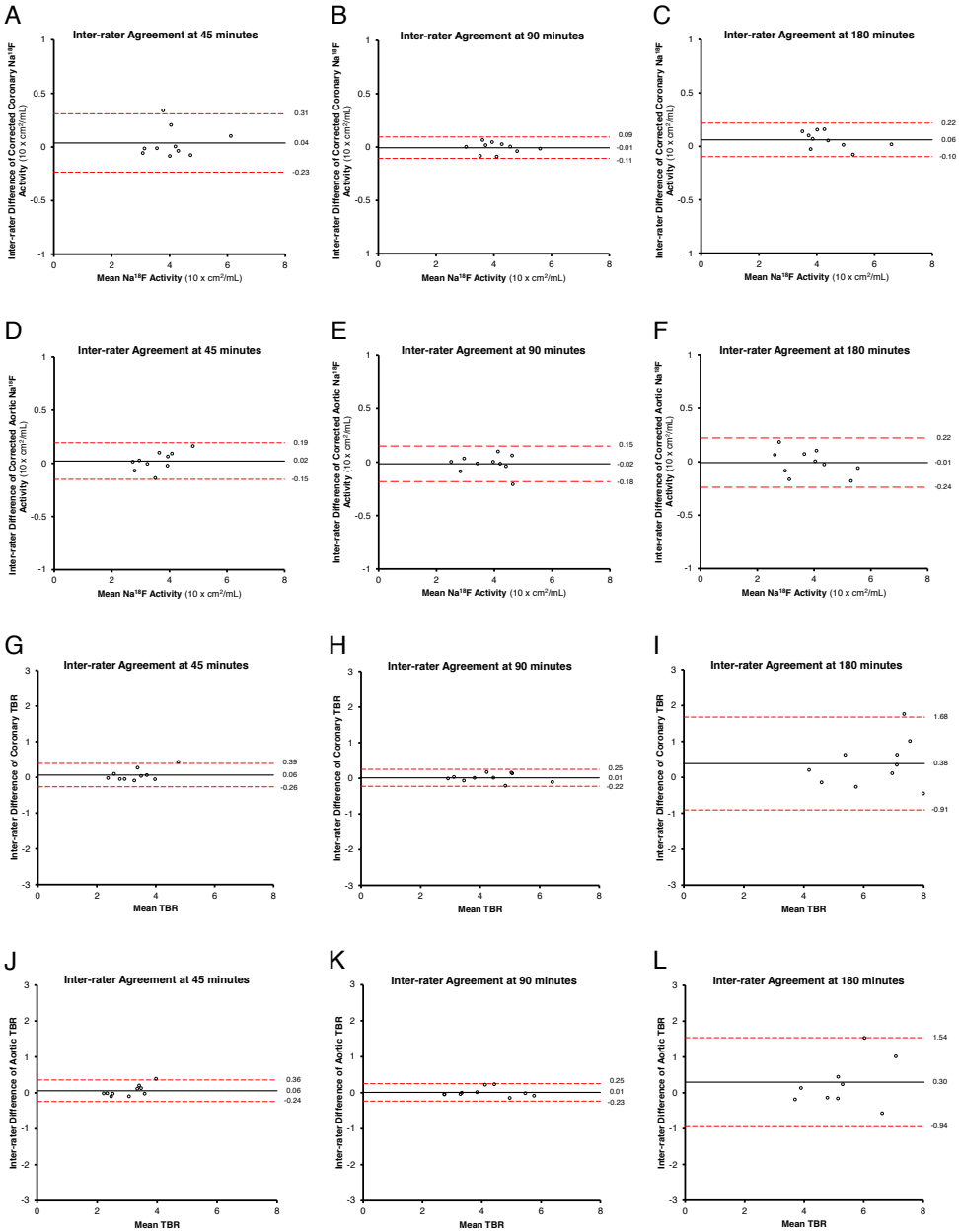

SUPPLEMENTARY FIGURE 2 – Inter-rater agreement of coronary $cSUV_{MAX}$ (**A**, **B**, **C**), aortic $cSUV_{MAX}$ (**D**, **E**, **F**), coronary TBR (**G**, **H**, **I**), and aortic TBR (**J**, **K**, **L**) at 45 (**A**, **D**, **G**, **J**), 90 (**B**, **E**, **H**, **K**), and 180 minutes (**C**, **F**, **I**, **L**).

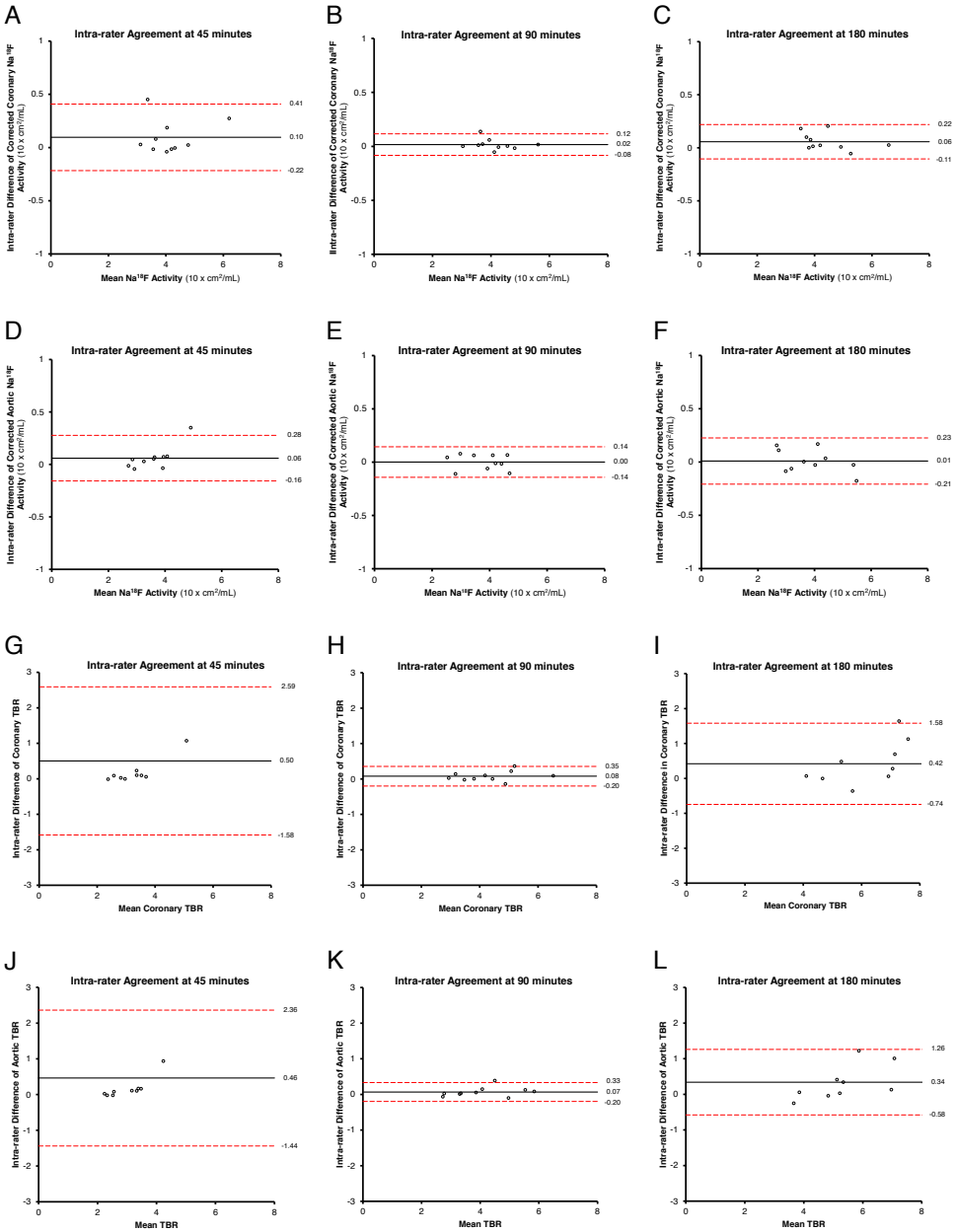

SUPPLEMENTARY FIGURE 3 – Intra-rater agreement of coronary cSUV$_{MAX}$ (**A**, **B**, **C**), aortic cSUV$_{MAX}$ (**D**, **E**, **F**), coronary TBR (**G**, **H**, **I**), and aortic TBR (**J**, **K**, **L**) at 45 (**A**, **D**, **G**, **J**), 90 (**B**, **E**, **H**, **K**), and 180 minutes (**C**, **F**, **I**, **L**).

SUPPLEMENTARY TABLES

SUPPLEMENTARY TABLE 1 – Inter-rater agreement

	ICC	95 % CI	Mean difference (10 x cm^2/mL)	95 % Limits of agreement
Coronary $cSUV_{MAX}$				
- 45 minutes	0.99 ***	0.96 to 1.00	0.04	-0.23 to 0.31
- 90 minutes	1.00 ***	0.99 to 1.00	-0.01	-0.11 to 0.09
- 180 minutes	1.00 ***	0.97 to 1.00	0.06	-0.10 to 0.22
Aortic $cSUV_{MAX}$				
- 45 minutes	0.99 ***	0.97 to 1.00	0.02	-0.15 to 0.19
- 90 minutes	1.00 ***	0.98 to 1.00	-0.02	-0.18 to 0.15
- 180 minutes	0.99 ***	0.98 to 1.00	-0.01	-0.24 to 0.22
Coronary TBR				
- 45 minutes	0.97 ***	0.90 to 0.99	0.06	-0.26 to 0.39
- 90 minutes	0.99 ***	0.98 to 1.00	0.01	-0.22 to 0.25
- 180 minutes	0.86 ***	0.51 to 0.96	0.38	-0.91 to 1.68
Aortic TBR				
- 45 minutes	0.97 ***	0.88 to 0.99	0.06	-0.24 to 0.36
- 90 minutes	0.99 ***	0.98 to 1.00	0.01	-0.23 to 0.25
- 180 minutes	0.93 ***	0.76 to 0.98	0.30	-0.94 to 1.54

ICC, CI, SUV_{MAX}, $cSUV_{MAX}$, and TBR indicate intraclass correlation coefficient (two-way random effects model assessing absolute agreement of single measures), confidence interval, radiotracer-decay and body surface area corrected maximum standardized uptake value, blood-pool corrected SUV_{MAX}, and target-to-background ratio, respectively. *** $P < .001$.

SUPPLEMENTARY TABLE 2 – Intra-rater agreement

	ICC	95 % CI	Mean difference (10 x cm^2/mL)	95 % Limits of agreement
Coronary cSUV$_{MAX}$				
- 45 minutes	0.98 ***	0.91 to 1.00	0.10	-0.22 to 0.41
- 90 minutes	1.00 ***	0.99 to 1.00	0.02	-0.08 to 0.12
- 180 minutes	1.00 ***	0.97 to 1.00	0.06	-0.11 to 0.22
Aortic cSUV$_{MAX}$				
- 45 minutes	0.98 ***	0.93 to 1.00	0.06	-0.16 to 0.28
- 90 minutes	1.00 ***	0.98 to 1.00	0.00	-0.14 to 0.14
- 180 minutes	1.00 ***	0.98 to 1.00	0.01	-0.21 to 0.23
Coronary TBR				
- 45 minutes	0.57 *	0.02 to 0.87	0.50	-1.58 to 2.59
- 90 minutes	0.99 ***	0.96 to 1.00	0.08	-0.20 to 0.35
- 180 minutes	0.88 ***	0.52 to 0.97	0.42	-0.74 to 1.58
Aortic TBR				
- 45 minutes	0.53 ***	-0.03 to 0.85	0.46	-1.44 to 2.36
- 90 minutes	0.99 ***	0.97 to 1.00	0.07	-0.20 to 0.33
- 180 minutes	0.95 ***	0.76 to 0.99	0.34	-0.58 to 1.26

Abbrevations as in **SUPPLEMENTARY TABLE 1**. * $P < .05$, *** $P < .001$.

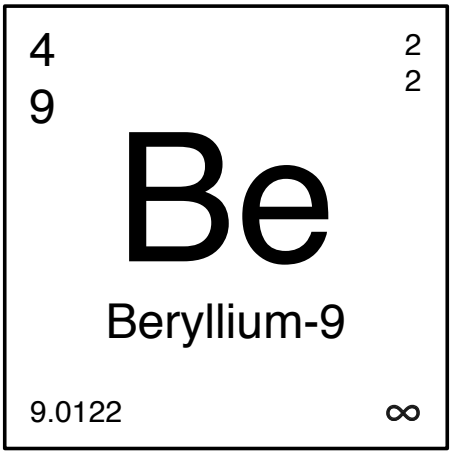
4
9
2
2
Be
Beryllium-9
9.0122
∞

Chapter 4

Quantifying [^{18}F]-Fluorodeoxyglucose Uptake in the Arterial Wall: The Effect of Dual Time-Point Imaging and Partial Volume Effect Correction

Björn A. Blomberg
Arjun Bashyam
Abhinay Ramachandran
Saeid Gholami
Sina Houshmand
Ali Salavati
Thomas J. Werner
Habib Zaidi
Abass Alavi

Published in the *European Journal of Nuclear Medicine and Molecular Imaging*, 2015

ABSTRACT

Background: The human arterial wall is smaller than the spatial resolution of current positron emission tomographs. Therefore, partial volume effects should be considered when quantifying arterial wall [^{18}F]-fluorodeoxyglucose (^{18}FDG) uptake. We evaluated the impact of a novel method for partial volume effect (PVE) correction with contrast-enhanced CT (CECT) assistance on quantification of arterial wall ^{18}FDG uptake at different imaging time-points.

Methods: Ten subjects were assessed by contrast enhanced CT (CECT) imaging and dual time-point PET/CT imaging at approximately 60 and 180 minutes after ^{18}FDG administration. For both time-points, uptake of ^{18}FDG was determined in the aortic wall by calculating the blood-pool-corrected maximum standardized uptake value ($cSUV_{MAX}$) and $cSUV_{MEAN}$. Also, the PVE-corrected SUV_{MEAN} ($pvcSUV_{MEAN}$) was calculated using ^{18}FDG PET/CT and CECT images. Finally, corresponding target-to-background ratios (TBR) were calculated.

Results: At 60 minutes, $pvcSUV_{MEAN}$ was on average 3.1 times greater than $cSUV_{MAX}$ ($P < .001$) and 8.5 times greater than $cSUV_{MEAN}$ ($P < .001$). At 180 minutes, $pvcSUV_{MEAN}$ was on average 2.6 times greater than $cSUV_{MAX}$ ($P < .001$) and 6.6 times greater than $cSUV_{MEAN}$ ($P < .001$).

Conclusions: This study demonstrated that CECT-assisted PVE correction significantly influences quantification of arterial wall ^{18}FDG uptake. Therefore, partial volume effects should be considered when quantifying arterial wall ^{18}FDG uptake with PET.

INTRODUCTION

[^{18}F]-fluorodeoxyglucose (^{18}FDG) positron emission tomography/computed tomography (PET/CT) is a promising non-invasive imaging technique for assessment of arterial wall inflammation. By targeting arterial plaque glycolysis, a surrogate of arterial inflammation and hypoxia **(1, 2)**, ^{18}FDG PET/CT imaging can potentially detect and quantitate arterial inflammation **(2, 3)**, evaluate response to treatment **(4, 5)**, and predict risk for cardiovascular events **(6)**.

Despite several promising studies in the literature **(7-10)**, ^{18}FDG PET/CT imaging of arterial inflammation suffers from significant limitations which relates to the partial volume effect (PVE) and to the low resolution of PET **(11)**. PVE is a well-known phenomenon and results in underestimation of the true quantity of radiotracer on PET images. PVE are significant in targeted structures that are two to three times smaller than the spatial resolution of PET **(12)**. Since the thickness of arterial walls (e.g. 1.5 to 2.5 mm for the aorta **(13, 14)**) is smaller than the spatial resolution of current positron emission tomographs (approximately 5 mm **(15)**), PVE should be considered in PET imaging of aortic inflammation.

We evaluated the impact of PVE correction with contrast-enhanced CT (CECT) assistence on quantification of arterial wall ^{18}FDG uptake at different imaging time-points. In addition, we evaluated the correlations between PVE-corrected measurements and other measurements indices of vessel wall ^{18}FDG uptake.

METHODS

This study was approved by the Institutional Review Board of the Philadelphia VA Medical Center and was conducted in accordance with the principles of the Declaration of Helsinki and the Health Insurance Portability and Accountability Act. Written informed consent was obtained from all subjects included in the study.

Subject Selection

Subjects were selected from a prospective cohort of patients recruited for the evaluation of lung cancer by multiple time-point ^{18}FDG PET/CT imaging. Only subjects with a CECT scan were included in the current study. Patients with tumour involvement near the aorta or other areas of interest were excluded. Ten subjects met the inclusion and exclusion criteria and were included in this study.

Study Design

As part of this prospective study, subjects were evaluated by questionnaires, blood pressure measurements, blood analyses, and dual time-point ^{18}FDG PET/CT imaging. Subjects also underwent CECT imaging. Questionnaires included questions about prescribed medications, history of cardiovascular disease, and cardiovascular risk factors. Systolic and diastolic blood pressure were obtained from blood pressure measurements. Blood analyses included fasting total serum cholesterol, serum LDL and HDL cholesterols, fasting blood glucose, and serum creatinine. The estimated glomerular filtration rate (eGFR) was determined using the Modification of Diet in Renal Disease (MDRD) equation. For each subject, the Framingham Risk Score was calculated based on age, gender, total serum cholesterol, serum HDL cholesterol, smoking status, systolic blood pressure, and antihypertensive medication status. ^{18}FDG PET/CT imaging was performed on an integrated Biograph TruePoint PET/CT scanner (Siemens Healthcare). This scanner combines a lutetium oxyorthosilicate scintillator with a 64-slice CT scanner. Each subject underwent dual time-point PET/CT imaging at 60 and 180 minutes after intravenous injection of approximately 5.2 MBq of ^{18}FDG per kilogram of body weight. ^{18}FDG was administered after the subject had fasted for at least 6 hours. Before ^{18}FDG injection, the blood glucose concentration was determined to ensure a value below 11 mmol/L. After injection and between scans, the subject rested in a warm and quiet room. For the 60 minute acquisition, the time per bed position was 2 minutes. For the 180-minute acquisition, the time per bed position was 4 minutes. PET images were acquired from the mid-skull to the mid-thigh and reconstructed in the transverse, coronal, and sagittal planes using a point spread function (three iterations, 21 subsets, 4 mm Gaussian filter, 168 × 168 reconstruction matrix). Corrections were applied for attenuation, scatter, random coincidences, and scanner dead time. Low-dose CT imaging was performed for attenuation correction and anatomic orientation. PET data were resampled to the CT voxel grid. No additional rebinning was performed. CECT imaging was performed as part of the routine clinical work-up. PET and CECT images were manually co-registered.

Quantitative Image Analysis

Quantitative image analysis was performed on a Philips Extended Brilliance Workspace platform. All quantitative analyses were performed on the descending aorta. The following parameters were calculated: area of the arterial lumen (mm^2), radius of the arterial lumen (mm), arterial wall area (mm^2), average arterial wall thickness (mm), area of the spillover activity (mm^2), average maximum and mean aortic ^{18}FDG activity (SUV_{MAX} and SUV_{MEAN}), average blood-pool ^{18}FDG activity (SUV_{MEAN}), and average background ^{18}FDG activity (SUV_{MEAN}). Based

TABLE 1 – Subject demographics

Demographic	Value
Age, years	66.3 (63.3 to 70.0)
Male, %	90
Active smoking, %	80
Pack years	55 [35 to 84.7]
Blood pressure, mmHg	
- Systolic	138.8 (125.2 to 152.6)
- Diastolic	77.2 (68.2 to 86.1)
Body mass index, kg/m^2	23.7 (20.5 to 27.2)
Diabetes mellitus, %	10
Cholesterol, mmol/L	
- Total	4.1 (3.6 to 4.5)
- LDL	2.4 (2.0 to 2.8)
- HDL	1.2 (1.0 to 1.4)
Triglycerides, mmol/L	1.0 (0.8 to 1.1)
Blood glucose, mmol/L	5.6 (5.3 to 5.9)
Creatinine, µmol/L	70.5 (60.5 to 81.1))
MDRD-eGFR, mL/min/1.73 m^2	88.6 (78.2 to 100.3)
Medication, %	
- Lipid lowering drugs	50
- Antihypertensive drugs	60
Framingham Risk Score, %	14.5 [8.5 to 21.8]

Values are mean (95 % confidence interval), %, or median [25 and 75 percentiles] for 10 subjects. The 95 % confidence interval was determined by a bootstrap of 2,000 samples.

on these parameters, the blood-pool-corrected SUV_{MAX} and SUV_{MEAN} ($cSUV_{MAX}$ and $cSUV_{MEAN}$) **(16)**, the maximum and mean target-to-background ratio (TBR_{MAX} and TBR_{MEAN}), and the PVE-corrected SUV_{MEAN} ($pvcSUV_{MEAN}$) were calculated. To determine the area and radius of the arterial lumen, a circular region of interest (ROI) was placed around the contrast-enhanced lumen on every axial slice of the CECT images. On the same images, a second ROI was drawn around the outer perimeter of the arterial wall to determine the area and radius of the descending aorta. Subtracting the luminal area and radius from the area and radius of the descending aorta yielded the arterial wall area and arterial wall thickness. The average arterial wall thickness was calculated as the sum of the arterial wall thickness obtained from all consecutive slices divided by the total number of slices. Based on the parameters obtained

Equation 1

$$\text{Bodyweight corrected SUV (g/mL)} = \frac{\text{Activity concentration (Bq/mL)} \cdot \text{decay correction factor} \cdot \text{bodyweight (g)}}{\text{Injected dosage (Bq)}}$$

Equation 2

$$\text{Background activity (Bq)} = \text{mean background activity (Bq/mL)} \cdot (\text{spillover area} - \text{arterial wall area} - \text{arterial lumen})\ (\text{mm}^2) \cdot \text{slice thickness (mm)}$$

Equation 3

$$\text{Spillover activity (Bq)} = \text{mean spillover activity (Bq/mL)} \cdot \text{spillover area (mm}^2) \cdot \text{slice thickness (mm)}$$

Equation 4

$$\text{Blood pool activity (Bq)} = \text{mean blood pool activity (Bq/mL)} \cdot \text{arterial lumen (mm}^2) \cdot \text{slice thickness (mm)}$$

Equation 5

$$\text{Partial volume corrected mean arterial wall activity concentration (Bq/mL)} = \frac{\text{Spillover activity (Bq)} - \text{blood pool activity (Bq)} - \text{background activity (Bq)}}{\text{Arterial wall area (mm}^2) \cdot \text{slice thickness (mm)}}$$

from the CECT images, the ROIs were replicated on the ^{18}FDG PET/CT images. This replication procedure was performed for every slice. On every slice, a third ROI was drawn to determine the area of spillover activity. The radius of the third ROI was equal to the radius of the second ROI plus the average arterial wall thickness. Per ROI, the maximum and mean ^{18}FDG activity concentration (Bq/mL) was determined and recalculated as the SUV_{MAX} and SUV_{MEAN} corrected for radiotracer decay and body weight (g) (**Equation 1**). The SUV_{MAX} and SUV_{MEAN} of consecutive slices were summed and divided by the number of slices, resulting in a single average SUV_{MAX} and SUV_{MEAN} value for each subject. Subsequently, the average values were corrected for blood-pool ^{18}FDG activity by subtracting the blood-pool SUV_{MEAN} to give $cSUV_{MAX}$ and $cSUV_{MEAN}$ **(16)**. The blood-pool activity was determined in the superior vena cava by placing a single circular ROI of 100 mm^2 to reduce spillover activity from the vessel wall and other adjacent ^{18}FDG-

avid structures. The TBR_{MAX} and TBR_{MEAN} were calculated by dividing the average SUV_{MAX} and SUV_{MEAN} by the blood-pool SUV_{MEAN}. The background activity was determined in the center of the left psoas major muscle at the level of the iliac crest by placing a single circular ROI of 100 mm^2 to reduce spillover activity from adjacent ^{18}FDG-avid structures. After calculating the background activity (**Equation 2**), spillover activity (**Equation 3**) and blood-pool activity (**Equation 4**), $pvcSUV_{MEAN}$ was calculated (**Equation 5**). All activity concentrations (Bq/mL) were converted to SUV (g/mL) via **Equation 1**. The quantitative image analysis is summarized in **Figure 1**.

Intra-Rater Agreement

Intra-rater agreement in determining arterial wall thickness on CECT images was assessed in five randomly selected patients 2 months after the initial analysis. Raters were masked from the results of the initial analysis. Inter-rater agreement was not determined.

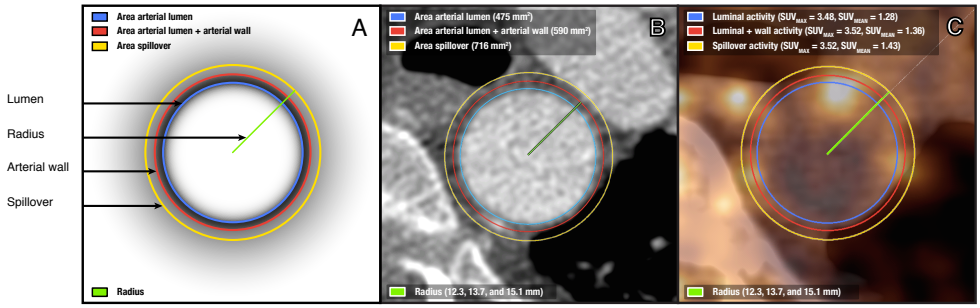

FIGURE 1 – Placement of regions of interest (ROI) around the arterial lumen (*blue line*), vessel wall (*red line*), and spillover area (*yellow line*) on (**A**) schematic, (**B**) contrast-enhanced CT image, and (**C**) superimposed ^{18}FDG PET/CT image. (**B**) First, the area of the arterial lumen (*blue ROI*) is determined on the contrast-enhanced CT image. On the same images, the area of the aorta (*red ROI*) is determined. Subtracting the luminal area (*blue*) from the aortic area (*red*) yields the arterial wall area. Subtracting their radiuses yields the arterial wall thickness. (**C**) Based on the area, arterial wall thickness, and the radiuses, the blue and red ROIs are replicated on the ^{18}FDG PET/CT image. Toward the outside of the artery, at 1.4 mm (arterial wall thickness) from the lateral border of the arterial wall, a spillover ROI (*yellow ROI*) is drawn to determine the spillover activity. Subtracting the blood-pool activity (0.89 × 475 = 423) and background activity (0.90 × (716 − 590) = 113) from the spillover activity (1.43 × 716 = 1,024), and dividing this number by the arterial wall area (590 − 475 = 115), results in the partial volume-corrected SUV_{MEAN} ($pvcSUV_{MEAN}$ = (1,024−(423+113))/115 = 4.24 g/mL). This value is 1.6 and 9.0 times greater than the blood-pool-corrected SUV_{MAX} ($cSUV_{MAX}$ = 3.52 − 0.89 = 2.63 g/mL) and SUV_{MEAN} ($cSUV_{MEAN}$ = 1.36 − 0.89 = 0.47 g/mL), respectively. Note that the blood-pool (SUV_{MEAN} = 0.89 g/mL) and background activity (SUV_{MEAN} = 0.90 g/mL) were determined in areas with minimal spillover activity from adjacent structures (i.e. the superior vena cava and the left psoas muscle, respectively) (*not shown*).

TABLE 2 – Quantitative analysis

	Mean	95 % Confidence Interval	*P* value
Aortic wall thickness, mm			.903
- 60 minutes	1.88	1.80 to 1.97	
- 180 minutes	1.89	1.80 to 1.98	
Background SUV_{MEAN}, g/mL			.079
- 60 minutes	1.20	0.93 to 1.60	
- 180 minutes	0.73	0.62 to 0.84	
Blood-pool SUV_{MEAN}, g/mL			**< .001**
- 60 minutes	1.40	1.26 to 1.56	
- 180 minutes	0.77	0.67 to 0.87	
$cSUV_{MAX}$, g/mL			**.013**
- 60 minutes	1.10	1.01 to 1.19	
- 180 minutes	1.41	1.32 to 1.49	
$cSUV_{MEAN}$, g/mL			**.008**
- 60 minutes	0.39	0.36 to 0.42	
- 180 minutes	0.54	0.51 to 0.58	
TBR_{MAX}			**.001**
- 60 minutes	1.78	1.61 to 1.96	
- 180 minutes	2.88	2.55 to 3.26	
TBR_{MEAN}			**.020**
- 60 minutes	1.28	1.17 to 1.41	
- 180 minutes	1.73	1.54 to 1.96	
$pvcSUV_{MEAN}$, g/mL			.087
- 60 minutes	3.33	3.24 to 3.40	
- 180 minutes	3.58	3.49 to 3.68	

P values and 95 % confidence interval was determined by a bootstrap of 2,000 samples. SUV, $cSUV_{MAX}$, $cSUV_{MEAN}$, TBR, and $pvcSUV_{MEAN}$ indicate standardized uptake value, blood-pool corrected SUV_{MAX}, blood-pool corrected SUV_{MEAN}, target to background ratio, and partial volume corrected SUV_{MEAN}, respectively.

Statistical Analysis

Subject demographics are summarized by descriptive statistics. Arterial ^{18}FDG uptake, quantified as $cSUV_{MAX}$, $cSUV_{MEAN}$, $pvcSUV_{MEAN}$, TBR_{MAX} and TBR_{MEAN}, are summarized and compared using the paired Student's *t* test. Differences in arterial ^{18}FDG uptake as a function of the PET acquisition time-point was also evaluated using the paired Student's *t* test. The linearity of the correlation between $pvcSUV_{MEAN}$ and $cSUV_{MAX}$, $cSUV_{MEAN}$, TBR_{MAX} and TBR_{MEAN}

was evaluated in terms of Pearson's correlation coefficient (*r*). Intra-rater agreement in determining arterial wall thickness was evaluated in terms of the intraclass correlation coefficient (ICC; two-way random effects model assessing absolute agreement of single measures) as well as 95 % limits of agreement according to the method of Bland and Altman **(17)**. A two-tailed *P* value less than .05 was regarded as statistically significant. The *P* values and 95 % confidence intervals were determined using a bootstrap of 2,000 samples. Statistical analyses were performed by IBM SPSS Statistics version 21.

RESULTS

Ten subjects at intermediate cardiovascular risk (median Framingham Risk Score of 14.5 %) underwent PET/CT imaging at 65 minutes (95 % CI = 62 to 68 minutes) and 184 minutes (95 % CI = 181 to 187 minutes) after ^{18}FDG administration (**Table 1**). Blood-pool SUV_{MEAN} significantly decreased with time (*P* < .001), whereas $cSUV_{MAX}$, $cSUV_{MEAN}$, TBR_{MAX}, and TBR_{MEAN} significantly increased with time (*P* = .013, *P* < .01, *P* < .005, and *P* = .020, respectively; **Figure 2**). Although background SUV_{MEAN} decreased and $pvcSUV_{MEAN}$ increased with time, the changes were not statistically significant (*P* = .079 and *P* = .087, respectively; **Table 2**).

TABLE 3 – The correlation between $pvcSUV_{MEAN}$ and $cSUV_{MAX}$, $cSUV_{MEAN}$, TBR_{MAX}, and TBR_{MEAN}

	Mean	95 % Confidence Interval	*P* value
$cSUV_{MAX}$, g/mL			
- 60 minutes	.69	.20 to .95	**.027**
- 180 minutes	.48	.07 to .96	.165
$cSUV_{MEAN}$, g/mL			
- 60 minutes	.66	.19 to .90	**.039**
- 180 minutes	.88	.73 to .99	**.001**
TBR_{MAX}			
- 60 minutes	.15	-.53 to .70	.671
- 180 minutes	.20	-.61 to .87	.579
TBR_{MEAN}			
- 60 minutes	.30	-.45 to .71	.404
- 180 minutes	.51	-.03 to .86	.131

P values and 95 % confidence interval was determined by a bootstrap of 2,000 samples. SUV, $cSUV_{MAX}$, $cSUV_{MEAN}$, TBR, and $pvcSUV_{MEAN}$ indicate standardized uptake value, blood-pool corrected SUV_{MAX}, blood-pool corrected SUV_{MEAN}, target to background ratio, and partial volume corrected SUV_{MEAN}, respectively.

At 60 minutes, $pvcSUV_{MEAN}$ was on average 3.1 times greater than $cSUV_{MAX}$ (3.33 g/mL [95 % CI = 3.24 to 3.40] *versus* 1.10 g/mL [95 % CI = 1.01 to 1.19]; $P < .001$) and 8.5 times greater than $cSUV_{MEAN}$ (3.33 g/mL [95 % CI = 3.24 to 3.40] *versus* 0.39 g/mL [95 % CI = 0.36 to 0.42]; $P < .001$). At 180 minutes, $pvcSUV_{MEAN}$ was on average 2.6 times greater than $cSUV_{MAX}$ (3.58 g/mL [95 % CI = 3.49 to 3.68] *versus* 1.41 g/mL [95 % CI = 1.32 to 1.49]; $P < .001$) and 6.6 times greater than $cSUV_{MEAN}$ (3.58 g/mL [95% CI = 3.49 to 3.68] *versus* 0.54 g/mL [95 % CI = 0.51 to 0.58]; $P < .001$).

At 60 minutes, both $cSUV_{MAX}$ and $cSUV_{MEAN}$ were linearly correlated with $pvcSUV_{MEAN}$ ($r = .69$; $P = .027$ and $r = .66$; $P = .039$, respectively). At 180 minutes, only $cSUV_{MEAN}$ was linearly correlated with $pvcSUV_{MEAN}$ ($r = .88$; $P = .001$; **Figure 3**). TBR_{MAX} and TBR_{MEAN} were not related to $pvcSUV_{MEAN}$, neither at 60 minutes nor at 180 minutes (**Table 3**).

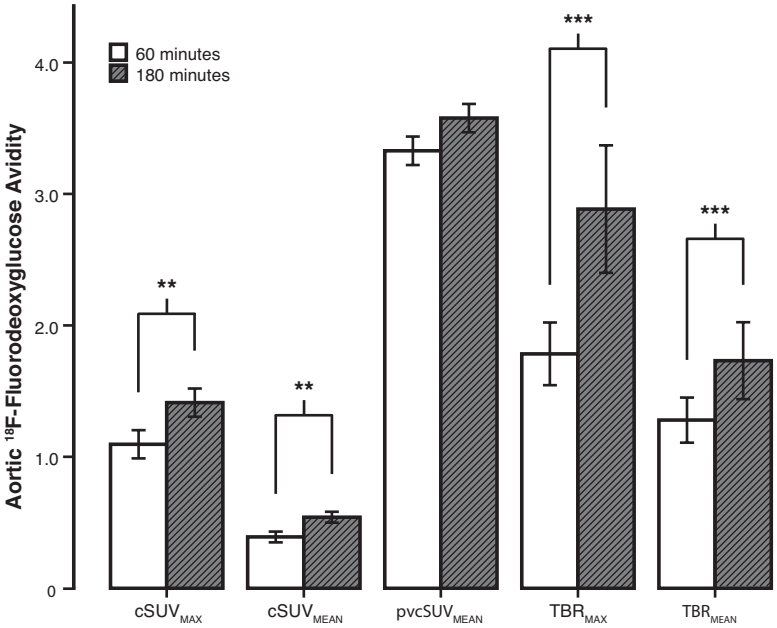

FIGURE 2 – Aortic ^{18}FDG activity at 60 and 180 minutes after ^{18}FDG administration. The blood-pool corrected SUV_{MAX} ($cSUV_{MAX}$), the blood-pool corrected SUV_{MEAN} ($cSUV_{MEAN}$), and corresponding target-to-background ratios (TBR), significantly increased with time. The partial volume corrected SUV_{MEAN} ($pvcSUV_{MEAN}$) was invariant to time. At 60 minutes, the $pvcSUV_{MEAN}$ was on average 3.1 times greater than the $cSUV_{MAX}$ ($P < .001$) and 8.5 times greater than the $cSUV_{MEAN}$ ($P < .001$). At 180 minutes, the $pvcSUV_{MEAN}$ was on average 2.6 times greater than the $cSUV_{MAX}$ ($P < .001$) and 6.6 times greater than the $cSUV_{MEAN}$ ($P < .001$). *Error bars* represent the 95 % confidence interval of the mean. ** $P < .01$, *** $P < .001$ established by the paired Student's *t* test.

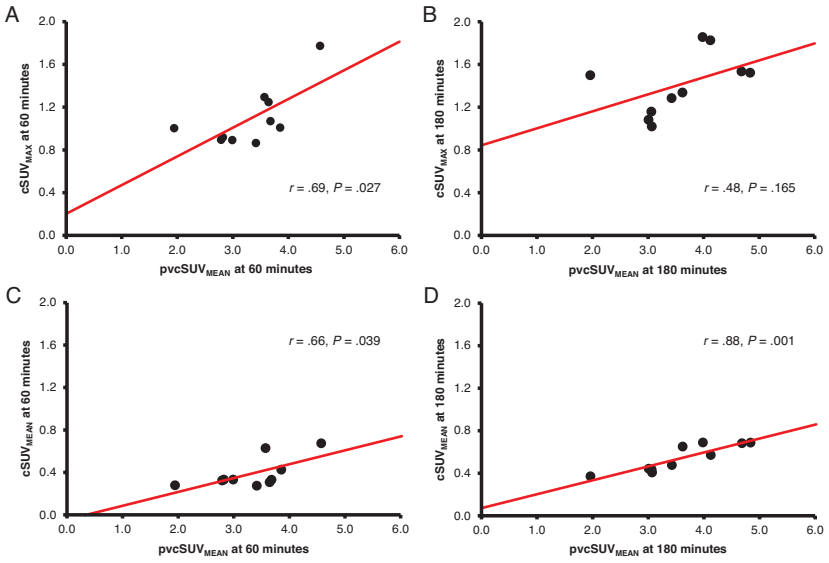

FIGURE 3 – Scatterplot depicting the correlation between the partial volume corrected SUV_{MEAN} ($pvcSUV_{MEAN}$) and the blood-pool corrected SUV_{MAX} ($cSUV_{MAX}$) (**A**, **B**) and $pvcSUV_{MEAN}$ and the blood-pool corrected SUV_{MEAN} ($cSUV_{MEAN}$) (**C**, **D**) at 60 (**A**, **C**) and 180 minutes (**B**, **D**) after ^{18}FDG administration.

Intra-rater agreement in determining aortic wall thickness calculated per slice was considered modest as indicated by an ICC of 0.38 (95 % CI = 0.31 to 0.45). The intra-rater agreement in determining average aortic wall thickness was considered excellent as indicated by an ICC of 0.98 (95 % CI = 0.81 to 1.00) with narrow 95 % limits of agreement (**Figure 4**).

DISCUSSION

Our study demonstrates that PVE significantly influences quantification of arterial wall ^{18}FDG uptake. Our findings indicate that CECT-assisted measurement of vessel wall $pvcSUV_{MEAN}$ is feasible and the numbers generated are likely to be more accurate than the currently employed ^{18}FDG PET indices (i.e. SUV_{MEAN}, SUV_{MAX}, $cSUV_{MEAN}$, $cSUV_{MAX}$, TBR_{MEAN}, TBR_{MAX}) at both 60 and 180 minutes after injection, but the method still needs to be confirmed in phantom studies. The increase in SUV after performing PVE correction is in line with studies investigating the impact of PVE on ^{18}FDG uptake in oncological and inflammatory diseases **(15, 18, 19)**. Nonetheless, among the indices, $cSUV_{MAX}$ and $cSUV_{MEAN}$ at 60 minutes and $cSUV_{MEAN}$ at 180 minutes were linearly correlated with $pvcSUV_{MEAN}$. $cSUV_{MEAN}$ at 180 minutes had the highest

linear correlation with PVE-corrected vessel wall ^{18}FDG uptake measurements and could be a reliable substitute for pvcSUV$_{MEAN}$.

The impact of PVE on quantification of arterial ^{18}FDG uptake has been previously studied. Izquierdo-Garcia and colleagues evaluated carotid ^{18}FDG uptake in seven patients with a recent transient ischaemic attack **(20)**. Stand-alone PET images were acquired 120 minutes after injection of 190 MBq of ^{18}FDG. In addition, MRI was performed for anatomic orientation. Arterial ^{18}FDG uptake was quantified as SUV$_{MEAN}$, TBR$_{MEAN}$ and ^{18}FDG influx rate determined by Patlak analysis. These parameters were corrected for PVE based on the geometric transfer matrix method **(21)**. PVE correction marginally increased the SUV$_{MEAN}$ by 5.7 %. The TBR$_{MEAN}$ and the influx rate did not significantly increase after PVE correction. These findings are in contrast to our study in which PVE correction significantly increased cSUV$_{MEAN}$ by over 800 % and 600 % at 60 and 180 minutes after ^{18}FDG administration, respectively. Despite differences in study methodology (i.e. assessment of the aorta *versus* carotid artery, CECT-based *versus* MRI-based PVE correction, and acquisition time-points of 60 and 180 minutes *versus* 120 minutes), it remains difficult to attribute the discrepant study results to methodological differences only. Differences in PVE correction algorithms are more likely to explain the discrepant results. This hypothesis finds support in a phantom study **(22)** in which the impact of PVE on quantification of aortic ^{18}FDG uptake was evaluated. Based on PET images which simulated the aorta at 60 minutes after administration of 300 MBq of ^{18}FDG, the TBR$_{MEAN}$ and the PVE-corrected TBR$_{MEAN}$ were calculated and compared to the true TBR which was primarily defined in the model. Two methods were used for PVE correction: a method based on arterial wall ^{18}FDG activity, arterial wall thickness, and a Gaussian point-spread function and another method called a geometric transfer matrix method **(21)**. The Gaussian point-spread function-corrected TBR$_{MEAN}$ was strongly correlated with the true TBR (R^2 = .94), but overestimated the true TBR by approximately 60 %. The geometric transfer matrix-corrected TBR$_{MEAN}$ significantly underestimated the true TBR (72 %), but also showed a strong correlation with the true TBR (R^2 = .89). On average, Gaussian point-spread function PVE correction increased TBR$_{MEAN}$ by 550 %. On average, geometric transfer matrix-based PVE correction increased TBR$_{MEAN}$ by 193 %. These results suggest that PVE correction algorithms strongly influence quantification of arterial ^{18}FDG avidity. Therefore, the discrepant results observed between the studies might be a reflection of the different PVE correction algorithms.

Although our study demonstrated that PVE correction significantly influenced quantification of arterial wall ^{18}FDG uptake, it remains to be seen whether correction for PVE

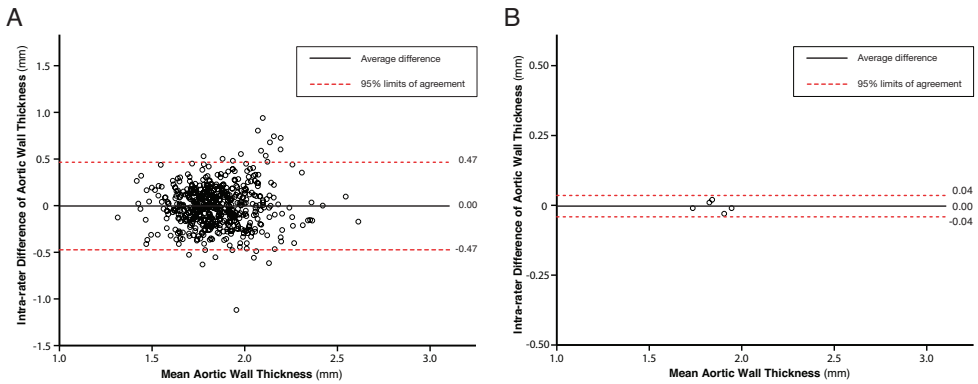

FIGURE 4 – Intra-rater agreement in determining aortic wall thickness as quantified on contrast-enhanced CT images in patients. (**A**) Analysis per slice. Although the average intra-rater difference is small, intra-rater reliability was modest (ICC = 0.38, 95 % CI = 0.31 to 0.45). (**B**) Average aortic wall thickness analysis. In contrast to the per slice analysis, both agreement and reliability are excellent (ICC = 0.98, 95 % CI = 0.81 to 1.00).

is relevant. In addition, our study lacks an accurate reference test of arterial inflammation. Histology of the arterial wall is generally regarded as the reference standard for assessment of arterial inflammation. However, ethical standards prevent collection of arterial specimens in humans. Phantom or animal studies are better suited for this purpose.

So far, only MRI has been successfully used for PVE correction of arterial ^{18}FDG uptake **(20)**. Our study demonstrated the feasibility of CECT imaging for this purpose. Based on arterial wall thickness on CECT, arterial ^{18}FDG uptake could be corrected for PVE. Our study demonstrated that the average aortic wall thickness could be determined with excellent intra-rater agreement. Previously, we have reported excellent inter-rater and intra-rater agreement in determining aortic wall ^{18}FDG uptake indices **(16)**. Therefore, CECT-based PVE correction of arterial ^{18}FDG uptake can be achieved with excellent intra-rater agreement. Nonetheless, we acknowledge that manual placement of ROIs for PVE correction can introduce variability among raters. To overcome variability among raters, automated algorithms for placement of ROIs around the aortic wall have been developed **(23)**. CECT-assisted PVE correction of arterial wall ^{18}FDG uptake may benefit from such computerized ROI placement algorithms.

Another potential source of error in our study relates to excessive spill-in activity from adjacent ^{18}FDG avid structures. Our study defined background activity by calculating the average ^{18}FDG activity in resting skeletal muscle. However, background ^{18}FDG activity

can exceed that of resting skeletal muscle, for example in tissues such as perivascular fat and bone marrow. This may result in overestimated values of arterial wall ^{18}FDG uptake with PVE correction. On the other hand, background ^{18}FDG activity can be lower than that of resting skeletal muscle, for example in tissues such as lung. This may result in underestimated values of arterial wall ^{18}FDG uptake with PVE correction. More sophisticated PVE correction techniques that take into account variations in background activity may further improve quantification of arterial wall ^{18}FDG uptake.

Lastly, patient movement, pulsatile blood flow, and the cardiac and respiratory cycles amplify PVE and may introduce misalignment between PET and coregistered CT images. The impact of these variations on quantification of arterial wall ^{18}FDG uptake was not part of the experimental design of this study, and was therefore not investigated. However, considering our observations that PVE correction significantly influenced quantification of arterial wall ^{18}FDG uptake, it seems likely that motion compensation could further improve quantification of arterial wall ^{18}FDG uptake.

Conclusions

In conclusion, CECT-assisted PVE correction seems to significantly influence quantification of arterial wall ^{18}FDG uptake. $pvcSUV_{MEAN}$ did not significantly increase with time. $cSUV_{MEAN}$ and $cSUV_{MAX}$ at 60 minutes after tracer injection were correlated with $pvcSUV_{MEAN}$, but $cSUV_{MEAN}$ at 180 minutes had the highest correlation with $pvcSUV_{MEAN}$. Therefore, $cSUV_{MEAN}$ determined at 180 minutes after injection of ^{18}FDG could be a substitute for $pvcSUV_{MEAN}$ as a measure of arterial ^{18}FDG uptake.

REFERENCES

1. Folco EJ, Sheikine Y, Rocha VZ, et al. Hypoxia but not Inflammation Augments Glucose Uptake in Human Macrophages: Implications for Imaging Atherosclerosis with ^{18}Fluorine-Labeled 2-Deoxy-D-Glucose Positron Emission Tomography. *J Am Coll Cardiol*. 2011; **58**: 603-14.

2. Rudd JH, Warburton EA, Fryer TD, et al. Imaging Atherosclerotic Plaque Inflammation with [^{18}F]-Fluorodeoxyglucose Positron Emission Tomography. *Circulation*. 2002; **105**: 2708-11.

3. Bural GG, Torigian DA, Botvinick E, et al. A Pilot Study of Changes in ^{18}F-FDG Uptake, Calcification and Global Metabolic Activity of the Aorta with Aging. *Hell J Nucl Med*. 2009; **12**: 123-8.

4. Tawakol A, Fayad ZA, Mogg R, et al. Intensification of Statin Therapy Results in a Rapid Reduction in Atherosclerotic Inflammation: Results of a Multi-Center FDG-PET/CT Feasibility Study. *J Am Coll Cardiol*. 2013; **62**: 909-17.

5. Tahara N, Kai H, Ishibashi M, et al. Simvastatin Attenuates Plaque Inflammation: Evaluation by Fluorodeoxyglucose Positron Emission Tomography. *J Am Coll Cardiol*. 2006; **48**: 1825-31.

6. Rominger A, Saam T, Wolpers S, et al. ^{18}F-FDG PET/CT Identifies Patients at Risk for Future Vascular Events in an Otherwise Asymptomatic Cohort with Neoplastic Disease. *J Nucl Med*. 2009; **50**: 1611-20.

7. Bucerius J, Mani V, Moncrieff C, et al. Impact of Non-Insulin-Dependent Type 2 Diabetes on Carotid Wall ^{18}F-Fluorodeoxyglucose Positron Emission Tomography Uptake. *J Am Coll Cardiol*. 2012;59:2080-8.

8. Rudd JH, Myers KS, Bansilal S, et al. Atherosclerosis Inflammation Imaging with ^{18}F-FDG PET: Carotid, Iliac, and Femoral Uptake Reproducibility, Quantification Methods, and Recommendations. *J Nucl Med*. 2008; **49**: 871-8.

9. Kim TN, Kim S, Yang SJ, et al. Vascular Inflammation in Patients with Impaired Glucose Tolerance and Type 2 Diabetes: Analysis with ^{18}F-Fluorodeoxyglucose Positron Emission Tomography. *Circ Cardiovasc Imaging*. 2010; **3**: 142-8.

10. Bucerius J, Duivenvoorden R, Mani V, et al. Prevalence and Risk Factors of Carotid Vessel Wall Inflammation in Coronary Artery Disease Patients: FDG-PET and CT Imaging Study. *J Am Coll Cardiol Img*. 2011; **4**: 1195-205.

11. Menezes LJ, Kotze CW, Hutton BF, et al. Vascular Inflammation Imaging with ^{18}F-FDG PET/CT: When to Image? *J Nucl Med*. 2009; **50**: 854-7.

12. Basu S, Zaidi H, Houseni M, et al. Novel Quantitative Techniques for Assessing Regional

and Global Function and Structure Based on Modern Imaging Modalities: Implications for Normal Variation, Aging, and Diseased States. *Semin Nucl Med*. 2007; **37**: 223-39.

13. Mensel B, Quadrat A, Schneider T, et al. MRI-Based Determination of Reference Values of Thoracic Aortic Wall Thickness in a General Population. *Eur Radiol*. 2014; **24**: 2038-44.

14. Shakeri A, Hafez Quran F, Javadrashid R, et al. Correlation Between Aortic Wall Thickness and Coronary Artery Disease by 64 Slice Multidetector Computed Tomography. *J Cardiovasc Thorac Res*. 2013; **5**: 91-5.

15. Sanchez-Crespo A, Andreo P, Larsson SA. Positron Flight in Human Tissues and Its Influence on PET Image Spatial Resolution. *Eur J Nucl Med Mol Imaging*. 2004; **31**: 44-51.

16. Blomberg BA, Thomassen A, Takx RA, et al. Delayed ^{18}F-Fluorodeoxyglucose PET/CT Imaging Improves Quantitation of Atherosclerotic Plaque Inflammation: Results from the CAMONA Study. *J Nucl Cardiol.* 2014; **21**: 588-97.

17. Bland JM, Altman DG. Statistical Methods for Assessing Agreement Between Two Methods of Clinical Measurement. *Lancet*. 1986; **1**: 307-10.

18. Salavati A, Borofsky S, Boon-Keng TK, et al. Application of Partial Volume Effect Correction and 4D PET in the Quantification of FDG Avid Lung Lesions. *Mol Imaging Biol*. 2015; **17**: 140-8.

19. Saboury B, Salavati A, Brothers A, et al. FDG PET/CT in Crohn's Disease: Correlation of Quantitative FDG PET/CT Parameters With Clinical and Endoscopic Surrogate Markers of Disease Activity. *Eur J Nucl Med Mol Imaging*. 2014; **41**: 605-14

20. Izquierdo-Garcia D, Davies JR, Graves MJ, et al. Comparison of Methods for Magnetic Resonance-Guided [^{18}F]-Fluorodeoxyglucose Positron Emission Tomography in Human Carotid Arteries: Reproducibility, Partial Volume Correction, and Correlation Between Methods. *Stroke*. 2009; **40**: 86-93.

21. Rousset OG, Ma Y, Evans AC. Correction for Partial Volume Effects in PET: Principle and Validation. *J Nucl Med*. 1998; **39**: 904-11.

22. Burg S, Dupas A, Stute S, Dieudonne A, et al. Partial Volume Effect Estimation and Correction in the Aortic Vascular Wall in PET Imaging. *Phys Med Biol*. 2013; **58**: 7527-42.

23. Reeps C, Bundschuh RA, Pellisek J, et al. Quantitative Assessment of Glucose Metabolism in the Vessel Wall of Abdominal Aortic Aneurysms: Correlation With Histology and Role of Partial Volume Correction. *Int J Cardiovasc Imaging*. 2013; **29**: 505-12

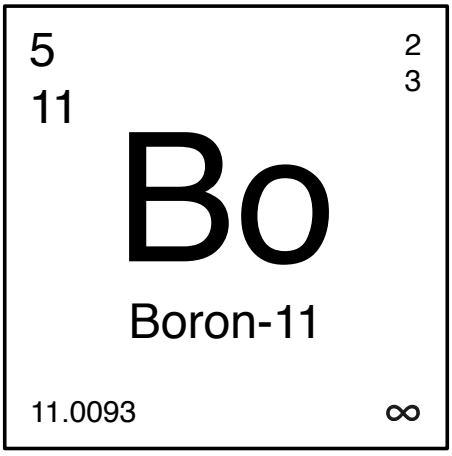
5
11
2
3
Bo
Boron-11
11.0093
∞

Chapter 5

Impact of Personal Characteristics and Technical Factors on Quantification of [^{18}F]-Fluorodeoxyglucose Uptake in Human Arteries: Prospective Evaluation of Healthy Subjects

Björn A. Blomberg
Anders Thomassen
Pim A. de Jong
Marnix G.E.H. Lam
Poul-Erik N. Braad
Axel C.P. Diederichsen
Werner Vach
Willem P.T.M. Mali
Abass Alavi
Poul F. Høilund-Carlsen

Submitted

ABSTRACT

Background: [^{18}F]-fluorodeoxyglucose (^{18}FDG) PET/CT is a promising imaging technique for assessment of atherosclerosis, but is hampered by a lack of validated quantification protocols. Both personal characteristics and technical factors can affect quantification of arterial ^{18}FDG uptake. This study investigated if blood activity, plasma glucose, renal function, body weight, circulating time, and PET/CT system affect quantification of arterial ^{18}FDG uptake.

Methods: Eighty-nine healthy subjects were prospectively examined by ^{18}FDG PET/CT imaging. Arterial ^{18}FDG uptake was quantified at the level of the ascending aorta, aortic arch, descending thoracic aorta, and carotid arteries by calculating the maximum ^{18}FDG activity (FDG_{MAX}), the maximum target-to-background ratio ($TBR_{MAX/MEAN}$), and the maximum blood subtracted ^{18}FDG activity ($_{BS}FDG_{MAX}$). Multivariable linear regression assessed the impact of personal characteristics and technical factors on quantification of arterial ^{18}FDG uptake.

Results: FDG_{MAX} and $TBR_{MAX/MEAN}$ were dependent on blood activity (β = .26 to .51; P < .026 and β = -.51 to -.32; P < .017) and PET/CT system (β = -.86 to -.26; P < .028 and β = -.78 to -.26; P < .021). $_{BS}FDG_{MAX}$ depended on PET/CT system (β = -.89 to -.27; P < .019), but not blood activity. This finding was observed at the level of the ascending aorta, aortic arch, descending thoracic aorta, as well as the carotid arteries. In addition to blood activity and PET/CT system, body weight affected quantification of arterial ^{18}FDG uptake, whereas plasma glucose, renal function, and circulating time did not.

Conclusion: Prospective evaluation of 89 healthy subjects demonstrated that quantification of arterial ^{18}FDG uptake is affected by blood activity, body weight, and PET/CT system. Therefore, blood activity, body weight, and PET/CT system should be taken into account to generate accurate estimates of arterial ^{18}FDG uptake.

INTRODUCTION

[^{18}F]-fluorodeoxyglucose (^{18}FDG) positron emission tomography/computed tomography (PET/CT) is a promising non-invasive imaging technique for assessment of atherosclerosis. By targeting atherosclerotic plaque glycolysis, a surrogate of plaque inflammation and hypoxia **(1, 2)**, ^{18}FDG PET/CT imaging can potentially detect and quantify atherosclerotic plaque inflammation **(2)**, evaluate response to treatment **(3, 4)**, and prognosticate risk for atherosclerosis related disease **(5)**.

Although ^{18}FDG PET/CT imaging of atherosclerosis is promising, implementing ^{18}FDG PET/CT imaging of atherosclerosis in research and clinical settings is hampered by a lack of validated and standardized quantification protocols **(6, 7)**. Lack of standardization led to introduction of numerous methods to quantify arterial ^{18}FDG uptake ranging from simple visual analysis to sophisticated techniques such as calculation of the ^{18}FDG influx rate by a Patlak plot **(7, 8)**. The optimal method to quantify arterial ^{18}FDG uptake remains undetermined. Moreover, quantification of arterial ^{18}FDG uptake can be affected by personal characteristics and technical factors, including blood ^{18}FDG activity, body weight, body surface area, plasma glucose, renal function, injected ^{18}FDG dose, ^{18}FDG circulating time, and PET/CT system. It is not known which factors affect quantification of arterial ^{18}FDG uptake. Standardized and unbiased quantification of arterial ^{18}FDG uptake is imperative for both research and clinical settings, being a prerequisite for generation of reference values for arterial ^{18}FDG uptake with healthy aging, for response evaluation requiring repeat ^{18}FDG PET/CT examinations, and to allow for comparison of quantitative imaging results among studies.

The purpose of this study was to determine the effect of personal characteristics and technical factors on quantification of arterial ^{18}FDG uptake. By studying these effects in a group of healthy subjects we aimed to generate accurate estimates of arterial ^{18}FDG uptake. Secondary aims were to elucidate the effects of quantification methods on estimates of arterial ^{18}FDG uptake, to determine the optimal location for assessment of blood activity, and, finally, to evaluate rater reliability and agreement.

METHODS

This study is part of the "Cardiovascular Molecular Calcification Assessed by ^{18}F-NaF PET/CT" (CAMONA) study. CAMONA was approved by the Danish National Committee on Health Research Ethics, registered at ClinicalTrials.gov (NCT01724749), and conducted in accordance

with the Declaration of Helsinki. Written informed consent was obtained from all study subjects.

Subject Selection

Healthy subjects were prospectively recruited from the general population by local advertisement or from the blood bank of Odense University Hospital, Denmark. Subjects free of oncologic disease, autoimmune disease, immunodeficiency syndromes, alcohol abuse, illicit drug use, (symptoms suggesting) cardiovascular disease, or prescription medication were considered healthy and were eligible for inclusion. Pregnant women were not considered for inclusion. Healthy subjects were recruited to limit bias from cardiovascular risk factors on study results. Subjects were preselected by sex and age to secure a balanced inclusion of males

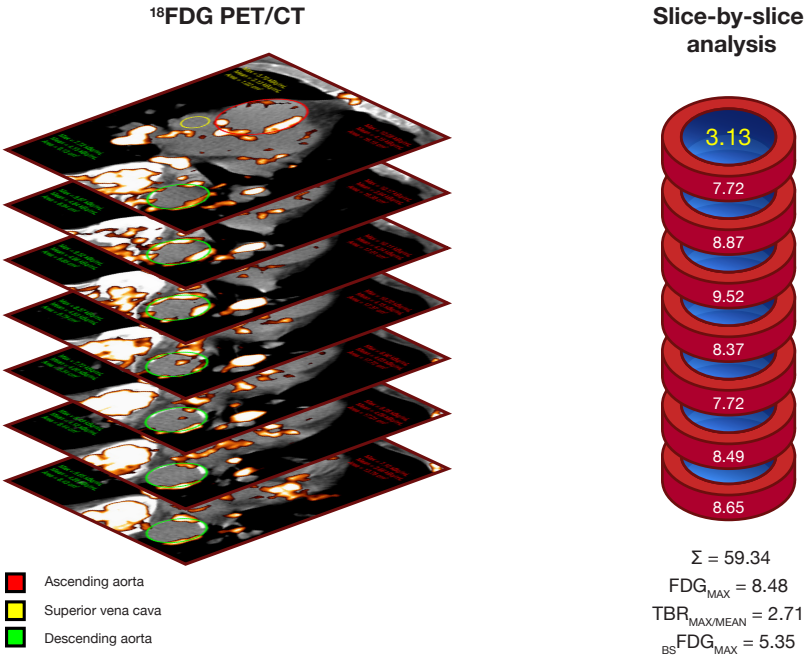

FIGURE 1 – Illustration demonstrating quantification of arterial [^{18}F]-fluorodeoxyglucose (^{18}FDG) uptake. A region of interest (ROI) is drawn around the arterial wall (*red* ROI = ascending aorta, *green* ROI = descending aorta) on every slice of the axially oriented ^{18}FDG PET/CT images. Per ROI, the maximum ^{18}FDG activity is determined. Values obtained per ROI are summed (Σ) and averaged (FDG_{MAX}) and subsequently divided or subtracted by the mean venous ^{18}FDG blood activity ($_{BLOOD}FDG_{MEAN}$). This provides the target-to-background ratio ($TBR_{MAX/MEAN}$) or the blood subtracted ^{18}FDG activity ($_{BS}FDG_{MAX}$), respectively. In this illustration, $_{BLOOD}FDG_{MEAN}$ was estimated in the superior vena cava (*yellow* ROI).

and females aged 20–29, 30–39, 40–49, 50–59, > 60 years. This allowed us to study a wide range of subjects to ensure translation of our findings to various settings.

Study Design

Healthy subjects were evaluated by blood pressure measurements, blood analyses, ^{18}FDG PET/CT imaging, and non-contrast enhanced cardiac CT imaging. Blood pressure measurements were performed thrice after a supine rest of at least 30 minutes. The average of the last two measurements determined the systolic and diastolic blood pressure. Blood analyses included fasting serum total cholesterol, serum LDL cholesterol, serum HDL cholesterol, serum triglycerides, fasting plasma glucose, glycated hemoglobin (HbA1c), serum creatinine, the latter being used to calculate the Modification of Diet and Renal Disease (MDRD) estimated glomerular filtration rate (eGFR). Furthermore, we determined body weight, body height, body mass index, and body surface area according to Du Bois. ^{18}FDG PET/CT imaging was performed on integrated PET/CT systems (GE Discovery 690/710, STE, VCT, and RX) at the PET center of Odense University Hospital, Denmark. Subjects were allocated to a PET/CT system at the discretion of the department's booking system. PET/CT system specifications and image reconstruction parameters are summarized in **SUPPLEMENTARY TABLE 1**. Each subject underwent PET/CT imaging at approximately 180 minutes after intravenous injection of approximately 4.0 MBq of ^{18}FDG per kilogram of body weight **(9)**. The ^{18}FDG was administered after an overnight fast of at least 8 hours. Prior to ^{18}FDG injection, the blood glucose concentration was determined to secure a value below 8 mmol/L. Subjects rested in a quiet and warm room between ^{18}FDG administration and PET/CT acquisition. The emission acquisition duration per bed position was 3.5 minutes. Total body PET images were acquired in 3D–mode and reconstructed into coronal, axial, and sagittal planes by an ordered subsets expectation maximization algorithm (GE VUE Point). PET images were corrected for attenuation, scatter, random coincidences, and scanner dead time. Low–dose CT imaging (140 kV, 30-110 mA, noise index 25, 0.8 seconds per rotation, slice thickness 3.75 mm) was performed for attenuation correction and anatomic orientation. To determine the coronary calcium score, non-contrast enhanced, breath-hold, cardiac CT imaging (120 kV, 100 mA, 0.4 seconds per rotation, slice thickness 2.5 mm) was performed with electrocardiogram gating at 50 % of the R–R interval. The effective radiation dosage received for the entire imaging protocol was approximately 14 mSv.

Quantitative Image Analyses

All images were analyzed by version 4.0 of the Philips IntelliSpace Portal client. The image

analyst was masked to subject demographics and PET/CT system specifications. For each subject, uptake of ^{18}FDG was determined in the ascending aorta, aortic arch, descending thoracic aorta, and carotid arteries according to previously published methods **(9)**. In summary, an oval region of interest (ROI) was manually placed around the outer perimeter of the artery on every slice of the attenuation corrected axially oriented PET/CT images. We carefully excluded cardiac and bone marrow derived ^{18}FDG activity by eliminating these areas from the ROI. Per ROI, the maximum radiotracer-decay corrected ^{18}FDG activity (kBq/mL) was determined. Per arterial bed, maximum values obtained per ROI were summed and divided by the number of ROIs resulting in a single averaged maximum value (FDG_{MAX}) for the ascending aorta, aortic arch, descending thoracic aorta, right carotid artery, and left carotid artery, respectively. Blood ^{18}FDG activity was determined in the lumen of the right atrium, aortic arch, right and left internal jugular vein, superior and inferior vena cava, and the right and left femoral vein. Blood ^{18}FDG activity was determined by drawing a single ROI in the center of each vessel (or atrium) and quantified as the radiotracer-decay corrected mean ^{18}FDG activity ($_{BLOOD}FDG_{MEAN}$). Quantification of blood ^{18}FDG activity is summarized in **SUPPLEMENTARY FIGURE 1**. To correct for blood ^{18}FDG activity, FDG_{MAX} was divided and subtracted by $_{BLOOD}FDG_{MEAN}$, respectively, to generate the maximum target-to-background ratio ($TBR_{MAX/MEAN}$) and maximum blood subtracted ^{18}FDG activity ($_{BS}FDG_{MAX}$). Quantification of arterial ^{18}FDG uptake is summarized in **FIGURE 1**. The coronary calcium score, obtained from the cardiac CT images, was quantified in arbitrary units according to Agatston and as a volumetric score (mm^3) **(10)**.

Rater Reliability and Agreement

Inter- and intra-rater reliability and agreement of FDG_{MAX} and $_{BLOOD}FDG_{MEAN}$ were assessed two months after the initial analysis in a randomly selected sample of 10 subjects. Raters were masked for subject demographics, imaging specifications, and results from the initial analysis.

Statistical Analysis

Subject demographics were summarized by descriptive statistics. Mean $_{BLOOD}FDG_{MEAN}$ was compared among vessel beds by the repeated measures one-way analysis of variance (ANOVA). Multivariable linear regression assessed the dependence of $_{BLOOD}FDG_{MEAN}$, FDG_{MAX}, $TBR_{MAX/MEAN}$, and $_{BS}FDG_{MAX}$ on personal characteristics and technical factors. We did not evaluate non-linear or interaction effects. First, we tested if the assumptions of no multicollinearity (tolerance statistic), independent errors (Durbin-Watson statistic), and homoscedasticity (graphically) between predictor variables were met. The assumption of no multicollinearity was violated

TABLE 1 - Subject demographics

	Total (*N* = 89)	**Minimum**	**Maximum**
Age, years	44 ± 14	21	75
Male, %	53		
Active smoking, %	3		
Blood pressure, mmHg			
- Systolic	128 ± 17	98	201
- Diastolic	77 ± 10	57	107
Body weight, kg	80 ± 18	50	145
Body surface area, m^2	1.93 ± 0.24	1.52	2.67
Body mass index, kg/m^2	27 ± 4	18	42
Cholesterol, mmol/L			
- Total	4.9 ± 0.9	2.9	7.4
- LDL	3.1 ± 0.8	1.3	5.0
- HDL	1.4 ± 0.5	0.7	3.2
Triglycerides, mmol/L	1.0 ± 0.7	0.3	4.5
Plasma glucose, mmol/L	5.5 ± 0.5	4.4	6.7
HbA1c (mmol/mol)	33.9 ± 4.1	24.0	49.0
Creatinine, µmol/L	79.3 ± 13.1	52.0	118.0
MDRD-eGFR, mL/min/1.73 m^2	82.9 ± 13.2	55.0	113.0
Coronary calcium score			
- Agatston score, arbitrary units	0 [0 to 0]	0	1046
- Volume, mm^3	0 [0 to 0]	0	430
Injected dose, MBq	306 ± 59	194	428
Circulation time, minutes	181 ± 4	174	192
FDG_{MAX}, kBq/mL			
- Ascending aorta	8.91 ± 2.70	4.92	16.74
- Aortic arch	8.64 ± 2.58	4.94	18.22
- Descending thoracic aorta	8.24 ± 2.04	4.93	15.60
- Right carotid artery	6.71 ± 1.86	3.49	13.98
- Left carotid artery	6.92 ± 2.53	3.73	19.63
PET/CT system, %			
- GE Discovery STE	24		
- GE Discovery VCT	20		
- GE Discovery RX	31		
- GE Discovery 690/710	25		

Values are mean ± standard deviation, %, or median [25 and 75 percentiles] for 89 subjects.

by our predictor variables. Multicollinearity existed between injected dose, body weight, and body surface area (**SUPPLEMENTARY FIGURE 2**). The issue of multicollinearity was resolved by removing injected dose and body surface area from the regression analyses. Subsequently, stepwise selection of variables, based on Akaike's information criterion, was performed by a backward elimination strategy. "PET/CT system" was entered as factor into the model with the GE Discovery 690/710 as reference system. Variables not selected by the model were considered not related to arterial ^{18}FDG uptake. Variability in variable selection was evaluated and adjusted for by a bootstrap of 2,000 samples **(11)**. Rater reliability was assessed by the intra-class correlation coefficient (ICC) (two-way random effects model assessing absolute agreement of single measures) **(12)**. Rater agreement was assessed by calculation of the 95

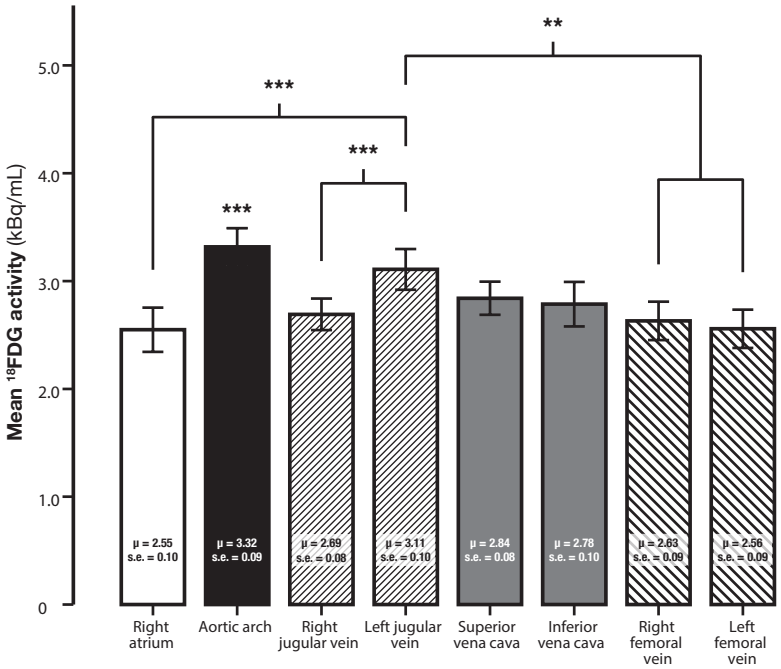

FIGURE 2 – Mean ^{18}FDG blood activity ($_{BLOOD}FDG_{MEAN}$) estimated in various vascular beds at 180 minutes after injection of ^{18}FDG. Blood activity in the aortic arch was significantly higher (P < .001) compared with other vascular beds, except for the left internal jugular vein (P = .999). Activity in the left internal jugular vein was significantly higher compared with the right internal jugular vein (P < .001), right atrium (P < .001), and femoral veins (P < .005). $_{BLOOD}FDG_{MEAN}$ in the right atrium, right internal jugular vein, superior vena cava, inferior vena cava, and femoral veins were not significantly different. *Error bars* represent the 95 % confidence interval of the mean. * P < .05, ** P < .01, *** P < .001 based on the repeated measures ANOVA with a Bonferroni correction. μ = mean; s.e. = standard error of the mean.

% limits of agreement according to Bland and Altman **(13)**. A two-tailed *P* value below .05 was regarded statistically significant. To internally validate our results, *P* values and 95 % confidence intervals were determined by a bootstrap of 2,000 samples. The sample size was based on the regression analysis. Statistical analyses were performed by statistical software R version 3.1.2 combined with the packages 'bootStepAIC' version 1.2-0, 'MASS' version 7.3-35, 'car' version 2.0-22, and 'QuantPsyc' version 1.5.

RESULTS

Between November 2012 and May 2014 we prospectively recruited 90 healthy subjects. One subject was excluded from the study because she refused the PET/CT examination due to claustrophobia. Subject demographics are summarized in **TABLE 1**.

$_{BLOOD}$**FDG$_{MEAN}$** was significantly different among vessel beds (F = 15.8; P < .001) (**FIGURE 2**). In particular, aortic arch $_{BLOOD}$FDG$_{MEAN}$ was up to 23 % higher than $_{BLOOD}$FDG$_{MEAN}$ in other vascular beds (t = 9.4; P < .001). Surprisingly, left internal jugular vein $_{BLOOD}$FDG$_{MEAN}$ was 14 % higher than $_{BLOOD}$FDG$_{MEAN}$ in the right internal jugular vein (t = 4.9; P < .001). No significant difference existed between $_{BLOOD}$FDG$_{MEAN}$ in the right atrium, right jugular vein, superior vena cava, inferior vena cava, and femoral veins. Subsequent analyses were performed with superior vena cava $_{BLOOD}$FDG$_{MEAN}$ only, since $_{BLOOD}$FDG$_{MEAN}$ was statistically similar in the majority of vascular beds. Superior vena cava $_{BLOOD}$FDG$_{MEAN}$ was not affected by variations in plasma glucose, renal function, body weight, circulating time, or PET/CT system (**TABLE 2**).

At all levels of the arterial tree, **FDG$_{MAX}$** was significantly affected by blood activity and PET/CT system. For every kBq/mL increase in $_{BLOOD}$FDG$_{MEAN}$, FDG$_{MAX}$ increased by 0.96 to 1.18 kBq/mL for the aorta and by 1.31 to 1.37 kBq/mL for the carotid arteries. FDG$_{MAX}$ was significantly higher among subjects examined by the GE Discovery 690/710 than subjects examined by the GE Discovery STE, VCT, or RX. In addition to blood activity and PET/CT system, ascending aorta FDG$_{MAX}$ was significantly affected by body weight. For every kilogram increase in body weight, ascending aorta FDG$_{MAX}$ increased by 0.03 kBq/mL. FDG$_{MAX}$ was not affected by variations in plasma glucose, renal function, or circulating time (**TABLE 3**, **SUPPLEMENTARY TABLES 2-5**).

At all levels of the arterial tree, **TBR$_{MAX/MEAN}$** was significantly affected by blood activity and PET/CT system. For every kBq/mL increase in $_{BLOOD}$FDG$_{MEAN}$, TBR$_{MAX/MEAN}$ decreased by 0.51

to 0.63 for the aorta and by 0.34 to 0.37 for the carotid arteries. $TBR_{MAX/MEAN}$ was significantly higher among subjects examined by the GE Discovery 690/710 than subjects examined by the GE Discovery STE, VCT, or RX. In addition to blood activity and PET/CT system, ascending aorta $TBR_{MAX/MEAN}$ was significantly affected by body weight. For every kilogram increase in body weight, ascending aorta $TBR_{MAX/MEAN}$ increased by 0.01. $TBR_{MAX/MEAN}$ was not affected by variations in plasma glucose, renal function, or circulating time (**TABLE 3**, **SUPPLEMENTARY TABLES 2-5**).

At all levels of the arterial tree, $_{BS}\mathbf{FDG_{MAX}}$ was significantly affected by PET/CT system. $_{BS}FDG_{MAX}$ was significantly higher among subjects examined by the GE Discovery 690/710 than subjects examined by the GE Discovery STE, VCT, or RX. In addition to PET/CT system, ascending aorta $_{BS}FDG_{MAX}$ was significantly affected by body weight. For every kilogram increase in body weight, ascending aorta $_{BS}FDG_{MAX}$ increased by 0.03 kBq/mL. $_{BS}FDG_{MAX}$ was not affected by variations in blood activity, plasma glucose, renal function, or circulating time (**TABLE 3**, **SUPPLEMENTARY TABLES 2-5**).

Inter- and intra-rater reliability and agreement of FDG_{MAX} and $_{BLOOD}FDG_{MEAN}$ were excellent as indicated by ICCs in the range of 0.98 to 1.00 for FDG_{MAX} and 0.91 to 0.92 for the superior vena cava $_{BLOOD}FDG_{MEAN}$, respectively. Furthermore, the 95 % limits of agreement were considered small (**SUPPLEMENTARY TABLES 6**, **7**).

TABLE 2 – Determinants of mean ^{18}FDG blood activity in the superior vena cava

	Regression coefficient	β	Adjusted R^2	*P* value
			0.06	.060
Intercept, kBq/mL	3.95 (2.80 to 5.15)			**< .001**
MDRD-eGFR, mL/min/1.73 m^2	-0.01 (-0.03 to 0.00)	-.23		.090
PET/CT system				
- GE Discovery STE	-0.16 (-0.60 to 0.38)	-.09		.516
- GE Discovery VCT	-0.31 (-0.63 to 0.02)	-.20		.068
- GE Discovery RX	0.24 (-0.10 to 0.60)	.14		.200

Multivariable linear regression assessing the dependence of mean ^{18}FDG blood activity on plasma glucose, renal function, body weight, circulating time, and PET/CT system. Plasma glucose, body weight, and circulating time were eliminated by the model. β = standardized regression coefficient. The 95 % confidence interval is presented in parentheses.

DISCUSSION

Prospective evaluation of 89 healthy subjects demonstrated that quantification of arterial ^{18}FDG uptake is significantly affected by blood ^{18}FDG activity, body weight, and PET/CT system, but not plasma glucose, renal function, or ^{18}FDG circulating time. Therefore, blood activity, body weight, and PET/CT system should be taken into account to generate unbiased estimates of arterial ^{18}FDG uptake.

To account for **blood activity**, it has been advocated to calculate the ratio between arterial wall ^{18}FDG uptake and blood ^{18}FDG activity, known as the target-to-background ratio ($TBR_{MAX/MEAN}$) **(14, 15)**. However, $TBR_{MAX/MEAN}$ has been criticized to be too dependent on variations in blood activity **(7, 9, 16)**. Our study confirmed that $TBR_{MAX/MEAN}$ is dependent on variations in blood activity. Therefore, quantifying arterial ^{18}FDG uptake as $TBR_{MAX/MEAN}$ may result in biased estimates of arterial ^{18}FDG uptake. Nonetheless, studies have demonstrated a strong association between $TBR_{MAX/MEAN}$ and histologic parameters of atherosclerotic plaque inflammation. For example, a strong association was observed between $TBR_{MAX/MEAN}$ and macrophage staining in 17 carotid atherosclerotic plaque specimens obtained by endarterectomy **(17)**. This association was present for both macrophage area (R^2 = 0.58; P < .001) and % anti-CD68 (R^2 = 0.72; P = < .001). The association weakened when carotid plaque ^{18}FDG uptake was quantified as the maximum standardized uptake value (SUV), a value related to FDG_{MAX} (macrophage area: R^2 = 0.24; P < .001 and % anti-CD68: R^2 = 0.34; P < .001). In contrast, the association between macrophage staining and carotid plaque ^{18}FDG activity strengthened when arterial ^{18}FDG uptake was quantified as the blood subtracted SUV_{MAX}, a value related to $_{BS}FDG_{MAX}$ (macrophage area: R^2 = 0.64; P < .001 and % anti-CD68: R^2 = 0.77; P < .001). The fact that blood subtracted SUV_{MAX} does not depend on blood activity might explain the improved association. The results of our study combined with empirical data from the literature suggest that quantification of arterial ^{18}FDG uptake by $TBR_{MAX/MEAN}$ is suboptimal compared to $_{BS}FDG_{MAX}$. Therefore, we prefer to quantify arterial ^{18}FDG uptake as $_{BS}FDG_{MAX}$ over $TBR_{MAX/MEAN}$.

In studies that evaluate atherosclerosis with ^{18}FDG PET/CT, blood activity is commonly estimated in the superior vena cava, inferior vena cava, or jugular veins **(15, 18-21)**. However, it is not known if estimates of blood activity are comparable among vessel beds. Theoretically, blood activity should be similar in intensity throughout the body, especially after prolonged circulating times. Nonetheless, our study demonstrated that estimates of blood activity differ significantly among vascular beds. In particular, recorded blood activity was higher in the

TABLE 3 – Determinants of ^{18}FDG uptake in the ascending aorta

	Regression coefficient	β	Adjusted R^2	*P* value
1. FDG_{MAX}, kBq/mL			0.66	**< .001**
Intercept, kBq/mL	7.65 (6.13 to 9.04)			**< .001**
Blood activity, kBq/mL	0.96 (0.54 to 1.36)	0.26		**< .001**
Body weight, kg	0.03 (0.02 to 0.05)	0.20		**.002**
PET/CT system				
- GE Discovery STE	-5.09 (-6.23 to -3.86)	-0.76		**< .001**
- GE Discovery VCT	-4.69 (-5.94 to -3.35)	-0.81		**< .001**
- GE Discovery RX	-5.33 (-6.58 to -4.09)	-0.86		**< .001**
2. $TBR_{MAX/MEAN}$			0.64	**< .001**
Intercept	5.40 (4.57 to 6.50)			
Blood activity, kBq/mL	-0.63 (-0.91 to -0.49)	-0.42		**< .001**
Body weight, kg	0.01 (0.01 to 0.02)	0.21		**< .001**
PET/CT system				
- GE Discovery STE	-1.76 (-2.24 to -1.35)	-0.66		**< .001**
- GE Discovery VCT	-1.70 (-2.15 to -1.28)	-0.73		**< .001**
- GE Discovery RX	-1.95 (-2.45 to -1.48)	-0.78		**< .001**
3. $_{BS}FDG_{MAX}$, kBq/mL			0.64	**< .001**
Intercept, kBq/mL	7.54 (5.78 to 9.19)			**< .001**
Body weight, kg	0.03 (0.02 to 0.05)	0.21		**.002**
PET/CT system				
- GE Discovery STE	-5.09 (-6.29 to -3.82)	-0.79		**< .001**
- GE Discovery VCT	-4.68 (-5.89 to -3.50)	-0.84		**< .001**
- GE Discovery RX	-5.34 (-6.49 to -4.15)	-0.89		**< .001**

Multivariable linear regression assessing the dependence of ascending aorta ^{18}FDG uptake on superior vena cava blood activity, plasma glucose, renal function, body weight, circulating time, and PET/CT system. Plasma glucose, renal function, and circulating time were eliminated by all models. In addition, blood activity was eliminated by model $_{BS}FDG_{MAX}$. The following quantifiers of arterial ^{18}FDG uptake were evaluated: FDG_{MAX}, $TBR_{MAX/MEAN}$, and $_{BS}FDG_{MAX}$. β = standardized regression coefficient. The 95 % confidence interval is presented in parentheses.

aortic arch and left internal jugular vein than other vascular beds. Spillover activity from adjacent ^{18}FDG avid structures likely accounts for this observation. For example, we believe that spillover activity from aortic atherosclerotic plaques increase blood ^{18}FDG activity estimates in the aortic arch. Similarly, we speculate that bone marrow and muscle ^{18}FDG activity increase blood ^{18}FDG activity estimates in the left internal jugular vein. Therefore, we advise to fix the location of blood ^{18}FDG activity estimation to either the lumen of the superior vena cava or right internal jugular vein, because these locations are easy to identify and are largely devoid from spillover activity from adjacent ^{18}FDG avid structures. Furthermore, our study demonstrated that blood ^{18}FDG activity could be determined with high inter- and intra-rater agreement at these locations. Standardized estimation of blood activity may reduce systematic errors and increase inter-study comparability.

In addition to blood activity, **body weight** affected quantification of arterial ^{18}FDG uptake. The impact of body weight is closely related to the distribution volume of ^{18}FDG. An increase in body size, and hence distribution volume, will negatively impact the uptake of ^{18}FDG in the target organ, such as the arterial wall. To overcome this problem, our study administered a ^{18}FDG dosage proportional to the subject's body weight. However, our regression models demonstrated that arterial ^{18}FDG uptake increased linearly to body weight for some arterial segments, which suggests overcompensation for the negative impact of body weight on arterial ^{18}FDG uptake. Calculation of the standardized uptake value (SUV) may account for variations in distribution volume **(22)**. The SUV is the decay-corrected tissue concentration of ^{18}FDG (kBq/mL) adjusted for injected dose (MBq) and body weight (kg) or body surface area (cm^2) and is a common method to quantify ^{18}FDG uptake. However, the observed multicollinearity between injected dose, body weight, and body surface area prevented SUV from adequately correcting for variations in distribution volume of the tracer (**SUPPLEMENTARY FIGURE 3**). Furthermore, SUV is associated with several other inherent limitations **(23)**. Therefore, it may be best to correct for variations in injected dose or body distribution volume via statistical approaches, such as regression modeling.

In addition to blood activity and body weight, quantification of arterial ^{18}FDG uptake was affected by differences in **PET/CT technology**. Even though our imaging protocol adhered to international practice guidelines **(24)** and our PET/CT systems were calibrated to a phantom, subjects examined by the GE Discovery 690/710 had significantly higher arterial ^{18}FDG uptake than subjects examined on our older PET/CT systems (i.e. GE Discovery STE, VCT, or RX). Differences in imaging hard- and software likely account for this observation

(**SUPPLEMENTARY TABLE 1**). It remains challenging to cross-calibrate PET/CT systems to overcome differences in imaging hard- and software. However, promising initiatives, such as the EARL ^{18}FDG PET/CT accreditation program **(25)**, can resolve issues surrounding differences in PET/CT technology and may contribute to improved inter-scan agreement in quantitative PET studies.

In contrast to blood activity, body weight, and PET/CT system, **plasma glucose** did not affect quantification of arterial ^{18}FDG uptake. International guidelines recommend adequate fasting before ^{18}FDG administration to ensure low plasma glucose and low insulinaemia **(25)**, because plasma glucose and insulin can affect ^{18}FDG uptake **(26)**. Our study confirms that adequate fasting ensures plasma glucose levels below the recommended threshold of 7.0 to 8.3 mmol/L **(25)**. We conclude that adequate controlled plasma glucose does not impact quantification of arterial ^{18}FDG uptake.

Similar to plasma glucose, **renal function** did not affect quantification of arterial ^{18}FDG uptake. Theoretically, impaired renal function prolongs tracer availability **(27)** and may contribute to increased ^{18}FDG accumulation in atherosclerotic plaques. Retrospective analysis of 50 oncologic patients demonstrated a negative correlation between renal function, expressed as MDRD-eGFR, and blood activity (Spearmen's ρ = -0.32; P = 0.03) **(16)**. In the same study, renal function associated negatively with the arterial wall maximum SUV (Spearmen's ρ = -0.50, P < .001) and positively with $TBR_{MAX/MEAN}$ (Spearmen's ρ = 0.21; P < .02). Therefore, this study concluded that renal function significantly affected arterial ^{18}FDG uptake. In contrast, our study could neither demonstrate an association between renal function and blood activity nor renal function and arterial ^{18}FDG uptake. Differences in study methodology might account for this observation. First, our study performed PET/CT imaging at 180 minutes versus 60 minutes after ^{18}FDG administration. A prolonged ^{18}FDG clearance time may have negated the effects of renal function on arterial ^{18}FDG uptake. Second, our study evaluated the relation between renal function and arterial ^{18}FDG uptake in a multivariable model versus univariate analysis only. Therefore, effects of renal function may co-correlate to other determinants of arterial ^{18}FDG uptake. For example, normalizing arterial ^{18}FDG uptake to blood activity may negate the impact of renal function on arterial ^{18}FDG uptake. Finally, our study contained a limited number of subjects with impaired renal function. Only 6 % of our subjects had an MDRD-eGFR below 60 mL/min/1.73 m^2 compared to 16 % in the other study **(16)**. Therefore, our results may only apply to subjects with a glomerular filtration rate of at least 60 mL/min/1.73 m^2.

As with plasma glucose and renal function, **^{18}FDG-circulating time** did not affect quantification of arterial ^{18}FDG uptake. In a previous study our group demonstrated that arterial ^{18}FDG uptake depends on ^{18}FDG circulating time **(9)**. In 40 subjects imaged at 90 and 180 minutes after ^{18}FDG administration, we could demonstrate that blood ^{18}FDG activity decreases with time (P < .001), whereas arterial ^{18}FDG uptake, quantified as the blood subtracted maximum SUV and the $TBR_{MAX/MEAN}$, significantly increases with time (P < .001). In the present study, we fixed the circulating time of ^{18}FDG to approximately 180 minutes and demonstrated that quantification of arterial ^{18}FDG uptake was not affected by small variations in circulating time. Consequently, a fixed time between ^{18}FDG administration and PET/CT acquisition negate the impact of circulating time on quantification of arterial ^{18}FDG uptake.

Finally, our study demonstrated that quantification of arterial ^{18}FDG uptake and blood ^{18}FDG activity can be achieved with excellent inter- and intra-rater reliability and agreement. This finding is consistent with previously published agreement studies **(9, 14, 15)**.

Strengths and Limitations

An important strength of the present study is that we prospectively evaluated the effect of personal characteristics and technical factors on quantification of arterial ^{18}FDG uptake in a group of healthy subjects. By studying healthy subjects we limited bias from cardiovascular disease on the generated results. However, studying a healthy population prevents extrapolating the results to a more diseased population. For example, only 2 % of subjects were glucose intolerant (HbA1c > 48 mmol/mol) and 6 % had impaired renal function (MDRD-eGFR < 60 mL/min/1.73 m^2). Therefore, we remain cautious in extrapolating our results to subjects with severe glucose intolerance or renal insufficiency. Second, although our study results were internally validated by bootstrap techniques, they lack external validation. To overcome this limitation, our study should preferably be repeated in a different population by different researchers. Third, ethical considerations prevented collection of arterial specimens for histological examination. Therefore, we could not associate arterial ^{18}FDG uptake to histologic markers of atherosclerotic plaque inflammation. For similar reasons, we could not collect invasive blood samples to determine and compare blood activity estimates obtained by PET/CT imaging to the true blood ^{18}FDG activity. Finally, the notion that quantification of arterial ^{18}FDG uptake by $TBR_{MAX/MEAN}$ is suboptimal compared to $_{BS}FDG_{MAX}$ cannot be substantiated by our data alone. Comparing arterial ^{18}FDG uptake to histologic analysis of atherosclerotic plaque inflammation may be able to confirm the notion that $_{BS}FDG_{MAX}$ is a preferred quantifier of arterial ^{18}FDG uptake.

Conclusions

Prospective evaluation of 89 healthy subjects demonstrated that quantification of arterial ^{18}FDG uptake is affected by blood ^{18}FDG activity, body weight, and PET/CT system. These factors should be accounted for in quantification methodologies to generate accurate estimates of arterial ^{18}FDG uptake.

REFERENCES

1. Folco EJ, Sheikine Y, Rocha VZ, et al. Hypoxia but not Inflammation Augments Glucose Uptake in Human Macrophages: Implications for Imaging Atherosclerosis with ^{18}Fluorine-Labeled 2-Deoxy-D-Glucose Positron Emission Tomography. *J Am Coll Cardiol*. 2011; **58**: 603-614.

2. Rudd JH, Warburton EA, Fryer TD, et al. Imaging Atherosclerotic Plaque Inflammation with [^{18}F]-Fluorodeoxyglucose Positron Emission Tomography. *Circulation*. 2002; **105**: 2708-2711.

3. Tawakol A, Fayad ZA, Mogg R, et al. Intensification of Statin Therapy Results in a Rapid Reduction in Atherosclerotic Inflammation: Results of a Multi-Center FDG-PET/CT Feasibility Study. *J Am Coll Cardiol*. 2013; **62**: 909-917.

4. Tahara N, Kai H, Ishibashi M, et al. Simvastatin Attenuates Plaque Inflammation: Evaluation by Fluorodeoxyglucose Positron Emission Tomography. *J Am Coll Cardiol*. 2006; **48**: 1825-1831.

5. Rominger A, Saam T, Wolpers S, et al. ^{18}F-FDG PET/CT Identifies Patients at Risk for Future Vascular Events in an Otherwise Asymptomatic Cohort with Neoplastic Disease. *J Nucl Med*. 2009; **50**: 1611-1620.

6. Sadeghi MM. ^{18}F-FDG PET and Vascular Inflammation: Time to Refine the Paradigm? *J Nucl Cardiol*. 2015; **22**: 319-324

7. Huet P, Burg S, Le Guludec D, et al. Variability and Uncertainty of FDG PET Imaging Protocols for Assessing Inflammation in Atherosclerosis: Suggestions for Improvement. *J Nucl Med*. 2015; **56**: 552-559

8. Izquierdo-Garcia D, Davies JR, Graves MJ, et al. Comparison of Methods for Magnetic Resonance-Guided [^{18}F]-Fluorodeoxyglucose Positron Emission Tomography in Human Carotid Arteries: Reproducibility, Partial Volume Correction, and Correlation Between Methods. *Stroke*. 2009; **40**: 86-93.

9. Blomberg BA, Thomassen A, Takx RA, et al. Delayed ^{18}F-fluorodeoxyglucose PET/CT Imaging Improves Quantitation of Atherosclerotic Plaque Inflammation: Results from the CAMONA Study. *J Nucl Cardiol*. 2014; **21**: 588-597.

10. Becker CR, Knez A, Ohnesorge B, et al. Visualization and Quantification of Coronary Calcifications with Electron Beam and Spiral Computed Tomography. *Eur Radiol*. 2000; **10**: 629-635.

11. Austin P, Tu J. Bootstrap Methods for Developing Predictive Models. *Am Stat*. 2004; **58**: 131-137.

12. Kottner J, Audige L, Brorson S, et al. Guidelines for Reporting Reliability and Agreement

Studies (GRRAS) Were Proposed. *J Clin Epidemiol*. 2011; **64**: 96-106.

13. Bland JM, Altman DG. Statistical Methods for Assessing Agreement Between Two Methods of Clinical Measurement. *Lancet*. 1986; **237**: 307-310.

14. Rudd JH, Myers KS, Bansilal S, et al. Atherosclerosis Inflammation Imaging with ^{18}F-FDG PET: Carotid, Iliac, and Femoral Uptake Reproducibility, Quantification Methods, and Recommendations. *J Nucl Med*. 2008; **49**: 871-878.

15. Rudd JH, Myers KS, Bansilal S, et al. ^{18}Fluorodeoxyglucose Positron Emission Tomography Imaging of Atherosclerotic Plaque Inflammation is Highly Reproducible: Implications for Atherosclerosis Therapy Trials. *J Am Coll Cardiol*. 2007; **50**: 892-896.

16. Derlin T, Habermann CR, Hahne JD, et al. Quantification of [^{18}F]-FDG Uptake in Atherosclerotic Plaque: Impact of Renal Function. *Ann Nucl Med*. 2011; **25**: 586-591.

17. Tawakol A, Migrino RQ, Bashian GG, et al. In Vivo ^{18}F-Fluorodeoxyglucose Positron Emission Tomography Imaging Provides a Noninvasive Measure of Carotid Plaque Inflammation in Patients. *J Am Coll Cardiol*. 2006; **48**: 1818-1824.

18. Tawakol A, Fayad ZA, Mogg R, et al. Intensification of Statin Therapy Results in a Rapid Reduction in Atherosclerotic Inflammation: Results of a Multicenter Fluorodeoxyglucose-Positron Emission Tomography/Computed Tomography Feasibility Study. *J Am Coll Cardiol*. 2013; **62**: 909-917.

19. Tawakol A, Singh P, Rudd JH, et al. Effect of Treatment for 12 Weeks with Rilapladib, a Lipoprotein-Associated Phospholipase A2 Inhibitor, on Arterial Inflammation as Assessed with ^{18}F-Fluorodeoxyglucose-Positron Emission Tomography Imaging. *J Am Coll Cardiol*. 2014; **63**: 86-88.

20. Figueroa AL, Subramanian SS, Cury RC, et al. Distribution of Inflammation within Carotid Atherosclerotic Plaques with High-Risk Morphological Features: A Comparison Between Positron Emission Tomography Activity, Plaque Morphology, and Histopathology. *Circ Cardiovasc Imaging*. 2012; **5**: 69-77.

21. Rudd JH, Myers KS, Bansilal S, et al. Relationships Among Regional Arterial Inflammation, Calcification, Risk Factors, and Biomarkers: A Prospective Fluorodeoxyglucose Positron-Emission Tomography/Computed Tomography Imaging Study. *Circ Cardiovasc Imaging*. 2009; **2**: 107-115.

22. Thie JA. Understanding the Standardized Uptake Value, Its Methods, and Implications for Usage. *J Nucl Med*. 2004; **45**: 1431-1434.

23. Keyes JW. SUV: Standard Uptake or Silly Useless Value? *J Nucl Med*. 1995; **36**: 1836-1839.

24. Boellaard R, O'Doherty MJ, Weber WA, et al. FDG PET and PET/CT: EANM Procedure Guidelines for Tumour PET Imaging: Version 1.0. *Eur J Nucl Med Mol Imaging*. 2010; **37**:

181-200.

25. Boellaard R, Delgado-Bolton R, Oyen WJ, et al. FDG PET/CT: EANM Procedure Guidelines for Tumour Imaging: Version 2.0. *Eur J Nucl Med Mol Imaging*. 2015; **42**: 328-354.

26. Belohlavek O, Jaruskova M. [^{18}F]FDG-PET Scan in Patients with Fasting Hyperglycaemia. *Q J Nucl Med Mol Imaging*. 2014; [Epub ahead of print]

27. Laffon E, Cazeau AL, Monet A, et al. The Effect of Renal Failure on ^{18}F-FDG Uptake: A Theoretic Assessment. *J Nucl Med Technol*. 2008; **36**: 200-202.

SUPPLEMENTARY FIGURES

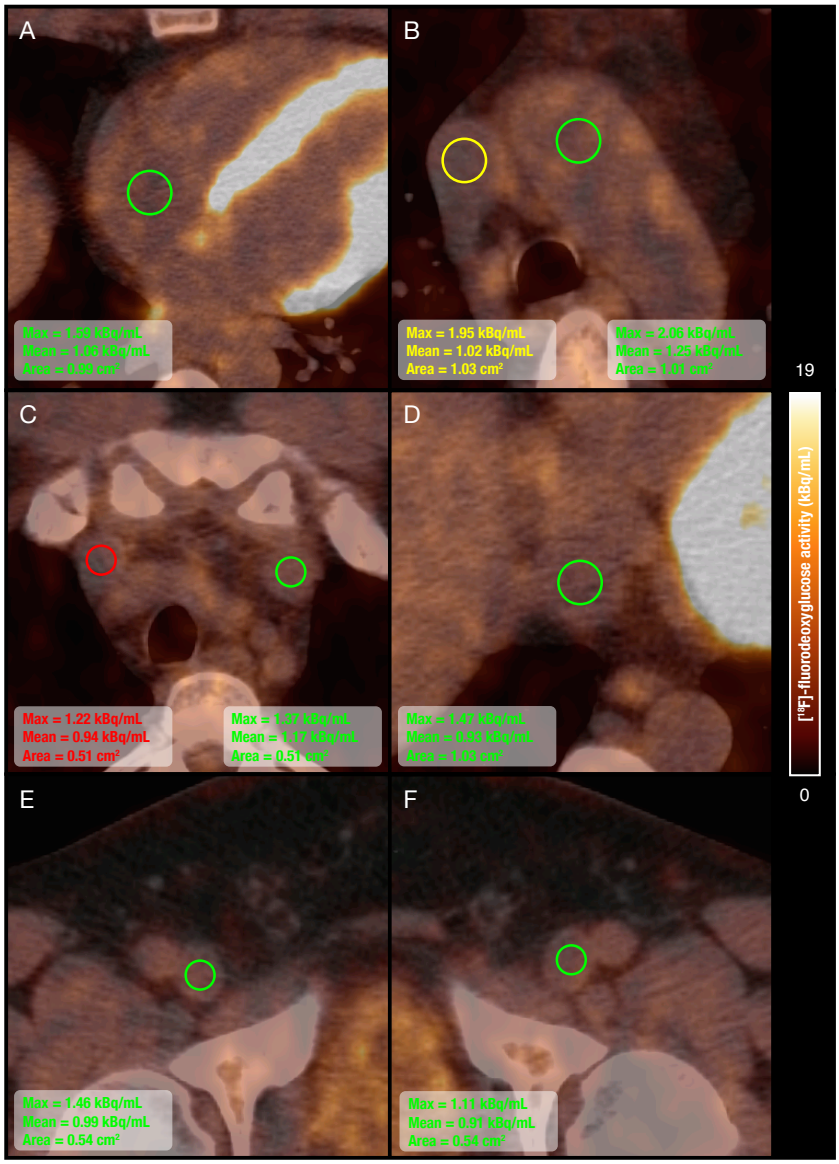

SUPPLEMENTARY FIGURE 1 – Illustration demonstrating quantification of mean ^{18}FDG blood activity ($_{BLOOD}FDG_{MEAN}$). On axially oriented ^{18}FDG PET/CT images, a circular region of interest (ROI), with an approximate area of 1 cm^2, was drawn in the center of the right atrium (**A**), superior vena cava (**B**), aortic arch (**B**), and proximal inferior vena cava (**D**). Similarly, a ROI, with an approximate area of 0.5 cm^2, was drawn in the right and left internal jugular vein (**C**) and right (**E**) and left femoral vein (**F**). Per ROI, the mean ^{18}FDG activity (kBq/mL) was determined.

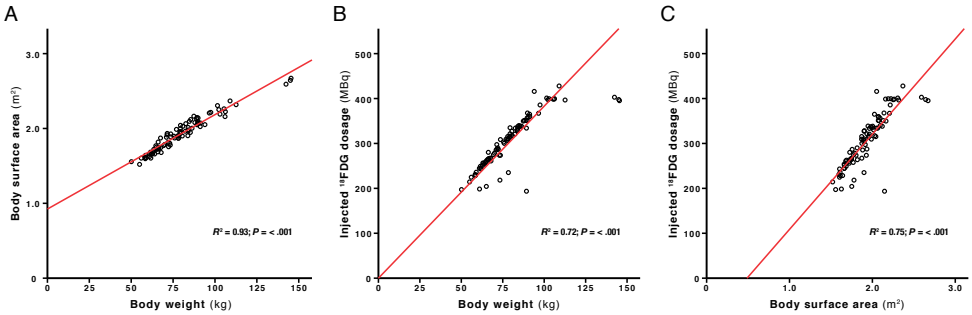

SUPPLEMENTARY FIGURE 2 – Scatter plot of (**A**) body surface area against body weight, (**B**) injected dose against body weight, and (**C**) injected dose against body surface area. The scatter plots together with the coefficients of determination (R^2) suggest multicollinearity between the variables. Multicollinearity was confirmed statistically by a tolerance statistic of 0.06, 0.07, and 0.25 for body surface area, body weight, and injected dose, respectively. Outliers observed in plot **B** and **C** are explained by differences in manual (n = 20) and automatic ^{18}FDG administration (n = 69).

$$\mathrm{SUV} = \frac{^{18}\mathrm{FDG\ activity\ (MBq \cdot mL^{-1}) \cdot body\ weight\ (kg)}}{\mathrm{Injected\ dose\ (MBq)}} =$$

$$= \frac{^{18}\mathrm{FDG\ activity\ (MBq \cdot mL^{-1}) \cdot body\ weight\ (kg)}}{\mathrm{4\ MBq \cdot kg^{-1} \cdot body\ weight\ (kg)}} =$$

$$= \frac{^{18}\mathrm{FDG\ activity\ (MBq \cdot mL^{-1})}}{\mathrm{4\ MBq \cdot kg^{-1}}}$$

SUPPLEMENTARY FIGURE 3 – Equation to normalize ^{18}FDG activity (MBq/mL) in the target of interest to injected dose (MBq) and body weight (kg) known as the standardized uptake value (SUV). Body weight dependent ^{18}FDG dose administration makes calculation of SUV ineffective.

SUPPLEMENTARY TABLES

SUPPLEMENTARY TABLE 1 – PET/CT system specifications and image reconstruction parameters

Vendor and type	System specifications		Image reconstruction parameters			
	PET scintillator	CT	Iterations/ Subsets	Post hoc filter	Reconstruction matrix	TOF/PSF
GE Discovery STE **(1)**	BGO	16-slice	2/28	6 mm	128x128	No/No
GE Discovery VCT **(1)**	BGO	64-slice	2/28	6 mm	128x128	No/No
GE Discovery RX **(2)**	LYSO	64-slice	2/21	6 mm	128x128	No/No
GE Discovery 690/710 **(3)**	LYSO	64-slice	3/24	5 mm	256x256	Yes/Yes

Summary of PET/CT system specifications and image reconstruction parameters. BGO, LYSO, and ToF/PSF indicate bismuth germanate, lutetium yttrium oxyorthosilicate, and time-of-flight and/or point spread function image reconstruction.

SUPPLEMENTARY TABLE 2 – Determinants of ^{18}FDG uptake in the aortic arch

	Regression coefficient	β	Adjusted R^2	*P* value
1. FDG_{MAX}, kBq/mL			0.47	**< .001**
Intercept, kBq/mL	7.01 (4.71 to 9.05)			**< .001**
Blood activity, kBq/mL	1.18 (0.76 to 1.73)	0.33		**< .001**
Body weight, kg	0.01 (-0.00 to 0.04)	0.10		.115
PET/CT system				
- GE Discovery STE	-3.84 (-5.03 to -2.67)	-0.60		**< .001**
- GE Discovery VCT	-3.40 (-4.71 to -2.08)	-0.62		**< .001**
- GE Discovery RX	-4.17 (-5.32 to -3.08)	-0.70		**< .001**
2. $TBR_{MAX/MEAN}$			0.46	**< .001**
Intercept	5.05 (4.13 to 5.90)			**< .001**
Blood activity, kBq/mL	-0.51 (-0.70 to -0.36)	-0.39		**< .001**
Body weight, kg	0.01 (-0.00 to 0.02)	0.13		.093
PET/CT system				
- GE Discovery STE	-1.27 (-1.76 to -0.83)	-0.54		**< .001**
- GE Discovery VCT	-1.19 (-1.71 to -0.68)	-0.58		**< .001**
- GE Discovery RX	-1.49 (-1.95 to -1.06)	-0.68		**< .001**
3. $_{BS}FDG_{MAX}$, kBq/mL			0.41	**< .001**
Intercept, kBq/mL	7.53 (5.61 to 9.24)			
Body weight, kg	0.02 (-0.00 to 0.04)	0.11		.140
PET/CT system				
- GE Discovery STE	-3.86 (-5.15 to -2.65)	-0.64		**< .001**
- GE Discovery VCT	-3.45 (-4.74 to -2.21)	-0.66		**< .001**
- GE Discovery RX	-4.14 (-5.42 to -2.96)	-0.74		**< .001**

Multivariable linear regression assessing the dependence of aortic arch ^{18}FDG uptake on superior vena cava blood activity, plasma glucose, renal function, body weight, circulating time, and PET/CT system. "PET/CT system" was entered as categorical variable into the model with the GE Discovery 690/710 as reference system. Stepwise selection of variables, based on Akaike's information criterion, was performed by a backward elimination strategy. The following quantifiers of arterial ^{18}FDG uptake were evaluated: FDG_{MAX}, $TBR_{MAX/MEAN}$, and $_{BS}FDG_{MAX}$. β = standardized regression coefficient. The 95 % confidence interval is presented in parentheses.

SUPPLEMENTARY TABLE 3 – Determinants of ^{18}FDG uptake in the descending thoracic aorta

	Regression coefficient	β	Adjusted R^2	*P* value
1. FDG_{MAX}, kBq/mL			0.54	**< .001**
Intercept, kBq/mL	8.99 (5.94 to 12.32)			**< .001**
Blood activity, kBq/mL	1.12 (0.76 to 1.44)	.40		**< .001**
MDRD-eGFR, mL/min/1.73 m^2	-0.02 (-0.05 to 0.01)	-.13		.172
PET/CT system				
- GE Discovery STE	-2.93 (-3.97 to -1.96)	-.58		**< .001**
- GE Discovery VCT	-2.81 (-3.88 to -1.82)	-.64		**< .001**
- GE Discovery RX	-2.99 (-3.88 to -2.20)	-.63		**< .001**
2. $TBR_{MAX/MEAN}$			0.51	**< .001**
Intercept	5.85 (4.67 to 7.23)			**< .001**
Blood activity, kBq/mL	-0.54 (-0.73 to -0.42)	-0.51		**< .001**
MDRD-eGFR, mL/min/1.73 m^2	-0.01 (-0.02 to 0.00)	-0.12		.195
PET/CT system				
- GE Discovery STE	-0.93 (-1.28 to -0.62)	-0.49		**< .001**
- GE Discovery VCT	-0.96 (-1.29 to -0.64)	-0.58		**< .001**
- GE Discovery RX	-1.04 (-1.35 to -0.76)	-0.59		**< .001**
3. $_{BS}FDG_{MAX}$, kBq/mL			0.44	**< .001**
Intercept, kBq/mL	9.44 (6.67 to 12.15)			**< .001**
MDRD-eGFR, mL/min/1.73 m^2	-0.02 (-0.05 to 0.01)	-.16		.131
PET/CT system				
- GE Discovery STE	-2.95 (-3.94 to -2.05)	-.65		**< .001**
- GE Discovery VCT	-2.85 (-3.85 to -1.90)	-.72		**< .001**
- GE Discovery RX	-2.96 (-3.88 to -2.16)	-.70		**< .001**

Multivariable linear regression assessing the dependence of aortic arch ^{18}FDG uptake on superior vena cava blood activity, plasma glucose, renal function, body weight, circulating time, and PET/CT system. "PET/CT system" was entered as categorical variable into the model with the GE Discovery 690/710 as reference system. Stepwise selection of variables, based on Akaike's information criterion, was performed by a backward elimination strategy. The following quantifiers of arterial ^{18}FDG uptake were evaluated: FDG_{MAX}, $TBR_{MAX/MEAN}$, and $_{BS}FDG_{MAX}$. β = standardized regression coefficient. The 95 % confidence interval is presented in parentheses.

SUPPLEMENTARY TABLE 4 – Determinants of ^{18}FDG uptake in the right carotid artery

	Regression coefficient	β	Adjusted R^2	*P* value
1. FDG_{MAX}, kBq/mL			0.59	**< .001**
Intercept, kBq/mL	4.92 (3.27 to 7.02)			**< .001**
Blood activity, kBq/mL	1.31 (0.68 to 1.78)	0.51		**< .001**
PET/CT system				
- GE Discovery STE	-2.45 (-3.18 to -1.77)	-0.53		**< .001**
- GE Discovery VCT	-2.14 (-2.80 to -1.50)	-0.54		**< .001**
- GE Discovery RX	-3.04 (-3.73 to -2.35)	-0.71		**< .001**
2. $TBR_{MAX/MEAN}$			0.52	**< .001**
Intercept	3.31 (2.25 to 4.62)			**< .001**
Blood activity, kBq/mL	-0.34 (-0.54 to -0.19)	-0.39		**< .001**
Plasma glucose, mmol/L	0.14 (-0.03 to 0.28)	0.11		.148
PET/CT system				
- GE Discovery STE	-0.83 (-1.11 to -0.60)	-0.53		**< .001**
- GE Discovery VCT	-0.76 (-1.00 to -0.52)	-0.56		**< .001**
- GE Discovery RX	-1.05 (-1.29 to -0.79)	-0.72		**< .001**
3. $_{BS}FDG_{MAX}$, kBq/mL			0.46	**< .001**
Intercept, kBq/mL	7.10 (4.94 to 9.11)			**< .001**
MDRD-eGFR, mL/min/1.73 m^2	-0.02 (-0.04 to 0.01)	-0.12		.133
PET/CT system				
- GE Discovery STE	-2.56 (-3.38 to -1.74)	-0.63		**< .001**
- GE Discovery VCT	-2.29 (-3.00 to -1.56)	-0.66		**< .001**
- GE Discovery RX	-2.93 (-3.59 to -2.31)	-0.78		**< .001**

Multivariable linear regression assessing the dependence of right carotid artery ^{18}FDG uptake on superior vena cava blood activity, plasma glucose, renal function, body weight, circulating time, and PET/CT system. "PET/CT system" was entered as categorical variable into the model with the GE Discovery 690/710 as reference system. Stepwise selection of variables, based on Akaike's information criterion, was performed by a backward elimination strategy. The following quantifiers of arterial ^{18}FDG uptake were evaluated: FDG_{MAX}, $TBR_{MAX/MEAN}$, and $_{BS}FDG_{MAX}$. β = standardized regression coefficient. The 95 % confidence interval is presented in parentheses.

SUPPLEMENTARY TABLE 5 – Determinants of ^{18}FDG uptake in the left carotid artery

	Regression coefficient	β	Adjusted R^2	*P* value
1. FDG_{MAX}, kBq/mL			0.15	**.001**
Intercept, kBq/mL	3.94 (1.40 to 7.08)			**.023**
Blood activity, kBq/mL	1.37 (0.44 to 2.12)	0.39		**.025**
PET/CT system				
- GE Discovery STE	-1.02 (-2.07 to 0.05)	-0.16		.126
- GE Discovery VCT	-1.01 (-2.11 to 0.26)	-0.19		.143
- GE Discovery RX	-1.52 (-2.55 to -0.37)	-0.26		**.017**
2. $TBR_{MAX/MEAN}$			0.14	**.007**
Intercept	3.85 (3.10 to 4.78)			**< .001**
Blood activity, kBq/mL	-0.37 (-0.65 to -0.14)	-0.32		**.016**
PET/CT system				
- GE Discovery STE	-0.32 (-0.71 to 0.03)	-0.16		.122
- GE Discovery VCT	-0.34 (-0.75 to 0.16)	-0.19		.163
- GE Discovery RX	-0.51 (-0.86 to -0.10)	-0.26		**.020**
3. $_{BS}FDG_{MAX}$, kBq/mL			0.02	.206
Intercept, kBq/mL	5.01 (4.49 to 5.54)			**< .001**
PET/CT system				
- GE Discovery STE	-1.06 (-2.14 to 0.18)	-0.18		.099
- GE Discovery VCT	-1.11 (-2.18 to 0.16)	-0.22		.096
- GE Discovery RX	-1.46 (-2.39 to -0.28)	-0.27		**.018**

Multivariable linear regression assessing the dependence of left carotid artery ^{18}FDG uptake on superior vena cava blood activity, plasma glucose, renal function, body weight, circulating time, and PET/CT system. "PET/CT system" was entered as categorical variable into the model with the GE Discovery 690/710 as reference system. Stepwise selection of variables, based on Akaike's information criterion, was performed by a backward elimination strategy. The following quantifiers of arterial ^{18}FDG uptake were evaluated: FDG_{MAX}, $TBR_{MAX/MEAN}$, and $_{BS}FDG_{MAX}$. β = standardized regression coefficient. The 95 % confidence interval is presented in parentheses.

SUPPLEMENTARY TABLE 6 – Intra-rater reliability and agreement of FDG_{MAX} and $_{BLOOD}FDG_{MEAN}$

	ICC	95 % CI	Mean difference (kBq/mL)	95 % Limits of agreement
FDG_{MAX}				
- Ascending aorta	0.99 *	0.97 to 1.00	-0.05	-0.24 to 0.15
- Aortic arch	1.00 *	0.97 to 1.00	0.06	-0.08 to 0.21
- Descending aorta	1.00 *	1.00 to 1.00	-0.01	-0.09 to 0.07
- Right carotid artery	1.00 *	0.98 to 1.00	0.01	-0.11 to 0.13
- Left carotid artery	1.00 *	0.99 to 1.00	-0.01	-0.10 to 0.08
$_{BLOOD}FDG_{MEAN}$				
- Right atrium	0.99 *	0.95 to 1.00	0.02	-0.10 to 0.14
- Aortic arch	0.92 *	0.69 to 0.98	0.07	-0.16 to 0.31
- Right jugular vein	1.00 *	0.99 to 1.00	-0.01	-0.06 to 0.03
- Left jugular vein	0.96 *	0.86 to 0.99	0.01	-0.11 to 0.13
- Superior vena cava	0.92 *	0.70 to 0.98	0.01	-0.14 to 0.17
- Inferior vena cava	0.84 *	0.48 to 0.96	0.07	-0.19 to 0.34
- Right femoral vein	0.95 *	0.83 to 0.99	-0.01	0.10 to -0.11
- Left femoral vein	0.96 *	0.85 to 0.99	0.00	-0.13 to 0.12

Intra-rater reliability and agreement of FDG_{MAX} and $_{BLOOD}FDG_{MEAN}$. ICC = intraclass correlation coefficient (two-way random effects model assessing absolute agreement of single measures). CI = confidence interval. * $P < .001$.

SUPPLEMENTARY TABLE 7 – Inter-rater reliability and agreement of FDG_{MAX} and $_{BLOOD}FDG_{MEAN}$

	ICC	95 % CI	Mean difference (kBq/mL)	95 % Limits of agreement
FDG_{MAX}				
- Ascending aorta	0.99 *	0.97 to 1.00	-0.05	-0.24 to 0.15
- Aortic arch	1.00 *	0.97 to 1.00	0.06	-0.08 to 0.21
- Descending aorta	1.00 *	1.00 to 1.00	-0.01	-0.09 to 0.07
- Right carotid artery	1.00 *	0.98 to 1.00	0.01	-0.11 to 0.13
- Left carotid artery	1.00 *	0.99 to 1.00	-0.01	-0.10 to 0.08
$_{BLOOD}FDG_{MEAN}$				
- Right atrium	0.99 *	0.95 to 1.00	0.02	-0.10 to 0.14
- Aortic arch	0.92 *	0.69 to 0.98	0.07	-0.16 to 0.31
- Right jugular vein	1.00 *	0.99 to 1.00	-0.01	-0.06 to 0.03
- Left jugular vein	0.96 *	0.86 to 0.99	0.01	-0.11 to 0.13
- Superior vena cava	0.92 *	0.70 to 0.98	0.01	-0.14 to 0.17
- Inferior vena cava	0.84 *	0.48 to 0.96	0.07	-0.19 to 0.34
- Right femoral vein	0.95 *	0.83 to 0.99	-0.01	0.10 to -0.11
- Left femoral vein	0.96 *	0.85 to 0.99	0.00	-0.13 to 0.12

Inter-rater reliability and agreement of FDG_{MAX} and $_{BLOOD}FDG_{MEAN}$. ICC = intraclass correlation coefficient (two-way random effects model assessing absolute agreement of single measures). CI = confidence interval. * $P < .001$.

SUPPLEMENTARY REFERENCES

1. Teräs M, Tolvanen T, Johansson JJ, et al. Performance of the New Generation of Whole-Body PET/CT Scanners: Discovery STE and Discovery VCT. *Eur J Nucl Med Mol Imaging*. 2007; **34**: 1683-92.

2. Kemp BJ, Kim C, Williams JJ, et al. NEMA NU 2-2001 Performance Measurements of an LYSO-based PET/CT system in 2D and 3D Acquisition Modes. *J Nucl Med*. 2006; **47**: 1960-7.

3. Bettinardi V, Presotto L, Rapisarda E, et al. Physical Performance of the New Hybrid PET/CT Discovery-690. *Med Phys*. 2011; **38**: 5394-411.

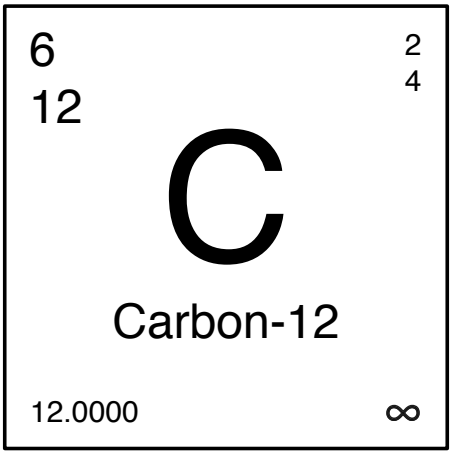
6
12
2
4
C
Carbon-12
12.0000
∞

Chapter 6

Impact of Personal Characteristics and Technical Factors on Quantification of Sodium [^{18}F]-Fluoride Uptake in Human Arteries: Prospective Evaluation of Healthy Subjects

Björn A. Blomberg
Anders Thomassen
Pim A. de Jong
Jane A. Simonsen
Marnix G.E.H. Lam
Anne L. Nielsen
Hans Mickley
Willem P.T.M. Mali
Abass Alavi
Poul F. Høilund-Carlsen

Published in *The Journal of Nuclear Medicine*, 2015

ABSTRACT

Background: Sodium [^{18}F]-fluoride PET/CT is a promising imaging technique for assessment of atherosclerosis, but is hampered by a lack of validated quantification protocols. Both personal characteristics and technical factors can affect quantification of arterial Na^{18}F uptake. This study investigated if blood activity, renal function, injected dose, circulating time, and PET/CT system affect quantification of arterial Na^{18}F uptake.

Methods: Eighty-nine healthy subjects were prospectively examined by Na^{18}F PET/CT imaging. Arterial Na^{18}F uptake was quantified at the level of the ascending aorta, aortic arch, descending thoracic aorta, and coronary arteries by calculating the maximum Na^{18}F activity (NaF_{MAX}), the maximum target-to-background ratio ($TBR_{MAX/MEAN}$), and the maximum blood subtracted Na^{18}F activity ($_{BS}NaF_{MAX}$). Multivariable linear regression assessed the effect of personal characteristics and technical factors on quantification of arterial Na^{18}F uptake.

Results: NaF_{MAX} and $TBR_{MAX/MEAN}$ were dependent on blood activity (β = .34 to .44; P < .001 and β = -.68 to -.58; P < .001, respectively) and PET/CT system (β = -.80 to -.53; P < .001 and β = -.80 to -.23; P < .031, respectively). $_{BS}NaF_{MAX}$ depended on PET/CT system (β = -.91 to -.57; P < .001), but not blood activity. This finding was observed at the level of the ascending aorta, aortic arch, descending thoracic aorta, as well as the coronary arteries. In addition to blood activity and PET/CT system, injected dose affected quantification of arterial Na^{18}F uptake, whereas renal function and circulating time did not.

Conclusions: Prospective evaluation of 89 healthy subjects demonstrated that quantification of arterial Na^{18}F uptake is affected by blood activity, injected dose, and PET/CT system. Therefore, blood activity, injected dose, and PET/CT system should be taken into account to generate accurate estimates of arterial Na^{18}F uptake.

INTRODUCTION

Sodium [^{18}F]-fluoride ($Na^{18}F$) positron emission tomography/computed tomography (PET/CT) is a promising non-invasive imaging technique for assessment of atherosclerosis. $Na^{18}F$ PET/CT targets the active exchange of fluoride with hydroxyl ions of hydroxylapatite crystals producing fluorapatite **(1)**. This process is believed to represent calcification metabolism of osseous tissue, including vascular calcification **(2-4)**. By imaging vascular calcification metabolism, $Na^{18}F$ PET/CT can potentially identify patients at high cardiovascular risk **(4)** and improve cardiovascular risk stratification **(5, 6)**.

Although $Na^{18}F$ PET/CT imaging of vascular calcification is promising, implementing $Na^{18}F$ PET/CT in research and clinical settings is hampered by a lack of validated and standardized quantification protocols. Most studies quantify arterial $Na^{18}F$ uptake as the ratio between arterial wall and blood $Na^{18}F$ activity, known as the target-to-background ratio ($TBR_{MAX/MEAN}$). However, this method has been criticized to be too dependent on blood activity **(6)**. In addition to blood activity, quantification of arterial $Na^{18}F$ uptake can be affected by personal characteristics and technical factors, including body weight, body surface area, renal function, injected $Na^{18}F$ dose, $Na^{18}F$ circulating time, and PET/CT system. It is not known which factors affect quantification of arterial $Na^{18}F$ uptake. Standardized and unbiased quantification of arterial $Na^{18}F$ uptake is imperative for both research and clinical settings, being a prerequisite for generation of reference values for arterial $Na^{18}F$ uptake with healthy aging, for response evaluation requiring repeat $Na^{18}F$ PET/CT examinations, and to allow for comparison of quantitative imaging results among studies.

The purpose of this study was to determine the effect of personal characteristics and technical factors on quantification of arterial $Na^{18}F$ uptake. By studying these effects in a group of healthy subjects we aimed to generate accurate estimates of arterial $Na^{18}F$ uptake. Secondary aims were to elucidate the effects of quantification methods on estimates of arterial $Na^{18}F$ uptake, to determine the optimal location for assessment of blood activity, and, finally, to evaluate rater reliability and agreement.

METHODS

This study is part of the "Cardiovascular Molecular Calcification Assessed by ^{18}F-NaF PET/CT" (CAMONA) study. CAMONA was approved by the Danish National Committee on Health Research Ethics, registered at ClinicalTrials.gov (NCT01724749), and conducted in accordance

with the Declaration of Helsinki. Written informed consent was obtained from all study subjects.

Subject Selection

Healthy subjects were prospectively recruited from the general population by local advertisement or from the blood bank of Odense University Hospital, Denmark. Subjects free of oncologic disease, autoimmune disease, immunodeficiency syndromes, alcohol abuse, illicit drug use, (symptoms suggesting) cardiovascular disease, or prescription medication were considered healthy and were eligible for inclusion. Pregnant women were not considered for inclusion. Healthy subjects were recruited to limit bias from cardiovascular risk factors on study results. Subjects were preselected by sex and age to secure a balanced inclusion of males

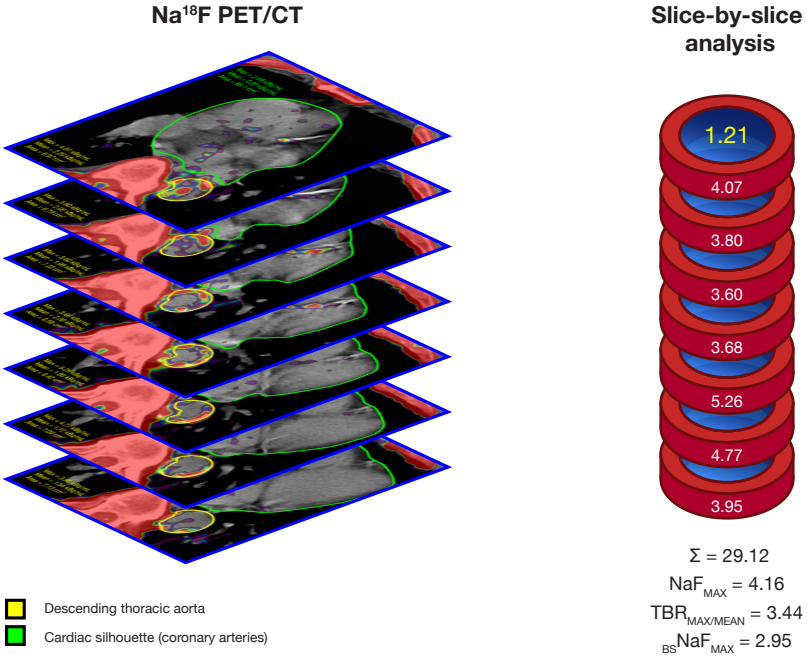

FIGURE 1 – Illustration demonstrating quantification of arterial sodium [^{18}F]-fluoride ($Na^{18}F$) uptake. A region of interest (ROI) is drawn around the arterial wall (*yellow* ROI = descending thoracic aorta) or cardiac silhouette (*green* ROI) on every slice of the axially oriented $Na^{18}F$ PET/CT images. Per ROI, the maximum $Na^{18}F$ activity is determined. Values obtained per ROI are summed (Σ) and averaged (NaF_{MAX}) and subsequently divided or subtracted by the mean $Na^{18}F$ blood activity ($_{BLOOD}NaF_{MEAN}$). This provides the target-to-background ratio ($TBR_{MAX/MEAN}$) or the blood subtracted $Na^{18}F$ activity ($_{BS}NaF_{MAX}$), respectively. Of note, $_{BLOOD}NaF_{MEAN}$ was estimated in the superior vena cava (not shown).

and females aged 20–29, 30–39, 40–49, 50–59, > 60 years. This allowed us to study a wide range of subjects to ensure translation of our findings to various settings.

Study Design

Healthy subjects were evaluated by blood pressure measurements, blood analyses, $Na^{18}F$ PET/CT imaging, and non-contrast enhanced cardiac CT imaging. Blood pressure measurements were performed thrice after a supine rest of at least 30 minutes. The average of the last two measurements determined the systolic and diastolic blood pressure. Blood analyses included fasting serum total cholesterol, serum LDL cholesterol, serum HDL cholesterol, serum triglycerides, fasting plasma glucose, glycated hemoglobin (HbA1c), serum creatinine, the latter being used to calculate the Modification of Diet and Renal Disease (MDRD) estimated glomerular filtration rate (eGFR). Furthermore, body weight, body height, body mass index, and body surface area according to Du Bois were determined. $Na^{18}F$ PET/CT imaging was performed on integrated PET/CT systems (GE Discovery 690/710, STE, VCT, and RX) at the PET center of Odense University Hospital, Denmark. Subjects were allocated to a PET/CT system at the discretion of the department's booking system. PET/CT system specifications and image reconstruction parameters are summarized in **SUPPLEMENTARY TABLE 1**. Each subject underwent PET/CT imaging at approximately 90 minutes after intravenous injection of approximately 2.2 MBq of $Na^{18}F$ per kilogram of body weight **(6)**. The emission acquisition duration per bed position was 2.5 minutes. Total body PET images were acquired in 3D–mode and reconstructed into coronal, axial, and sagittal planes by an ordered subsets expectation maximization algorithm (GE VUE Point). PET images were corrected for attenuation, scatter, random coincidences, and scanner dead time. Low–dose CT imaging (140 kV, 30-110 mA, noise index 25, 0.8 seconds per rotation, slice thickness 3.75 mm) was performed for attenuation correction and anatomic orientation. To determine the coronary calcium score, non-contrast enhanced, breath-hold, cardiac CT imaging (120 kV, 100 mA, 0.4 seconds per rotation, slice thickness 2.5 mm) was performed with electrocardiogram gating at 50 % of the R–R interval. The effective radiation dose received for the entire imaging protocol was approximately 14 mSv.

Quantitative Image Analyses

All images were analyzed by version 4.0 of the Philips IntelliSpace Portal client. The image analyst was masked to subject demographics and PET/CT system specifications. For each subject, uptake of $Na^{18}F$ was determined in the ascending aorta, aortic arch, descending thoracic aorta, and coronary arteries according to previously published methods **(6)**. In summary,

for the coronary arteries, we manually drew a free-hand region of interest (ROI) around the cardiac silhouette on every slice of the axially oriented PET/CT images. We carefully excluded $Na^{18}F$ activity originating from bone tissue and cardiac valves by eliminating these areas from the ROI. For the aorta, we manually drew a free-hand ROI around the outer perimeter of the artery on every slice of the axially oriented PET/CT images. We carefully excluded skeletal-derived $Na^{18}F$ activity by eliminating these areas from the ROI. Per ROI, the maximum radiotracer-decay corrected $Na^{18}F$ activity (kBq/mL) was determined. Per arterial bed, maximum values obtained per ROI were summed and divided by the number of ROIs resulting in a single averaged maximum value (NaF_{MAX}) for the ascending aorta, aortic arch, descending thoracic aorta, and coronary arteries, respectively. Blood $Na^{18}F$ activity was determined in the lumen of the right atrium, aortic arch, right and left internal jugular vein, superior and inferior vena cava, and right and left femoral vein. Blood $Na^{18}F$ activity was determined by drawing a single ROI in the center of each vessel (or atrium) and was quantified as the radiotracer-decay corrected mean $Na^{18}F$ activity ($_{BLOOD}NaF_{MEAN}$). Quantification of blood $Na^{18}F$ activity is summarized in **SUPPLEMENTARY FIGURE 1**. To correct for blood $Na^{18}F$ activity, NaF_{MAX} was divided and subtracted by $_{BLOOD}NaF_{MEAN}$, respectively, to generate the maximum target-to-background ratio ($TBR_{MAX/MEAN}$) and maximum blood subtracted $Na^{18}F$ activity ($_{BS}NaF_{MAX}$). Blood-pool correction was performed with superior vena cava $_{BLOOD}NaF_{MEAN}$ only, because this location was least subject to spillover activity from adjacent $Na^{18}F$ avid structures. In addition, super vena cava $_{BLOOD}NaF_{MEAN}$ could be determined with excellent inter- and intra-rater agreement (**SUPPLEMENTARY TABLES 5** and **6**). Quantification of arterial $Na^{18}F$ uptake is summarized in **FIGURE 1**. The coronary calcium score, obtained from the cardiac CT images, was quantified in arbitrary units according to Agatston and as a volumetric score (mm^3) **(7)**.

Rater Reliability and Agreement

Inter- and intra-rater reliability and agreement of NaF_{MAX} and $_{BLOOD}NaF_{MEAN}$ were assessed two months after the initial analysis in a randomly selected sample of 10 subjects. Raters were masked for subject demographics, imaging specifications, and results from the initial analysis.

Statistical Analysis

Subject demographics were summarized by descriptive statistics. Mean $_{BLOOD}NaF_{MEAN}$ was compared among vascular beds by the repeated measures one-way analysis of variance (ANOVA). Multivariable linear regression assessed the dependence of $_{BLOOD}NaF_{MEAN}$, NaF_{MAX}, $TBR_{MAX/MEAN}$, and $_{BS}NaF_{MAX}$ on personal characteristics and technical factors. We did not evaluate non-linear or interaction effects. First, we tested if the assumptions of no multicollinearity

TABLE 1 - Subject demographics

	Total (*N* = 89)	**Minimum**	**Maximum**
Age, years	44 ± 14	21	75
Male, %	53		
Active smoking, %	3		
Blood pressure, mmHg			
- Systolic	128 ± 17	98	201
- Diastolic	77 ± 10	57	107
Body weight, kg	80 ± 18	50	145
Body surface area, m^2	1.93 ± 0.24	1.52	2.67
Body mass index, kg/m^2	27 ± 4	18	42
Cholesterol, mmol/L			
- Total	4.9 ± 0.9	2.9	7.4
- LDL	3.1 ± 0.8	1.3	5.0
- HDL	1.4 ± 0.5	0.7	3.2
Triglycerides, mmol/L	1.0 ± 0.7	0.3	4.5
Plasma glucose, mmol/L	5.5 ± 0.5	4.4	6.7
HbA1c (mmol/mol)	33.9 ± 4.1	24.0	49.0
Creatinine, µmol/L	79.3 ± 13.1	52.0	118.0
MDRD-eGFR, mL/min/1.73 m^2	82.9 ± 13.2	55.0	113.0
Coronary calcium score			
- Agatston score, arbitrary units	0 [0 to 0]	0	1046
- Volume, mm^3	0 [0 to 0]	0	430
Injected dose, MBq	174 ± 39	109	348
Circulation time, minutes	92 ± 4	90	109
NaF_{MAX}, kBq/mL			
- Ascending aorta	3.32 ± 1.17	1.69	6.43
- Aortic arch	3.25 ± 1.07	1.36	7.16
- Descending thoracic aorta	3.22 ± 0.88	1.64	5.92
- Coronary arteries	3.75 ± 0.91	2.03	6.13
PET/CT system, %			
- GE Discovery STE	25		
- GE Discovery VCT	21		
- GE Discovery RX	31		
- GE Discovery 690/710	22		

Values are mean ± standard deviation, %, or median [25 and 75 percentiles] for 89 subjects.

(tolerance statistic), independent errors (Durbin-Watson statistic), and homoscedasticity (graphically) between predictor variables were met. The assumption of no multicollinearity was violated by our predictor variables. Multicollinearity existed between injected dose, body weight, and body surface area (**SUPPLEMENTARY FIGURE 2**). The issue of multicollinearity was resolved by removing body weight and body surface area from the regression analyses. Subsequently, stepwise selection of variables, based on Akaike's information criterion, was performed by a backward elimination strategy. The categorical variable "PET/CT system" was entered as factor into the model with the GE Discovery 690/710 as reference system. Variables not selected by the model were considered not related to arterial $Na^{18}F$ uptake. Variability in variable selection was evaluated and adjusted for by a bootstrap of 2,000 samples **(8)**. Rater reliability was assessed by the intra-class correlation coefficient (ICC) (two-way random effects model assessing absolute agreement of single measures) **(9)**. Rater agreement was

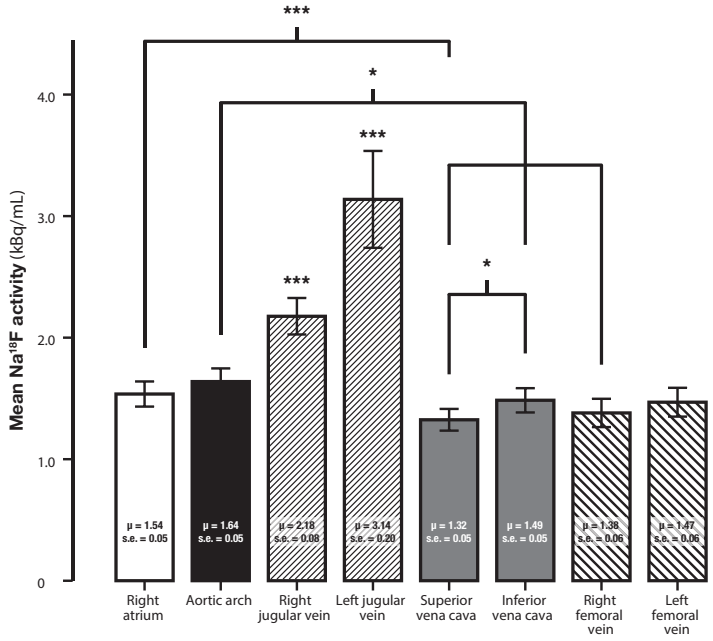

FIGURE 2 – Mean $Na^{18}F$ blood activity ($_{BLOOD}NaF_{MEAN}$) estimated in various vascular beds at 90 minutes after injection of $Na^{18}F$. Blood activity in the right and left internal jugular vein was significantly higher ($P < .001$) compared with other vascular beds. Activity in the aortic arch was significantly higher compared with the superior vena cava ($P < .001$), inferior vena cava ($P = .017$), and right femoral vein ($P = .001$). $_{BLOOD}NaF_{MEAN}$ was significantly lower in the superior vena cava than in the right atrium ($P < .001$) and inferior vena cava ($P = 0.010$). *Error bars* represent the 95 % confidence interval of the mean. * $P < .05$, P ** $< .01$, *** $P < .001$ based on the repeated measures ANOVA with a Bonferroni correction. μ = mean; s.e. = standard error of the mean.

assessed by calculation of the 95 % limits of agreement according to Bland and Altman **(10)**. A two-tailed *P* value below .05 was regarded statistically significant. To internally validate our results, *P* values and 95 % confidence intervals were determined by a bootstrap of 2,000 samples. The sample size was based on the regression analysis. For every predictor variable (i.e. six continuous and one categorical variable) we aimed to include 10 subjects resulting in a sample size of 90 subjects. Statistical analyses were performed by statistical software R version 3.1.2 combined with the packages 'bootStepAIC' version 1.2-0, 'MASS' version 7.3-35, 'car' version 2.0-22, and 'QuantPsyc' version 1.5.

RESULTS

Between November 2012 and May 2014 we prospectively recruited 90 healthy subjects. One subject was excluded from the analysis because she refused the PET/CT examination due to claustrophobia. Subject demographics are summarized in **TABLE 1**.

$_{\text{BLOOD}}\mathbf{NaF}_{\mathbf{MEAN}}$ was significantly different among vessel beds (F = 66.6; P < .001) (**FIGURE 2**). In particular, left internal jugular vein $_{\text{BLOOD}}\text{NaF}_{\text{MEAN}}$ was up to 58 % higher than $_{\text{BLOOD}}\text{NaF}_{\text{MEAN}}$ in other vascular beds (t = 10.2; P < .001). Similarly, right internal jugular vein $_{\text{BLOOD}}\text{NaF}_{\text{MEAN}}$ was up to 39 % higher than $_{\text{BLOOD}}\text{NaF}_{\text{MEAN}}$ in other vascular beds (t = 12.0; P < .001). Smaller, yet statistically significant, differences were observed between $_{\text{BLOOD}}\text{NaF}_{\text{MEAN}}$ in the right atrium, aortic arch, superior vena cava, inferior vena cava, and femoral veins. Subsequent analyses were performed with superior vena cava $_{\text{BLOOD}}\text{NaF}_{\text{MEAN}}$ only, because superior vena cava $_{\text{BLOOD}}\text{NaF}_{\text{MEAN}}$ was least subject to spillover activity from adjacent Na^{18}F avid structures and demonstrated excellent rater agreement (**FIGURE 2**, **SUPPLEMENTARY TABLES 5** and **6**). Superior vena cava $_{\text{BLOOD}}\text{NaF}_{\text{MEAN}}$ significantly depended on injected dose and PET/CT system (**TABLE 2**). For every 100 MBq increase in injected dose, $_{\text{BLOOD}}\text{NaF}_{\text{MEAN}}$ increased by 0.35 kBq/mL. $_{\text{BLOOD}}\text{NaF}_{\text{MEAN}}$ was significantly higher among subjects examined by the GE Discovery 690/710 than subjects examined by the GE Discovery VCT. Superior vena cava $_{\text{BLOOD}}\text{NaF}_{\text{MEAN}}$ did not depend on variations in renal function or circulating time.

At all levels of the arterial tree, $\mathbf{NaF}_{\mathbf{MAX}}$ was significantly affected by blood activity and PET/CT system. For every kBq/mL increase in $_{\text{BLOOD}}\text{NaF}_{\text{MEAN}}$, NaF_{MAX} increased by 0.92 to 0.97 kBq/mL for the aorta and by 0.86 kBq/mL for the coronary arteries. NaF_{MAX} was significantly higher among subjects examined by the GE Discovery 690/710 than subjects examined by the GE Discovery STE, VCT, or RX. In addition to blood activity and PET/CT system, descending

thoracic aortac NaF_{MAX} was significantly affected by renal function (β = -.15; *P* = .014) and ascending aorta NaF_{MAX} was significantly affected by renal function (β = -.11; *P* = .020) and injected dose (β = .19; *P* = .008). NaF_{MAX} was not affected by variations in circulating time (**TABLE 3** and **SUPPLEMENTARY TABLES 2-4**).

At all levels of the arterial tree, $\mathbf{TBR_{MAX/MEAN}}$ was significantly affected by blood activity and PET/CT system. For every kBq/mL increase in $_{BLOOD}NaF_{MEAN}$, $TBR_{MAX/MEAN}$ decreased by 1.15 to 1.27 for the aorta and 1.63 for the coronary arteries. $TBR_{MAX/MEAN}$ was significantly higher among subjects examined by the GE Discovery 690/710 than subjects examined by the GE Discovery STE, VCT, or RX. In addition to blood activity and PET/CT system, coronary $TBR_{MAX/MEAN}$ was significantly affected by injected dose (β = .30; *P* = .020) and ascending aorta $TBR_{MAX/MEAN}$ was significantly affected by injected dose (β = .33; *P* = .001) and renal function (β = -.12; *P* = .034). $TBR_{MAX/MEAN}$ was not affected by variations in circulating time (**TABLE 3** and **SUPPLEMENTARY TABLES 2-4**).

At all levels of the arterial tree, $\mathbf{_{BS}NaF_{MAX}}$ was significantly affected by PET/CT system. $_{BS}NaF_{MAX}$ was significantly higher among subjects examined by the GE Discovery 690/710 than subjects examined by the GE Discovery STE, VCT, or RX. In addition to PET/CT system, descending thoracic aorta $_{BS}NaF_{MAX}$ was significantly affected by renal function (β = -.18; *P* = .016) and ascending aorta $_{BS}NaF_{MAX}$ was significantly affected by renal function (β = -.13; *P* = .019) and injected dose (β = .21; *P* = .006). $_{BS}NaF_{MAX}$ was not affected by variations in blood activity or circulating time (**TABLE 3** and **SUPPLEMENTARY TABLES 2-4**).

TABLE 2 – Determinants of mean $Na^{18}F$ blood activity in the superior vena cava

	Regression coefficient	β	Adjusted R^2	*P* value
			.23	**< .001**
Intercept, kBq/mL	0.84 (0.42 to 1.49)			**.001**
Injected dose, 100 MBq	0.35 (0.03 to 0.55)	.32		**.011**
PET/CT system				
- GE Discovery STE	-0.14 (-0.36 to 0.13)	-.14		.310
- GE Discovery VCT	-0.39 (-0.61 to -0.16)	-.37		**< .001**
- GE Discovery RX	-0.01 (-0.23 to 0.19)	-.01		.948

Multivariable linear regression assessing the dependence of mean $Na^{18}F$ blood activity on renal function, injected dose, circulating time, and PET/CT system. Renal function and circulating time were eliminated by the model. β = standardized regression coefficient. The 95 % confidence interval is presented in parentheses.

DISCUSSION

Prospective evaluation of 89 healthy subjects demonstrated that quantification of arterial $Na^{18}F$ uptake is significantly affected by blood $Na^{18}F$ activity, $Na^{18}F$ injected dose, and PET/CT system, but not renal function and $Na^{18}F$ circulating time. Therefore, blood activity, injected dose, and PET/CT system should be taken into account to generate unbiased estimates of arterial $Na^{18}F$ uptake.

To account for **blood activity**, it has been proposed to calculate the ratio between arterial wall $Na^{18}F$ uptake and blood $Na^{18}F$ activity, known as the target-to-background ratio ($TBR_{MAX/MEAN}$) **(3, 5)**. However, the $TBR_{MAX/MEAN}$ has been criticized to be too dependent on variations in blood activity **(6)**. Our study confirmed that $TBR_{MAX/MEAN}$ is dependent on variations in blood activity. Therefore, quantifying arterial $Na^{18}F$ uptake as $TBR_{MAX/MEAN}$ may result in biased estimates of arterial $Na^{18}F$ uptake. In contrast, our study demonstrated that ${}_{BS}NaF_{MAX}$ does not depend on blood activity. Therefore, we prefer to quantify arterial $Na^{18}F$ uptake as ${}_{BS}NaF_{MAX}$ over $TBR_{MAX/MEAN}$. It should be noted that our preference cannot be substantiated by our data alone. For that, autoradiographic and histologic analysis of arterial $Na^{18}F$ uptake is necessary.

In studies that investigate vascular calcification metabolism with $Na^{18}F$ PET/CT, blood activity is commonly estimated in the superior vena cava, inferior vena cava, or right atrium **(3-6, 11-14)**. However, it is not known if estimates of blood activity are comparable among vessel beds. Theoretically, blood activity should be similar in intensity throughout the body, especially after prolonged circulating times. Nonetheless, our study demonstrated that estimates of blood activity differ significantly among vascular beds. In particular, recorded blood activity was higher in the right and left internal jugular vein compared with other vascular beds. Spillover activity from adjacent $Na^{18}F$ avid structures likely accounts for this observation. For example, we believe that spillover activity from the skeleton, including the sternum, clavicles, and cervical spine, increase blood $Na^{18}F$ activity estimates in the internal jugular veins. Similarly, we speculate that spillover activity from vascular calcifications may increase blood $Na^{18}F$ activity estimates in the aortic arch. Therefore, we advise to fix the location of blood $Na^{18}F$ activity estimation to the lumen of the superior vena cava, because this location is easy to identify and is largely devoid from spillover activity from adjacent $Na^{18}F$ avid structures. In addition, our study demonstrated that blood $Na^{18}F$ activity could be determined with higher inter- and intra-rater agreement at this location. The excellent rater agreement suggests that blood activity can be accurately estimated via placement of a

TABLE 3 – Determinants of $Na^{18}F$ uptake in the ascending aorta

	Regression coefficient	β	Adjusted R^2	*P* value
1. NaF_{MAX}, kBq/mL			.80	**< .001**
Intercept, kBq/mL	3.54 (2.59 to 4.23)			**< .001**
Blood activity, kBq/mL	0.94 (0.65 to 1.21)	.34		**< .001**
MDRD-eGFR, mL/min/1.73 m^2	-0.01 (-0.02 to -0.00)	-.11		**.020**
Injected dose, 100 MBq	0.57 (0.18 to 1.23)	.19		**.008**
PET/CT system				
- GE Discovery STE	-2.16 (-2.56 to -1.76)	-.80		**< .001**
- GE Discovery VCT	-2.14 (-2.55 to -1.74)	-.75		**< .001**
- GE Discovery RX	-1.99 (-2.37 to -1.61)	-.79		**< .001**
2. $TBR_{MAX/MEAN}$			.69	**< .001**
Intercept	4.89 (4.03 to 5.68)			**< .001**
Blood activity, kBq/mL	-1.27 (-1.75 to -0.90)	-.60		**< .001**
MDRD-eGFR, mL/min/1.73 m^2	-0.01 (-0.02 to -0.00)	-.12		**.034**
Injected dose, 100 MBq	0.77 (0.39 to 1.34)	.33		**.001**
PET/CT system				
- GE Discovery STE	-1.67 (-2.03 to -1.33)	-.80		**< .001**
- GE Discovery VCT	-1.54 (-1.89 to -1.20)	-.70		**< .001**
- GE Discovery RX	-1.55 (-1.86 to -1.24)	-.80		**< .001**
3. $_{BS}NaF_{MAX}$, kBq/mL			.74	**< .001**
Intercept, kBq/mL	3.47 (2.63 to 4.10)			**< .001**
MDRD-eGFR, mL/min/1.73 m^2	-0.01 (-0.02 to -0.00)	-.13		**.019**
Injected dose, 100 MBq	0.55 (0.24 to 1.13)	.21		**.006**
PET/CT system				
- GE Discovery STE	-2.15 (-2.52 to -1.78)	-.91		**< .001**
- GE Discovery VCT	-2.12 (-2.49 to -1.78)	-.86		**< .001**
- GE Discovery RX	-1.99 (-2.33 to -1.62)	-.91		**< .001**

Multivariable linear regression assessing the dependence of ascending aorta ^{18}FDG uptake on superior vena cava blood activity, plasma glucose, renal function, injected dose, circulating time, and PET/CT system. Plasma glucose, renal function, injected dose, and circulating time were eliminated by all models. In addition, blood activity was eliminated by model $_{BS}FDG_{MAX}$. The following quantifiers of arterial ^{18}FDG uptake were evaluated: FDG_{MAX}, $TBR_{MAX/MEAN}$, and $_{BS}FDG_{MAX}$. β = standardized regression coefficient. The 95 % confidence interval is presented in parentheses.

single ROI as compared to multiple ROIs over several slices as propagated by some authors **(13)**. In summary, standardized estimation of blood activity may reduce systematic errors and increase inter-study comparability.

In addition to blood activity, **renal function** affected quantification of arterial $Na^{18}F$ uptake. Renal function, expressed as MDRD-eGFR, negatively associated with NaF_{MAX}, $TBR_{MAX/MEAN}$, and ${}_{BS}NaF_{MAX}$. Theoretically, impaired renal function prolongs tracer availability and may contribute to increased $Na^{18}F$ accumulation in vascular calcifications. However, our study demonstrated that blood $Na^{18}F$ activity did not depend on variations in MDRD-eGFR. Therefore, it seems unlikely that impaired renal function influences quantification of arterial $Na^{18}F$ uptake by prolonging tracer availability. We believe that impaired renal function is a risk factor for the development of vascular calcification and consequently drives the degree of arterial $Na^{18}F$ uptake, instead of affecting its quantification. This view finds support in studies that demonstrated strong positive associations between impaired renal function and increased prevalence of vascular calcifications **(15-17)**.

In addition to blood activity and renal function, **injected $Na^{18}F$ dose** affected quantification of arterial $Na^{18}F$ uptake. The impact of injected $Na^{18}F$ dose is related to the distribution volume of $Na^{18}F$. An increase in body size, and hence distribution volume, may negatively impact the uptake of $Na^{18}F$ in the target organ, such as the arterial wall. To overcome this problem, our study administered a $Na^{18}F$ dosage proportional to the subject's body weight. However, our regression models demonstrated that arterial $Na^{18}F$ uptake increased linearly to injected dose for some arterial segments, which suggests overcompensation for the negative impact of distribution volume on arterial $Na^{18}F$ uptake. Calculation of the standardized uptake value (SUV) may account for variations in injected dose and distribution volume. The SUV is the decay-corrected activity concentration of $Na^{18}F$ (kBq/mL) adjusted for injected dose (MBq) and body surface area (cm^2) or body weight (g). However, the observed multicollinearity between injected dose, body weight, and body surface area prevented SUV from adequately correcting for variations in injected dose and distribution volume of the tracer (**SUPPLEMENTARY FIGURE 3**). To overcome issues surrounding injected $Na^{18}F$ dose, we advise to administer a fixed $Na^{18}F$ dose in studies evaluating vascular calcification with $Na^{18}F$ PET/CT and to take the effect of distribution volume of the tracer separately into account.

In addition to blood activity, renal function, and injected dose, quantification of arterial $Na^{18}F$ uptake was affected by differences in **PET/CT technology**. Even though our

imaging protocol adhered to international practice guidelines **(18)** and our PET/CT systems were calibrated to a phantom, subjects examined by the GE Discovery 690/710 had significantly higher arterial $Na^{18}F$ uptake than subjects examined on our older PET/CT systems (i.e. GE Discovery STE, VCT, or RX). Differences in imaging hard- and software likely account for this observation (**SUPPLEMENTARY TABLE 1**). It remains challenging to cross-calibrate PET/CT systems to overcome differences in imaging hard- and software, even if PET/CT systems are from the same vendor, as was the case in our study. However, promising initiatives in [^{18}F]-fluorodeoxyglucose (^{18}FDG) PET/CT imaging, such as the EARL ^{18}FDG PET/CT accreditation program **(19)**, can resolve issues surrounding differences in PET/CT technology and may contribute to improved inter-scan agreement in quantitative PET studies.

In contrast to blood activity, renal function, injected dose, and PET/CT system, **$Na^{18}F$-circulating time** did not affect quantification of arterial $Na^{18}F$ uptake. In a previous study our group demonstrated that circulating time affects quantification of arterial $Na^{18}F$ uptake **(6)**. In 38 subjects imaged at 45, 90 and 180 minutes after $Na^{18}F$ administration, we could demonstrate that the maximum SUV, a value related to NaF_{MAX}, and blood $Na^{18}F$ activity significantly decreases with time ($P < .001$ and $P < .001$, respectively), whereas the $TBR_{MAX/MEAN}$ significantly increases with time ($P < .001$). The blood subtracted maximum SUV, a value related to $_{BS}NaF_{MAX}$, was not affected by the circulating time ($P = 0.65$). In the present study, we fixed the circulating time of $Na^{18}F$ to approximately 90 minutes and demonstrated that quantification of arterial $Na^{18}F$ uptake was not affected by small variations in circulating time. Consequently, a fixed time between $Na^{18}F$ administration and PET/CT acquisition can adequately negate the impact of circulating time on quantification of arterial $Na^{18}F$ uptake.

Finally, our study demonstrated that quantification of arterial $Na^{18}F$ uptake and blood $Na^{18}F$ activity can be achieved with excellent inter- and intra-rater reliability and agreement (**SUPPLEMENTARY TABLES 5** and **6**). This finding is consistent with previously published reports **(5, 6)**.

Strengths and Limitations

An important strength of the present study is that we prospectively evaluated the effect of personal characteristics and technical factors on arterial $Na^{18}F$ uptake in a group of healthy subjects. By studying healthy subjects we limited bias from cardiovascular risk factors on the generated results. However, studying a healthy population prevents extrapolating the results to a more diseased population. For example, only 6 % of subjects had impaired renal function

(MDRD-eGFR < 60 mL/min/1.73 m^2). Therefore, we remain cautious in extrapolating our results to subjects with severe renal insufficiency. Second, although our study results were internally validated by bootstrap techniques, they lack external validation. To overcome this limitation, our study should preferably be repeated in a different study population by different researchers. Third, ethical considerations prevented collection of arterial specimens for histologic examination. Therefore, we could not associate arterial $Na^{18}F$ uptake to histologic markers of vascular calcification. For similar reasons, we could not collect invasive blood samples to determine and compare blood activity estimates obtained by PET/CT imaging to the true blood $Na^{18}F$ activity. Finally, the notion that quantification of arterial $Na^{18}F$ uptake by $TBR_{MAX/MEAN}$ is suboptimal compared to ${}_{BS}NaF_{MAX}$ cannot be substantiated by our data alone. Comparing arterial $Na^{18}F$ uptake to autoradiographic and histologic analysis of vascular calcification may be able to confirm the notion that ${}_{BS}NaF_{MAX}$ is a preferred quantifier of arterial $Na^{18}F$ uptake.

Conclusions

Prospective evaluation of 89 healthy subjects demonstrated that quantification of arterial $Na^{18}F$ uptake is affected by blood $Na^{18}F$ activity, injected dose, and PET/CT system. These factors should be accounted for in quantification methodologies to generate accurate estimates of arterial $Na^{18}F$ uptake.

REFERENCES

1. Czernin J, Satyamurthy N, Schiepers C. Molecular Mechanisms of Bone ^{18}F-NaF Deposition. *J Nucl Med*. 2010; **51**: 1826-1829.
2. Derlin T, Richter U, Bannas P, et al. Feasibility of ^{18}F-Sodium Fluoride PET/CT for Imaging of Atherosclerotic Plaque. *J Nucl Med*. 2010; **51**: 862-865.
3. Derlin T, Wisotzki C, Richter U, et al. In Vivo Imaging of Mineral Deposition in Carotid Plaque Using ^{18}F-Sodium Fluoride PET/CT: Correlation with Atherogenic Risk Factors. *J Nucl Med*. 2011; **52**: 362-368.
4. Joshi NV, Vesey AT, Williams MC, et al. ^{18}F-Fluoride Positron Emission Tomography for Identification of Ruptured and High-Risk Coronary Atherosclerotic Plaques: A Prospective Clinical Trial. *Lancet*. 2014; **383**: 705-713.
5. Dweck MR, Chow MW, Joshi NV, et al. Coronary Arterial ^{18}F-Sodium Fluoride Uptake: A Novel Marker of Plaque Biology. *J Am Coll Cardiol*. 2012; **59**: 1539-1548.
6. Blomberg BA, Thomassen A, Takx RA, et al. Delayed Sodium ^{18}F-Fluoride PET/CT Imaging Does not Improve Quantification of Vascular Calcification Metabolism: Results from the CAMONA Study. *J Nucl Cardiol*. 2014; **21**: 293-304.
7. Becker CR, Knez A, Ohnesorge B, et al. Visualization and Quantification of Coronary Calcifications with Electron Beam and Spiral Computed Tomography. *Eur Radiol*. 2000; **10**: 629-635.
8. Austin P, Tu J. Bootstrap Methods for Developing Predictive Models. *Am Stat*. 2004; **58**: 131-137.
9. Kottner J, Audige L, Brorson S, et al. Guidelines for Reporting Reliability and Agreement Studies (GRRAS) Were Proposed. *J Clin Epidemiol*. 2011; **64**: 96-106.
10. Bland JM, Altman DG. Statistical Methods for Assessing Agreement Between Two Methods of Clinical Measurement. *Lancet*. 1986; **327**: 307-310.
11. Derlin T, Janssen T, Salamon J, et al. Age-Related Differences in the Activity of Arterial Mineral Deposition and Regional Bone Metabolism: A ^{18}F-Sodium Fluoride Positron Emission Tomography Study. *Osteoporos Int*. 2015; **26**: 199-207.
12. Derlin T, Toth Z, Papp L, et al. Correlation of Inflammation Assessed by ^{18}F-FDG PET, Active Mineral Deposition Assessed by ^{18}F-Fluoride PET, and Vascular Calcification in Atherosclerotic Plaque: A Dual-Tracer PET/CT Study. *J Nucl Med*. 2011; **52**: 1020-1027.
13. Janssen T, Bannas P, Herrmann J, et al. Association of Linear ^{18}F-Sodium Fluoride Accumulation in Femoral Arteries as a Measure of Diffuse Calcification with Cardiovascular Risk Factors: A PET/CT Study. *J Nucl Cardiol*. 2013; **20**: 569-577.
14. Morbelli S, Fiz F, Piccardo A, et al. Divergent Determinants of ^{18}F-NaF Uptake and Visible

Calcium Deposition in Large Arteries: Relationship with Framingham Risk Score. *Int J Cardiovasc Imaging*. 2014; **30**: 439-447.

15. Demer LL, Tintut Y. Vascular Calcification: Pathobiology of a Multifaceted Disease. *Circulation*. 2008; **117**: 2938-2948.

16. Lamprea-Montealegre JA, McClelland RL, Astor BC, et al. Chronic Kidney Disease, Plasma Lipoproteins, and Coronary Artery Calcium Incidence: The Multi-Ethnic Study of Atherosclerosis. *Arterioscler Thromb Vasc Biol*. 2013; **33**: 652-658.

17. Sage AP, Tintut Y, Demer LL. Regulatory Mechanisms in Vascular Calcification. *Nat Rev Cardiol*. 2010; **7**: 528-536.

18. Segall G, Delbeke D, Stabin MG, et al. SNM Practice Guideline for Sodium ^{18}F-Fluoride PET/CT Bone Scans 1.0. *J Nucl Med*. 2010; **51**: 1813-1820.

19. Boellaard R, Delgado-Bolton R, Oyen WJ, et al. FDG PET/CT: EANM Procedure Guidelines for Tumour Imaging: Version 2.0. *Eur J Nucl Med Mol Imaging*. 2015; **42**: 328-354.

SUPPLEMENTARY FIGURES

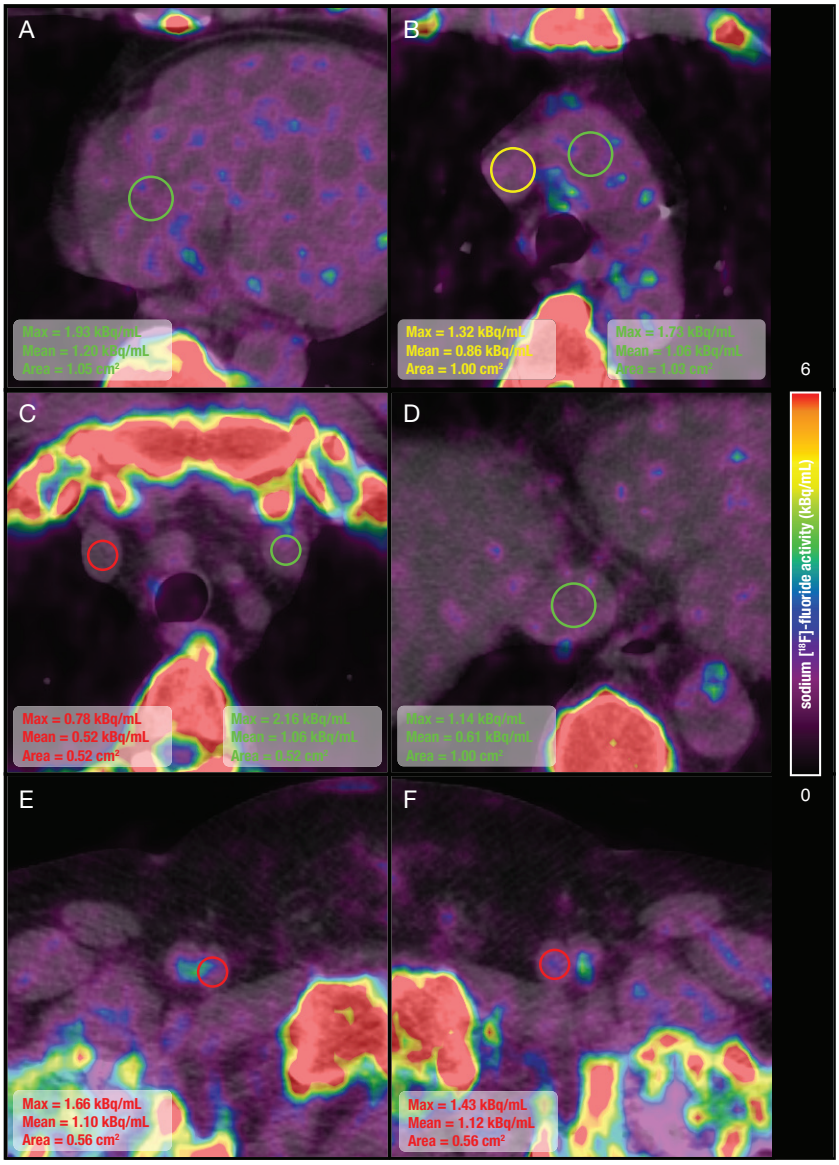

SUPPLEMENTARY FIGURE 1 – Illustration demonstrating quantification of mean $Na^{18}F$ blood activity ($_{BLOOD}NaF_{MEAN}$). On axially oriented $Na^{18}F$ PET/CT images, a circular region of interest (ROI), with an approximate area of 1 cm^2, was drawn in the center of the right atrium (**A**), superior vena cava (**B**), aortic arch (**B**), and proximal inferior vena cava (**D**). Similarly, a ROI, with an approximate area of 0.5 cm^2, was drawn in the right and left internal jugular vein (**C**) and right (**E**) and left femoral vein (**F**). Per ROI, the mean $Na^{18}F$ activity (kBq/mL) was determined.

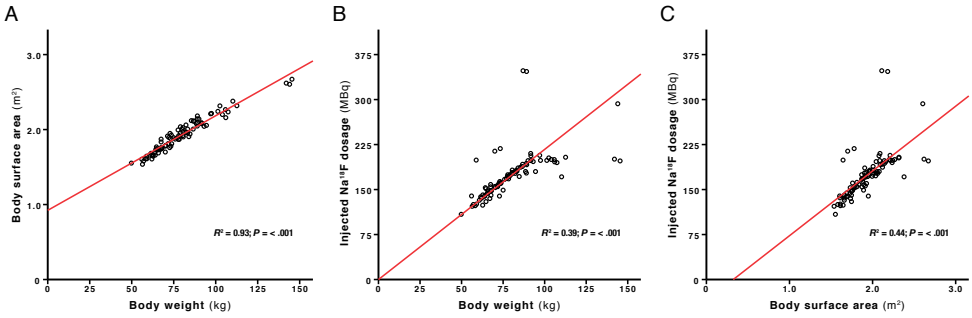

SUPPLEMENTARY FIGURE 2 – Scatter plot of (**A**) body surface area against body weight, (**B**) injected dose against body weight, and (**C**) injected dose against body surface area. The scatter plots together with the coefficients of determination (R^2) suggest multicollinearity between the variables. Multicollinearity was confirmed statistically by a tolerance statistic of 0.05, 0.06, and 0.35 for body surface area, body weight, and injected dose, respectively. Outliers observed in plot **B** and **C** are explained by differences in manual (n = 17) and automatic Na^{18}F administration (n = 72).

$$\mathrm{SUV} = \frac{\mathrm{Na}^{18}\mathrm{F\ activity\ (kBq \cdot mL^{-1}) \cdot body\ weight\ (g)}}{\mathrm{Injected\ dose\ (MBq)}} =$$

$$= \frac{\mathrm{Na}^{18}\mathrm{F\ activity\ (kBq \cdot mL^{-1}) \cdot body\ weight\ (g)}}{2.2\ \mathrm{MBq \cdot kg^{-1} \cdot body\ weight\ (kg)}} =$$

$$= \frac{\mathrm{Na}^{18}\mathrm{F\ activity\ (kBq \cdot mL^{-1})}}{2.2\ \mathrm{kBq \cdot kg^{-1}}}$$

SUPPLEMENTARY FIGURE 3 – Equation to normalize Na^{18}F uptake (kBq/mL) in the target of interest to injected dose (MBq) and body weight (g) known as the standardized uptake value (SUV). Body weight dependent Na^{18}F dose administration makes calculation of SUV ineffective.

SUPPLEMENTARY TABLES

SUPPLEMENTARY TABLE 1 – PET/CT system specifications and image reconstruction parameters

Vendor and type	System specifications		Image reconstruction parameters			
	PET scintillator	CT	Iterations/ Subsets	Post hoc filter	Reconstruction matrix	ToF/PSF
GE Discovery STE **(1)**	BGO	16-slice	2/28	6 mm	128x128	No/No
GE Discovery VCT **(1)**	BGO	64-slice	2/28	6 mm	128x128	No/No
GE Discovery RX **(2)**	LYSO	64-slice	2/21	6 mm	128x128	No/No
GE Discovery 690/710 **(3)**	LYSO	64-slice	3/24	5 mm	256x256	Yes/Yes

Summary of PET/CT system specifications and image reconstruction parameters. BGO, LYSO, and ToF/PSF indicate bismuth germanate, lutetium yttrium oxyorthosilicate, and time-of-flight and/or point spread function image reconstruction.

SUPPLEMENTARY TABLE 2 – Determinants of $Na^{18}F$ uptake in the aortic arch

	Regression coefficient	β	Adjusted R^2	*P* value
1. NaF_{MAX}, kBq/mL			.65	**< .001**
Intercept, kBq/mL	3.23 (2.62 to 3.77)			**< .001**
Blood activity, kBq/mL	0.97 (0.68 to 1.40)	0.39		**< .001**
PET/CT system				
- GE Discovery STE	-1.78 (-2.26 to -1.26)	-0.72		**< .001**
- GE Discovery VCT	-1.78 (-2.27 to -1.29)	-0.68		**< .001**
- GE Discovery RX	-1.42 (-1.85 to -1.00)	-0.62		**< .001**
2. $TBR_{MAX/MEAN}$			.52	**< .001**
Intercept	4.24 (3.44 to 4.91)			**< .001**
Blood activity, kBq/mL	-1.15 (-1.64 to -0.75)	-0.58		**< .001**
Injected dose, 100 MBq	0.46 (-0.04 to 1.09)	0.21		.058
PET/CT system				
- GE Discovery STE	-1.33 (-1.75 to -0.96)	-0.69		**< .001**
- GE Discovery VCT	-1.19 (-1.62 to -0.79)	-0.58		**< .001**
- GE Discovery RX	-1.15 (-1.47 to -0.84)	-0.63		**< .001**
3. $_{BS}NaF_{MAX}$, kBq/mL			.55	**< .001**
Intercept, kBq/mL	3.18 (2.82 to 3.59)			**< .001**
PET/CT system				
- GE Discovery STE	-1.78 (-2.28 to -1.31)	-0.82		**< .001**
- GE Discovery VCT	-1.76 (-2.24 to -1.33)	-0.78		**< .001**
- GE Discovery RX	-1.42 (-1.90 to -0.98)	-0.71		**< .001**

Multivariable linear regression assessing the dependence of aortic arch $Na^{18}F$ uptake on superior vena cava blood activity, renal function, injected dose, circulating time, and PET/CT system. "PET/CT system" was entered as categorical variable into the model with the GE Discovery 690/710 as reference system. Stepwise selection of variables, based on Akaike's information criterion, was performed by a backward elimination strategy. The following quantifiers of arterial $Na^{18}F$ uptake were evaluated: NaF_{MAX}, $TBR_{MAX/MEAN}$, and $_{BS}NaF_{MAX}$. β = standardized regression coefficient. The 95 % confidence interval is presented in parentheses.

SUPPLEMENTARY TABLE 3 – Determinants of $Na^{18}F$ uptake in the descending thoracic aorta

	Regression coefficient	β	Adjusted R^2	*P* value
1. NaF_{MAX}, kBq/mL			.69	**< .001**
Intercept, kBq/mL	3.84 (2.94 to 4.66)			**< .001**
Blood activity, kBq/mL	0.92 (0.69 to 1.20)	.44		**< .001**
MDRD-eGFR, mL/min/1.73 m^2	-0.01 (-0.02 to -0.00)	-.15		**.014**
PET/CT system				
- GE Discovery STE	-1.40 (-1.78 to -1.01)	-.69		**< .001**
- GE Discovery VCT	-1.36 (-1.76 to -0.95)	-.63		**< .001**
- GE Discovery RX	-1.16 (-1.51 to -0.80)	-.61		**< .001**
2. $TBR_{MAX/MEAN}$			.57	**< .001**
Intercept	4.83 (4.01 to 5.71)			**< .001**
Blood activity, kBq/mL	-1.21 (-1.70 to -0.87)	-.67		**< .001**
MDRD-eGFR, mL/min/1.73 m^2	-0.01 (-0.02 to 0.00)	-.14		.086
Injected dose, 100 MBq	0.42 (-0.06 to 0.89)	.21		.054
PET/CT system				
- GE Discovery STE	-1.06 (-1.46 to -0.73)	-.60		**< .001**
- GE Discovery VCT	-0.85 (-1.26 to -0.47)	-.46		**< .001**
- GE Discovery RX	-0.93 (-1.28 to -0.66)	-.57		**< .001**
3. $_{BS}NaF_{MAX}$, kBq/mL			.44	**< .001**
Intercept, kBq/mL	3.71 (2.91 to 4.46)			**< .001**
MDRD-eGFR, mL/min/1.73 m^2	-0.01 (-0.02 to -0.00)	-0.18		**.016**
PET/CT system				
- GE Discovery STE	-1.39 (-1.77 to -1.04)	-0.81		**< .001**
- GE Discovery VCT	-1.33 (-1.69 to -0.97)	-0.73		**< .001**
- GE Discovery RX	-1.16 (-1.51 to -0.82)	-0.73		**< .001**

Multivariable linear regression assessing the dependence of descending thoracic aorta $Na^{18}F$ uptake on superior vena cava blood activity, renal function, injected dose, circulating time, and PET/CT system. "PET/CT system" was entered as categorical variable into the model with the GE Discovery 690/710 as reference system. Stepwise selection of variables, based on Akaike's information criterion, was performed by a backward elimination strategy. The following quantifiers of arterial $Na^{18}F$ uptake were evaluated: NaF_{MAX}, $TBR_{MAX/MEAN}$, and $_{BS}NaF_{MAX}$. β = standardized regression coefficient. The 95 % confidence interval is presented in parentheses.

SUPPLEMENTARY TABLE 4 – Determinants of $Na^{18}F$ uptake in coronary arteries

	Regression coefficient	β	Adjusted R^2	*P* value
1. NaF_{MAX}, kBq/mL			.57	**< .001**
Intercept, kBq/mL	0.32 (-3.80 to 3.11)			.841
Blood activity, kBq/mL	0.86 (0.54 to 1.25)	.40		**< .001**
Injected dose, 100 MBq	0.40 (-0.04 to 1.14)	.17		.156
Circulating time, minutes	0.03 (-0.00 to 0.07)	.13		.091
PET/CT system				
- GE Discovery STE	-1.33 (-1.71 to -0.94)	-.63		**< .001**
- GE Discovery VCT	-1.17 (-1.56 to -0.75)	-.53		**< .001**
- GE Discovery RX	-1.39 (-1.79 to -1.01)	-.71		**< .001**
2. $TBR_{MAX/MEAN}$			.55	**< .001**
Intercept	4.55 (3.58 to 5.30)			**< .001**
Blood activity, kBq/mL	-1.63 (-2.37 to -1.09)	-.68		**< .001**
Injected dose, 100 MBq	0.79 (0.26 to 1.61)	.30		**.020**
PET/CT system				
- GE Discovery STE	-1.04 (-1.47 to -0.67)	-.44		**< .001**
- GE Discovery VCT	-0.58 (-1.00 to -0.16)	-.23		**.031**
- GE Discovery RX	-1.13 (-1.48 to -0.81)	-.51		**< .001**
3. $_{BS}NaF_{MAX}$, kBq/mL			.43	**< .001**
Intercept, kBq/mL	0.19 (-3.73 to 2.87)			.910
Injected dose, 100 MBq	0.35 (-0.00 to 1.09)	.17		.168
Circulating time, minutes	0.03 (-0.00 to 0.07)	.15		.076
PET/CT system				
- GE Discovery STE	-1.32 (-1.67 to -0.93)	-.72		**< .001**
- GE Discovery VCT	-1.11 (-1.49 to -0.73)	-.57		**< .001**
- GE Discovery RX	-1.39 (-1.78 to -1.00)	-.81		**< .001**

Multivariable linear regression assessing the dependence of coronary artery $Na^{18}F$ uptake on superior vena cava blood activity, renal function, injected dose, circulating time, and PET/CT system. "PET/CT system" was entered as categorical variable into the model with the GE Discovery 690/710 as reference system. Stepwise selection of variables, based on Akaike's information criterion, was performed by a backward elimination strategy. The following quantifiers of arterial $Na^{18}F$ uptake were evaluated: NaF_{MAX}, $TBR_{MAX/MEAN}$, and $_{BS}NaF_{MAX}$. β = standardized regression coefficient. The 95 % confidence interval is presented in parentheses.

SUPPLEMENTARY TABLE 5 – Intra-rater reliability and agreement of NaF_{MAX} and $_{BLOOD}NaF_{MEAN}$

	ICC	95 % CI	Mean difference (kBq/mL)	95 % Limits of agreement
NaF_{MAX}				
- Ascending aorta	0.99 *	0.98 to 1.00	0.02	-0.09 to 0.12
- Aortic arch	1.00 *	0.99 to 1.00	-0.02	-0.11 to 0.07
- Descending aorta	1.00 *	0.99 to 1.00	0.01	-0.09 to 0.11
- Coronary arteries	1.00 *	1.00 to 1.00	0.00	-0.04 to 0.04
$_{BLOOD}NaF_{MEAN}$				
- Right atrium	0.90 *	0.60 to 0.97	-0.06	-0.23 to 0.11
- Aortic arch	0.94 *	0.63 to 0.99	-0.08	-0.27 to 0.10
- Right jugular vein	0.95 *	0.81 to 0.99	-0.04	-0.18 to 0.10
- Left jugular vein	0.58	-0.01 to 0.88	0.12	-0.62 to 0.86
- Superior vena cava	0.94 *	0.77 to 0.98	-0.02	-0.13 to 0.10
- Inferior vena cava	0.98 *	0.93 to 1.00	0.00	-0.10 to 0.11
- Right femoral vein	0.97 *	0.79 to 0.99	0.06	-0.08 to 0.19
- Left femoral vein	0.88 *	0.60 to 0.97	-0.03	-0.32 to 0.26

Intra-rater reliability and agreement of NaF_{MAX} and $_{BLOOD}NaF_{MEAN}$. ICC = intraclass correlation coefficient (two-way random effects model assessing absolute agreement of single measures). CI = confidence interval. * $P < .001$.

SUPPLEMENTARY TABLE 6 – Inter-rater reliability and agreement of NaF_{MAX} and $_{BLOOD}NaF_{MEAN}$

	ICC	95 % CI	Mean difference (kBq/mL)	95 % Limits of agreement
NaF_{MAX}				
- Ascending aorta	0.98 *	0.90 to 1.00	0.06	-0.11 to 0.23
- Aortic arch	1.00 *	0.98 to 1.00	0.00	-0.14 to 0.13
- Descending aorta	0.99 *	0.97 to 1.00	0.00	-0.15 to 0.16
- Coronary arteries	1.00 *	1.00 to 1.00	0.01	-0.05 to 0.06
$_{BLOOD}NaF_{MEAN}$				
- Right atrium	0.79 *	0.28 to 0.94	-0.11	-0.39 to 0.17
- Aortic arch	0.95 *	0.82 to 0.99	-0.05	-0.24 to 0.14
- Right jugular vein	0.95 *	0.82 to 0.99	0.01	-0.16 to 0.17
- Left jugular vein	0.45	-0.17 to 0.83	-0.16	-1.04 to 0.72
- Superior vena cava	0.98 *	0.94 to 1.00	-0.01	-0.07 to 0.05
- Inferior vena cava	1.00 *	0.99 to 1.00	0.00	-0.04 to 0.05
- Right femoral vein	0.96 *	0.88 to 0.99	-0.03	-0.20 to 0.14
- Left femoral vein	0.89 *	0.61 to 0.97	0.01	-0.29 to 0.31

Inter-rater reliability and agreement of NaF_{MAX} and $_{BLOOD}NaF_{MEAN}$. ICC = intraclass correlation coefficient (two-way random effects model assessing absolute agreement of single measures). CI = confidence interval. * $P < .001$.

SUPPLEMENTARY REFERENCES

1. Teräs M, Tolvanen T, Johansson JJ, et al. Performance of the New Generation of Whole-Body PET/CT Scanners: Discovery STE and Discovery VCT. *Eur J Nucl Med Mol Imaging*. 2007; **34**: 1683-92.

2. Kemp BJ, Kim C, Williams JJ, et al. NEMA NU 2-2001 Performance Measurements of an LYSO-based PET/CT system in 2D and 3D Acquisition Modes. *J Nucl Med*. 2006; **47**: 1960-7.

3. Bettinardi V, Presotto L, Rapisarda E, et al. Physical Performance of the New Hybrid PET/CT Discovery-690. *Med Phys*. 2011; **38**: 5394-411.

PART II

Clinical Perspectives

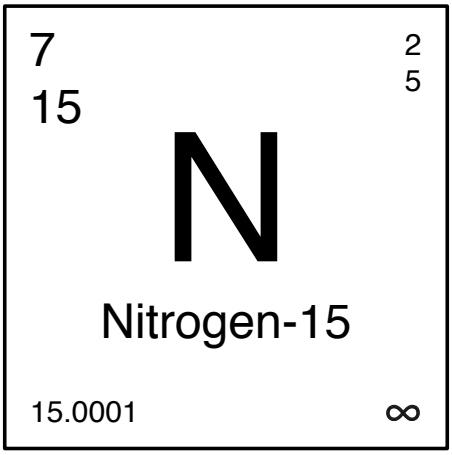
7
15
2
5
N
Nitrogen-15
15.0001
∞

Chapter 7

Reference Values for [^{18}F]-Fluorodeoxyglucose and Sodium [^{18}F]-Fluoride Uptake in Human Arteries: Prospective Evaluation of 89 Healthy Adults

Björn A. Blomberg
Anders Thomassen
Pim A. de Jong
Marnix G.E.H. Lam
Søren Hess
Michael H. Olsen
Werner Vach
Willem P.T.M. Mali
Abass Alavi
Poul F. Høilund-Carlsen

Submitted

ABSTRACT

Background: Reference values of [^{18}F]-fluorodeoxyglucose (^{18}FDG) and sodium [^{18}F]-fluoride (Na^{18}F) uptake in human arteries are unknown. The aim of this study was to determine age- and sex-specific reference values of arterial ^{18}FDG and Na^{18}F uptake.

Methods: Uptake of ^{18}FDG and Na^{18}F was determined in the ascending aorta, aortic arch, and descending thoracic aorta. In addition, ^{18}FDG uptake was determined in the carotid arteries and Na^{18}F uptake was determined in the coronary arteries. Arterial ^{18}FDG and Na^{18}F uptake were quantified as the blood-pool subtracted maximum activity concentration in kBq/mL ($_{BS}FDG_{MAX}$ and $_{BS}NaF_{MAX}$, respectively). In addition to determining reference values, we evaluated the dependence of $_{BS}FDG_{MAX}$ and $_{BS}NaF_{MAX}$ on aging and sex.

Results: Arterial ^{18}FDG and Na^{18}F uptake was assessed in 89 healthy adults aged 21-75 years (53 % males). Both $_{BS}FDG_{MAX}$ and $_{BS}NaF_{MAX}$ increased with aging. The increase in $_{BS}FDG_{MAX}$ with aging was significant for the descending aorta ($\beta = 0.28$; $P = .003$), whereas the increase in $_{BS}NaF_{MAX}$ with aging was significant for the ascending aorta ($\beta = 0.18$; $P < .001$), aortic arch ($\beta = 0.19$; $P = .006$), descending aorta ($\beta = 0.33$; $P < .001$), and coronary arteries ($\beta = 0.20$; $P = .009$), respectively. $_{BS}FDG_{MAX}$ and $_{BS}NaF_{MAX}$ did not associate with sex, except for ascending aorta $_{BS}FDG_{MAX}$.

Conclusions: Prospective evaluation of 89 healthy adults generated age- and sex-specific reference values of arterial ^{18}FDG and Na^{18}F uptake. Our findings indicate that arterial ^{18}FDG and Na^{18}F uptake tend to increase with aging.

INTRODUCTION

Atherosclerosis develops early in life **(1, 2)**, but remains asymptomatic for decades **(3)**. This provides an opportunity for early disease detection and initiation of treatment before symptoms occur **(3)**. Imaging atherosclerosis with [^{18}F]-fluorodeoxyglucose (^{18}FDG) and sodium [^{18}F]-fluoride (Na^{18}F) positron emission tomography/computed tomography (PET/CT) offers new prospects for early disease detection, risk stratification, and treatment monitoring, in addition to improving our understanding of atherosclerosis biology **(4, 5)**.

^{18}FDG and Na^{18}F PET/CT imaging of atherosclerosis has been validated in patients with advanced atherosclerotic disease, including patients with angina pectoris **(6, 7)**, myocardial infarction **(6, 7)**, high-grade carotid stenosis **(8)**, and stroke **(9)**. These studies demonstrated positive associations between arterial ^{18}FDG and Na^{18}F uptake and atherosclerotic disease severity. Few ^{18}FDG and Na^{18}F PET/CT studies, however, have been performed in subjects with moderate or mild atherosclerotic disease. Therefore, it remains unknown if ^{18}FDG and Na^{18}F PET/CT can detect early signs of atherosclerosis. Moreover, reference values of arterial ^{18}FDG and Na^{18}F uptake are not available, because arterial ^{18}FDG and Na^{18}F uptake were never assessed in healthy subjects. Reference values are important to determine if ^{18}FDG and Na^{18}F PET/CT imaging can detect early signs of atherosclerosis and distinguish subjects at low cardiovascular risk from those at increased cardiovascular risk.

The aim of this cross-sectional study was to determine age- and sex-specific reference values of arterial ^{18}FDG and Na^{18}F uptake.

METHODS

This study is part of the "Cardiovascular Molecular Calcification Assessed by ^{18}F-NaF PET/CT" (CAMONA) study. CAMONA was approved by the Danish National Committee on Health Research Ethics, registered at ClinicalTrials.gov (NCT01724749), and conducted in accordance with the Declaration of Helsinki. All study participants provided written informed consent. Details of CAMONA have been published previously **(10, 11)**.

Subject Selection

Healthy adults were recruited from the general population by local advertisement or from the blood bank of Odense University Hospital, Denmark. Subjects free of oncologic disease, autoimmune disease, immunodeficiency syndromes, alcohol abuse, illicit drug use, (symptoms

suggesting) cardiovascular disease, or prescription medication were considered healthy and were eligible for inclusion. Pregnant women were not considered for inclusion. Adults were preselected by age and sex to secure a balanced inclusion of males and females aged 20-29, 30-39, 40-49, 50-59, and ≥ 60 years.

Study Design

Study participants were evaluated by questionnaires, blood pressure measurements, blood analyses, the Systematic COronary Risk Evaluation (SCORE) tool **(12)**, ^{18}FDG PET/CT imaging, Na^{18}F PET/CT imaging, and non-contrast enhanced cardiac CT imaging. In addition, body weight (kg) and body mass index (kg/m^2) were determined. Questionnaires collected information about smoking habits. Blood pressure measurements were performed thrice after a supine rest of at least 30 minutes. The average of the last two measurements determined the systolic and diastolic blood pressure. Blood analyses determined fasting serum total cholesterol, serum LDL cholesterol, serum HDL cholesterol, serum triglycerides, fasting plasma glucose, glycated hemoglobin (HbA1c), and the Modification of Diet and Renal Disease (MDRD) estimated glomerular filtration rate (eGFR). For each subject, the 10-year risk for fatal cardiovascular disease was estimated based on SCORE. SCORE estimates the 10-year risk for fatal cardiovascular disease based on age, gender, systolic blood pressure, total serum cholesterol, serum HDL cholesterol, and smoking habits **(12)**. ^{18}FDG and Na^{18}F PET/CT imaging were performed according to previously published protocols **(10, 11)**. In summary, ^{18}FDG and Na^{18}F PET/CT imaging were performed on hybrid PET/CT systems (GE Discovery STE, VCT, RX, and 690/710). ^{18}FDG PET/CT imaging was performed at 180 minutes after intravenous injection of 4.0 MBq of ^{18}FDG per kilogram of body weight **(10)**. The ^{18}FDG was administered after an overnight fast of at least 8 hours. Prior to ^{18}FDG injection, the blood glucose concentration was determined to secure a value below 8 mmol/L. On average, Na^{18}F PET/CT imaging was performed within two weeks of ^{18}FDG PET/CT imaging. Na^{18}F PET/CT imaging was performed at 90 minutes after intravenous injection of 2.2 MBq of Na^{18}F per kilogram of body weight **(11)**. Positron emission tomography images were corrected for attenuation, scatter, random coincidences, and scanner dead time. Low–dose CT imaging (140 kV, 30-110 mA, noise index 25, 0.8 seconds per rotation, slice thickness 3.75 mm) was performed for attenuation correction and anatomic orientation. To determine the calcium volume (mm^3) in the coronary arteries, non-contrast enhanced, breath-hold, cardiac CT imaging (120 kV, 100 mA, 0.4 seconds per rotation, slice thickness 2.5 mm) was performed with electrocardiogram gating at 50 % of the R–R interval. The effective radiation dose received for the entire imaging protocol was approximately 14 mSv.

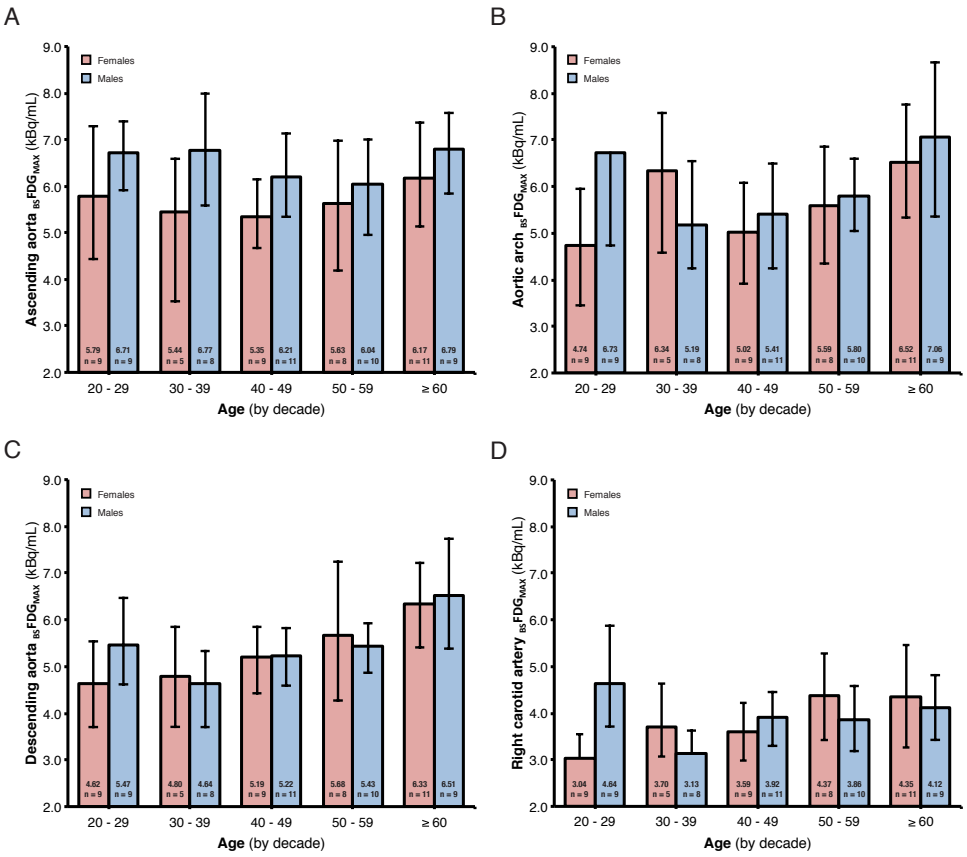

FIGURE 1 – Reference values of arterial ^{18}FDG uptake ($_{BS}$FDG$_{MAX}$) in the ascending aorta (**A**), aortic arch (**B**), descending thoracic aorta (**C**), and right carotid artery (**D**) stratified to sex and age by decade. *Error bars* represent the 95 % confidence interval of the mean. $_{BS}$FDG$_{MAX}$ indicates the blood-pool subtracted maximum [^{18}F]-fluorodeoxyglucose activity concentration (kBq/mL) adjusted for body weight and PET/CT scanner.

Quantitative Image Analyses

All images were analyzed by version 4.0 of the Philips IntelliSpace Portal client. The image analyst was masked to subject demographics and image specifications. Quantification of arterial ^{18}FDG and Na^{18}F uptake was performed according to previously published methods **(10, 11)**. In summary, uptake of ^{18}FDG in the ascending aorta, aortic arch, descending thoracic aorta, and carotid arteries was determined by manually placing an oval region of interest (ROI) around the outer perimeter of the artery on every slice of the axially oriented PET/

CT images. Per ROI, the maximum radiotracer-decay corrected ^{18}FDG activity concentration (kBq/mL) was determined. Per arterial bed, maximum values obtained per ROI were summed and divided by the number of ROIs resulting in a single averaged maximum value (FDG_{MAX}). Subsequently, FDG_{MAX} was adjusted for blood ^{18}FDG activity by subtracting blood activity from FDG_{MAX}. This yielded the blood-pool subtracted maximum ^{18}FDG activity concentration ($_{BS}FDG_{MAX}$). Blood ^{18}FDG activity was determined by drawing a single ROI in the lumen of superior vena cava. Blood ^{18}FDG was quantified as the radiotracer-decay corrected mean ^{18}FDG activity concentration (kBq/mL). Similarly, we calculated $_{BS}NaF_{MAX}$ for the ascending aorta, aortic arch, and descending aorta. Blood $Na^{18}F$ activity was determined by drawing a single ROI in the lumen of the superior vena cava. Blood $Na^{18}F$ was quantified as the radiotracer-decay corrected mean $Na^{18}F$ activity concentration (kBq/mL). Coronary artery $Na^{18}F$ uptake was determined by manually placing a free-hand region of interest (ROI) around the cardiac silhouette on every slice of the axially oriented PET/CT images. Per ROI, the maximum radiotracer-decay corrected $Na^{18}F$ activity concentration (kBq/mL) was determined. Maximum values obtained per ROI were summed and divided by the number of ROIs resulting in a single averaged maximum value (NaF_{MAX}). Subsequently, NaF_{MAX} was adjusted for blood $Na^{18}F$ activity by subtracting blood activity from NaF_{MAX}. This yielded the blood-pool subtracted maximum $Na^{18}F$ activity concentration ($_{BS}NaF_{MAX}$). Finally, we determined vascular calcium volumes (mm^3). The coronary calcium volume was determined on cardiac CT images **(13)**. The calcium volume (mm^3) in the ascending aorta, aortic arch, and descending aorta were determined on low-dose CT images obtained as part of PET/CT imaging. The detection threshold for vascular calcium was set at 130 Hounsfield units.

Statistical Analysis

First, $_{BS}FDG_{MAX}$ and $_{BS}NaF_{MAX}$ were adjusted for body weight and PET/CT technology by the factorial analysis of covariance (ANCOVA), because previous studies indicated that these parameters significantly affect quantification of arterial ^{18}FDG and $Na^{18}F$ uptake **(14)**. Second, reference values of arterial ^{18}FDG and $Na^{18}F$ uptake were determined by calculating mean values of $_{BS}FDG_{MAX}$ and $_{BS}NaF_{MAX}$ for five age strata (i.e. 20-29, 30-39, 40-49, 50-59, and ≥ 60). This was achieved by adding the categorical variable "age by decade" to the factorial ANCOVA. Reference values were determined separately for females and males. Third, subject demographics were summarized by descriptive statistics and compared between females and males by the unpaired Student's *t* test, Mann-Whitney *U* test, or Fisher's exact test. Fourth, the dependence of $_{BS}FDG_{MAX}$ and $_{BS}NaF_{MAX}$ on aging was evaluated. This was achieved by adding the continuous variable "age" to the factorial ANCOVA. Because $_{BS}FDG_{MAX}$ and $_{BS}NaF_{MAX}$ did not

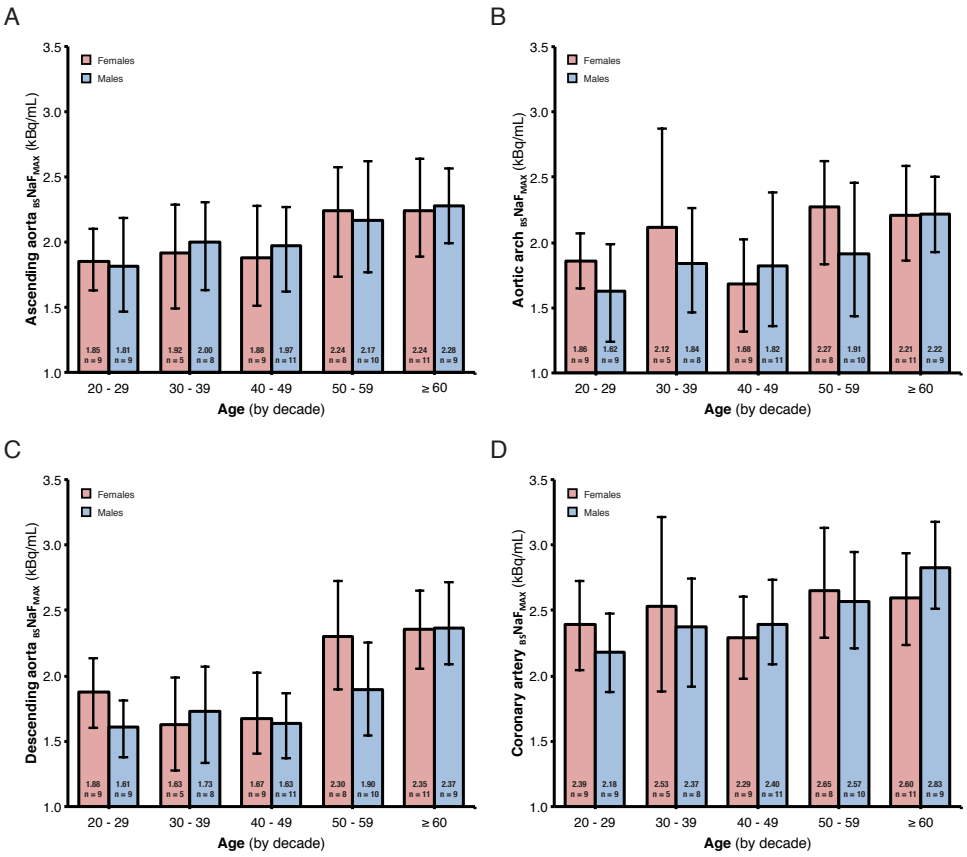

FIGURE 2 – Reference values of arterial Na^{18}F uptake ($_{BS}NaF_{MAX}$) in the ascending aorta (**A**), aortic arch (**B**), descending thoracic aorta (**C**), and coronary arteries (**D**) stratified to sex and age by decade. *Error bars* represent the 95 % confidence interval of the mean. $_{BS}NaF_{MAX}$ indicates the blood-pool subtracted maximum [^{18}F]-sodium fluoride activity concentration (kBq/mL) adjusted for body weight and PET/CT scanner.

associate with sex, the association with aging was evaluated in the entire study population. All ANCOVA models met the assumption of independency of covariates and homogeneity of regression slopes. A two-tailed *P* value below .05 was regarded statistically significant. To internally validate our results, *P* values and 95 % confidence intervals were determined by a bootstrap of 2,000 samples. Statistical analyses were performed by statistical software IBM SPSS Statistics version 21.

RESULTS

Between November 2012 and May 2014 we prospectively recruited 90 healthy adults. One subject was excluded from the study because she refused the PET/CT examination due to claustrophobia. The study population was considered very healthy (**TABLE 1**). On average, all modifiable cardiovascular risk factors, except body mass index, remained below recommended levels. Nonetheless, some individuals (n = 18) had cardiovascular risk factors, including elevated blood pressure (n = 2), increased serum total cholesterol (n = 5), and coronary calcifications (n = 14). Seventeen out of 18 adults with risk factors were aged 50 years or older. Therefore, we considered these risk factors part of normal aging and decided against excluding these individuals from the study.

Reference values of ${}_{BS}FDG_{MAX}$ and ${}_{BS}NaF_{MAX}$ are presented in **TABLE 2** and **TABLE 3**, respectively. Both ${}_{BS}FDG_{MAX}$ and ${}_{BS}NaF_{MAX}$ increased with aging (**FIGURE 1** and **2**, **TABLE 4**). The increase in ${}_{BS}FDG_{MAX}$ with aging was significant for the descending aorta (β = 0.28; P = .003), whereas the increase in ${}_{BS}NaF_{MAX}$ with aging was significant for the ascending aorta (β = 0.18; P < .001), aortic arch (β = 0.19; P = .006), descending aorta (β = 0.33; P < .001), and coronary arteries (β = 0.20; P = .009), respectively. The increase in ${}_{BS}FDG_{MAX}$ and ${}_{BS}NaF_{MAX}$ with aging is illustrated in **Figure 3**. ${}_{BS}FDG_{MAX}$ and ${}_{BS}NaF_{MAX}$ did not associate with sex, except for ascending aorta ${}_{BS}FDG_{MAX}$ (**TABLE 1**).

DISCUSSION

Prospective evaluation of 89 healthy adults generated age- and sex-specific reference values of arterial ^{18}FDG and Na^{18}F uptake. Our findings indicate that arterial ^{18}FDG and Na^{18}F uptake tend to increase with aging.

^{18}FDG PET/CT targets atherosclerotic plaque inflammation **(4)**. Particularly, ^{18}FDG accumulates in plaque macrophages and uptake strongly correlates with macrophage density **(15-17)**. Macrophages play an important role in atherosclerotic plaque formation, plaque evolution, and inception of plaque vulnerability **(18)**. Arterial ^{18}FDG retention also seems to depend on plaque hypoxia **(19)**, another determinant of plaque vulnerability **(20)**. By targeting plaque macrophages and hypoxia, ^{18}FDG PET/CT can potentially detect asymptomatic patients at high risk for cardiovascular events **(21)**. Although ^{18}FDG PET/CT is a promising non-invasive imaging technique for assessment of atherosclerosis, it has solely been applied in patients at high cardiovascular risk. Therefore, it remains unknown if ^{18}FDG PET/CT can detect signs of

TABLE 1 - Subject demographics

	Female (*n* = 42)	**Male** (*n* = 47)	***P* value**	**Total** (*N* = 89)
Age, years	45 ± 14	44 ± 14	.748	44 ± 14
Smokers, %				
- Former	43	30	.664	36
- Current	2	4	.660	3
Blood pressure, mmHg				
- Systolic	124 ± 17	131 ± 17	**.041**	128 ± 17
- Diastolic	75 ± 10	78 ± 10	.112	77 ± 10
Body weight, kg	70 ± 10	89 ± 10	**< .001**	80 ± 18
Body mass index, kg/m^2	25 ± 3	27 ± 5	**.021**	27 ± 4
Cholesterol, mmol/L				
- Total	5.0 ± 0.9	4.8 ± 0.9	.315	4.9 ± 0.9
- LDL	3.0 ± 0.8	3.1 ± 0.8	.605	3.1 ± 0.8
- HDL	1.7 ± 0.5	1.2 ± 0.3	**< .001**	1.4 ± 0.5
Triglycerides, mmol/L	0.8 ± 0.3	1.2 ± 0.8	**.014**	1.0 ± 0.7
Plasma glucose, mmol/L	5.4 ± 0.5	5.7 ± 0.5	**.009**	5.5 ± 0.5
HbA1c, mmol/mol	33.0 ± 3.4	34.7 ± 4.5	**.041**	33.9 ± 4.1
eGFR, mL/min/1.73 m^2	81.3 ± 14.5	84.3 ± 11.7	.306	82.9 ± 13.2
SCORE, %	0 [0 to 0.3]	0 [0 to 1]	**.005**	0 [0 to 1]
Vascular calcification, mm^3				
- Ascending aorta	0 [0 to 0]	0 [0 to 0]	.198	0 [0 to 0]
- Aortic arch	0 [0 to 0]	0 [0 to 0]	.973	0 [0 to 0]
- Descending aorta	0 [0 to 0]	0 [0 to 0]	.863	0 [0 to 0]
- Carotid arteries	0 [0 to 0]	0 [0 to 0]	.999	0 [0 to 0]
- Coronary arteries	0 [0 to 0]	0 [0 to 9]	**.008**	0 [0 to 0]
Injected dose, MBq				
- [^{18}F]-fluorodeoxyglucose	271 ± 43	338 ± 53	**< .001**	306 ± 59
- [^{18}F]-sodium fluoride	156 ± 25	190 ± 42	**< .001**	174 ± 39
Circulating time, minutes				
- [^{18}F]-fluorodeoxyglucose	181 ± 4	181 ± 4	.691	181 ± 4
- [^{18}F]-sodium fluoride	92 ± 5	91 ± 3	.268	92 ± 4

Continued on page 160

TABLE 1 - Subject demographics, *continued*

	Female (*n* = 42)	**Male** (*n* = 47)	***P* value**	**Total** (*N* = 89)
$_{BS}$FDG$_{MAX}$, kBq/mL				
- Ascending aorta	5.70 ± 1.71	6.49 ± 1.63	**.031**	6.12 ± 1.67
- Aortic arch	5.51 ± 1.80	6.13 ± 2.47	.234	5.84 ± 2.15
- Descending thoracic aorta	5.30 ± 1.53	5.56 ± 1.60	.490	5.44 ± 1.57
- Right carotid artery	3.76 ± 1.56	4.00 ± 1.25	.458	3.89 ± 1.40
- Left carotid artery	4.11 ± 2.22	4.09 ± 2.73	.982	4.10 ± 2.49
$_{BS}$NaF$_{MAX}$, kBq/mL				
- Ascending aorta	2.03 ± 0.56	2.06 ± 0.53	.777	2.05 ± 0.54
- Aortic arch	2.01 ± 0.64	1.89 ± 0.79	.479	1.95 ± 0.72
- Descending thoracic aorta	1.98 ± 0.54	1.87 ± 0.50	.325	1.92 ± 0.52
- Coronary arteries	2.49 ± 0.56	2.47 ± 0.57	.868	2.48 ± 0.57
PET/CT system, % (^{18}FDG / Na^{18}F)				
- GE Discovery STE	21 / 33	19 / 17		20 / 25
- GE Discovery VCT	31 / 21	32 / 21		31 / 21
- GE Discovery RX	17 / 21	32 / 40		25 / 31
- GE Discovery 690/710	31 / 24	17 / 21		24 / 22

Values are mean ± standard deviation, %, or median [25 and 75 percentiles]. HbA1c, eGFR, $_{BS}$FDG$_{MAX}$, and $_{BS}$NaF$_{MAX}$ indicates glycated hemoglobin, estimated glomerular filtration rate, blood-pool subtracted maximum [^{18}F]-fluorodeoxyglucose activity concentration (kBq/mL) adjusted for body weight and PET/CT scanner, and blood-pool subtracted maximum [^{18}F]-sodium fluoride activity concentration (kBq/mL) adjusted for body weight and PET/CT scanner.

atherosclerosis in subjects at low cardiovascular risk. Moreover, reference values of arterial wall ^{18}FDG uptake are unavailable, because arterial ^{18}FDG uptake was never assessed in healthy subjects.

Na^{18}F PET/CT targets the exchange of fluoride with hydroxyl ions of hydroxylapatite crystals producing fluorapatite **(22)**. Hydroxylapatite is the structural component of vascular calcification and is laid down in the earliest and most active stages of atherosclerotic plaque calcification **(23)**. Traditionally, vascular calcification is detected and quantified by computed tomography (CT) imaging **(13)**. CT imaging studies have demonstrated that vascular calcification is a strong independent predictor of cardiovascular morbidity and mortality **(24, 25)**. Nonetheless, CT imaging of vascular calcification has inherent limitations. First, CT's

limited sensitivity prevents detection of vascular calcification at the molecular level **(26)**. Second, CT imaging cannot distinguish active from indolent vascular calcification, a possible biomarker for vulnerable and stabilized atherosclerotic plaque, respectively **(6, 27, 28)**. Imaging vascular calcification with Na^{18}F PET/CT can possibly overcome these limitations. By targeting fluorapatite formation, Na^{18}F PET/CT can detect vascular calcification at the molecular level as well as discriminate active from indolent vascular calcification **(11)**. As such, arterial Na^{18}F PET/CT imaging may improve cardiovascular risk stratification beyond established approaches, such as the SCORE tool or the CT coronary calcium score. Although Na^{18}F PET/CT is a promising non-invasive imaging technique for assessment of atherosclerosis, it has solely been validated in patients at high cardiovascular risk **(6, 29)**. Therefore, it remains unknown if Na^{18}F PET/CT can detect signs of atherosclerosis in subjects at low cardiovascular risk. Moreover, reference values of arterial Na^{18}F uptake are unavailable, because arterial Na^{18}F uptake was never assessed in healthy subjects.

For the first time, we have generated age- and sex-specific reference values by studying arterial ^{18}FDG and Na^{18}F uptake in very healthy adults expected to have low prevalence of atherosclerosis. The generated reference values provide a baseline to which results of other

TABLE 2 - Reference values of arterial ^{18}FDG and Na^{18}F uptake in females

	Age by decade				
	20 – 29 (*n* = 9)	**30 – 39** (*n* = 5)	**40 – 49** (*n* = 9)	**50 – 59** (*n* = 8)	**≥ 60** (*n* = 11)
$_{BS}$**FDG**$_{MAX}$, kBq/mL					
- Ascending aorta	5.79 ± 2.26	5.44 ± 1.51	5.35 ± 1.06	5.63 ± 1.98	6.17 ± 1.90
- Aortic arch	4.74 ± 1.70	6.34 ± 1.75	5.02 ± 1.61	5.59 ± 1.72	6.52 ± 1.92
- Descending thoracic aorta	4.62 ± 1.40	4.80 ± 1.09	5.19 ± 1.06	5.68 ± 2.25	6.33 ± 1.46
- Right carotid artery	3.04 ± 0.78	3.70 ± 1.03	3.59 ± 0.91	4.37 ± 1.35	4.35 ± 1.99
- Left carotid artery	3.23 ± 1.01	3.51 ± 1.25	4.17 ± 1.11	4.49 ± 1.82	5.21 ± 2.95
$_{BS}$**NaF**$_{MAX}$, kBq/mL					
- Ascending aorta	1.85 ± 0.37	1.92 ± 0.41	1.88 ± 0.59	2.24 ± 0.56	2.24 ± 0.59
- Aortic arch	1.86 ± 0.33	2.12 ± 0.97	1.68 ± 0.53	2.27 ± 0.56	2.21 ± 0.56
- Descending thoracic aorta	1.88 ± 0.41	1.63 ± 0.36	1.67 ± 0.45	2.30 ± 0.60	2.35 ± 0.48
- Coronary arteries	2.39 ± 0.52	2.53 ± 0.73	2.29 ± 0.48	2.65 ± 0.54	2.60 ± 0.61

Reference values of arterial ^{18}FDG and Na^{18}F uptake in females stratified to age by decade. Values are mean ± standard deviation. Abbreviations as in **TABLE 1**.

TABLE 3 - Reference values of arterial ^{18}FDG and Na^{18}F uptake in males

	Age by decade				
	20 – 29 (*n* = 9)	**30 – 39** (*n* = 8)	**40 – 49** (*n* = 11)	**50 – 59** (*n* = 10)	**≥ 60** (*n* = 9)
$_{BS}$FDG$_{MAX}$, kBq/mL					
- Ascending aorta	6.71 ± 1.24	6.77 ± 1.72	6.21 ± 1.53	6.04 ± 1.58	6.79 ± 1.28
- Aortic arch	6.73 ± 2.60	5.19 ± 1.68	5.41 ± 2.05	5.80 ± 1.35	7.06 ± 2.78
- Descending thoracic aorta	5.47 ± 1.39	4.64 ± 1.18	5.22 ± 1.08	5.43 ± 0.93	6.51 ± 1.96
- Right carotid artery	4.64 ± 1.21	3.13 ± 1.23	3.92 ± 1.23	3.86 ± 1.19	4.12 ± 1.17
- Left carotid artery	6.01 ± 4.46	2.64 ± 1.50	3.97 ± 3.38	3.56 ± 1.52	3.88 ± 2.02
$_{BS}$NaF$_{MAX}$, kBq/mL					
- Ascending aorta	1.81 ± 0.52	2.00 ± 0.48	1.97 ± 0.56	2.17 ± 0.70	2.28 ± 0.47
- Aortic arch	1.62 ± 0.55	1.84 ± 0.56	1.82 ± 0.98	1.91 ± 0.78	2.22 ± 0.45
- Descending thoracic aorta	1.61 ± 0.30	1.73 ± 0.49	1.63 ± 0.44	1.90 ± 0.58	2.37 ± 0.51
- Coronary arteries	2.18 ± 0.44	2.37 ± 0.68	2.40 ± 0.56	2.57 ± 0.65	2.83 ± 0.53

Reference values of arterial ^{18}FDG and Na^{18}F uptake in males stratified to age by decade. Values are mean ± standard deviation. Abbreviations as in **TABLE 1**.

studies can be compared. For example, comparing our reference values to data obtained in subjects at increased cardiovascular risk may help determine if ^{18}FDG and Na^{18}F PET/CT can distinguish subjects at low cardiovascular risk from those at increased cardiovascular risk.

Quantitative PET results in general and reference values of arterial ^{18}FDG and Na^{18}F uptake in particular should be interpreted cautiously. Namely, PET/CT imaging is associated with inherent limitations, which may cause wrong conclusions. Notably, our quantitative image analysis detected substantial arterial ^{18}FDG and Na^{18}F activity in arteries of young adults. As the prevalence of atherosclerosis is low in young adults **(30)**, we expected to quantify negligible ^{18}FDG and Na^{18}F uptake in arteries of the young. Our expectations were supported by post hoc visual inspection of the PET images. We occasionally detected ^{18}FDG and Na^{18}F uptake in arteries of the young, whereas uptake was regularly observed in arteries of elderly subjects (**Figure 3**). Nonetheless, our quantitative approach detected substantial arterial ^{18}FDG and Na^{18}F activity in the young, which only gradually increased with aging. Although the activity observed in the young may partly reflect true disease activity, it likely represents non-specific background activity as a consequence of partial volume and scatter effects. Partial volume and scatter effects may overestimate arterial tracer uptake in subjects

with low disease activity and underestimate arterial tracer uptake in subjects with high disease activity. Although our PET images were corrected for scatter effects, partial volume effects were not considered. This may partly explain why our quantitative approach detected only small differences in arterial tracer uptake between young and elderly arteries, whereas post hoc visual analysis suggested a more sizeable difference in arterial tracer uptake between the young and elderly. Interpreting reference values of arterial ^{18}FDG and Na^{18}F is further complicated by an incomplete understanding of the metabolic pathways that govern ^{18}FDG and Na^{18}F uptake in atherosclerotic arteries **(31)**. Although a fair number of histopathology studies have linked arterial ^{18}FDG uptake to plaque inflammation **(15-17)** and arterial Na^{18}F uptake to atherosclerotic plaque calcification **(6)**, these studies were solely performed in patients with advanced atherosclerotic disease. In addition, these studies investigated a relatively small

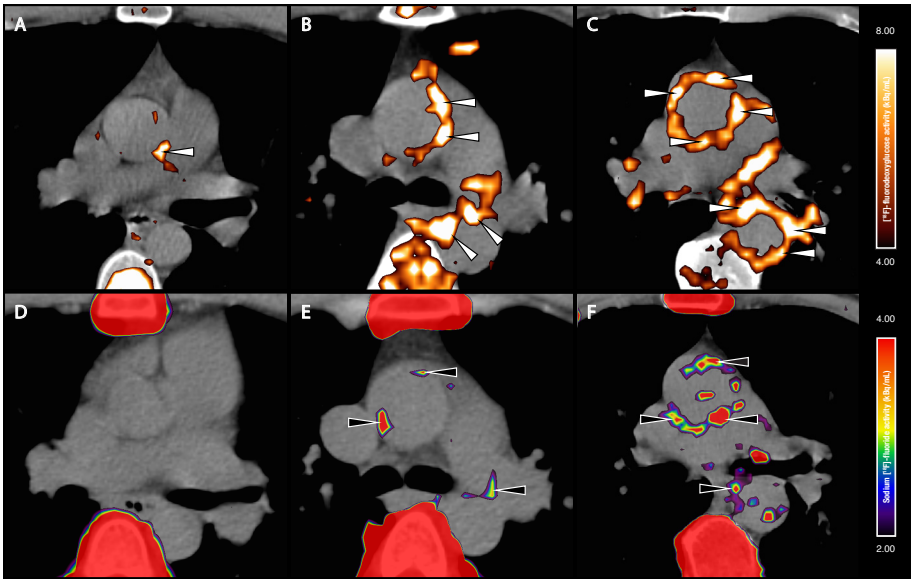

FIGURE 3 – Axial ^{18}FDG (*top*) and Na^{18}F PET/CT images (*bottom*) showing the ascending and descending aorta at the level of the pulmonary artery. Image **A** and **D** were obtained in a 25-year old male without traditional cardiovascular risk factors, a body mass index of 24 kg/m^2, a negative coronary calcium score, and a SCORE of 0 %. ^{18}FDG accumulated in the ascending aorta (*white arrowhead*). Image **B** and **E** were obtained in a 44-year old male without traditional cardiovascular risk factors, a body mass index of 24 kg/m^2, a negative coronary calcium score, and a SCORE 0 %. Both ^{18}FDG and Na^{18}F accumulated in the ascending and descending aorta (*white* and *black arrowheads*). Image **C** and **F** were obtained in a 65-year old male without traditional cardiovascular risk factors, a body mass index of 21 kg/m^2, a coronary calcium score of 292 mm^3, and a SCORE of 3 %. Significant uptake of ^{18}FDG and Na^{18}F was observed in both the ascending and descending aorta (*white* and *black arrowheads*).

TABLE 4 - Dependence of arterial ^{18}FDG and Na^{18}F uptake on aging

	Constant	*B*	β	*P* value
$_{BS}$**FDG**$_{MAX}$, kBq/mL				
- Ascending aorta	2.04	0.03 (-0.24 to 0.31)	0.02	.804
- Aortic arch	1.91	0.29 (-0.03 to 0.62)	0.17	.086
- Descending thoracic aorta	2.48	0.38 (0.17 to 0.59)	0.28	**.003**
- Right carotid artery	1.35	0.17 (-0.01 to 0.35)	0.15	.082
- Left carotid artery	1.94	0.09 (-0.40 to 0.49)	0.06	.676
$_{BS}$**NaF**$_{MAX}$, kBq/mL				
- Ascending aorta	-0.23	0.13 (0.07 to 0.19)	0.18	**< .001**
- Aortic arch	0.41	0.13 (0.04 to 0.21)	0.19	**.006**
- Descending thoracic aorta	0.36	0.18 (0.12 to 0.24)	0.33	**< .001**
- Coronary arteries	0.05	0.12 (0.03 to 0.19)	0.20	**.009**

Dependence of arterial ^{18}FDG and Na^{18}F uptake on aging. *B* = regression coefficient of age in decades. β = standardized regression coefficient of age. The 95 % confidence interval is presented in parentheses. Abbreviations as in **TABLE 1**.

number of patients (n < 20) and only carotid artery plaques were evaluated. Therefore, the biological basis of ^{18}FDG and Na^{18}F uptake in atherosclerotic arteries remain ambiguous **(31, 32)**, especially in arteries other than carotid arteries and in arteries with moderate, mild, or no atherosclerotic disease. The incomplete understanding of the arterial ^{18}FDG and Na^{18}F signal impedes adequate interpretation of imaging results aimed at quantifying active metabolic processes that govern the early stages of atherosclerosis. Validation studies substantiating arterial ^{18}FDG and Na^{18}F uptake to histopathology, either performed in humans or animals, are clearly needed to overcome this important limitation.

The findings from this study should be interpreted in light of its other limitations. First, study participants were examined on three generations of PET/CT scanner. Differences in imaging hardware- and software can influence results of quantitative PET studies **(33, 34)**. To overcome this limitation, we applied statistical corrections. Nonetheless, our reference values should be interpreted cautiously when compared to data generated on hardware- and software that differ in generation and possibly vendor. Second, our quantitative image analysis did not correct for partial volume effects. Partial volume effects may result in under- or overestimated values of arterial tracer uptake **(35)**. Although methods for partial volume correction have been described **(36)**, they are rarely applied in arterial PET studies. Third, we could not assess

^{18}FDG uptake in coronary arteries and Na^{18}F uptake in the carotid arteries. High myocardial ^{18}FDG retention and cardiac motion artifacts prevented accurate detection of coronary ^{18}FDG uptake. Similarly, high Na^{18}F retention in the spine and skull prevented accurate detection of carotid Na^{18}F uptake. Fourth, we fixed the tracer circulating time to 180 and 90 minutes for ^{18}FDG and Na^{18}F, respectively. Differences in circulating time can affect results in quantitative PET studies **(10, 11)**. Particularly, arterial ^{18}FDG uptake seems to depend on the circulating time of the tracer **(10)**. Therefore, our results should be interpreted cautiously when compared to studies that applied different circulating times. Fifth, the dependence of arterial ^{18}FDG and Na^{18}F uptake on sex and age was evaluated in a cross-sectional study with a relatively small sample size. Large within-subject variability in arterial tracer uptake and statistical type II errors may explain the lack of association with sex and the limited association between arterial ^{18}FDG uptake and age.

Conclusions

Prospective evaluation of 89 healthy adults generated age- and sex-specific reference values of arterial ^{18}FDG and Na^{18}F uptake. Our findings indicate that arterial ^{18}FDG and Na^{18}F uptake are dependent on aging.

REFERENCES

1. Berenson GS, Srinivasan SR, Bao W, et al. Association Between Multiple Cardiovascular Risk Factors and Atherosclerosis in Children and Young Adults. The Bogalusa Heart Study. *N Engl J Med*. 1998; **338**: 1650-6.

2. McGill HC, McMahan CA. Determinants of Atherosclerosis in the Young. Pathobiological Determinants of Atherosclerosis in Youth (PDAY) Research Group. *Am J Cardiol*. 1998; **82**: 30T-36T.

3. Arbab-Zadeh A, Fuster V. The Myth of the "Vulnerable Plaque": Transitioning from a Focus on Individual Lesions to Atherosclerotic Disease Burden for Coronary Artery Disease Risk Assessment. *J Am Coll Cardiol*. 2015; **65**: 846-55.

4. Tarkin JM, Joshi FR, Rudd JH. PET Imaging of Inflammation in Atherosclerosis. *Nat Rev Cardiol*. 2014; **11**: 443-57.

5. Dweck MR, Joshi FR, Newby DE, et al. Noninvasive Imaging in Cardiovascular Therapy: The Promise of Coronary Arterial ^{18}F-Sodium Fluoride Uptake as a Marker of Plaque Biology. *Expert Rev Cardiovasc Ther*. 2012; **10**: 1075-7.

6. Joshi NV, Vesey AT, Williams MC, et al. ^{18}F-Fluoride Positron Emission Tomography for Identification of Ruptured and High-Risk Coronary Atherosclerotic Plaques: A Prospective Clinical Trial. *Lancet*. 2014; **383**: 705-13.

7. Rogers IS, Nasir K, Figueroa AL, et al. Feasibility of FDG Imaging of the Coronary Arteries: Comparison Between Acute Coronary Syndrome and Stable Angina. *J Am Coll Cardiol Img*. 2010; **3**: 388-97.

8. Menezes LJ, Kotze CW, Agu O, et al. Investigating Vulnerable Atheroma Using Combined ^{18}F-FDG PET/CT Angiography of Carotid Plaque with Immunohistochemical Validation. *J Nucl Med*. 2011; **52**: 1698-703.

9. Marnane M, Merwick A, Sheehan OC, et al. Carotid Plaque Inflammation on ^{18}F-Fluorodeoxyglucose Positron Emission Tomography Predicts Early Stroke Recurrence. *Ann Neurol*. 2012; **71**: 709-18.

10. Blomberg BA, Thomassen A, Takx RA, et al. Delayed ^{18}F-Fluorodeoxyglucose PET/CT Imaging Improves Quantitation of Atherosclerotic Plaque Inflammation: Results from the CAMONA Study. *J Nucl Cardiol*. 2014; **21**: 588-97.

11. Blomberg BA, Thomassen A, Takx RA, et al. Delayed Sodium ^{18}F-Fluoride PET/CT Imaging Does not Improve Quantification of Vascular Calcification Metabolism: Results from the CAMONA Study. *J Nucl Cardiol*. 2014; **21**: 293-304.

12. Conroy RM, Pyorala K, Fitzgerald AP, et al. Estimation of Ten-Year Risk of Fatal Cardiovascular Disease in Europe: The SCORE Project. *Eur Heart J*. 2003; **24**: 987-1003.

13. Becker CR, Knez A, Ohnesorge B, et al. Visualization and Quantification of Coronary Calcifications with Electron Beam and Spiral Computed Tomography. *Eur Radiol*. 2000; **10**: 629-35.

14. Huet P, Burg S, Le Guludec D, et al. Variability and Uncertainty of FDG PET Imaging Protocols for Assessing Inflammation in Atherosclerosis: Suggestions for Improvement. *J Nucl Med*. 2015; **56**: 552-9.

15. Rudd JH, Warburton EA, Fryer TD, et al. Imaging Atherosclerotic Plaque Inflammation with [^{18}F]-Fluorodeoxyglucose Positron Emission Tomography. *Circulation*. 2002; **105**: 2708-11.

16. Tawakol A, Migrino RQ, Bashian GG, et al. In Vivo ^{18}F-Fluorodeoxyglucose Positron Emission Tomography Imaging Provides a Noninvasive Measure of Carotid Plaque Inflammation in Patients. *J Am Coll Cardiol*. 2006; **48**: 1818-24.

17. Figueroa AL, Subramanian SS, Cury RC, et al. Distribution of Inflammation within Carotid Atherosclerotic Plaques with High-Risk Morphological Features: A Comparison Between Positron Emission Tomography Activity, Plaque Morphology, and Histopathology. *Circ Cardiovasc Imaging*. 2012; **5**: 69-77.

18. Moore KJ, Tabas I. Macrophages in the Pathogenesis of Atherosclerosis. *Cell*. 2011; **145**: 341-55.

19. Folco EJ, Sheikine Y, Rocha VZ, et al. Hypoxia but not Inflammation Augments Glucose Uptake in Human Macrophages: Implications for Imaging Atherosclerosis with ^{18}Fluorine-Labeled 2-Deoxy-D-Glucose Positron Emission Tomography. *J Am Coll Cardiol*. 2011; **58**: 603-14.

20. Libby P, Folco E. Tension in the Plaque: Hypoxia Modulates Metabolism in Atheroma. *Circ Res*. 2011; **109**: 1100-2.

21. Figueroa AL, Abdelbaky A, Truong QA, et al. Measurement of Arterial Activity on Routine FDG PET/CT Images Improves Prediction of Risk of Future CV Events. *J Am Coll Cardiol Img*. 2013; **6**: 1250-9.

22. Czernin J, Satyamurthy N, Schiepers C. Molecular Mechanisms of Bone ^{18}F-NaF Deposition. *J Nucl Med*. 2010; **51**: 1826-9.

23. Aikawa E, Nahrendorf M, Figueiredo JL, et al. Osteogenesis Associates with Inflammation in Early-Stage Atherosclerosis Evaluated by Molecular Imaging In Vivo. *Circulation*. 2007; **116**: 2841-50.

24. Budoff MJ, Shaw LJ, Liu ST, et al. Long-Term Prognosis Associated with Coronary Calcification: Observations from a Registry of 25,253 Patients. *J Am Coll Cardiol*. 2007; **49**: 1860-70.

25. Hou ZH, Lu B, Gao Y, et al. Prognostic Value of Coronary CT Angiography and Calcium Score for Major Adverse Cardiac Events in Outpatients. *J Am Coll Cardiol Img*. 2012; **5**: 990-9.

26. Ehara S, Kobayashi Y, Yoshiyama M, et al. Spotty Calcification Typifies the Culprit Plaque in Patients with Acute Myocardial Infarction: An Intravascular Ultrasound Study. *Circulation*. 2004; **110**: 3424-9.

27. Virmani R, Burke AP, Farb A, et al. Pathology of the Vulnerable Plaque. *J Am Coll Cardiol*. 2006; **47**: C13-8.

28. Demer LL, Tintut Y. Vascular Calcification: Pathobiology of a Multifaceted Disease. *Circulation*. 2008; **117**: 2938-48.

29. Dweck MR, Chow MW, Joshi NV, et al. Coronary Arterial ^{18}F-Sodium Fluoride Uptake: A Novel Marker of Plaque Biology. *J Am Coll Cardiol*. 2012; **59**: 1539-48.

30. Webber BJ, Seguin PG, Burnett DG, et al. Prevalence of and Risk Factors for Autopsy-Determined Atherosclerosis Among US Service Members, 2001-2011. *JAMA*. 2012; **308**: 2577-83.

31. Sadeghi MM. ^{18}F-FDG PET and Vascular Inflammation: Time to Refine the Paradigm? *J Nucl Cardiol*. 2015; **22**: 319-24

32. Sheikine Y, Akram K. FDG-PET Imaging of Atherosclerosis: Do we Know what we See? *Atherosclerosis*. 2010; **211**: 371-80.

33. Boellaard R, Delgado-Bolton R, Oyen WJ, et al. FDG PET/CT: EANM Procedure Guidelines for Tumour Imaging: Version 2.0. *Eur J Nucl Med Mol Imaging*. 2015; **42**: 328-54.

34. Boellaard R, O'Doherty MJ, Weber WA, et al. FDG PET and PET/CT: EANM Procedure Guidelines for Tumour PET Imaging: Version 1.0. *Eur J Nucl Med Mol Imaging*. 2010; **37**: 181-200.

35. Soret M, Bacharach SL, Buvat I. Partial-Volume Effect in PET Tumor Imaging. *J Nucl Med*. 2007; **48**: 932-45.

36. Izquierdo-Garcia D, Davies JR, Graves MJ, et al. Comparison of Methods for Magnetic Resonance-Guided [^{18}F]-Fluorodeoxyglucose Positron Emission Tomography in Human Carotid Arteries: Reproducibility, Partial Volume Correction, and Correlation Between Methods. *Stroke*. 2009; **40**: 86-93.

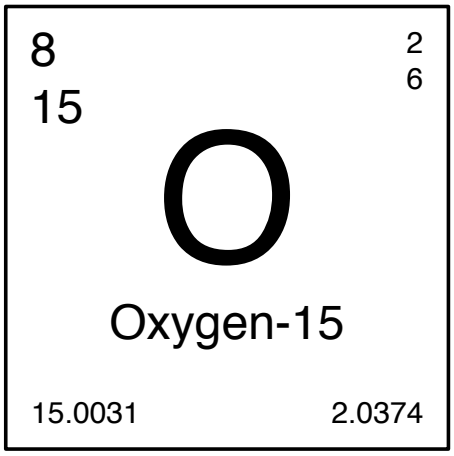
8
15
2
6
O
Oxygen-15
15.0031
2.0374

Chapter 8

Coronary Sodium [^{18}F]-Fluoride Uptake is Increased in Healthy Adults with an Unfavorable Cardiovascular Risk Profile: Results from the CAMONA Study

Björn A. Blomberg
Anders Thomassen
Pim A. de Jong
Marnix G.E.H. Lam
Axel C.P. Diederichsen
Michael H. Olsen
Hans Mickley
Willem P.T.M. Mali
Abass Alavi
Poul F. Høilund-Carlsen

Submitted

ABSTRACT

Background: Coronary artery sodium [^{18}F]-fluoride ($Na^{18}F$) uptake reflects coronary artery calcification metabolism and is considered to be an early prognostic marker of coronary heart disease. This study evaluated the relationship between coronary artery $Na^{18}F$ uptake and cardiovascular risk in healthy adults at low cardiovascular risk.

Methods: Study participants underwent blood pressure measurements, blood analyses, and coronary artery $Na^{18}F$ PET/CT imaging. In addition, the 10-year risk for development of cardiovascular disease, based on the Framingham Risk Score, was estimated. Multivariable linear regression evaluated the dependence of coronary artery $Na^{18}F$ uptake on cardiovascular risk factors.

Results: We recruited 89 healthy adults (47 males, 42 females) aged 21 to 75 years. Female sex (0.40 kBq/mL; $P = .005$), age (0.13 kBq/mL per SD; $P = .021$), body mass index (0.26kBq/mL per SD; $P = .041$), and diastolic blood pressure (0.12 kBq/mL per SD; $P = .028$) were independent determinants of increased coronary artery $Na^{18}F$ uptake (adjusted $R^2 = 0.12$; $P < .001$). Coronary artery $Na^{18}F$ uptake increased linearly to the number of cardiovascular risk factors present ($P < .001$ for a linear trend). The estimated 10-year risk for development of cardiovascular disease was on average 3.1 times higher in adults with coronary artery $Na^{18}F$ uptake in the highest quartile compared with those in the lowest quartile of the distribution (10.1 % *versus* 3.3 %; $P < .001$).

Conclusions: Our findings indicate that coronary artery $Na^{18}F$ PET/CT imaging is feasible in healthy adults at low cardiovascular risk and that an unfavorable cardiovascular risk profile is associated with a marked increase in coronary artery $Na^{18}F$ uptake.

INTRODUCTION

Atherosclerosis in coronary arteries develops gradually and silently over decades **(1)**. This provides an opportunity for early disease detection and initiation of preventive strategies before the onset of symptoms. Preventive measures taken early in life may delay development of coronary atherosclerosis and, hence, postpone or avert the occurrence of coronary heart disease later in life.

Sodium [^{18}F]-fluoride ($Na^{18}F$) positron emission tomography/computed tomography (PET/CT) imaging is a non-invasive method for assessment of coronary atherosclerosis **(2)**. By targeting the earliest stages of plaque calcification, coronary $Na^{18}F$ PET/CT imaging can potentially detect atherosclerosis early on, improve cardiovascular risk stratification, and guide preventive strategies **(3)**. Coronary $Na^{18}F$ PET/CT imaging has been validated in patients at high cardiovascular risk **(2, 4)**. These studies demonstrated that coronary $Na^{18}F$ uptake is increased in subjects with unfavorable cardiovascular risk profiles. Moreover, increased coronary $Na^{18}F$ uptake is associated with high-risk atherosclerotic plaque features **(4)**. Few studies, however, have assessed coronary $Na^{18}F$ uptake in subjects at low cardiovascular risk. Therefore, it remains unknown if coronary $Na^{18}F$ PET/CT imaging is feasible in low risk populations and whether the associations observed in high-risk populations also exist in populations at low cardiovascular risk.

To explore if coronary $Na^{18}F$ PET/CT imaging is feasible in populations at low cardiovascular risk, we evaluated the relationship between coronary $Na^{18}F$ uptake and cardiovascular risk factors in 89 healthy adults aged 21 to 75 years.

METHODS

This study is part of the "Cardiovascular Molecular Calcification Assessed by ^{18}F-NaF PET/CT" (CAMONA) study. The CAMONA study was approved by the Danish National Committee on Health Research Ethics, registered at ClinicalTrials.gov (NCT01724749), and conducted in accordance with the Declaration of Helsinki. All study participants provided written informed consent. Details of CAMONA have been published previously **(5)**.

Subject Selection

Healthy adults were recruited from the general population by local advertisement or from the blood bank of Odense University Hospital, Denmark. Subjects free of oncologic disease,

autoimmune disease, immunodeficiency syndromes, alcohol abuse, illicit drug use, (symptoms suggesting) cardiovascular disease, or any prescription medication were considered healthy and were eligible for inclusion. Pregnant women were not considered for inclusion. Adults were preselected by sex and age to secure a balanced inclusion of males and females aged 20–29, 30–39, 40–49, 50–59, ≥ 60 years.

Study Design

Healthy adults were evaluated by questionnaires, blood pressure measurements, blood analyses, the Framingham Risk Score (FRS) **(6, 7)**, $Na^{18}F$ PET/CT imaging, and non-contrast enhanced cardiac CT imaging. In addition, body mass index (kg/m^2) was determined. CAMONA participants were also evaluated by [^{18}F]-fluorodeoxyglucose (^{18}FDG) PET/CT imaging, a marker of atherosclerotic plaque inflammation. However, high myocardial ^{18}FDG retention prevented accurate detection of coronary ^{18}FDG uptake. Therefore, this study does not report data on coronary ^{18}FDG uptake. Questionnaires collected information about smoking habits and family history of coronary heart disease. Blood pressure measurements were performed thrice after a supine rest of at least 30 minutes. The average of the last two measurements determined the systolic and diastolic blood pressure. Blood analyses determined fasting serum total cholesterol, serum LDL cholesterol, serum HDL cholesterol, serum triglycerides, fasting plasma glucose, glycated hemoglobin (HbA1c), and the Modification of Diet and Renal Disease (MDRD) estimated glomerular filtration rate (eGFR). For each subject, the 10-year **(6)** and 30-year risk **(7)** for cardiovascular disease was estimated based on the FRS. The FRS estimates the cardiovascular disease risk (i.e. coronary death, myocardial infarction, and fatal or non-fatal stroke) based on age, gender, systolic blood pressure, total serum cholesterol, serum HDL cholesterol, and smoking habits. $Na^{18}F$ PET/CT imaging was performed according to a previously published protocol **(5)**. In summary, $Na^{18}F$ PET/CT imaging was performed on integrated PET/CT systems (GE Discovery STE, VCT, RX, and 690/710) at 90 minutes after intravenous injection of 2.2 MBq of $Na^{18}F$ per kilogram of body weight. The emission acquisition duration per bed position was 2.5 minutes. Total body PET images were acquired in 3D–mode and reconstructed into coronal, axial, and sagittal planes by an ordered subsets expectation maximization algorithm (GE VUE Point). PET images were corrected for attenuation, scatter, random coincidences, and scanner dead time. Low–dose CT imaging (140 kV, 30-110 mA, noise index 25, 0.8 seconds per rotation, slice thickness 3.75 mm) was performed for attenuation correction and anatomic orientation. To determine the coronary calcium score, non-contrast enhanced, breath-hold, cardiac CT imaging (120 kV, 100 mA, 0.4 seconds per rotation, slice thickness 2.5 mm) was performed with electrocardiogram gating at 50 % of the R–R interval.

The effective radiation dose received for the entire imaging protocol was approximately 14 mSv.

Quantitative Image Analyses

All images were analyzed by version 4.0 of the Philips IntelliSpace Portal client. The image analyst was masked to subject demographics and image specifications. Quantification of coronary $Na^{18}F$ uptake was performed according to previously published methods **(5, 8)**. In summary, coronary $Na^{18}F$ uptake was determined by manually placing a free-hand region of interest (ROI) around the cardiac silhouette on every slice of the axially oriented PET/CT images. We carefully excluded $Na^{18}F$ activity originating from the skeleton, the aortic wall, and cardiac valves by eliminating these areas from the ROI. Per ROI, the radiotracer-decay corrected maximum $Na^{18}F$ activity concentration (kBq/mL) was determined. Maximum values obtained per ROI were summed and divided by the number of ROIs resulting in a single averaged maximum value (NaF_{MAX}). We also determined $Na^{18}F$ activity in blood by drawing a single ROI in the lumen of superior vena cava. Blood $Na^{18}F$ activity was quantified as the radiotracer-decay corrected mean $Na^{18}F$ activity concentration (kBq/mL). Finally, the coronary calcium volume (mm^3) was determined on cardiac CT images **(9)**. The detection threshold for coronary calcium was set at 130 Hounsfield units.

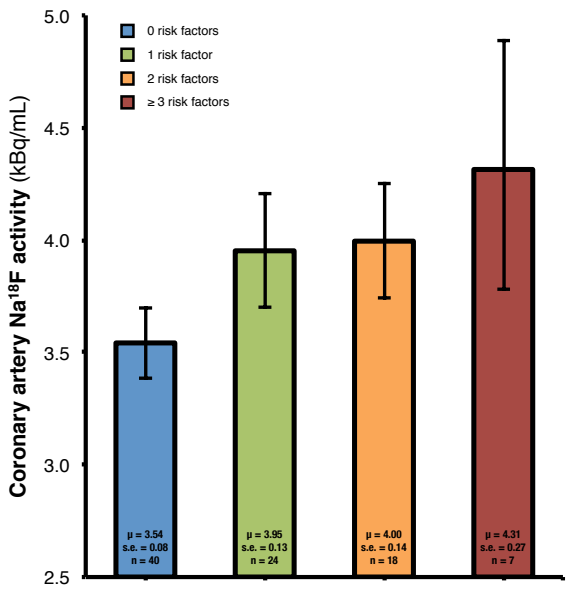

FIGURE 1 – Bar graph showing coronary artery $Na^{18}F$ uptake (kBq/mL), adjusted for blood $Na^{18}F$ activity, body weight, and PET/CT technology, in relation to the number of cardiovascular risk factors (i.e. body mass index, systolic blood pressure, serum triglyceride concentration, and serum LDL-cholesterol concentration) present. Coronary $Na^{18}F$ uptake increased linearly to the number of risk factors present (P < .001 for a linear trend). Coronary $Na^{18}F$ uptake was significantly lower in absence of risk factors compared with the presence of one or more risk factors (3.54 *versus* 3.95, 4.00, and 4.31 kBq/mL, respectively; P < .012). *Error bars* represent the 95 % confidence interval of the mean.

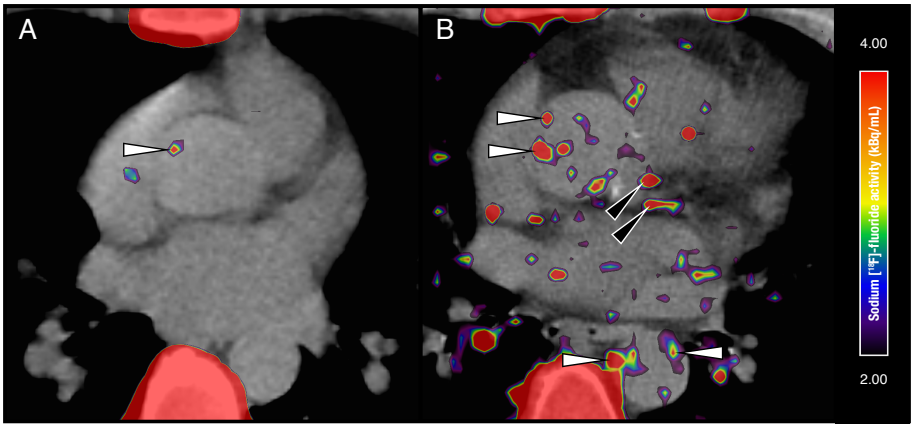

FIGURE 2 – Axial sodium [^{18}F]-fluoride (Na^{18}F) PET/CT images showing the heart at the level of the left main coronary artery. Image **A** was obtained in a 42-year old female without cardiovascular risk factors, a negative calcium score, and an estimated 10-year CVD risk of 2 %. Sporadic aortic Na^{18}F uptake (*white arrowhead*) was seen, whereas no marked Na^{18}F activity could be detected in the coronary arteries. Image **B** was obtained in a 65-year old female with 3 cardiovascular risk factors, a calcium score of 46 mm^3, and an estimated 10-year CVD risk of 12 %. Marked Na^{18}F uptake was seen in the left coronary artery (*black arrowheads*). In addition, Na^{18}F uptake was observed in the ascending and descending aorta (*white arrowheads*). Note the intense uptake of Na^{18}F in the sternum, vertebra, and ribs.

Statistical Analysis

First, coronary NaF_{MAX} was adjusted for blood Na^{18}F activity, body weight, and PET/CT technology by the factorial analysis of covariance (ANCOVA), because previous studies indicated that these parameters significantly influence quantification of arterial Na^{18}F uptake **(10)**. Second, subject demographics were summarized by descriptive statistics and compared between males and females by the unpaired Student's *t* test, Mann-Whitney *U* test, or Fisher's exact test. Third, the dependence of adjusted coronary NaF_{MAX} on cardiovascular risk factors was evaluated by univariate linear regression. Risk factors that significantly associated with adjusted coronary NaF_{MAX} were adjusted for sex, age, and body mass index. Linear models were extended by interaction terms to evaluate if the dependence of coronary NaF_{MAX} on cardiovascular risk factors was modified by sex. Because no significant interactions were observed, we did not separate results for males and females. We also performed multivariable linear regression to establish independent determinants of adjusted coronary NaF_{MAX}. Variables entered in the multivariable regression were selected based on results from univariate analyses. Fourth, to evaluate the combined effect of multiple risk factors on adjusted coronary NaF_{MAX} we applied the methodology used by the Bogalusa Heart Study **(11)**. The Bogalusa Heart Study considered body mass index, systolic blood pressure, serum triglycerides, and serum LDL cholesterol

TABLE 1 - Subject demographics

	Male (*n* = 47)	**Female** (*n* = 42)	***P* value**	**Total** (*N* = 89)
Age, years	44 ± 14	45 ± 14	.748	44 ± 14
Smokers, %				
- Former	30	43	.664	36
- Current	4	2	.660	3
Positive family history, %	19	17	.790	18
Blood pressure, mmHg				
- Systolic	131 ± 17	124 ± 17	**.041**	128 ± 17
- Diastolic	78 ± 10	75 ± 10	.112	77 ± 10
Body weight, kg	89 ± 19	70 ± 10	**< .001**	80 ± 18
Body mass index, kg/m^2	27 ± 5	25 ± 3	**.021**	27 ± 4
Cholesterol, mmol/L				
- Total	4.8 ± 0.9	5.0 ± 0.9	.315	4.9 ± 0.9
- LDL	3.1 ± 0.8	3.0 ± 0.8	.605	3.1 ± 0.8
- HDL	1.2 ± 0.3	1.7 ± 0.5	**< .001**	1.4 ± 0.5
Triglycerides, mmol/L	1.2 ± 0.8	0.8 ± 0.3	**.014**	1.0 ± 0.7
Plasma glucose, mmol/L	5.7 ± 0.5	5.4 ± 0.5	**.009**	5.5 ± 0.5
HbA1c, mmol/mol	34.7 ± 4.5	33.0 ± 3.4	**.041**	33.9 ± 4.1
eGFR, mL/min/1.73 m^2	84.3 ± 11.7	81.3 ± 14.5	.306	82.9 ± 13.2
10-year FRS, %	6 [2 to 12]	3 [1 to 3]	**.003**	4 [2 to 9]
30-year FRS, %	15 [5 to 24]	8 [4 to 18.5]	**.001**	13 [5 to 21]
Coronary artery calcification				
- Volume, mm^3	0 [0 to 9]	0 [0 to 0]	**.008**	0 [0 to 0]
- %	26	5	**.008**	16
Injected Na^{18}F dose, MBq	190 ± 42	156 ± 25	**< .001**	174 ± 39
Circulating time, minutes	91 ± 3	92 ± 5	.268	92 ± 4
Coronary NaF$_{MAX}$, kBq/mL	3.63 ± 0.78	3.97 ± 0.73	**.049**	3.79 ± 0.76
PET/CT system, %				
- GE Discovery STE	17	33		25
- GE Discovery VCT	21	21		21
- GE Discovery RX	40	21		31
- GE Discovery 690/710	21	24		22

Values are mean ± standard deviation, %, or median [25 and 75 percentiles]. HbA1c, FRS, eGFR, and NaF$_{MAX}$ indicate glycated hemoglobin, Framingham Risk Score, estimated glomerular filtration rate, and maximum [^{18}F]-sodium fluoride (Na^{18}F) activity concentration (kBq/mL) adjusted for blood Na^{18}F activity, body weight, and PET/CT technology.

above the sex-specific 75th percentile for the study group as risk factors for cardiovascular disease **(11)**. Mean adjusted coronary NaF_{MAX} was compared between groups with 0, 1, 2, and 3 or 4 cardiovascular risk factors by the factorial ANCOVA. Lastly, we estimated the 10-year and 30-year risk for cardiovascular disease and compared these risk estimates across quartiles of adjusted coronary NaF_{MAX} using factorial ANCOVA. A two-tailed *P* value below .05 was regarded statistically significant. *P* values and 95 % confidence intervals were determined by a bootstrap of 2,000 samples. Statistical analyses were performed by statistical software IBM SPSS Statistics version 21.

RESULTS

Between November 2012 and May 2014 we prospectively recruited 90 healthy adults. One subject was excluded from the study because she refused the PET/CT examination due to claustrophobia.

Among 89 participants, 47 were male. Males had significantly higher systolic blood pressure, body weight, body mass index, serum triglycerides, plasma glucose, and HbA1c compared with females. In addition, males had more coronary calcifications, were administered a higher $Na^{18}F$ dose, and had a higher median FRS than females, whereas adjusted coronary NaF_{MAX} and HDL cholesterol were significantly lower in males than females. No sex differences were seen for age, smoking habits, total cholesterol, and LDL cholesterol (**TABLE 1**).

Univariate analyses established that female sex, age, smoking habits, family history of coronary heart disease, blood pressure, body mass index, and the serum concentration of total cholesterol were positively associated with an increase in adjusted coronary NaF_{MAX} (**TABLE 2**). Adjustments for sex, age, and body mass index attenuated most of these associations. Multivariable linear regression established that female sex (0.40 kBq/mL; *P* = .005), age (0.13 kBq/mL per SD; *P* = .021), body mass index (0.26 kBq/mL per SD; *P* = .041), and diastolic blood pressure (0.12 kBq/mL per SD; *P* = .028) were independent determinants of adjusted coronary NaF_{MAX} in our population and explained an additional 12 % of variation in adjusted coronary NaF_{MAX} (adjusted R^2 increased from 0.65 to 0.77; *P* < .001). Blood $Na^{18}F$ activity, body weight, and PET/CT technology explained the initial 55 % of variation in the data.

For males, the 75th percentile for systolic blood pressure, serum LDL cholesterol, serum triglycerides, and body mass index was 139 mmHg, 3.8 mmol/L, 1.3 mmol/L, and

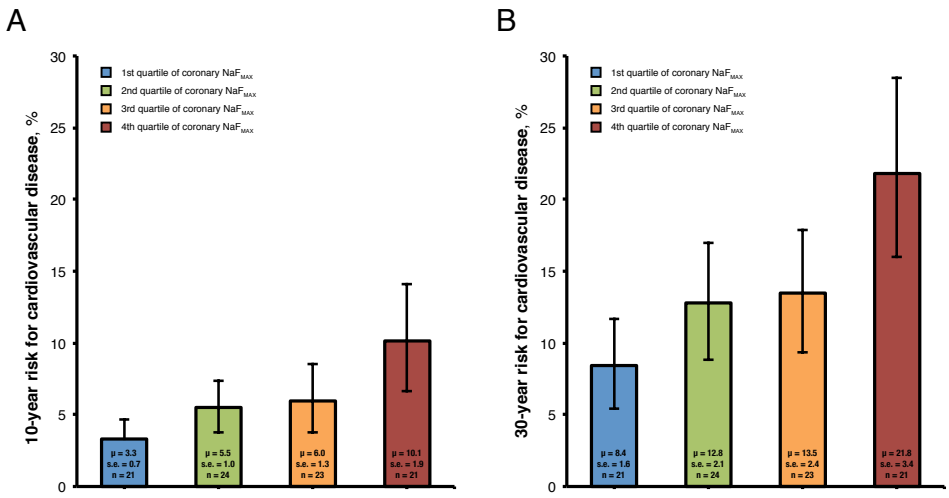

FIGURE 3 – Bar graph showing the estimated 10-year (**A**) and 30-year (**B**) risk for cardiovascular disease against quartiles of coronary artery $Na^{18}F$ uptake (NaF_{MAX}). Cardiovascular disease risk was significantly lower in the first quartile of coronary NaF_{MAX} compared with the fourth quartile (3.3 % *versus* 10.1 %; *P* = .005 for the 10-year risk and 8.4 % *versus* 21.8 %; *P* = .002 for the 30-year risk, respectively). In addition, cardiovascular disease risk increased linearly to quartiles of coronary NaF_{MAX} (*P* < .001 for a linear trend). *Error bars* represent the 95 % confidence interval of the mean. Coronary artery $Na^{18}F$ uptake (kBq/mL) was adjusted for blood $Na^{18}F$ activity, body weight, and PET/CT technology.

29.2 kg/m^2, respectively. For females, the 75th percentile for systolic blood pressure, serum LDL cholesterol, serum triglycerides, and body mass index was 139 mmHg, 3.4 mmol/L, 1.0 mmol/L, and 27 kg/m^2, respectively.

Adjusted coronary NaF_{MAX} increased linearly to the number of cardiovascular risk factors present (*P* < .001 for a linear trend)(**FIGURE 1**). Adults without cardiovascular risk factors (21 males and 19 females, mean age of 43 ± 13 years) had the lowest adjusted coronary NaF_{MAX} (3.54 kBq/mL [95 % CI = 3.39 to 3.70]), whereas those with 3 or 4 cardiovascular risk factors (4 males and 3 females, mean age of 43 years ± 13 years) had the highest adjusted coronary NaF_{MAX} (4.31 kBq/mL [95% CI = 3.78 to 4.89])(**FIGURE 1** and **2**).

The estimated 10-year and 30-year risk for cardiovascular disease increased linearly to quartiles of adjusted coronary NaF_{MAX} (*P* < .001 for a linear trend)(**FIGURE 3**). The estimated 10-year risk for cardiovascular disease increased from 3.3 % (95 % CI = 2.1 to 4.6) for adults in the lowest quartile to 10.1 % (95 % CI = 6.6 to 14.1) for adults in the highest quartile of adjusted

coronary NaF_{MAX}. The estimated 30-year risk for cardiovascular disease increased from 8.4 % (95 % CI = 5.4 to 11.7) for adults in the lowest quartile to 21.8 % (95 % CI = 16.0 to 28.4) for adults in the highest quartile of adjusted coronary NaF_{MAX}.

DISCUSSION

This study demonstrates that sex, age, body mass index, and diastolic blood pressure are independent determinants of coronary $Na^{18}F$ uptake in healthy adults. Furthermore, we have shown that coronary $Na^{18}F$ uptake increases linearly to the number of cardiovascular risk factors present. Moreover, we demonstrated that the estimated 10-year and 30-year risk for development of cardiovascular disease increases linearly to the increase in coronary $Na^{18}F$ uptake. Our findings indicate that an unfavorable cardiovascular risk profile is associated with a marked increase in coronary $Na^{18}F$ uptake.

Arterial $Na^{18}F$ uptake is believed to reflect vascular calcification metabolism **(12)**. Traditionally, vascular calcification is detected and quantified by computed tomography (CT) imaging **(9)**. Prospective follow-up studies have demonstrated that CT detectable vascular calcification is an important independent predictor of cardiovascular morbidity and mortality **(13, 14)**. Nevertheless, CT imaging of vascular calcification is associated with limitations. First, CT's limited sensitivity prevents accurate detection of vascular calcification at the molecular level **(15)**. Second, CT imaging cannot distinguish active from indolent vascular calcification, a possible biomarker for vulnerable and stabilized atherosclerotic plaque, respectively **(4, 16, 17)**.

Imaging vascular calcification with $Na^{18}F$ PET/CT can possibly overcome these limitations. $Na^{18}F$ PET/CT imaging targets the exchange of fluoride with hydroxyl ions of hydroxylapatite crystals producing fluorapatite **(18)**. Hydroxylapatite is the structural component of vascular calcification and is laid down in the earliest stages of atherosclerotic plaque calcification **(19)**. By imaging fluorapatite formation, $Na^{18}F$ PET/CT can detect vascular calcification at the molecular level as well as discriminate active from indolent vascular calcification **(5)**. As such, coronary $Na^{18}F$ PET/CT imaging may improve cardiovascular risk stratification beyond CT's coronary calcium score.

Although calcification of atherosclerotic plaques is a strong prognostic marker of cardiovascular disease, its triggers remain debated. It has been suggested that atherosclerotic

TABLE 2 – Determinants of coronary artery $Na^{18}F$ uptake

Determinant	Crude †	Sex adjusted	Age and sex adjusted	Sex, age, and BMI adjusted
Sex, male	-0.56 (-0.79 to -0.33)		-0.59 (-0.80 to -0.40)	-0.36 (-0.61 to -0.13)
Age, years	0.15 (0.04 to 0.26)	0.18 (0.08 to 0.28)		0.15 (0.07 to 0.24)
Smoking, former or current	0.37 (0.14 to 0.57)	0.29 (0.05 to 0.52)	0.22 (0.00 to 0.41)	0.17 (-0.05 to 0.37)
Positive family history, yes	0.33 (0.02 to 0.63)	0.30 (-0.02 to 0.60)		
Blood pressure, mmHg				
- Systolic	0.12 (-0.02 to 0.22)			
- Diastolic	0.20 (0.08 to 0.31)	0.20 (0.07 to 0.30)	0.15 (0.03 to 0.26)	0.12 (0.00 to 0.23)
Mean arterial pressure, mmHg	0.18 (0.06 to 0.27)	0.18 (0.05 to 0.28)	0.13 (0.01 to 0.25)	0.09 (-0.01 to 0.20)
Body mass index, kg/m^2	0.56 (0.36 to 0.79)	0.41 (0.15 to 0.69)	0.34 (0.10 to 0.63)	
Cholesterol, mmol/L				
- Total	0.15 (0.02 to 0.28)	0.12 (0.01 to 0.22)	0.06 (-0.04 to 0.18)	
- LDL	0.08 (-0.06 to 0.22)			
- HDL	0.09 (-0.02 to 0.23)			
Triglycerides, mmol/L	0.10 (-0.01 to 0.37)			
Plasma glucose, mmol/L	0.09 (-0.06 to 0.22)			
HbA1c, mmol/mol	0.11 (-0.02 to 0.25)			
eGFR, mL/min/1.73 m^2	-0.08 (-0.21 to 0.07)			
Coronary calcification, *n*	0.13 (-0.18 to 0.43)			

Determinants of coronary artery $Na^{18}F$ uptake (NaF_{MAX}). Values are expressed as linear regression coefficients (95 % confidence interval) per standard deviation of change in the determinant. To illustrate, a regression coefficient of 0.43 for BMI signifies that an increase in BMI with 1 standard deviation (5 for males and 3 for females) relates to an increase in NaF_{MAX} of 0.43 kBq/mL. † Crude values of NaF_{MAX} were adjusted for blood $Na^{18}F$ activity, body weight, and PET/CT technology. Abbreviations as in **TABLE 1**.

plaque calcification is part of a healing process that occurs after plaque rupture **(20-22)**. In addition, vascular calcification might occur in response to intense and chronic atherosclerotic plaque inflammation **(23)**. Longitudinal studies performing serial $Na^{18}F$ PET/CT imaging in combination with ^{18}FDG PET/CT imaging (vascular inflammation) might help elucidate some of these hypotheses.

Uptake of $Na^{18}F$ has been described in the aorta **(12)**, carotid arteries **(24)**, femoral arteries **(25)**, and coronary arteries **(2, 4, 8)**. Retrospective studies performed in oncology patients have demonstrated positive associations between large artery $Na^{18}F$ uptake and cardiovascular risk factors **(24, 25)**. These studies could also demonstrate that the prevalence of marked carotid and femoral $Na^{18}F$ uptake increased linearly to the number of cardiovascular risk factors present **(24, 25)**. Besides risk factors, arterial $Na^{18}F$ uptake associated with increased risk for cardiovascular disease. In a study that examined patients with and without aortic valve disease (n = 119), the 10-year risk for cardiovascular disease was 36 % higher in those with increased coronary $Na^{18}F$ uptake (n = 40) compared to those from a control group (n = 13)(34 % *versus* 25 %, $P < .05$) **(2)**. In another study, coronary $Na^{18}F$ uptake was assessed in patients that suffered a myocardial infarction (n = 40). This study demonstrated that uptake of $Na^{18}F$ was 34 % higher in ruptured coronary plaques compared with non-ruptured coronary plaques (1.66 *versus* 1.24, $P < .001$) **(4)**. In the same study, coronary $Na^{18}F$ uptake was evaluated in patients with angina pectoris (n = 39). Increased coronary artery $Na^{18}F$ uptake was associated with high-risk plaque features, including micro-calcification and a large necrotic core, as assessed by intra-vascular ultrasonography imaging. In summary, studies that investigated populations at high cardiovascular risk have shown positive associations between arterial $Na^{18}F$ uptake and atherosclerosis severity. The fact that our study found similar associations in healthy adults support the notion that $Na^{18}F$ PET/CT imaging is feasible in subjects at low cardiovascular risk. Moreover, the finding that coronary $Na^{18}F$ uptake is increased in relation to cardiovascular risk factors, indicate that $Na^{18}F$ PET/CT can detect subtle changes in atherosclerosis activity and possibly distinguish early from intermediate or advanced atherosclerotic disease. Future studies that compare healthy adults to patients with overt cardiovascular disease may substantiate this claim.

Our observations find support in autopsy studies that investigated coronary atherosclerosis in deceased adults **(11, 26, 27)**. Autopsy studies observed strong associations between coronary atherosclerosis prevalence and cardiovascular risk factors, including age, sex, body mass index, blood pressure, smoking habits, and serum concentration of triglycerides

and LDL cholesterol. Importantly, these studies revealed that multiple cardiovascular risk factors are associated with formation of fatty streaks and fibrous plaques in coronary arteries. Our observation that multiple cardiovascular risk factors are associated with increased coronary $Na^{18}F$ uptake expands the findings of these studies. Particularly, it seems that multiple risk factors are not only associated with formation of fatty streaks and fibrous plaques, but also with calcification of atherosclerotic plaques.

Surprisingly, our study observed that males, on average, had lower coronary $Na^{18}F$ uptake compared with females. This observation stands in sharp contrast to the estimated median risk for cardiovascular disease, which was approximately twice as high in males compared with females. Temporal differences in pathobiology or evolution of atherosclerosis between males and females might explain some of the observed sex difference in coronary $Na^{18}F$ uptake. Nevertheless, we acknowledge that an incomplete understanding of the arterial $Na^{18}F$ signal impedes adequate interpretation of unexpected imaging results. Validation studies substantiating arterial $Na^{18}F$ uptake to histopathology, either performed in humans or animals, are clearly needed to explain this apparently paradoxical finding.

Strengths and Limitations

An important strength of the present study is that we prospectively investigated healthy adults aged 21 to 75 years. The majority of studies investigating arterial $Na^{18}F$ uptake were either performed retrospectively in oncology patients **(12, 24, 25, 28)** or involved elderly patients with advanced cardiovascular disease **(2, 4)**. Such studies are limited by imaging protocols not optimized for imaging arteries **(5)**, suffer from selection bias, or both. In contrast, our study was performed prospectively, included a uniform population of healthy adults, and utilized an imaging protocol optimized for artery imaging **(5)**. As such, we were able to demonstrate that coronary $Na^{18}F$ PET/CT imaging is feasible in populations at low cardiovascular risk. Moreover, we demonstrated that an unfavorable cardiovascular risk profile is associated with a marked increase in $Na^{18}F$ uptake in coronary arteries of healthy adults.

The findings of our study, however, should be interpreted in light of its limitations. First, our quantitative image analysis did not correct for partial volume effects, which could have influenced study results **(29)**. Partial volume effects encompass the phenomena that small volumes of $Na^{18}F$ activity appear larger in size but weaker in signal on PET images. Because the coronary arterial wall is smaller than the spatial resolution of PET, partial volume effects should be considered when quantifying coronary $Na^{18}F$ uptake. Moreover, patient movement,

pulsatile blood flow, and the cardiac and respiratory cycle, amplify partial volume effects. This is particularly problematic for coronary arteries, because of their anatomic location. To accurately quantify coronary $Na^{18}F$ uptake, partial volume corrections need to be applied. This was not attempted in our study and likely resulted in underestimated values of coronary $Na^{18}F$ uptake.

Second, coronary $Na^{18}F$ uptake was determined by global assessment. Global assessment has been criticized to be too dependent on bleed-in effects from non-coronary derived $Na^{18}F$ activity **(30)**. However, in previous studies we have demonstrated that excluding non-coronary $Na^{18}F$ activity, such as activity originating from the aortic wall or cardiac valves, can be achieved with high inter- and intra-observer agreement **(5)**. In addition, global assessment has advantages over focal quantification of coronary $Na^{18}F$ uptake. First, global assessment is not limited by difficulties in localizing coronary arteries on non-ECG-gated CT images acquired during PET/CT imaging. Second, global assessment evaluates the entire coronary vasculature and is not limited to focal segments of the coronary tree. Therefore, we prefer global assessment to focal assessment, especially when coronary $Na^{18}F$ uptake is evaluated in populations at low cardiovascular risk.

Third, the dependence of coronary $Na^{18}F$ uptake on cardiovascular risk factors was evaluated in a cross-sectional study. Therefore, we could not assess within-subject variation in coronary $Na^{18}F$ uptake. Longitudinal studies evaluating possible temporal within-subject changes in coronary $Na^{18}F$ uptake in relation to risk factors may give a more precise picture of the processes which are behind the associations we observed in our cross-sectional study.

Conclusions

The findings from our study indicate that coronary $Na^{18}F$ PET/CT imaging is feasible in healthy adults at low cardiovascular risk and that an unfavorable cardiovascular risk profile is associated with a marked increase in coronary $Na^{18}F$ uptake. Our results represent initial steps in determining the feasibility and clinical benefit of $Na^{18}F$ PET/CT imaging of coronary atherosclerosis in low risk populations. Prospective long-term follow-up studies are required to assess the risk stratification capabilities of coronary $Na^{18}F$ PET/CT beyond standard approaches, such as FRS and CT's coronary calcium score.

REFERENCES

1. Libby P. Mechanisms of Acute Coronary Syndromes and Their Implications for Therapy. *N Engl J Med.* 2013; **368**: 2004-13.
2. Dweck MR, Chow MW, Joshi NV, et al. Coronary Arterial ^{18}F-Sodium Fluoride Uptake: A Novel Marker of Plaque Biology. *J Am Coll Cardiol*. 2012; **59**: 1539-48.
3. Dweck MR, Joshi FR, Newby DE, et al. Noninvasive Imaging in Cardiovascular Therapy: The Promise of Coronary Arterial ^{18}F-Sodium Fluoride Uptake as a Marker of Plaque Biology. *Expert Rev Cardiovasc Ther.* 2012; **10**: 1075-7.
4. Joshi NV, Vesey AT, Williams MC, et al. ^{18}F-Fluoride Positron Emission Tomography for Identification of Ruptured and High-Risk Coronary Atherosclerotic Plaques: A Prospective Clinical Trial. *Lancet*. 2014; **383**: 705-13.
5. Blomberg BA, Thomassen A, Takx RA, et al. Delayed Sodium ^{18}F-Fluoride PET/CT Imaging Does Not Improve Quantification of Vascular Calcification Metabolism: Results from the CAMONA Study. *J Nucl Cardiol.* 2014; **21**: 293-304.
6. D'Agostino RB, Vasan RS, Pencina MJ, et al. General Cardiovascular Risk Profile for Use in Primary Care: The Framingham Heart Study. *Circulation.* 2008; **117**: 743-53.
7. Pencina MJ, D'Agostino RB, Larson MG, et al. Predicting the 30-Year Risk of Cardiovascular Disease: The Framingham Heart Study. *Circulation.* 2009; **119**: 3078-84.
8. Beheshti M, Saboury B, Mehta NN, et al. Detection and Global Quantification of Cardiovascular Molecular Calcification by ^{18}F-Fluoride Positron Emission Tomography/Computed Tomography: A Novel Concept. *Hell J Nucl Med.* 2011; **14**: 114-20.
9. Becker CR, Knez A, Ohnesorge B, et al. Visualization and Quantification of Coronary Calcifications with Electron Beam and Spiral Computed Tomography. *Eur Radiol.* 2000; **10**: 629-35.
10. Blomberg BA, Thomassen A, de Jong PA, et al. Impact of Personal Characteristics and Technical Factors on Quantification of Sodium ^{18}F-Fluoride Uptake in Human Arteries: Prospective Evaluation of Healthy Subjects. *J Nucl Med*. 2015; [Epub ahead of print].
11. Berenson GS, Srinivasan SR, Bao W, et al. Association Between Multiple Cardiovascular Risk Factors and Atherosclerosis in Children and Young Adults. The Bogalusa Heart Study. *N Engl J Med.* 1998; **338**: 1650-6.
12. Derlin T, Richter U, Bannas P, et al. Feasibility of ^{18}F-Sodium Fluoride PET/CT for Imaging of Atherosclerotic Plaque. *J Nucl Med.* 2010; **51**: 862-5.
13. Budoff MJ, Shaw LJ, Liu ST, et al. Long-Term Prognosis Associated with Coronary Calcification: Observations from a Registry of 25,253 Patients. *J Am Coll Cardiol.* 2007; **49**: 1860-70.

14. Hou ZH, Lu B, Gao Y, et al. Prognostic Value of Coronary CT Angiography and Calcium Score for Major Adverse Cardiac Events in Outpatients. *J Am Coll Cardiol Img.* 2012; **5**: 990-9.

15. Ehara S, Kobayashi Y, Yoshiyama M, et al. Spotty Calcification Typifies the Culprit Plaque in Patients with Acute Myocardial Infarction: An Intravascular Ultrasound Study. *Circulation.* 2004; **110**: 3424-9.

16. Virmani R, Burke AP, Farb A, et al. Pathology of the Vulnerable Plaque. *J Am Coll Cardiol.*2006; **47**: C13-8.

17. Demer LL, Tintut Y. Vascular Calcification: Pathobiology of a Multifaceted Disease. *Circulation.* 2008; **117**: 2938-48.

18. Czernin J, Satyamurthy N, Schiepers C. Molecular Mechanisms of Bone ^{18}F-NaF Deposition. *J Nucl Med.* 2010; **51**: 1826-9.

19. Aikawa E, Nahrendorf M, Figueiredo JL, et al. Osteogenesis Associates with Inflammation in Early-Stage Atherosclerosis Evaluated by Molecular Imaging In Vivo. *Circulation.* 2007; **116**: 2841-50.

20. Stary HC, Chandler AB, Dinsmore RE, et al. A Definition of Advanced Types of Atherosclerotic Lesions and a Histological Classification of Atherosclerosis. A Report from the Committee on Vascular Lesions of the Council on Arteriosclerosis, American Heart Association. *Circulation.* 1995; **92**: 1355-74.

21. Ueda M. Clinical Relevance of Coronary Artery Calcification, as a Risk Factor for Plaque Rupture: Viewpoint from Pathology. *Clin Calcium*. 2010; **20**: 1656-62.

22. McEvoy JW, Blaha MJ, Defilippis AP, et al. Coronary Artery Calcium Progression: An Important Clinical Measurement? A Review of Published Reports. *J Am Coll Cardiol.* 2010; **56**: 1613-22.

23. Abdelbaky A, Corsini E, Figueroa AL, et al. Focal Arterial Inflammation Precedes Subsequent Calcification in the Same Location: A Longitudinal FDG-PET/CT Study. *Circ Cardiovasc Imaging.* 2013; **6**: 747-54.

24. Derlin T, Wisotzki C, Richter U, et al. In Vivo Imaging of Mineral Deposition in Carotid Plaque Using ^{18}F-Sodium Fluoride PET/CT: Correlation with Atherogenic Risk Factors. *J Nucl Med.* 2011; **52**: 362-8.

25. Janssen T, Bannas P, Herrmann J, et al. Association of Linear ^{18}F-Sodium Fluoride Accumulation in Femoral Arteries as a Measure of Diffuse Calcification with Cardiovascular Risk Factors: A PET/CT Study. *J Nucl Cardiol*. 2013; **20**: 569-77.

26. McGill HC, McMahan CA. Determinants of Atherosclerosis in the Young. Pathobiological Determinants of Atherosclerosis in Youth (PDAY) Research Group. *Am J Cardiol.* 1998; **82**:

30T-36T.

27. Webber BJ, Seguin PG, Burnett DG, et al. Prevalence of and Risk Factors for Autopsy-Determined Atherosclerosis Among US Service Members, 2001-2011. *JAMA.* 2012; **308**: 2577-83.

28. Morbelli S, Fiz F, Piccardo A, et al. Divergent Determinants of ^{18}F-NaF Uptake and Visible Calcium Deposition in Large Arteries: Relationship with Framingham Risk Score. *Int J Cardiovasc Imaging.* 2014; **30**: 439-47.

29. Soret M, Bacharach SL, Buvat I. Partial-Volume Effect in PET Tumor Imaging. *J Nucl Med.* 2007; **48**: 932-45.

30. Mohler ER, Alavi A, Wilensky RL. ^{18}F-Fluoride Imaging for Atherosclerosis. *J Am Coll Cardiol.* 2012; **60**: 1711-3.

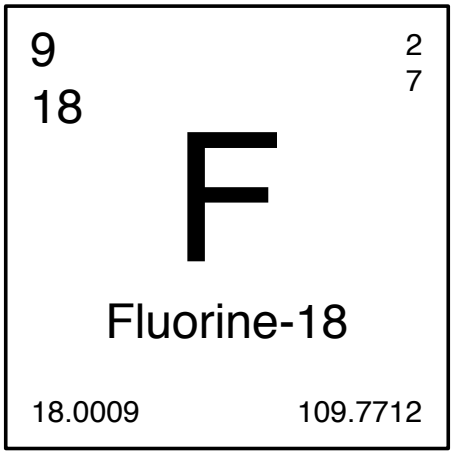
9
18
2
7
F
Fluorine-18
18.0009
109.7712

Chapter 9

Thoracic Aorta Calcification but not Inflammation is Associated with Increased Cardiovascular Disease Risk: Results from the CAMONA Study

Björn A. Blomberg
Pim A. de Jong
Anders Thomassen
Marnix G.E.H. Lam
Werner Vach
Michael H. Olsen
Willem P.T.M. Mali
Jagat Narula
Abass Alavi
Poul F. Høilund-Carlsen

Submitted

ABSTRACT

Background: The relationship between cardiovascular disease (CVD) risk and arterial inflammation (^{18}FDG PET/CT imaging), vascular calcification metabolism (Na^{18}F PET/CT imaging), and vascular calcium burden (CT imaging) of the thoracic aorta was investigated in a population at low CVD risk.

Methods: Study participants underwent blood pressure measurements, blood analyses, and ^{18}FDG and Na^{18}F PET/CT imaging. In addition, the 10-year risk for development of CVD, based on the Framingham Risk Score (FRS), was estimated. CVD risk was compared across quartiles of thoracic aorta ^{18}FDG uptake, Na^{18}F uptake, and CT calcium burden.

Results: In total, we evaluated 139 subjects (52 % males, mean age of 49 years, age range 21 to 75 years, median FRS of 6 %). CVD risk was, on average, 3.5 times higher among subjects with thoracic aorta Na^{18}F uptake in the highest quartile compared with those in the lowest quartile of the distribution (14.7 % *versus* 4.2 %; $P < .001$). CVD risk was, on average, 3.6 times higher among subjects with thoracic aorta CT calcium burden in the highest quartile compared with those in the lowest two quartiles of the distribution (17.7 % *versus* 4.9 %; $P < .001$). CVD risk remained similar across quartiles of thoracic aorta ^{18}FDG uptake.

Conclusions: Our findings indicate that an unfavorable CVD risk profile is associated with marked increases in vascular calcification metabolism and vascular calcium burden of the thoracic aorta, but not arterial inflammation.

INTRODUCTION

Adverse cardiovascular events and their sequelae are a major health concern in Western societies **(1)**. Efforts to prevent adverse cardiovascular events have focused on identifying asymptomatic individuals at high cardiovascular disease (CVD) risk, the so-called "vulnerable" patient **(2, 3)**. In theory, vulnerable patients benefit most from intensive evidence-based medical interventions. However, identifying the vulnerable patient remains a major ongoing challenge **(2)**.

Recent developments in cardiovascular imaging, aimed at visualizing key pathophysiological processes of CVD, offer new opportunities to assess patient vulnerability. Amongst others, arterial inflammation **(4)** and vascular calcification **(5)** have gained interest as potent markers of increased CVD risk **(6-8)**. [^{18}F]-fluorodeoxyglucose (^{18}FDG) positron emission tomography/computed tomography (PET/CT) imaging can non-invasively assess arterial inflammation, whereas [^{18}F]-sodium fluoride (Na^{18}F) PET/CT and X-ray computed tomography (CT) imaging can non-invasively assess vascular calcification (**FIGURE 1**).

Although CVD risk in relation to arterial inflammation (^{18}FDG PET/CT imaging), vascular calcification metabolism (Na^{18}F PET/CT imaging), and vascular calcium burden (CT imaging) has been previously studied, a limited number of studies have applied a combined approach **(9, 10)**. Moreover, few investigations evaluated these cardiovascular imaging modalities in relation to CVD risk in a population at low CVD risk. Therefore, the aim of this study was to evaluate the relationship between CVD risk and arterial inflammation, vascular calcification metabolism, and vascular calcium burden in a cohort of subjects at low CVD risk, namely healthy volunteers and patients evaluated for chest pain syndromes.

METHODS

This study is part of the "Cardiovascular Molecular Calcification Assessed by ^{18}F-NaF PET/CT" (CAMONA) study. The CAMONA study was approved by the Danish National Committee on Health Research Ethics, registered at ClinicalTrials.gov (NCT01724749), and conducted in accordance with the Declaration of Helsinki. All study participants provided written informed consent.

Subject Selection

We recruited a heterogeneous population of subjects, including healthy volunteers and patients

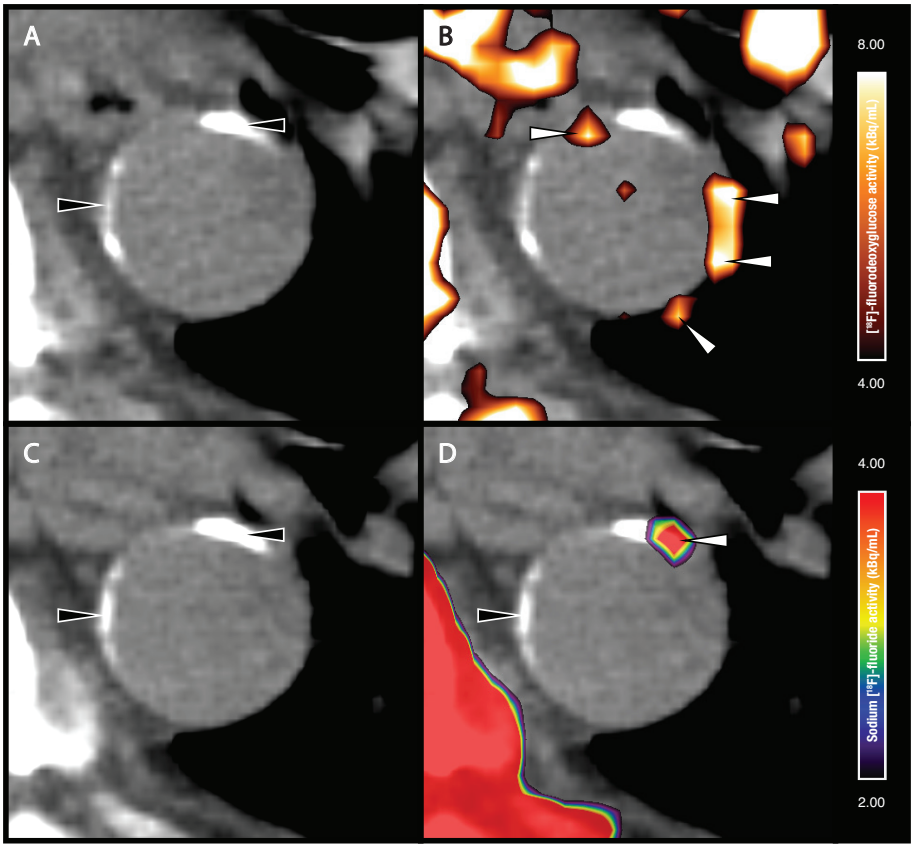

FIGURE 1 – Axial CT (**A**, **C**), ^{18}FDG PET/CT (**B**), and Na^{18}F PET/CT (**D**) images obtained at the same location in 69-year old male with hypertension, a body mass index of 28 kg/m^2, and a Framingham Risk Score of 26 %. ^{18}FDG accumulated in the descending thoracic aorta (*white arrowheads* in image **B**), but did not accumulate at sites with structural calcium deposits (*black arrowheads* in images **A** and **C**). Na^{18}F PET/CT appeared to distinguish active (*white arrowhead* in image **D**) from indolent vascular calcifications (*black arrowhead* in image **D**).

evaluated for chest pain syndromes. This allowed us to study the relationship between CVD risk and arterial inflammation, vascular calcification metabolism, and vascular calcium burden in a heterogeneous, but clinically relevant, group of subjects regarded to be at low CVD risk. Healthy volunteers were recruited from the general population by local advertisement or from the blood bank of Odense University Hospital, Denmark. Volunteers free of oncologic disease, autoimmune disease, immunodeficiency syndromes, alcohol abuse, illicit drug use, (symptoms suggesting) CVD, or any prescription medication were considered healthy and were eligible for inclusion. Patients evaluated for chest pain syndromes were recruited from those referred for a coronary CT-angiography. Only patients with a 10-year risk for fatal CVD equal to or above 1

TABLE 1 - Subject demographics

	Controls (*n* = 89)	**Patients** (*n* = 50)	***P* value**	**Total** (*N* = 139)
Age, years	44 ± 14	57 ± 11	**< .001**	49 ± 14
Male, %	53	50	.860	52
Smokers, %				
- Former	36	44	.370	39
- Current	3	20	**.002**	9
Family history, %	18	38	**.014**	25
Blood pressure, mmHg				
- Systolic	128 ± 17	131 ± 17	.277	129 ± 17
- Diastolic	77 ± 10	79 ± 8	.105	78 ± 10
Body weight, kg	80 ± 18	81 ± 16	.784	80 ± 18
Body mass index, kg/m^2	27 ± 4	27 ± 4	.291	27 ± 4
Cholesterol, mmol/L				
- Total	4.9 ± 0.9	5.4 ± 0.9	**.006**	5.1 ± 0.9
- LDL	3.1 ± 0.8	3.4 ± 0.9	**.037**	3.2 ± 0.8
- HDL	1.4 ± 0.5	1.4 ± 0.4	.834	1.4 ± 0.4
Triglycerides, mmol/L	1.0 ± 0.7	1.2 ± 0.7	.224	1.1 ± 0.7
Plasma glucose, mmol/L	5.5 ± 0.5	5.9 ± 0.9	**.011**	5.6 ± 0.7
HbA1c, mmol/mol	33.9 ± 4.1	37.4 ± 5.0	**< .001**	35.1 ± 4.7
eGFR, mL/min/1.73 m^2	82.9 ± 13.2	75.1 ± 14.3	**.002**	80.4 ± 14.1
Framingham Risk Score, %	4 [2 to 9]	9 [6 to 22]	**< .001**	6 [2 to 12]
Medication, %				
- Statines	0	35	**< .001**	12
- Antihypertensive drugs	0	46	**< .001**	17
Calcium burden				
- Thoracic aorta, %	20	60	**< .001**	35
- Thoracic aorta, mm^3	0 [0 to 0]	1 [0 to 5]	**< .001**	0 [0 to 1]
Injected dose, MBq				
- [^{18}F]-fluorodeoxyglucose	306 ± 59	315 ± 65	.410	309 ± 61
- [^{18}F]-sodium fluoride	174 ± 39	175 ± 28	.851	174 ± 35
Circulating time, minutes				
- [^{18}F]-fluorodeoxyglucose	181 ± 4	182 ± 5	.500	181 ± 4
- [^{18}F]-sodium fluoride	92 ± 4	91 ± 4	.339	91 ± 4
Radiotracer activity, kBq/mL				
- FDG_{MAX}	6.58 ± 1.38	7.05 ± 1.93	.098	6.75 ± 2.18
- NaF_{MAX}	2.05 ± 0.46	2.42 ± 0.63	**< .001**	1.61 ± 0.56

Continued on page 194

TABLE 1 - Subject demographics, *continued*

	Controls (*n* = 89)	**Patients** (*n* = 50)	***P* value**	**Total** (*N* = 139)
PET/CT system, % (^{18}FDG / Na^{18}F)				
- GE Discovery STE	20 / 25	16 / 28		19 / 26
- GE Discovery VCT	31 / 21	20 / 18		27 / 20
- GE Discovery RX	25 / 31	31 / 20		27 / 27
- GE Discovery 690/710	24 / 22	31 / 34		27 / 27

Values are mean ± standard deviation, %, or median [25 and 75 percentiles]. HbA1c, eGFR, FDG_{MAX}, and NaF_{MAX} indicate glycated hemoglobin, estimated glomerular filtration rate, maximum [^{18}F]-fluorodeoxyglucose activity concentration (kBq/mL) adjusted for blood activity, body weight, and PET/CT technology, and maximum [^{18}F]-sodium fluoride activity concentration (kBq/mL) adjusted for blood activity, body weight, and PET/CT technology, respectively.

%, as estimated by the body mass index (kg/m^2) based Systematic COronary Risk Evaluation tool **(11)**, were eligible for inclusion. Pregnant women were not considered for inclusion.

Study Design

Study participants were evaluated by questionnaires, blood pressure measurements, blood analyses, the Framingham Risk Score (FRS) **(12)**, ^{18}FDG PET/CT imaging, and Na^{18}F PET/CT imaging. In addition, body weight (kg) and body mass index (kg/m^2) were determined. Questionnaires collected information about smoking habits, family history of CVD, and prescription medication. Blood pressure measurements were performed thrice after a supine rest of at least 30 minutes. The average of the last two measurements determined the systolic and diastolic blood pressure. Blood analyses determined fasting serum total cholesterol, serum LDL cholesterol, serum HDL cholesterol, serum triglycerides, fasting plasma glucose, glycated hemoglobin (HbA1c), and the Modification of Diet and Renal Disease (MDRD) estimated glomerular filtration rate (eGFR). For each subject, the FRS estimated the 10-year risk for development of CVD. FRS estimates CVD risk (i.e. risk of coronary death, myocardial infarction, coronary insufficiency, angina, ischemic stroke, hemorrhagic stroke, transient ischemic attack, peripheral artery disease, heart failure) based on age, gender, systolic blood pressure, total serum cholesterol, serum HDL cholesterol, smoking habits, and treatment for hypertension **(12)**. ^{18}FDG and Na^{18}F PET/CT imaging were performed according to previously published methods **(13, 14)**. In summary, ^{18}FDG and Na^{18}F PET/CT imaging were performed on hybrid PET/CT systems (GE Discovery STE, VCT, RX, and 690/710). ^{18}FDG PET/CT imaging was performed at 180 minutes after intravenous injection of 4.0 MBq of ^{18}FDG per kilogram of body

weight **(13)**. ^{18}FDG was administered after an overnight fast of at least 8 hours. Prior to ^{18}FDG injection, the blood glucose concentration was determined to secure a value below 8 mmol/L. On average, Na^{18}F PET/CT imaging was performed within two weeks of ^{18}FDG PET/CT imaging. Na^{18}F PET/CT imaging was performed at 90 minutes after intravenous injection of 2.2 MBq of Na^{18}F per kilogram of body weight **(14)**. PET images were corrected for attenuation, scatter, random coincidences, and scanner dead time. Low–dose CT imaging (140 kV, 30-110 mA, noise index 25, 0.8 seconds per rotation, slice thickness 3.75 mm) was performed for attenuation correction, anatomic orientation, and to determine the thoracic aorta CT calcium burden. The effective radiation dose received for the entire imaging protocol was approximately 14 mSv.

Quantitative Image Analyses

All images were analyzed by version 4.0 of the Philips IntelliSpace Portal client. The image analyst was masked to subject demographics and image specifications. Quantification of arterial ^{18}FDG and Na^{18}F uptake was performed according to previously published methods **(13, 14)**. In summary, uptake of ^{18}FDG in the thoracic aorta was determined by manually placing an oval region of interest (ROI) around the outer perimeter of the artery on every slice of the axially oriented PET/CT images. Per ROI, the maximum radiotracer-decay corrected

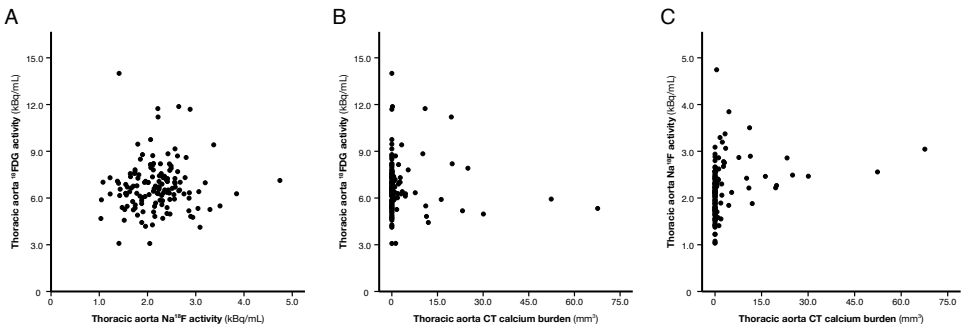

FIGURE 2 – (**A**) Scatter plot of thoracic aorta ^{18}FDG activity (FDG_{MAX}) against thoracic aorta Na^{18}F activity (NaF_{MAX}). FDG_{MAX} did not correlate with NaF_{MAX} (Spearman's ρ = 0.09; P = .316). (**B**) Scatter plot of FDG_{MAX} against thoracic aorta CT calcium burden (mm^3). FDG_{MAX} did not correlate with thoracic aorta CT calcium burden (Spearman's ρ = 0.04; P = .663). (**C**) Scatter plot of NaF_{MAX} against thoracic aorta CT calcium burden. NaF_{MAX} positively correlated with thoracic aorta CT calcium burden (Spearman's ρ = 0.44; P < .001). FDG_{MAX} and NaF_{MAX} indicate maximum [^{18}F]-fluorodeoxyglucose activity concentration (kBq/mL) adjusted for blood activity, body weight, and PET/CT technology and maximum [^{18}F]-sodium fluoride activity concentration (kBq/mL) adjusted for blood activity, body weight, and PET/CT technology, respectively.

^{18}FDG activity concentration (kBq/mL) was calculated. Maximum values obtained per ROI were summed and divided by the number of ROIs resulting in a single averaged maximum value (FDG_{MAX}). Similarly, we calculated thoracic aorta NaF_{MAX}. Blood ^{18}FDG activity and blood Na^{18}F activity were determined by drawing a single ROI in the lumen of superior vena cava. Blood ^{18}FDG activity and blood Na^{18}F activity were quantified as the radiotracer-decay corrected mean activity concentration (kBq/mL). Finally, we calculated the thoracic aorta CT calcium burden. The CT calcium burden was determined on low-dose CT images obtained as part of PET/CT imaging. The CT calcium burden was determined by calculating the calcium volume (mm^3) on every slice of the axially oriented CT images. Volumes obtained per slice were summed and divided by the number of slices resulting in a single mean CT calcium volume (mm^3). The detection threshold for vascular calcium was set at 130 Hounsfield units. To assess inter-scan agreement of mean CT calcium volume, the mean CT calcium volume was calculated on CT images obtained as part of ^{18}FDG and as part of Na^{18}F PET/CT imaging. Since inter-scan agreement of mean CT calcium volume was excellent, the CT images of the ^{18}FDG PET/CT portion were used as reference for the statistical analysis. We could not assess inter-scan agreement of FDG_{MAX} and NaF_{MAX}, since the ^{18}FDG PET/CT and Na^{18}F PET/CT scan was acquired only once.

Statistical Analysis

First, FDG_{MAX} and NaF_{MAX} were adjusted for blood activity, body weight, and PET/CT technology by multivariable linear regression, because previous studies indicated that these parameters significantly affect quantification of arterial ^{18}FDG and Na^{18}F uptake **(15)**. Second, subject demographics were summarized by descriptive statistics and compared between healthy volunteers and patients by the unpaired Student's *t* test, Mann-Whitney *U* test, or Fisher's exact test. Third, the correlations between thoracic aorta FDG_{MAX}, thoracic aorta NaF_{MAX}, and thoracic aorta CT calcium burden, were evaluated by the Spearman's rank correlation coefficient (ρ). Fourth, the dependence of thoracic aorta FDG_{MAX}, NaF_{MAX}, and CT calcium burden on cardiovascular risk factors was evaluated by univariate regression analyses. Subsequently, cardiovascular risk factors that significantly associated with FDG_{MAX}, NaF_{MAX}, or CT calcium burden were adjusted for age and sex. Linear models were extended by interaction terms to evaluate if associations between cardiovascular risk factors and FDG_{MAX}, NaF_{MAX}, or CT calcium burden were modified by sex, subject recruitment (i.e. volunteers *versus* patients), or prescription medication. Because no significant interactions were observed, we did not separate results for sex, volunteers, patients, or those on prescription medication. Finally, we performed multivariable linear regression to establish independent determinants of thoracic

aorta FDG_{MAX}, NaF_{MAX}, and CT calcium burden. Variables entered in the multivariable regression were selected based on results from univariate analyses. Fifth, we estimated the 10-year risk for CVD, based on FRS, and compared these risk estimates across quartiles of FDG_{MAX}, NaF_{MAX}, and CT calcium burden using the factorial analysis of covariance (ANCOVA). Additionally, we assessed the relation between FRS and FDG_{MAX}, NaF_{MAX}, and CT calcium burden continuously via Spearman's ρ and via multivariable linear regression analysis. Lastly, we assessed inter-scan agreement (i.e. ^{18}FDG PET/CT *versus* Na^{18}F PET/CT) of mean CT calcium volume by calculating the 95 % limits of agreement according to Bland and Altman **(16)**. A two-tailed *P* value below .05 was regarded statistically significant. *P* values and 95 % confidence intervals were determined by a bootstrap of 2,000 samples. Statistical analyses were performed by statistical software IBM SPSS Statistics version 21.

Results

Between November 2012 and May 2014 we prospectively recruited 89 healthy volunteers and 50 patients evaluated for chest pain syndromes. Several differences in subject demographics were observed between volunteers and patients (**TABLE 1**). These differences were mainly driven by age, except for smoking habits, family history, HbA1c, FRS, and prescription medication, which remained significantly higher among patients compared with volunteers after adjustment for age. The age and FRS of the study population ranged between 21 to 75 years and 0.3 to 30.0 %, respectively.

TABLE 2 – Determinants of the 10-year risk for CVD

Determinant	Regression coefficient	β	Adjusted R^2	*P* value
			0.37	**< .001**
Intercept, %	-7.53 (-14.41 to -2.19)			**.022**
FDG_{MAX}, kBq/mL	0.61 (-0.04 to 1.38)	0.11		.062
NaF_{MAX}, kBq/mL	5.05 (3.01 to 7.82)	0.34		**< .001**
CT calcium burden, mm^3	0.42 (0.28 to 0.89)	0.43		**.003**

Multivariable linear regression assessing the dependence of the 10-year cardiovascular disease (CVD) risk, estimated by the Framingham Risk Score, on thoracic aorta ^{18}FDG activity (FDG_{MAX}), thoracic aorta Na^{18}F activity (NaF_{MAX}), and the thoracic aorta CT calcium burden. β = standardized regression coefficient. The 95 % confidence interval is presented in parentheses. Abbreviations as in **TABLE 1**.

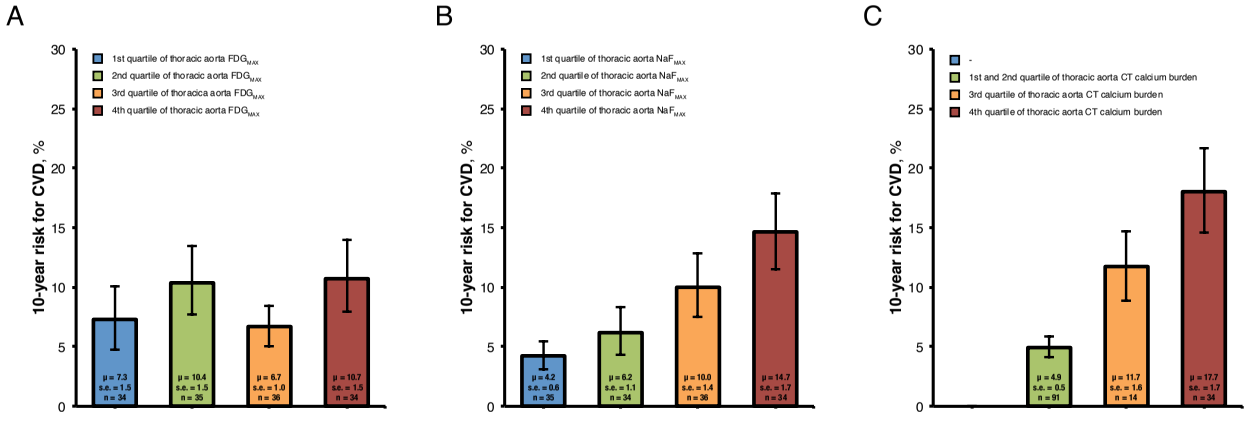

FIGURE 3 – Bar graph showing the 10-year cardiovascular disease (CVD) risk, estimated by the Framingham Risk Score, against quartiles of thoracic aorta ^{18}FDG activity (FDG$_{MAX}$) (**A**), quartiles of thoracic aorta Na^{18}F activity (NaF$_{MAX}$) (**B**), and quartiles of thoracic aorta CT calcium burden (mm^3) (**C**). CVD risk remained similar across quartiles of thoracic aorta FDG$_{MAX}$, whereas CVD risk increased linearly to quartiles of thoracic aorta NaF$_{MAX}$ (*P* < .001 for a linear trend) and quartiles of thoracic aorta CT calcium burden (*P* < .001 for a linear trend). *Error bars* represent the 95 % confidence interval of the mean. Abbreviations as in **FIGURE 2**.

Thoracic aorta ^{18}FDG uptake neither correlated with thoracic aorta Na^{18}F uptake nor with thoracic aorta CT calcium burden, whereas thoracic aorta Na^{18}F uptake positively correlated with thoracic aorta CT calcium burden (Spearman's ρ = 0.44; P < .001)(**FIGURE 2**).

Results from univariate analyses are presented in **SUPPLEMENTARY TABLES 1-3**. Multivariable linear regression established that age (0.41 kBq/mL per SD; P = .007) and family history (0.69 kBq/mL; P = .034) were independent determinants of thoracic aorta ^{18}FDG uptake in our population and explained an additional 3 % of variation in thoracic aorta FDG_{MAX} (adjusted R^2 increased from 0.60 to 0.63; P = .001). Blood ^{18}FDG activity, body weight, and PET/CT technology explained the initial 60 % of variation in the data. Multivariable linear regression established that age (0.26 kBq/mL per SD; P < .001), renal function (-0.08 kBq/mL per SD; P = .046), and thoracic aorta CT calcium burden (0.07 kBq/mL per SD; P = .015) were independent determinants of thoracic aorta Na^{18}F uptake in our population and explained an additional 8 % of variation in thoracic aorta NaF_{MAX} (adjusted R^2 increased from 0.72 to 0.80; P < .001). Blood Na^{18}F activity, body weight, and PET/CT technology explained the initial 72 % of variation in the data. Multivariable linear regression established that age (1.47 mm^3 per SD; P = .013) and anti-hypertensive treatment (10.17 mm^3; P = .030) were independent determinants of thoracic aorta CT calcium burden in our population and explained 28 % of variation in thoracic aorta mean CT calcium volume (adjusted R^2 = 0.28; P < .001).

FRS remained similar across quartiles of thoracic aorta ^{18}FDG uptake (P = .298 for a linear trend, Spearman's ρ = 0.15; P = .090). In contrast, FRS increased linearly to quartiles of thoracic aorta Na^{18}F uptake (P < .001 for a linear trend, Spearman's ρ = 0.49; P < .001). FRS was, on average, 3.5 times higher among subjects with thoracic aorta Na^{18}F uptake in highest quartile compared with those in the lowest quartile of the distribution (14.7 % *versus* 4.2 %; P < .001). FRS also increased linearly to quartiles of thoracic aorta CT calcium burden (P < .001 for a linear trend, Spearman's ρ = 0.63; P < .001). FRS was, on average, 3.6 times higher among subjects with thoracic aorta CT calcium burden in the highest quartile compared with those in the lowest two quartile of the distribution (17.7 % *versus* 4.9 %; P < .001)(**FIGURE 3**). Multivariable linear regression established that aortic Na^{18}F uptake (β = 0.34; P < .001) and aorta CT calcium burden (β = 0.43; P = .003), but not aortic ^{18}FDG uptake (β = 0.11; P = .062), were independent determinants of FRS (adjusted R^2 = 0.37; P < .001)(**Table 2**)(**FIGURE 4**).

Inter-scan agreement of thoracic aorta CT calcium burden was considered excellent as indicated by a small inter-scan difference (**SUPPLEMENTARY FIGURE 1**).

DISCUSSION

This study demonstrates that an elevated risk for CVD, as estimated by the FRS, is associated with marked increases in vascular calcification metabolism, as assessed by $Na^{18}F$ PET/CT imaging, and vascular calcium burden, as assessed by CT imaging, but not arterial inflammation, as assessed by ^{18}FDG PET/CT imaging. For the purpose of identifying the vulnerable patient, our data support a role for arterial $Na^{18}F$ PET/CT imaging, whereas this role seems less obvious for arterial ^{18}FDG PET/CT imaging.

Arterial inflammation and vascular calcification are regarded key processes in the pathogenesis of various cardiovascular diseases, in particular atherosclerosis **(4,5)**. Atherosclerotic plaque inflammation is characterized by accumulation of macrophages, which are attracted to plaques in response to lipids retained in the arterial intima **(17)**. Plaque macrophages secret chemokines, pro-inflammatory cytokines, and matrix metalloproteinases, which contribute to a non-resolving inflammatory response that lead to plaque hypoxia, plaque necrosis, weakening of the protective fibrous cap, and, ultimately, plaque rupture **(17, 18)**. Plaque rupture is considered the single-most frequent cause of adverse cardiovascular events, such as acute coronary syndromes and stroke **(18, 19)**. In response to chronic inflammation and necrosis, atherosclerotic plaque calcify **(20)**. It is believed that atherosclerotic plaque calcification retards the inflammatory response, stabilizes the atherosclerotic plaque, and reduces the risk of plaque rupture. Nonetheless, the earliest stages of plaque calcification are associated with increased plaque instability and an elevated risk of rupture **(21)**, whereas only advanced stages of plaque calcification are associated with stabilized plaques **(22)**. A possible explanation for the increased risk of plaque rupture during early stages of plaque calcification reside in that plaque micro-calcifications increase local tissue stress, which facilitate plaque vulnerability **(23)**. Although plaque calcification is associated with plaque stabilization, the presence and degree of vascular macro-calcifications is strongly predictive of adverse cardiovascular events **(7)**. It appears that vascular calcification, independent of its association with plaque stability, is a marker of the overall atherosclerotic disease burden, and thus, the vulnerable patient **(3, 24)**.

By inference, imaging techniques, aimed at visualizing arterial inflammation and vascular calcification, are potent markers of CVD risk. ^{18}FDG PET/CT imaging can non-invasively assess arterial inflammation, whereas $Na^{18}F$ PET/CT and CT imaging can non-invasively assess vascular calcification. ^{18}FDG uptake reflects the rate of glycolysis, which is particularly increased in atherosclerotic plaque that retain macrophages **(25)** and plaque

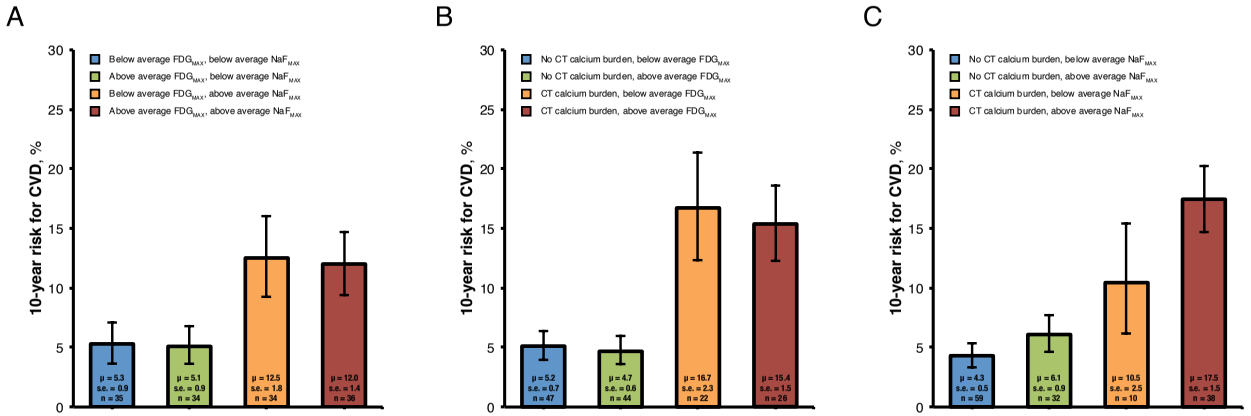

FIGURE 4 – Bar graph showing the 10-year cardiovascular disease (CVD) risk, estimated by the Framingham Risk Score, against groups below or above average thoracic aorta ^{18}FDG activity (FDG_{MAX}) and below or above average thoracic aorta Na^{18}F activity (NaF_{MAX}) (**A**), groups with or without thoracic aorta CT calcium burden and below or above average FDG_{MAX} (**B**), groups with or without thoracic aorta CT calcium burden and below or above average NaF_{MAX} (**C**). NaF_{MAX} and thoracic aorta CT calcium burden differentiated subjects at high CVD risk from subjects at low CVD risk, whereas FDG_{MAX} did not. *Error bars* represent the 95 % confidence interval of the mean. Abbreviations as in **FIGURE 2**.

that endure hypoxic stress **(26)**. In addition to atherosclerotic plaque, aortic ^{18}FDG retention has been linked to formation of aneurysms and dissection of the aorta, which are diseases associated with inflammation of the arterial media and arterial adventitia **(27)**. It has been reported that arterial ^{18}FDG uptake increases in proportion to CVD risk factors **(28)** and that aortic ^{18}FDG retention predicts adverse cardiovascular events beyond traditional CVD risk factors **(6)**. Na^{18}F uptake reflects the active exchange of fluoride with hydroxyl groups of hydroxyapatite crystals producing fluorapatite **(29)**. This process is believed to reflect calcification metabolism of osseous tissue, including calcification of atherosclerotic plaque **(30-32)**. Next to calcification of atherosclerotic plaque, which is regarded a disease of the arterial intima, arterial Na^{18}F retention is believed to reflect calcification of the arterial media, a condition associated with arterial stiffening, increased pulse pressure, left ventricular hypertrophy, and reduced myocardial perfusion **(33, 34)**. Similar to arterial ^{18}FDG retention, arterial Na^{18}F retention has also been reported to increase in proportion to CVD risk factors **(30, 31)**. CT imaging targets structural vascular calcifications. Numerous follow-up studies have established that the vascular calcium burden, as detected by CT imaging, is a strong independent marker of CVD risk **(7, 8)**.

Our study confirms findings from previous investigations. First, it confirms that arterial ^{18}FDG retention neither correlates with arterial Na^{18}F retention **(10)** nor with the CT calcium burden **(9)**. A previous investigation demonstrated that ^{18}FDG avid plaques rarely (~ 7 %) accumulate Na^{18}F and only occasionally (~ 15 %) collocate with structural calcium deposits **(9)**. These findings suggest that arterial retention of ^{18}FDG and Na^{18}F represent different stages of the cardiovascular atherosclerotic disease process and may help differentiate early from advanced stages of the disease **(9)** or may carry independent prognostic value. Second, our study confirms that arterial Na^{18}F retention positively correlates with the CT calcium burden **(9)**. A previous study reported that structural calcium deposits accompany approximately 77 % of Na^{18}F avid plaques, whereas only 21 % of vascular macro-calcifications retain Na^{18}F **(9)**. These findings suggest that arterial Na^{18}F retention may discriminate active from indolent vascular calcifications, associated with vulnerable and stabilized plaques, respectively **(10)**. Lastly, our study confirms that CVD risk, as estimated by the FRS, increases linearly with the increase in arterial Na^{18}F uptake and CT calcium burden **(10, 35)**.

Despite confirming several findings from previous investigations, our observations challenge the notion that arterial inflammation, as assessed by ^{18}FDG PET/CT, is associated with an elevated risk for CVD **(6)**. Several considerations may explain our discrepant finding.

First, our study evaluated subjects at low CVD risk (i.e. median FRS of 6 %), whereas the majority of studies that investigated arterial ^{18}FDG retention in relation to CVD risk were performed in subjects at high CVD risk **(6)**. Therefore, our study might have detected early stages of atherosclerotic plaque inflammation, but not inflammation to a degree that provokes plaque or patient vulnerability. Second, our study included subjects with a broad age range, namely between 21 and 75 years old. Therefore, we assume to have included subjects with a spectrum of atherosclerosis severity, ranging from mild to severe disease. Both fatty streaks, the hallmark of mild atherosclerosis, and high-risk vulnerable plaques, the hallmark of severe atherosclerosis, are densely populated by macrophages **(17)**. Because ^{18}FDG is primarily retained in plaque macrophages **(36-38)**, ^{18}FDG PET/CT imaging may have difficulty differentiating fatty streaks from high-risk vulnerable plaques, and thus differentiating mild from severe atherosclerosis. Third, our study estimated CVD risk solely based on FRS. A previous investigation demonstrated that aortic ^{18}FDG retention predicts CVD risk beyond FRS **(6)**. Moreover, that study demonstrated that adding the aortic ^{18}FDG retention index to FRS resulted in a net reclassification improvement of approximately 25 % compared with FRS alone **(6)**. Because our study estimated CVD risk solely via FRS, the incremental value of arterial ^{18}FDG retention over FRS in predicting CVD risk could not be assessed by our study. The three considerations mentioned above may explain the lack of association between arterial ^{18}FDG retention and CVD risk as observed by our study.

Strengths and Limitations

An important strength of the present study is that we prospectively investigated the relationship between CVD risk and arterial inflammation, vascular calcification metabolism, and vascular calcium burden in a heterogeneous group of subjects at low CVD risk. Studies that investigated similar relations were either performed retrospectively in oncology patients **(9)** or involved exclusively elderly patients with advanced CVD **(10)**. Such studies are limited by imaging protocols not necessarily optimized for imaging arteries, may suffer from selection bias, or both. In contrast, our study was performed prospectively, included a heterogeneous group of subjects at low CVD risk, and utilized imaging protocols optimized for artery imaging **(13, 14)**. As such, we were able to demonstrate that CVD risk positively associated with increases in thoracic aorta Na^{18}F uptake and thoracic aortic CT calcium burden, whereas no such relation existed with thoracic aorta ^{18}FDG uptake.

The findings of our study, however, should be interpreted in light of three limitations. First, CVD risk was estimated via the FRS. Although the renewed FRS performs good in terms

of discrimination and calibration **(12)**, it still tends to overestimate risk in those at low CVD risk and underestimate risk in those at high CVD risk. As such, our estimates of CVD risk may be inaccurate and may have biased the association between CVD risk and our imaging findings. However, given the cross-sectional nature of our study we had to rely on an estimated CVD risk. Second, the relationship between CVD risk and arterial inflammation, vascular calcification metabolism, and vascular calcium burden was evaluated in a cross-sectional study. A previous investigation, which performed serial ^{18}FDG PET/CT examinations, demonstrated that baseline arterial ^{18}FDG uptake predicted formation of vascular calcium deposits on the follow-up examination, suggesting a temporal relationship between arterial inflammation and vascular calcification **(39)**. Temporal relations are difficult to assess in cross-sectional studies and preferably require a longitudinal approach. Therefore, our finding that arterial inflammation neither relates to vascular calcification metabolism nor to the vascular calcium burden could be attributed to our cross-sectional design. Third, ethical considerations prevented collection of arterial specimens for histological examination. Therefore, we could not relate our imaging findings to the exact structure, biological composition, and inflammatory state of the detected atherosclerotic plaques **(9)**. Substantiating arterial ^{18}FDG and Na^{18}F uptake to histopathology, preferably in the early stages of the disease, might contribute to a better understanding of the metabolic pathways that govern CVD risk.

Conclusions

Our findings indicate that an unfavorable cardiovascular risk profile is associated with marked increases in thoracic aorta vascular calcification metabolism and thoracic aorta vascular calcium burden, but not arterial inflammation. For the purpose of identifying the vulnerable patient, our data support a role for arterial Na^{18}F PET/CT imaging, whereas this role seems less obvious for arterial ^{18}FDG PET/CT imaging. Nonetheless, prospective long-term follow-up studies are required to assess the risk stratification capabilities of arterial ^{18}FDG and Na^{18}F PET/CT imaging beyond standard approaches, such as the FRS and CT's calcium score.

REFERENCES

1. Mozaffarian D, Benjamin EJ, Go AS, et al. Heart Disease and Stroke Statistics--2015 Update: A Report From the American Heart Association. *Circulation.* 2015; **131**: e29-322.

2. Franco M, Cooper RS, Bilal U, et al. Challenges and Opportunities for Cardiovascular Disease Prevention. *Am J Med.* 2011; **124**: 95-102.

3. Arbab-Zadeh A, Fuster V. The Myth of the "Vulnerable Plaque": Transitioning From a Focus on Individual Lesions to Atherosclerotic Disease Burden for Coronary Artery Disease Risk Assessment. *J Am Coll Cardiol.* 2015; **65**: 846-55.

4. Hansson GK. Inflammation, Atherosclerosis, and Coronary Artery Disease. *N Engl J Med.* 2005; **352**: 1685-95.

5. Demer LL, Tintut Y. Vascular Calcification: Pathobiology of a Multifaceted Disease. *Circulation.* 2008; **117**: 2938-48.

6. Figueroa AL, Abdelbaky A, Truong QA, et al. Measurement of Arterial Activity on Routine FDG PET/CT images Improves Prediction of Risk of Future CV Events. *J Am Coll Cardiol Img.* 2013; **6**: 1250-9.

7. Budoff MJ, Shaw LJ, Liu ST, et al. Long-Term Prognosis Associated with Coronary Calcification: Observations From a Registry of 25,253 Patients. *J Am Coll Cardiol.* 2007; **49**: 1860-70.

8. Hou ZH, Lu B, Gao Y, et al. Prognostic Value of Coronary CT Angiography and Calcium Score for Major Adverse Cardiac Events in Outpatients. *J Am Coll Cardiol Img.* 2012; **5**: 990-9.

9. Derlin T, Toth Z, Papp L, et al. Correlation of Inflammation Assessed by ^{18}F-FDG PET, Active Mineral Deposition Assessed by ^{18}F-fluoride PET, and Vascular Calcification in Atherosclerotic Plaque: A Dual-Tracer PET/CT Study. *J Nucl Med.* 2011; **52**: 1020-7.

10. Dweck MR, Chow MW, Joshi NV, et al. Coronary Arterial ^{18}F-Sodium Fluoride Uptake: A Novel Marker of Plaque Biology. *J Am Coll Cardiol.* 2012; **59**: 1539-48.

11. Conroy RM, Pyorala K, Fitzgerald AP, et al. Estimation of Ten-Year Risk of Fatal Cardiovascular Disease in Europe: The SCORE Project. *Eur Heart J.* 2003; **24**: 987-1003.

12. D'Agostino RB, Vasan RS, Pencina MJ, et al. General Cardiovascular Risk Profile For Use in Primary Care: The Framingham Heart Study. *Circulation.* 2008; **117**: 743-53.

13. Blomberg BA, Thomassen A, Takx RA, et al. Delayed ^{18}F-Fluorodeoxyglucose PET/CT Imaging Improves Quantitation of Atherosclerotic Plaque Inflammation: Results from the CAMONA Study. *J Nucl Cardiol* 2014; **21**: 588-97.

14. Blomberg BA, Thomassen A, Takx RA, et al. Delayed Sodium ^{18}F-Fluoride PET/CT Imaging Does Not Improve Quantification of Vascular Calcification Metabolism: Results from the

CAMONA Study. *J Nucl Cardiol.* 2014; **21**: 293-304.

15. Huet P, Burg S, Le Guludec D, et al. Variability and Uncertainty of FDG PET Imaging Protocols for Assessing Inflammation in Atherosclerosis: Suggestions for Improvement. *J Nucl Med*. 2015; **56**: 552-9.

16. Bland JM, Altman DG. Statistical Methods for Assessing Agreement Between Two Methods of Clinical Measurement. *Lancet*. 1986; **327**: 307-10.

17. Moore KJ, Tabas I. Macrophages in the Pathogenesis of Atherosclerosis. *Cell*. 2011; **145**: 341-55.

18. Libby P. Mechanisms of Acute Coronary Syndromes and Their Implications for Therapy. *N Engl J Med.* 2013; **368**: 2004-13.

19. Weber C, Noels H. Atherosclerosis: Current Pathogenesis and Therapeutic Options. *Nat Med*. 2011; **17**: 1410-22.

20. Demer LL, Tintut Y. Inflammatory, Metabolic, and Genetic Mechanisms of Vascular Calcification. *Arterioscler Thromb Vasc Biol*. 2014; **34**: 715-23.

21. Ehara S, Kobayashi Y, Yoshiyama M, et al. Spotty Calcification Typifies the Culprit Plaque in Patients with Acute Myocardial Infarction: An Intravascular Ultrasound Study. *Circulation*. 2004; **110**: 3424-9.

22. Otsuka F, Finn AV, Virmani R. Do Vulnerable and Ruptured Plaques Hide in Heavily Calcified Arteries? *Atherosclerosis.* 2013; **229**: 34-7.

23. Kelly-Arnold A, Maldonado N, Laudier D, et al. Revised Microcalcification Hypothesis for Fibrous Cap Rupture in Human Coronary Arteries. *Proc Natl Acad Sci*. 2013; **110**: 10741-6.

24. Mauriello A, Servadei F, Zoccai GB, et al. Coronary Calcification Identifies the Vulnerable Patient Rather than the Vulnerable Plaque. *Atherosclerosis.* 2013; **229**: 124-9.

25. Tarkin JM, Joshi FR, Rudd JH. PET Imaging of Inflammation in Atherosclerosis. *Nat Rev Cardiol*. 2014; **11**: 443-57.

26. Folco EJ, Sheikine Y, Rocha VZ, et al. Hypoxia but not Inflammation Augments Glucose Uptake in Human Macrophages: Implications for Imaging Atherosclerosis with ^{18}Fluorine-Labeled 2-Deoxy-D-Glucose Positron Emission Tomography. *J Am Coll Cardiol.* 2011; **58**: 603-14.

27. Golestani R, Sadeghi MM. Emergence of Molecular Imaging of Aortic Aneurysm: Implications for Risk Stratification and Management. *J Nucl Cardiol.* 2014; **21**: 251-67.

28. Blomberg BA, Hoilund-Carlsen PF. [^{18}F]-Fluorodeoxyglucose PET Imaging of Atherosclerosis. *PET Clin.* 2015; **10**: 1-7.

29. Czernin J, Satyamurthy N, Schiepers C. Molecular Mechanisms of Bone ^{18}F-NaF Deposition.

J Nucl Med. 2010; **51**: 1826-9.

30. Derlin T, Richter U, Bannas P, et al. Feasibility of ^{18}F-Sodium Fluoride PET/CT for Imaging of Atherosclerotic Plaque. *J Nucl Med.* 2010; **51**: 862-5.

31. Derlin T, Wisotzki C, Richter U, et al. In Vivo Imaging of Mineral Deposition in Carotid Plaque Using ^{18}F-Sodium Fluoride PET/CT: Correlation With Atherogenic Risk Factors. *J Nucl Med.* 2011; **52**: 362-8.

32. Joshi NV, Vesey AT, Williams MC, et al. ^{18}F-Fluoride Positron Emission Tomography for Identification of Ruptured and High-Risk Coronary Atherosclerotic Plaques: A Prospective Clinical Trial. *Lancet*. 2014; **383**: 705-13.

33. Johnson LL. Novel Application of ^{18}F-Sodium Fluoride an Old Tracer to a Clinically Neglected Condition. *J Nucl Cardiol.* 2013; 20: 506-9.

34. Janssen T, Bannas P, Herrmann J, et al. Association of Linear ^{18}F-Sodium Fluoride Accumulation in Femoral Arteries as a Measure of Diffuse Calcification with Cardiovascular Risk Factors: A PET/CT Study. *J Nucl Cardiol*. 2013; **20**: 569-77.

35. Morbelli S, Fiz F, Piccardo A, et al. Divergent Determinants of ^{18}F-NaF Uptake and Visible Calcium Deposition in Large Arteries: Relationship with Framingham Risk Score. *Int J Cardiovasc Imaging*. 2014; **30**: 439-47.

36. Rudd JH, Warburton EA, Fryer TD, et al. Imaging Atherosclerotic Plaque Inflammation with [^{18}F]-Fluorodeoxyglucose Positron Emission Tomography. *Circulation*. 2002; **105**: 2708-11.

37. Tawakol A, Migrino RQ, Bashian GG, et al. In Vivo ^{18}F-Fluorodeoxyglucose Positron Emission Tomography Imaging Provides a Noninvasive Measure of Carotid Plaque Inflammation in Patients. *J Am Coll Cardiol.* 2006; **48**: 1818-24.

38. Figueroa AL, Subramanian SS, Cury RC, et al. Distribution of Inflammation Within Carotid Atherosclerotic Plaques With High-Risk Morphological Features: A Comparison Between Positron Emission Tomography Activity, Plaque Morphology, and Histopathology. *Circ Cardiovasc Imaging.* 2012; **5**: 69-77.

39. Abdelbaky A, Corsini E, Figueroa AL, et al. Focal Arterial Inflammation Precedes Subsequent Calcification in the Same Location: A Longitudinal FDG-PET/CT Study. *Circ Cardiovasc Imaging.* 2013; **6**: 747-54.

SUPPLEMENTARY FIGURES

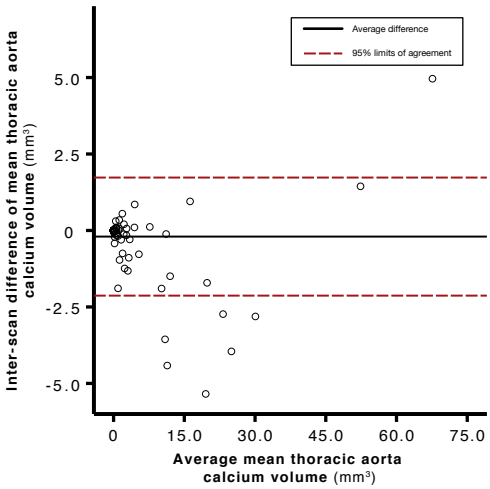

SUPPLEMENTARY FIGURE 1 – Difference plot depicting the inter-scan agreement of thoracic aorta CT calcium burden. The inter-scan agreement was considered good (average difference of 0.20 mm^3; 95 % limits of agreement 1.73 to -2.13).

SUPPLEMENTARY TABLES

SUPPLEMENTARY TABLE 1 – Determinants of thoracic aorta ^{18}FDG uptake

Determinant	Crude †	Age adjusted	Age and sex adjusted
Sex, male	-0.04 (-0.70 to 0.61)		
Age, years	0.45 (0.16 to 0.77)		0.46 (0.16 to 0.78)
Smoking, former or current	-0.08 (-0.69 to 0.54)		
Positive family history	0.79 (0.23 to 1.34)	0.69 (0.09 to 1.32)	0.69 (0.09 to 1.32)
Blood pressure, mmHg			
- Systolic	0.06 (-0.24 to 0.39)		
- Diastolic	0.15 (-0.13 to 0.42)		
Body mass index, kg/m^2	0.26 (-0.38 to 0.89)		
Cholesterol, mmol/L			
- Total	0.17 (-0.06 to 0.40)		
- LDL	0.05 (-0.23 to 0.30)		
- HDL	0.16 (-0.18 to 0.55)		
Triglycerides, mmol/L	0.09 (-0.28 to 0.46)		
Plasma glucose, mmol/L	-0.06 (-0.32 to 0.28)		
HbA1c, mmol/mol	0.23 (-0.03 to 0.71)		
eGFR, mL/min/1.73 m^2	-0.37 (-0.73 to -0.04)	-0.25 (-0.62 to 0.08)	
Medication, yes			
- Statines	0.74 (-0.18 to 1.83)		
- Antihypertensive drugs	0.46 (-0.53 to 1.54)		

Continued on page 211

SUPPLEMENTARY TABLE 1 – Determinants of thoracic aorta ^{18}FDG uptake, *continued*

Determinant	Crude †	Age adjusted	Age and sex adjusted
Vascular calcification, yes	0.30 (-0.51 to 1.11)		
Vascular calcification, mm^3	-0.07 (-0.42 to 0.59)		
Aortic radioactivity, kBq/mL			
- [^{18}F]-sodium fluoride	0.13 (-0.29 to 0.54)		

Determinants of thoracic aorta ^{18}FDG uptake (FDG_{MAX}). Values are expressed as linear regression coefficients (95 % confidence interval) per standard deviation of change in the determinant. To illustrate, a regression coefficient of 0.45 for age signifies that an increase in age with 1 standard deviation (i.e. 14 years) relates to an increase in FDG_{MAX} of 0.45 kBq/mL. † Crude values of FDG_{MAX} were adjusted for blood ^{18}FDG activity, body weight, and PET/CT technology. Abbreviations as in **TABLE 1**.

SUPPLEMENTARY TABLE 2 – Determinants of thoracic aorta $Na^{18}F$ uptake

Determinant	Crude †	Age adjusted	Age and sex adjusted
Sex, male	0.05 (-0.17 to 0.26)		
Age, years	0.31 (0.24 to 0.38)		0.31 (0.24 to 0.39)
Smoking, former or current	0.17 (-0.01 to 0.33)		
Positive family history	0.05 (-0.21 to 0.28)		
Blood pressure, mmHg			
- Systolic	0.08 (-0.02 to 0.18)		
- Diastolic	0.07 (-0.04 to 0.16)		
Body mass index, kg/m^2	0.11 (-0.09 to 0.29)		
Cholesterol, mmol/L			
- Total	0.13 (0.06 to 0.21)	0.03 (-0.04 to 0.11)	
- LDL	0.10 (0.02 to 0.18)	0.04 (-0.04 to 0.11)	
- HDL	-0.02 (-0.13 to 0.09)		
Triglycerides, mmol/L	0.17 (0.06 to 0.33)	0.12 (0.00 to 0.27)	0.12 (0.00 to 0.27)
Plasma glucose, mmol/L	0.14 (0.03 to 0.28)	0.05 (-0.08 to 0.20)	
HbA1c, mmol/mol	0.15 (0.06 to 0.30)	0.03 (-0.08 to 0.12)	
eGFR, mL/min/1.73 m^2	-0.18 (-0.27 to -0.09)	-0.07 (-0.15 to 0.00)	-0.07 (-0.15 to 0.00)
Medication, yes			
- Statines	0.18 (-0.10 to 0.45)		
- Antihypertensive drugs	0.43 (0.11 to 0.73)	0.12 (-0.15 to 0.39)	

Continued on page 213

SUPPLEMENTARY TABLE 2 – Determinants of thoracic aorta Na^{18}F uptake, *continued*

Determinant	Crude †	Age adjusted	Age and sex adjusted
Vascular calcification, yes	0.53 (0.36 to 0.71)	0.20 (-0.04 to 0.46)	
Vascular calcification, mm^3	0.15 (0.09 to 0.34)	0.06 (0.00 to 0.13)	0.06 (0.00 to 0.12)
Aortic radioactivity, kBq/mL			
- [^{18}F]-fluorodeoxyglucose	0.04 (-0.07 to 0.16)		

Determinants of thoracic aorta Na^{18}F uptake (NaF_{MAX}). Values are expressed as linear regression coefficients (95 % confidence interval) per standard deviation of change in the determinant. To illustrate, a regression coefficient of 0.31 for age signifies that an increase in age with 1 standard deviation (i.e. 14 years) relates to an increase in NaF_{MAX} of 0.31 kBq/mL. † Crude values of NaF_{MAX} were adjusted for blood Na^{18}F activity, body weight, and PET/CT technology. Abbreviations as in **TABLE 1**.

SUPPLEMENTARY TABLE 3 – Determinants of thoracic aorta CT calcium burden

Determinant	Crude †	Age adjusted	Age and sex adjusted
Sex, male	1.97 (-0.31 to 4.61)		
Age, years	3.15 (1.75 to 4.88)		3.30 (1.70 to 5.16)
Smoking, former or current	2.90 (0.02 to 5.75)	1.62 (-1.92 to 4.52)	
Positive family history	-2.04 (-4.13 to -0.14)	-2.60 (-5.29 to -0.56)	-2.32 (-4.67 to -0.56)
Blood pressure, mmHg			
- Systolic	1.26 (0.31 to 2.54)	0.33 (-0.88 to 1.59)	
- Diastolic	0.44 (-0.57 to 1.36)		
Body mass index, kg/m^2	-0.10 (-1.29 to 0.99)		
Cholesterol, mmol/L			
- Total	0.47 (-0.54 to 1.43)		
- LDL	0.17 (-1.18 to 1.44)		
- HDL	-0.09 (-0.84 to 0.84)		
Triglycerides, mmol/L	0.94 (-0.46 to 2.67)		
Plasma glucose, mmol/L	3.17 (0.47 to 5.27)	2.35 (-0.51 to 4.54)	
HbA1c, mmol/mol	3.57 (1.08 to 5.28)	2.70 (-0.03 to 4.71)	
eGFR, mL/min/1.73 m^2	-0.86 (-2.99 to 1.08)		
Medication, yes			
- Statines	8.18 (2.12 to 15.39)	5.16 (-1.70 to 12.80)	
- Antihypertensive drugs	12.00 (5.86 to 19.37)	10.17 (4.06 to 17.33)	9.85 (4.55 to 16.53)

Continued on page 215

SUPPLEMENTARY TABLE 3 – Determinants of thoracic aorta CT calcium burden, *continued*

Determinant	Crude †	Age adjusted	Age and sex adjusted
Aortic radioactivity, kBq/mL			
- [^{18}F]-fluorodeoxyglucose	-0.41 (-2.27 to 1.08)		
- [^{18}F]-sodium fluoride	2.56 (1.05 to 4.86)	0.91 (-0.21 to 2.62)	

Determinants of thoracic aorta CT calcium burden (mm^3). Values are expressed as linear regression coefficients (95 % confidence interval) per standard deviation of change in the determinant. To illustrate, a regression coefficient of 3.15 for age signifies that an increase in age with 1 standard deviation (i.e. 14 years) relates to an increase in CT calcium burden of 3.15 mm^3. Abbreviations as in **TABLE 1**.

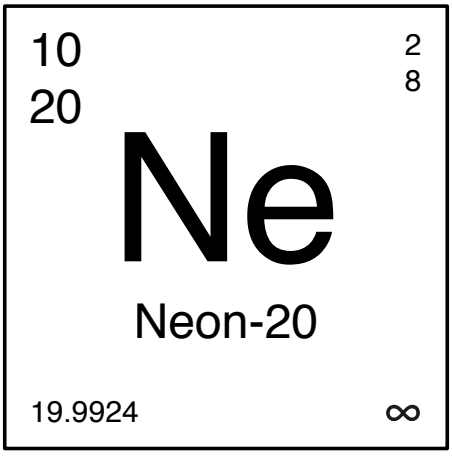
10
20
2
8
Ne
Neon-20
19.9924
∞

Chapter 10

General Discussion

The first major finding of this thesis is that PET/CT imaging of atherosclerosis is challenging and that several technical aspects need to be considered before quantitative imaging of atherosclerosis with [^{18}F]-fluorodeoxyglucose (^{18}FDG) and sodium ^{18}F-fluoride (Na^{18}F) PET/CT can be reliably attempted.

Most importantly, this thesis demonstrates that delayed ^{18}FDG PET/CT imaging improves quantification of arterial inflammation, whereas delayed Na^{18}F PET/CT imaging does not improve quantification of vascular calcification. Furthermore, it confirms the finding that quantification of ^{18}FDG and Na^{18}F uptake in human arteries can be achieved with low inter-observer and intra-observer variability **(1-3)**. Moreover, it shows that partial volume effects significantly influence quantification of arterial inflammation, as assessed by ^{18}FDG PET/CT imaging, and that partial volume correction may improve quantification of arterial inflammation. In addition, it demonstrates that blood ^{18}FDG activity, body weight, and PET/CT instrumentation affect assessment of arterial inflammation by ^{18}FDG PET/CT imaging. Similarly, blood Na^{18}F activity, injected dose, and PET/CT instrumentation affect assessment of vascular calcification by Na^{18}F PET/CT imaging. Therefore, blood activity, body weight, injected dose, and PET/CT instrumentation should be taken into account to generate accurate estimates of arterial ^{18}FDG and Na^{18}F uptake. Finally, this thesis demonstrates that quantification of ^{18}FDG and Na^{18}F uptake in human arteries by calculation of the target-to-background ratio—the current reference standard for this purpose **(1, 2, 4)**—is suboptimal compared to calculation of the blood-pool subtracted maximum arterial wall activity.

Although these findings improve the technical validity of atherosclerosis imaging with PET/CT, the results indicate that a lack of consensus and standardization of protocols for imaging atherosclerosis with PET/CT imaging can result in substantial variability and uncertainty in the retrieved signal. Numerous factors, including injected dose, body distribution volume, acquisition duration, tracer circulating time, reconstruction algorithm, voxel size, spatial resolution, effective number of iterations, and post-filtering can influence the arterial tracer signal retrieved by PET/CT imaging. The impact of these parameters on the images generated has been thoroughly investigated by Huet and colleagues in 2015 **(5)**. Their results, together with the findings from this thesis, stress that standardized protocols for imaging atherosclerosis with PET/CT are imperative for reliable research, being a prerequisite for generation of reference values, and to allow for comparison of quantitative imaging results among studies. Most strikingly, the results of this thesis embarked a discussion regarding the relative impact of injected dose and body distribution volume on uptake of tracer in human

arteries. Under the assumption that tracer amounts do not saturate the uptake of ^{18}FDG and Na^{18}F in atherosclerotic plaque, arterial tracer uptake positively correlates with injected dose and negatively correlates with body distribution volume. It remains undetermined, however, whether these correlations are linear, exponential, or logarithmic under biological circumstances. The standardized uptake value, a common method to quantify tracer uptake in PET/CT imaging, assumes that the impact of injected dose and body distribution volume, as estimated via either body weight, body surface area, or lean body mass, on arterial tracer uptake is strictly linear. If this assumption was true, administration of injected dose proportional to body weight would eliminate the relative impact of injected dose and body distribution volume on arterial tracer uptake altogether. The results of this thesis, however, suggests that, even if injected dose is given proportional to body weight, the combined effect of injected dose and body weight remains positively related to the degree of tracer uptake in the arterial wall. This might explain the equivocal use of body weight, body surface area, and lean body mass as surrogates of body distribution volume in the equation of the standardized uptake value. Because injected dose was administered proportional to body weight in the CAMONA study, which resulted in significant collinearity between these two variables, this thesis could not assess the individual impact of injected dose and body distribution volume on arterial tracer uptake. Despite this limitation, we need to consider that in absence of atherosclerosis, there should be little to no uptake of tracer in the arterial wall. As a consequence, arterial tracer uptake no longer depends on administrated dose or distribution volume, but starts to rely on blood activity, non-specific background activity, and scatter effects. Under such circumstances, calculation of the standardized uptake value may result into biased estimated of arterial tracer uptake. These considerations seem to support the suggestion that it is best to administer a fixed tracer dose in studies evaluating atherosclerosis with PET/CT imaging and to take the effect of distribution volume of the tracer separately into account, for instance via regression modeling. The data of this thesis further questions whether the assumption of no saturation is defensible, particularly for arterial Na^{18}F PET/CT imaging, where arterial Na^{18}F uptake seemed to saturate after 45 minutes. Saturation of tracer uptake would be another argument for fixed dose administration in examining atherosclerosis with PET/CT imaging.

Similar to problems with imaging protocols, a lack of consensus and standardization of protocols for quantification hampers the accurate translation of the generated PET/CT images to reliable quantitative numbers. The lack of standardized quantification protocols led to introduction of numerous methods to quantify arterial ^{18}FDG and Na^{18}F uptake ranging from simple visual analysis to sophisticated techniques such as calculation of the tracers influx rate

by a Patlak plot. The optimal method to quantify arterial tracer uptake remains undetermined. This thesis, for example, demonstrates that quantification of ^{18}FDG and Na^{18}F uptake in human arteries by calculation of the target-to-background ratio—a prevalent method to quantify tracer uptake in the arterial wall—is suboptimal compared to calculation of the blood-pool subtracted maximum arterial wall activity. Future studies are required to establish the most accurate methodology to quantify arterial tracer uptake on PET/CT images.

The second major finding of this thesis is that vascular calcification, as assessed by Na^{18}F PET/CT imaging, is associated with an elevated risk for adverse cardiovascular events, while arterial inflammation, as assessed by [^{18}F]-fluorodeoxyglucose (^{18}FDG) PET/CT imaging, is not associated with an elevated risk for adverse cardiovascular events. The former observation is in line with the current literature and the hypothesis that the degree of arterial Na^{18}F uptake reflects atherosclerosis severity, while the latter observation challenges the current literature and the hypothesis that arterial ^{18}FDG uptake reflects atherosclerosis severity.

Numerous studies have reported positive associations between arterial ^{18}FDG uptake and atherosclerosis severity. The first study to link arterial ^{18}FDG avidity to atherosclerosis was published in 2001 by Yun and colleagues **(6)**. They demonstrated that half of patients referred for ^{18}FDG PET had evidence of ^{18}FDG retention in various parts of the arterial tree. Furthermore, they suggested that arterial ^{18}FDG uptake likely represents arterial inflammation and could be associated with the number and activity level of macrophages present in atherosclerotic plaque. In 2002, Rudd and colleagues **(7)** confirmed the suggestion that ^{18}FDG accumulates in plaque macrophages. This was an important confirmation, mainly because plaques with high numbers of macrophages are considered vulnerable and vulnerable plaques are associated with an elevated risk for adverse cardiovascular events. Therefore, by targeting plaque macrophages, ^{18}FDG PET/CT imaging can potentially evaluate risk for adverse cardiovascular events. Figueroa and colleagues later confirmed this suggestion in 2013 **(8)**. They demonstrated that ^{18}FDG PET/CT imaging of atherosclerosis could predict risk for adverse cardiovascular events, independent of traditional cardiovascular risk factors. Adding the aortic ^{18}FDG retention index to the Framingham Risk Score resulted in a net reclassification index of approximately 25 % compared with the Framingham Risk Score alone. In addition, aortic ^{18}FDG uptake was inversely related to the timing of the adverse cardiovascular event. These data suggest that arterial ^{18}FDG uptake is helpful in risk stratification of patients at risk for cardiovascular disease, beyond standard tools, such as the Framingham Risk Score. In 2007,

Rudd and colleagues demonstrated that ^{18}FDG PET/CT imaging of atherosclerosis meets two important criteria for treatment evaluation purposes **(2)**. Namely, that spontaneous changes in plaque ^{18}FDG avidity are low within a time frame of two weeks and that plaque ^{18}FDG avidity can be determined with excellent inter-rater agreement. Based on these results, Tawakol and colleagues designed a study that investigated whether high-dose statin treatment would attenuate arterial ^{18}FDG activity more than low-dose statin treatment **(9)**. To this end, 76 patients with established atherosclerosis were randomized to receive either daily 10 mg or 80 mg of atorvastatin. Treatment effects were assessed by ^{18}FDG PET/CT at 4 and 12 weeks after the baseline ^{18}FDG PET/CT examination. At 4 weeks, arterial ^{18}FDG activity was significantly reduced compared with baseline for both the 10 mg and 80 mg groups (6.4 % *versus* 12.5 % reduction, respectively). At 12 weeks, an additional relative reduction was observed for the 80 mg group only (10.6 % relative reduction), suggesting a dose-response relationship between statin therapy and attenuation of arterial ^{18}FDG activity.

Although these studies demonstrate a positive relationship between arterial ^{18}FDG avidity and atherosclerosis severity, our study could not demonstrate such a relationship. Several considerations may explain this discrepant finding. First, CAMONA evaluated subjects at low risk for adverse cardiovascular events, whereas the majority of studies that investigated arterial ^{18}FDG retention in relation to cardiovascular disease risk were performed in subjects at high risk for adverse cardiovascular events **(8)**. Therefore, CAMONA might have detected early stages of atherosclerotic plaque inflammation, but not inflammation to a degree that provokes plaque or patient vulnerability. Second, CAMONA recruited subjects with a broad age range, namely between 21 and 75 years old. Therefore, CAMONA included subjects with a spectrum of atherosclerosis severity, ranging from mild to severe disease. Both fatty streaks, the hallmark of mild atherosclerosis, and high-risk vulnerable plaques, the hallmark of severe atherosclerosis, are densely populated by macrophages **(10)**. Because ^{18}FDG is primarily retained in plaque macrophages **(4, 7, 11)**, ^{18}FDG PET/CT imaging may have difficulty differentiating fatty streaks from high-risk vulnerable plaques, and thus differentiating mild from severe atherosclerosis. Third, our study estimated cardiovascular disease risk solely based on the Framingham Risk Score. A previous investigation demonstrated that aortic ^{18}FDG retention predicts cardiovascular disease risk beyond the Framingham Risk Score **(8)**. Moreover, that study demonstrated that adding the aortic ^{18}FDG retention index to the Framingham Risk Score resulted in a net reclassification improvement of approximately 25 % compared with the Framingham Risk Score alone **(8)**. Because our study estimated risk for adverse cardiovascular events solely via the Framingham Risk Score, the incremental value

of arterial ^{18}FDG retention over the Framingham Risk Score in predicting risk for adverse cardiovascular events could not be assessed. The three considerations mentioned above may explain the lack of association between arterial ^{18}FDG retention and risk for adverse cardiovascular events as observed in the CAMONA study.

In contrast to ^{18}FDG PET/CT imaging of atherosclerosis, only a limited number of studies have investigated the relationship between arterial Na^{18}F uptake and atherosclerosis severity or risk for adverse cardiovascular events. In 2010, Derlin and colleagues were able to demonstrate the feasibility of Na^{18}F PET/CT for the purpose of imaging mineral deposition in the arterial walls of large arteries **(12)**. A subsequent study by the same authors demonstrated that arterial Na^{18}F uptake related to the cardiovascular risk profile of the patient **(13)**. In 2012, Dweck and colleagues demonstrated the feasibility of Na^{18}F PET/CT imaging of mineral deposition in coronary arteries **(3)**. In addition, this study was able to demonstrate that coronary Na^{18}F uptake was higher in patients with clinically manifest cardiovascular disease compared to control subjects and that the degree of coronary Na^{18}F uptake increased according to the cardiovascular risk profile of the patient. In 2015, Irkle and colleagues published another important study in the field of Na^{18}F PET/CT imaging of atherosclerosis **(14)**. This study helped unravel the mechanisms underlying Na^{18}F uptake in the vasculature. Using electron microprobe analysis on carotid atherosclerotic plaques obtained as part of carotid endarterectomy surgery, it was demonstrated that fluoride directly adsorbs to calcified areas in mineralized vascular tissue. The binding of Na^{18}F to vascular calcium was highly specific, because localization to soft tissue was not observed. Furthermore, it was demonstrated that the extent of Na^{18}F uptake was highly dependent on the surface area of the calcification, being able to adsorb only to the outer layer of calcifications without deeper penetration. These data suggest that Na^{18}F PET/CT imaging of vascular calcification is prone to detect micro-calcifications, since micro-calcifications, relative to its size, have large surface areas whereas macro-calcifications, relative to its size, have small surface areas.

By demonstrating a positive correlation between arterial Na^{18}F avidity and risk for adverse cardiovascular events, the results of this thesis confirm findings from previous investigations. Most importantly, the results obtained with Na^{18}F PET/CT imaging of vascular calcification are in line with results obtained with CT imaging of vascular calcification. Namely, the presence and degree of vascular macro-calcification, as assessed by CT imaging, is also predictive of risk for adverse cardiovascular events **(15).** It remains surprising though that vascular calcification on the one hand is positively associated with risk for adverse

cardiovascular events and on the other hand is regarded to be feature of atherosclerotic plaque stabilization. This apparent paradox might be explained by the fact that vascular calcification, independent of its association with plaque stability, is a marker of the overall atherosclerotic disease burden, and thus, the vulnerable patient **(16, 17)**. Consequently, it comes as no surprise that visualization of micro-calcifications via $Na^{18}F$ PET/CT imaging, similar to visualization of macro-calcifications via CT imaging, is positively related to risk for adverse cardiovascular events. By targeting the earliest stages of atherosclerotic plaque calcification, $Na^{18}F$ PET/CT imaging of vascular calcification offers new opportunities for early and individual atherosclerotic cardiovascular disease risk assessment and possibly identification of new pathobiological targets for anti-atherosclerotic therapies. This makes $Na^{18}F$ PET/CT imaging of molecular vascular calcification an imaging modality with merit for further investigations.

FUTURE PERSPECTIVES

First and foremost, imaging and quantification protocols need to be standardized before reliable and reproducible research can be attempted with PET/CT imaging. Most of the aforementioned methodological and technical limitations of PET/CT imaging of atherosclerosis can be overcome by performing studies that investigate whether ^{18}FDG PET/CT and $Na^{18}F$ PET/CT have incremental prognostic value over currently established methods for determining risk for adverse cardiovascular events, such as the Framingham Risk Score **(18)** and HeartSCORE **(19)**. Such studies can set a standard for imaging and quantification protocols that can be copied and applied by other imaging centers. Unfortunately, such studies require large prospective long-term follow-up studies that can be financially and logistically challenging. Notwithstanding the challenges, some research groups are currently attempting such studies. Examples are "The Progression and Early Detection of Subclinical Atherosclerosis" (PESA) study **(20)** and "The Prediction of Recurrent Events with ^{18}F-Fluoride to Identify Ruptured and High-Risk Coronary Artery Plaques in Patients with Myocardial Infarction" ($PRE^{18}FFIR$) study. The PESA study aims to examine the presence of subclinical atherosclerosis by means of non-invasive imaging, including ^{18}FDG PET/CT imaging, and relate imaging characteristics to the cardiovascular outcome of the patient. To this end, almost 4,000 asymptomatic subjects will be recruited and examined. The $PRE^{18}FFIR$ study has similar aims as PESA, but follows 700 high-risk patients with coronary artery disease for 2 years to determine whether baseline $Na^{18}F$ PET/CT imaging can identify patients who go on to sustain myocardial infarction and predict coronary arterial disease progression. The results of PESA and $PRE^{18}FFIR$ are feverishly awaited with the first results expected to become available in the second half of 2016.

GENERAL CONCLUSION

In conclusion, positron emission tomography imaging of atherosclerosis offers exciting new opportunities to assess a patient's vulnerability for adverse cardiovascular events. It remains to be seen, however, whether functional imaging of atherosclerosis will translate into improved cardiovascular risk stratification and ultimately reduced rates of adverse cardiovascular events.

REFERENCES

1. Rudd JH, Myers KS, Bansilal S, et al. Atherosclerosis Inflammation Imaging with ^{18}F-FDG PET: Carotid, Iliac, and Femoral Uptake Reproducibility, Quantification Methods, and Recommendations. *J Nucl Med.* 2008; **49**: 871-878.

2. Rudd JH, Myers KS, Bansilal S, et al. ^{18}Fluorodeoxyglucose Positron Emission Tomography Imaging of Atherosclerotic Plaque Inflammation is Highly Reproducible: Implications for Atherosclerosis Therapy Trials. *J Am Coll Cardiol.* 2007; **50**: 892-896.

3. Dweck MR, Chow MW, Joshi NV, et al. Coronary Arterial ^{18}F-Sodium Fluoride Uptake: A Novel Marker of Plaque Biology. *J Am Coll Cardiol.* 2012; **59**: 1539-1548.

4. Tawakol A, Migrino RQ, Bashian GG, et al. In Vivo ^{18}F-Fluorodeoxyglucose Positron Emission Tomography Imaging Provides a Noninvasive Measure of Carotid Plaque Inflammation in Patients. *J Am Coll Cardiol.* 2006; **48**: 1818-1824.

5. Huet P, Burg S, Le Guludec D, et al. Variability and Uncertainty of ^{18}F-FDG PET Imaging Protocols for Assessing Inflammation in Atherosclerosis: Suggestions for Improvement. *J Nucl Med.* 2015; **56**: 552-559.

6. Yun M, Yeh D, Araujo LI, et al. ^{18}F-FDG Uptake in the Large Arteries: A New Observation. *Clin Nucl Med.* 2001; **26**: 314-319.

7. Rudd JH, Warburton EA, Fryer TD, et al. Imaging Atherosclerotic Plaque Inflammation with [^{18}F]-Fluorodeoxyglucose Positron Emission Tomography. *Circulation.* 2002; **105**: 2708-2711.

8. Figueroa AL, Abdelbaky A, Truong QA, et al. Measurement of Arterial Activity on Routine FDG PET/CT Images Improves Prediction of Risk of Future CV Events. *J Am Coll Cardiol Img.* 2013; **6**: 1250-1259.

9. Tawakol A, Fayad ZA, Mogg R, et al. Intensification of Statin Therapy Results in a Rapid Reduction in Atherosclerotic Inflammation: Results of a Multicenter Fluorodeoxyglucose-Positron Emission Tomography/Computed Tomography Feasibility Study. *J Am Coll Cardiol.* 2013; **62**: 909-917.

10. Moore KJ, Tabas I. Macrophages in the Pathogenesis of Atherosclerosis. *Cell.* 2011; **145**: 341-355.

11. Figueroa AL, Subramanian SS, Cury RC, et al. Distribution of Inflammation within Carotid Atherosclerotic Plaques with High-Risk Morphological Features: A Comparison Between Positron Emission Tomography Activity, Plaque Morphology, and Histopathology. *Circ Cardiovasc Imaging.* 2012; **5**: 69-77.

12. Derlin T, Richter U, Bannas P, et al. Feasibility of ^{18}F-Sodium Fluoride PET/CT for Imaging of Atherosclerotic Plaque. *J Nucl Med.* 2010; **51**: 862-865.

13. Derlin T, Wisotzki C, Richter U, et al. In Vivo Imaging of Mineral Deposition in Carotid Plaque Using ^{18}F-Sodium Fluoride PET/CT: Correlation with Atherogenic Risk Factors. *J Nucl Med.* 2011; **52**: 362-368.

14. Irkle A, Vesey AT, Lewis DY, et al. Identifying Active Vascular Microcalcification by ^{18}F-Sodium Fluoride Positron Emission Tomography. *Nat Commun.* 2015; **6**: 7495.

15. Budoff MJ, Shaw LJ, Liu ST, et al. Long-Term Prognosis Associated with Coronary Calcification: Observations from a Registry of 25,253 Patients. *J Am Coll Cardiol.* 2007; **49**: 1860-1870.

16. Arbab-Zadeh A, Fuster V. The Myth of the "Vulnerable Plaque": Transitioning from a Focus on Individual Lesions to Atherosclerotic Disease Burden for Coronary Artery Disease Risk Assessment. *J Am Coll Cardiol.* 2015; **65**: 846-855.

17. Mauriello A, Servadei F, Zoccai GB, et al. Coronary Calcification Identifies the Vulnerable Patient Rather than the Vulnerable Plaque. *Atherosclerosis.* 2013; **229**: 124-129.

18. D'Agostino RB, Vasan RS, Pencina MJ, et al. General Cardiovascular Risk Profile for Use in Primary Care: The Framingham Heart Study. *Circulation.* 2008; **117**: 743-753.

19. Conroy RM, Pyorala K, Fitzgerald AP, et al. Estimation of Ten-Year Risk of Fatal Cardiovascular Disease in Europe: The SCORE Project. *Eur Heart J.* 2003; **24**: 987-1003.

20. Fernandez-Ortiz A, Jimenez-Borreguero LJ, Penalvo JL, et al. The Progression and Early Detection of Subclinical Atherosclerosis (PESA) Study: Rationale and Design. *Am Heart J.* 2013; **166**: 990-998.

Samenvatting

INTRODUCTIE

Slagaderverkalking is een hart- en vaatziekte die wordt gekenmerkt door de vorming van plaques in de slagaderwand. Plaques bestaan voornamelijk uit vetten, kalk en ontstekingscellen. Plaques ontwikkelen zich langzaam en geven zelden klachten. Echter, in uitzonderlijke gevallen kan een plaque scheuren. Op de scheur vormt zich een bloedstolsel dat de slagader gedeeltelijk of geheel kan afsluiten. Het weefsel achter de afsluiting krijgt hierdoor onvoldoende zuurstof en sterft af. Zo ontstaat een klinische episode zoals een hartaanval of beroerte.

Klinische episoden en hun complicaties leggen een zware druk op de Nederlandse gezondheidszorg. Het adagium "voorkomen is beter dan genezen" is dan ook van toepassing. De voornaamste strategie om klinische episoden te voorkomen is het identificeren van personen zonder symptomen, maar met een verhoogd risico op hart- en vaatziekten, de zogenoemde kwetsbare patiënt. Kwetsbare patiënten hebben in theorie de meeste baat bij leefstijladviezen en behandeling met medicijnen. Het vroegtijdig opsporen van kwetsbare patiënten blijkt echter een enorme uitdaging. Hoewel verschillende factoren, zoals roken, overgewicht en een verhoogde bloeddruk geassocieerd zijn met een verhoogd risico op hart- en vaatziekten, zijn de risico's die hiermee gepaard gaan te klein voor individueel cardiovasculair risicomanagement. Dat wil zeggen, de meerderheid van de klinische episoden komt voor bij mensen zonder risicofactoren terwijl de meerderheid van de mensen met risicofactoren nooit een klinische episode zal doormaken. Derhalve is de medische wetenschap naarstig op zoek naar nieuwe en betere methoden voor het inschatten van het risico op hart- en vaatziekten.

Recente ontwikkelingen binnen de medische specialismen radiologie en nucleaire geneeskunde bieden nieuwe perspectieven voor het inschatten van het risico op hart- en vaatziekten. Met name functionele beeldvorming van slagaderverkalking, gericht op het afbeelden van de ziektemechanismen van slagaderverkalking, bieden goede mogelijkheden om cardiovasculair risicomanagement te verbeteren. Voorbeelden van ziektemechanismen die het risico op klinische episoden vergroten zijn ontsteking en verkalking van de slagaderwand. Deze twee mechanismen kunnen in beeld worden gebracht met behulp van, respectievelijk, de functionele beeldvormende technieken [^{18}F]-fluorodeoxyglucose positronemissietomografie en natrium [^{18}F]-fluoride positronemissietomografie.

Positronemissietomografie, afgekort PET, is een beeldvormende techniek die met behulp van kleine hoeveelheden radioactief materiaal lichaamsfuncties in beeld brengt. PET wordt daarom beschouwd als een functionele beeldvormende techniek in tegenstelling tot

computertomografie en MRI, die beide structurele beeldvormende technieken zijn. De meeste PET-scans worden gemaakt met behulp van [^{18}F]-fluorodeoxyglucose, afgekort FDG. FDG is een radioactief suiker. Suikers, waaronder FDG, worden in groten getale opgenomen in metabool actieve cellen en in mindere mate in metabool inactieve cellen. Zo ontstaat er een contrast tussen actieve en inactieve lichaamscellen. Dit principe wordt bijvoorbeeld toegepast om kanker op te sporen. Kankercellen delen zich sneller dan goedaardige cellen en verbruiken hierbij veel energie in de vorm van suikers. Zodoende hoopt FDG zich op in het kankergezwel en wordt deze zichtbaar op een PET-scan. Een vergelijkbaar principe wordt toegepast bij het in beeld brengen van slagaderverkalking. Plaque met veel ontstekingscellen verbruikt meer suikers dan plaque met weinig ontstekingscellen. Zo worden plaques met veel ontstekingscellen zichtbaar op een FDG PET-scan. Een plaque met veel ontstekingscellen scheurt makkelijker dan een plaque met weinig ontstekingscellen. Het risico op klinische episoden is dan ook groter in mensen met veel ontstoken plaques.

PET-scans kunnen ook gemaakt worden met behulp van natrium [^{18}F]-fluoride, afgekort NaF. NaF is een radioactief zout dat zich aan de bouwstenen van botweefsel bindt. NaF PET wordt dan ook voornamelijk toegepast om ziekten van het skelet te detecteren, zoals uitzaaiingen van kanker in bot. Ook slagaderverkalking kan in beeld worden gebracht met NaF PET. Sommige plaques bevatten namelijk kalk. De naam slagaderverkalking verwijst hiernaar. De bouwstenen van plaquekalk tonen grote gelijkenissen met de bouwstenen van botweefsel. NaF bindt, naast bot, dan ook aan plaquekalk. Zodoende kunnen plaques met veel kalk zichtbaar gemaakt worden op een NaF PET-scan. Het risico op klinische episoden is groter in mensen met veel verkalkte plaques.

Hoewel FDG PET en NaF PET veelbelovende methoden zijn voor het bepalen van het cardiovasculaire risicoprofiel van de patiënt, zal zorgvuldig medisch wetenschappelijk onderzoek moeten uitwijzen of deze functionele beeldvormende technieken daadwerkelijk van toegevoegde waarden zijn bovenop de reeds gangbare risicofactoren voor hart- en vaatziekten.

PROEFSCHRIFT

Het doel van dit proefschrift is het valideren van FDG PET en NaF PET voor cardiovasculair risicomanagement.

Het proefschrift bevat twee delen. **Deel I**, bestaande uit 5 hoofdstukken, is gericht op de technische validatie van FDG PET en NaF PET. In **hoofdstukken 2** en **3** is de invloed van tijd tussen het toedienen van het radioactief materiaal en het maken van de PET-scan op de beeldkwaliteit bestudeerd. Voor FDG bleek de tijd tussen het toedienen van het radioactief materiaal en het maken van de PET-scan van invloed te zijn op de beeldkwaliteit. FDG PET-scans die gemaakt werden na 180 minuten toonden een verhoogde opname van FDG in plaque in vergelijking met FDG PET-scans die gemaakt werden na 90 minuten. Echter, voor NaF PET bleek de tijd tussen het toedienen van het radioactief materiaal en het maken van de PET-scan niet van invloed op de beeldkwaliteit. Op basis van deze resultaten is besloten om de FDG PET-scan altijd na 180 minuten en de NaF PET-scan altijd na 90 minuten te maken. In **hoofdstuk 4** is de invloed van het partiële volume effect op de beeldkwaliteit bestudeerd. Het partiële volume effect omvat een scala aan effecten waarbij kleine volumes radioactiviteit op PET-scans groter in volume lijken, maar zwakker in intensiteit. Aangezien plaques erg klein zijn, zorgt het partiële volume effect ervoor dat de intensiteit van radioactiviteit in plaque wordt onderschat. In **hoofdstuk 4** wordt een methode beschreven waarmee voor het partiële volume effect gecorrigeerd kan worden. In **hoofdstukken 5** en **6** is de rol van persoonlijke karakteristieken, waaronder nierfunctie, lichaamsgewicht en de bloedglucosespiegel, als ook de rol van technische factoren, waaronder de geïnjecteerde dosis, circulatietijd, bloedactiviteit en het PET instrumentarium, op de beeldkwaliteit bestudeerd. Voor zowel FDG als voor NaF bleken de geïnjecteerde dosis, de resterende bloedactiviteit en het PET instrumentarium van invloed te zijn op de beeldkwaliteit. De overige factoren, waaronder de nierfunctie, de bloedglucosespiegel en het lichaamsgewicht, bleken niet van invloed op de beeldkwaliteit. Daarnaast worden in deze hoofstukken methoden beschreven waarmee gecorrigeerd kan worden voor variatie in de geïnjecteerde dosis, de resterende bloedactiviteit en het PET instrumentarium.

Deel II, bestaande uit 3 hoofdstukken, is gericht op de klinische validatie van FDG PET en NaF PET. In **hoofdstuk 7** worden de resultaten besproken van onderzoek dat normaalwaarden heeft vastgesteld voor FDG en NaF opname in de slagaderwand. Normaalwaarden zijn belangrijk om gezond van ziek te kunnen onderscheiden. Naast het vaststellen van normaalwaarden is gekeken naar leeftijds- en geslachtsverschillen. Het onderzoek toonde aan dat de opname van

zowel FDG als NaF in de slagaderwand met de leeftijd toeneemt. Geslacht daarentegen had geen invloed op de opname van FDG en NaF in de slagaderwand. In **hoofdstuk 8** wordt het resultaat besproken van onderzoek waarin NaF opname in de kransslagaders werd vergeleken met het cardiovasculair risicoprofiel van de patiënt. De opname van NaF in de kransslagaders was hoger bij vrouwen dan bij mannen en nam toe met zowel de leeftijd, lichaamsgewicht, als de bloeddruk. Het onderzoek toonde verder aan dat het risico op hart- en vaatziekten gemiddeld 3,1 keer hoger was bij personen met veel NaF opname in de kransslagaders dan in personen met weinig NaF opname. Samenvattend toonde het onderzoek aan dat personen met een ongunstig cardiovasculair risicoprofiel meer NaF stapelen in hun kransslagaders dan personen met een gunstig cardiovasculair risicoprofiel. Tot slot wordt in **hoofdstuk 9** het cardiovasculair risicoprofiel van de patiënt vergeleken met de aanwezigheid van vaatkalk in de grote lichaamsslagader, zoals vastgesteld met een computertomografie-scan, alsmede de mate waarin FDG en NaF zich stapelen in de grote lichaamsslagader. Het onderzoek toonde aan dat zowel de mate van NaF stapeling als de aanwezigheid van vaatkalk geassocieerd waren met een verhoogd risico op hart- en vaatziekten. FDG stapeling daarentegen bleek niet geassocieerd te zijn met een verhoogd risico op hart- en vaatziekten. Het hoogste risico op hart- en vaatziekten werd gevonden in mensen met vaatkalk en met een hoge NaF waarde. De resultaten van **hoofdstuk 9** suggereren dat NaF PET een belangrijke rol kan spelen in het detecteren van de kwetsbare patiënt, terwijl de rol van FDG PET beperkter lijkt voor dit doel.

CONCLUSIE

Dit proefschrift concludeert dat NaF PET een veelbelovende techniek is voor identificatie van kwetsbare patiënten. FDG PET daarentegen speelt geen rol van betekenis bij de identificatie van de kwetsbare patiënt. Naast klinische validatie levert dit proefschrift een bijdrage aan de technische validatie van zowel FDG PET als NaF PET voor de toepassing van cardiovasculair risicomanagement. Ondanks de bemoedigende resultaten toont dit proefschrift niet aan dat functionele beeldvorming van slagaderverkalking van toegevoegde waarde is bovenop de reeds gangbare risicofactoren voor hart- en vaatziekten. Dit zal vervolgonderzoek moeten uitwijzen.

ADDENDA

Review Committee

Prof. dr. Pieter A.F.M. Doevendans
Professor of Cardiology
Department of Cardiology, University Medical Center Utrecht

Prof. dr. ir. Yvonne T. van der Schouw
Professor of Epidemiology
Department of Epidemiology, University Medical Center Utrecht

Prof. dr. Tim Leiner
Professor of Radiology
Department of Radiology and Nuclear Medicine, University Medical Center Utrecht

Prof. dr. Marianne C. Verhaar
Professor of Nephrology
Department of Nephrology and Hypertension, University Medical Center Utrecht

Prof. dr. Riemer H.J.A. Slart
Professor of Molecular Imaging
Department of Nuclear Medicine, University Medical Center Groningen

Authors and Affiliations

Abass Alavi Department of Radiology, Hospital of the University of Pennsylvania, Philadelphia, Pennsylvania, United States of America

Arjun Bashyam Department of Radiology, Hospital of the University of Pennsylvania, Philadelphia, Pennsylvania, United States of America

Poul-Erik N. Braad Department of Nuclear Medicine, Odense University Hospital, Odense, Denmark

Karen M. Buch-Olsen Department of Nuclear Medicine, Odense University Hospital, Odense, Denmark

Axel C.P. Diederichsen Department of Cardiology, Odense University Hospital, Odense, Denmark

Saeid Gholami Department of Radiology, Hospital of the University of Pennsylvania, Philadelphia, Pennsylvania, United States of America

Søren Hess Department of Nuclear Medicine, Odense University Hospital, Odense, Denmark

Malene G. Hildebrandt Department of Nuclear Medicine, Odense University Hospital, Odense, Denmark

Poul F. Høilund-Carlsen Department of Nuclear Medicine, Odense University Hospital, Odense, Denmark and Institute of Clinical Research, University of Southern Denmark, Odense, Denmark

Sina Houshmand Department of Radiology, Hospital of the University of Pennsylvania, Philadelphia, Pennsylvania, United States of America

Pim A. de Jong Department of Radiology and Nuclear Medicine, University Medical Center Utrecht, Utrecht, the Netherlands

Marnix G.E.H. Lam Department of Radiology and Nuclear Medicine, University Medical Center Utrecht, Utrecht, the Netherlands

Willem P.T.M. Mali Department of Radiology and Nuclear Medicine, University Medical Center Utrecht, Utrecht, the Netherlands

Hans Mickley Department of Cardiology, Odense University Hospital, Odense, Denmark

Jagat Narula Icahn School of Medicine, Mount Sinai Hospital, New York, New York, United States of America

Anne L. Nielsen Department of Nuclear Medicine, Odense University Hospital, Odense, Denmark

Michael H. Olsen The Cardiovascular and Metabolic Preventive Clinic, Department of Endocrinology, Center for Individualized Medicine in Arterial Diseases, Odense University Hospital, Odense, Denmark

Abhinay Ramachandran Department of Radiology, Hospital of the University of Pennsylvania, Philadelphia, Pennsylvania, United States of America

Ali Salavati Department of Radiology, Hospital of the University of Pennsylvania, Philadelphia, Pennsylvania, United States of America

Jane A. Simonsen Department of Nuclear Medicine, Odense University Hospital, Odense, Denmark

Richard A.P. Takx Department of Radiology and Nuclear Medicine, University Medical Center Utrecht, Utrecht, the Netherlands and Department of Radiology, Massachusetts General Hospital, Boston, Massachusetts, United States of America

Anders Thomassen Department of Nuclear Medicine, Odense University Hospital, Odense, Denmark

Werner Vach Department of Clinical Epidemiology, Institute of Medical Biometry and Medical Informatics, University Medical Center Freiburg, Freiburg, Germany

Mie H. Vilstrup Department of Nuclear Medicine, Odense University Hospital, Odense, Denmark

Thomas J. Werner Department of Radiology, Hospital of the University of Pennsylvania, Philadelphia, Pennsylvania, United States of America

Habib Zaidi Division of Nuclear Medicine and Molecular Imaging, Geneva University Hospital, Geneva, Switzerland and Department of Nuclear Medicine and Molecular Imaging, University Medical Center Groningen, Groningen, the Netherlands

Scientific Communications

PEER REVIEWED PUBLICATIONS

1. Oudkerk SF, de Jong PA, Blomberg BA, Scholtens AM, Mali WP, Spiering W. Whole-Body Visualization of Ectopic Bone Formation of Arteries and Skin in Pseudoxanthoma Elasticum. *J Am Coll Cardiol Img*. 2015; [Epub ahead of print].

2. Blomberg BA, Thomassen A, De Jong PA, Simonsen JA, Lam GE, Nielsen AL, Mickley H, Mali WP, Alavi A, Højlund-Carlsen PF. Impact of Personal Characteristics and Technical Factors on Quantification of Sodium ^{18}F-Fluoride Uptake in Human Arteries: Prospective Evaluation of Healthy Subjects. *J Nucl Med*. 2015; **56**: 1534-1540.

3. Blomberg BA, Bashyam A, Ramachandran A, Gholami S, Houshmand S, Salavati A, Werner TJ, Zaidi H, Alavi A. Quantifying [^{18}F]-Fluorodeoxyglucose Uptake in the Arterial Wall: The Effects of Dual Time-Point Imaging and Partial Volume Effect Correction. *Eur J Nucl Med Mol Imaging*. 2015**; 42**: 1414-1422.

4. Pasha AK, Moghbel M, Saboury B, Gharavi MH, Blomberg BA, Torigian DA, Kwee TC, Basu S, Mohler ER, Alavi A. Effects of Age and Cardiovascular Risk Factors on ^{18}F-FDG PET/CT Quantification of Atherosclerosis in the Aorta and Peripheral Arteries. *Hell J Nucl Med*. 2015; **18**: 5-10.

5. Takx RA, Blomberg BA, Aidi HE, Habets J, de Jong PA, Nagel E, Hoffmann U, Leiner T. Diagnostic Accuracy of Stress Myocardial Perfusion Imaging Compared to Invasive Coronary Angiography with Fractional Flow Reserve Meta-Analysis. *Circ Cardiovasc Imaging*. 2015; **8**: [Epub ahead of print].

6. Thomassen A, Nielsen AL, Lauridsen JK, Blomberg BA, Hess S, Petersen H, Johansen A, Asmussen JT, Sørensen JR, Johansen J, Godballe C, Højlund-Carlsen PF. FDG-PET/CT Can Rule Out Malignancy in Patients With Vocal Cord Palsy. *Am J Nucl Med Mol Imaging*. 2014; **4**: 193-201.

7. Hess S, Blomberg BA, Rakheja R, Friedman K, Kwee TC, Højlund-Carlsen PF, Alavi A. A Brief Overview of Novel Approaches to FDG PET Imaging and Quantification. *Clin Transl Imaging.* 2014; **2**: 187-98.

8. Blomberg BA, Thomassen A, Takx RA, Hildebrandt MG, Simonsen JA, Buch-Olsen KM,

Diederichsen AC, Mickley H, Alavi A, Høilund-Carlsen PF. Delayed ^{18}F-Fluorodeoxyglucose PET/CT Imaging Improves Quantitation of Atherosclerotic Plaque Inflammation: Results from the CAMONA Study. *J Nucl Cardiol*. 2014; **21**: 588-97.

9. Blomberg BA, Thomassen A, Takx RA, Vilstrup MH, Hess S, Nielsen A, Diederichsen AC, Mickley H, Alavi A, Høilund-Carlsen PF. Delayed Sodium ^{18}F-Fluoride PET/CT Imaging Does Not Improve Quantification of Vascular Calcification Metabolism: Results from the CAMONA Study. *J Nucl Cardiol*. 2014; **21**: 293-304.

10. Hess S, Blomberg BA, Zhu HJ, Høilund-Carlsen PF, Alavi A. The Pivotal Role of FDG-PET/CT in Modern Medicine. *Acad Radiol.* 2014; **21**: 232-49.

11. Mauritz FA, Blomberg BA, Stellato RK, van der Zee DC, Siersema PD, van Herwaarden-Lindeboom MY. Complete Versus Partial Fundoplication in Children with Gastroesophageal Reflux Disease: Results of a Systematic Review and Meta-analysis. *J Gastrointest Surg*. 2013; **17**: 1883-92.

12. Blomberg BA, Akers SR, Saboury B, Mehta NN, Cheng G, Torigian DA, Lim E, Del Bello C, Werner TJ, Alavi A. Delayed Time-Point ^{18}F-FDG PET CT Imaging Enhances Assessment of Atherosclerotic Plaque Inflammation. *Nucl Med Commun*. 2013; **34**: 860-7.

13. Blomberg BA, Codreanu I, Cheng G, Werner TJ, Alavi A. Beta-cell Imaging: Call for Evidence-Based and Scientific Approach. *Mol Imaging Biol*. 2013; **15**: 123-30.

14. Blomberg BA, Eriksson O, Saboury B, Alavi A. β-Cell Mass Imaging with DTBZ Positron Emission Tomography: Is it Possible? *Mol Imaging Biol*. 2012; **15**: 1-2.

15. Blomberg BA, Moghbel MC, Saboury S, Stanley CA, Alavi A. The Value of Radiologic Interventions and ^{18}F-DOPA PET in Diagnosing and Localizing Focal Congenital Hyperinsulinism: Systematic Review and Meta-Analysis. *Mol Imaging Biol*. 2012; **15**: 97-105.

16. Blomberg BA, Moghbel MC, Alavi A. PET Imaging of β-Cell Mass: Is it Feasible? *Diabetes Metab Res Rev*. 2012; **28**: 601-602.

BOOK CHAPTERS

1. Blomberg BA, Høilund-Carlsen PF. [^{18}F]-Fluorodeoxyglucose PET Imaging of Atherosclerosis. *PET Clin*. 2015; 10: 1-7.

CONFERENCE PROCEEDINGS

The 20th Annual Scientific Session of the American Society of Nuclear Cardiology, Washington, District of Columbia, United States of America

1. Blomberg BA. Coronary [^{18}F]-Sodium Fluoride is Increased in Healthy Adults With an Unfavorable Cardiovascular Risk Profile. *J Nucl Cardiol*. 2015; [Epub ahead of print].

2014 Annual Congress of the European Association of Nuclear Medicine, Gothenburg, Sweden

1. Blomberg BA, Takx RA, Høilund-Carlsen PF. Stress Myocardial Perfusion Imaging Versus Invasive Coronary Angiography with Fractional Flow Reserve: A Meta-Analysis. *Eur J Nucl Med Mol Imaging*. 2014; **41**: S201.

80th European Atherosclerosis Society Congress, Lyon, France

1. Blomberg BA, Thomassen A, Simonsen JA, Hildebrandt MG, Diederichsen AC, Mickley H, Alavi A, Høilund-Carlsen PF. The Effect of Aging on Atherosclerotic Plaque Inflammation and Molecular Calcification: A PET CT Imaging Study.

Society of Nuclear Medicine and Molecular Imaging 2013 Annual Meeting, Vancouver, British Columbia, Canada

1. Blomberg BA, Thomassen A, Hildebrandt GE, Vilstrup M, Nielsen A, Simonsen JA, Diederichsen AC, Mickley H, Alavi A, Høilund-Carlsen PF. Assessment of Atherosclerotic Plaque Inflammation can be Improved by Delayed Time Point FDG PET/CT Imaging. *J Nucl Med*. 2013; **54**: 1720.

2. Blomberg BA, Thomassen A, Hildebrandt GE, Vilstrup M, Nielsen A, Simonsen JA, Hess S, Alavi A, Høilund-Carlsen PF. The Relation Between Aging, Aortic NaF Avidity and

Coronary Artery NaF Avidity: A NaF PET/CT Study. *J Nucl Med*. 2013; **54**: 1721.

3. Blomberg BA, Thomassen A, Hildebrandt GE, Nielsen A, Simonsen JA, Hess S, Alavi A, Høilund-Carlsen PF. The Effect of Aging on Aortic Atherosclerotic Plaque Inflammation and Molecular Calcification: A FDG and NaF PET/CT Study. *J Nucl Med*. 2013; **54**: 1722.

Society of Nuclear Medicine and Molecular Imaging 2012 Annual Meeting, Miami, Florida, United States of America

1. Blomberg BA, Gharavi MH, Saboury B, Werner TJ, Torigian D, Cheng G, Lim E, Akers SR, Alavi A. Effect of Aging and Smoking on FDG-Uptake in Atherosclerotic Plaques Assessed By Multiple-Time-Point PET/CT Imaging. *J Nucl Med*. 2012; **53**: 1850.

3rd Multimodality Cardiovascular Molecular Imaging Symposium, Bethesda, Maryland, United States of America

1. Blomberg BA, Gharavi MH, Saboury B, Werner TJ, Torigian D, Cheng G, Lim E, Akers SR, Alavi A. Effect of Aging and Smoking on FDG-Uptake in Atherosclerotic Plaques Assessed By Multiple-Time-Point PET/CT Imaging. *J Nucl Med*. 2012; **53**: 665.

Grants and Awards

GRANTS

Anna Marie and Christian Rasmussen's Memorial Foundation, University of Southern Denmark, Odense, Denmark

MD-PhD 'Alexandre Suerman' Stipend, University Medical Center Utrecht, Utrecht, the Netherlands

AWARDS

2015 Young Investigator Award, American Society of Nuclear Cardiology

Acknowledgements

(Dankwoord)

Dit proefschrift kwam tot stand door de inzet van velen. Enkelen van hen wil ik in het bijzonder bedanken.

Professor Mali, promotor, beste Willem, ik ben u zeer dankbaar voor alle mogelijkheden die u mij heeft geboden tijdens mijn promotietraject. Het gegeven vertrouwen om mijn eigen onderzoek uit te voeren heb ik beschouwd als een enorm voorrecht. Dankzij uw inspanningen heb ik, naast mijn werkzaamheden in Nederland, onderzoek kunnen doen in de Verenigde Staten van Amerika en Denemarken. Deze ervaringen zijn bepalend geweest voor het succes van mijn onderzoek. Daarnaast heb ik op uw advies de studie tot klinisch epidemioloog gevolgd; een waardevolle opleiding voor mijn toekomstige carrière als arts-onderzoeker.

I'm extremely grateful to Professor Poul Flemming Høilund-Carlsen for supervising the work described in this thesis. His assistance, from initial approval of the study protocol to journal publication and all stops in between, has been invaluable and this work would not have come to fruition without his guidance and enthusiasm. In addition, I am grateful for all the opportunities he provided me with, particularly the opportunity to spend a year in Denmark and to work with his wonderful team at Odense University Hospital. Poul, you are an indescribably inspiring person and I'm looking forward to work with you for many years to come.

Doctor De Jong, copromotor, beste Pim, ik wil u hartelijk bedanken voor de dagelijkse begeleiding van mijn promotieonderzoek. U heeft in belangrijke mate bijgedragen aan de kwaliteit van dit proefschrift. Daarnaast stond u altijd voor mij klaar en had u voor elk probleem een passende oplossing. Ik heb dan ook met plezier met u samengewerkt.

Doctor Lam, copromotor, beste Marnix, ook u wil ik hartelijk bedanken voor de begeleiding van mijn promotieonderzoek. In het bijzonder wil ik u bedanken voor de kritische blik op mijn artikelen. U was altijd bereid om in een vroeg stadium de artikelen te lezen en te voorzien van constructief commentaar. Bedankt voor deze betrokkenheid.

De leden van de beoordelingscommissie, prof. dr. Doevendans, prof. dr. Van der Schouw, prof. dr. Leiner, prof. dr. Verhaar en prof. dr. Slart, ik wil u allen hartelijk bedanken voor het lezen en beoordelen van mijn proefschrift.

I would like to express sincere thanks to Professor Abass Alavi whose wisdom and wit were invaluable to the success of this thesis. His enthusiasm towards medical research aspired me

to become a physician-scientist. For this and many other things, I am forever grateful. I am proud to be part of the Alavi family.

I would also like to express sincere thanks to Anders Thomassen. This thesis would not have been possible without your kind and generous help regarding all things CAMONA. In addition, I really enjoyed our trips to Lyon, Vancouver, and Boston. Hopefully we can continue our collaborative work in the future.

I would like to thank the entire CAMONA team, consisting of Poul Flemming Høilund-Carlsen, Axel Diederichsen, Anders Thomassen, Peter Grupe, Mie Vilstrup, Anne Nielsen, Jane Simonsen, Malene Hildebrandt, Søren Hess, Karen Buch-Olsen, Allan Johansen, Henrik Petersen, Oke Gerke, Michael Hecht Olsen, Kim Brixen, Werner Vach, Hans Mickley, and Abass Alavi, for all their efforts. In addition, I would like to thank Mette Høilund-Carlsen and Marianne Knudsen for their excellent logistical assistance. Without their assistance CAMONA was not possible. Finally, I would like to express my sincere thanks to all those involved in scanning the study volunteers and producing the radiotracers for the countless CAMONA examinations.

Marja Kool en Annet Bleumink-Houtman wil ik hartelijk bedanken voor de secretariële ondersteuning. Roy Sanders wil ik hartelijk bedanken voor het printen van het concept proefschrift voor de beoordelingscommissie.

Anouk, beste collega, maatje, jouw tomeloze energie, enthousiasme en humor hebben het werken op de afdeling radiologie tot een waar feest gemaakt. Onze vriendschap waardeer ik enorm.

Hugo, beste collega, maat, jouw enthousiaste doch kritische blik op medisch-wetenschappelijk onderzoek hebben mij tot een betere onderzoeker gemaakt. Dank voor de vele goede gesprekken en de gezellige koffiemomenten.

Richard, Annemarie en Marjolein, beste kamergenoten, bedankt voor de gezelligheid en alle goede gesprekken. Bij jullie kon ik mijn ei kwijt, kon ik mijn ervaringen relativeren en mijn successen delen. Dit heb ik enorm gewaardeerd. Ik wens jullie heel veel succes met het afronden van jullie promotietrajecten.

Lieve zus, beste Ellen, wat fijn dat je mijn paranimf wilt zijn.

Beste Christian, maat vanaf het eerste uur in Utrecht. Ik vind het een eer dat je mijn paranimf wilt zijn. Daarnaast wens ik je veel succes met het afronden van je promotieonderzoek aan de Universiteit van Oxford.

Peter en Hilma, dit proefschrift is voor jullie. Ik ben jullie ontzettend dankbaar voor de warme en liefdevolle opvoeding. Zonder jullie onvoorwaardelijke steun was dit proefschrift er nooit gekomen. Ik kan mij geen betere ouders voorstellen.

Lieve Alexandra, mijn grote liefde. Wat ben ik blij dat ik jou heb versierd en ingepakt. Je hebt mij laten zien dat er nog zoveel meer is dan studie, werk en onderzoek. Het lijkt me heerlijk om de rest van mijn leven met jou te delen.

Curriculum Vitae

Björn Blomberg was born December 4, 1987 in Rockanje, the Netherlands. After graduating from the Atheneum at G.S.G. Helinium in Hellevoetsluis, he attended Utrecht University School of Medicine in Utrecht. As part of his medical training he visited the Perelman School of Medicine at the University of Pennsylvania in Philadelphia, United States of America and performed clinical research at the Department of Radiology at the Hospital of the University of Pennsylvania under supervision of Abass Alavi. After graduating with honors (judicium cum laude) from Utrecht University School of Medicine in 2012, he moved to Denmark to conduct cardiovascular research at the Department of Nuclear Medicine at Odense University Hospital in Odense under supervision of Poul Flemming Høilund-Carlsen. After his return to the Netherlands, he initiated a collaboration between the Department of Nuclear Medicine at Odense University Hospital, the Department of Radiology at the Hospital of the University of Pennsylvania, and the Department of Radiology and Nuclear Medicine at the University Medical Center Utrecht. The efforts of this collaboration are presented in this thesis. During his time at the University Medical Center Utrecht he obtained a Postgraduate Master of Science degree in Clinical Epidemiology from Utrecht University. Björn is currently pursuing a career in surgery.